DEVELOPMENT OF HPLC STATIONARY PHASES WITH UNIQUE SELECTIVITIES AND INTRODUCTION OF MOLECULAR ROTATIONAL RESONANCE SPECTROSCOPY IN GAS CHROMATOGRAPHY

by

NIMISHA THAKUR

Presented to the Faculty of the Graduate School of

The University of Texas at Arlington in Partial Fulfillment

of the Requirements for the Degree of

DOCTOR OF PHILOSOPHY

THE UNIVERSITY OF TEXAS AT ARLINGTON

December 2020

Dedicated to all the women around the world who are following their passions despite the odds

Acknowledgment

I have been incredibly fortunate to have Dr. Daniel W. Armstrong as my Ph.D. supervisor and would like to express my most profound appreciation. It was his excellent mentorship, constant support, and counsel, which made this long scientific journey smooth and fulfilling. He is a teacher par excellence. His scientific expertise, enthusiasm, and constructive feedback helped me achieve various milestones throughout my graduate school. I want to record my gratitude to my committee members, Dr. Kevin Schug, Dr. Peter Kroll, and Dr. Morteza Khaledi, for their support.

I would like to thank Dr. M. Farooq Wahab for his constant and noble assistance whenever I needed it. I have learned a great deal from him about science, attention to detail, designing experiments, as well as soft skills like presentation and writing skills. His benevolence is his hallmark.

I am also grateful to my colleagues and friends, Siqi, Mohsen, Daipayan, Elizabeth, Abiud, Diego, Saba, and Michael for providing fun and positive learning environment. I would especially like to thank Rahul and Chandan for their valuable mentoring throughout my Ph.D. I would like to thank Anne Ellis, Angel Escalante, Stephanie Henry, and Barbara Smith for their administrative assistance.

I heartily thank my friends, Priyanka, Megha, and Vijit, who are my lifelines. This journey would not have been possible without their humor, silliness, light-heartedness, and selfless friendships.

Finally, I would like to thank my father, Prof. Ravinder Thakur, mother, Anju Thakur, and brother, Vidit, for all their love, care, support, and encouragement. A special thanks to my sister, Ankita, whom I have always looked up to for inspiration and direction.

Oct 7th, 2020

Abstract

DEVELOPMENT OF HPLC STATIONARY PHASES WITH UNIQUE SELECTIVITIES AND INTRODUCTION OF MOLECULAR ROTATIONAL RESONANCE SPECTROSCOPY IN GAS CHROMATOGRAPHY

Nimisha Thakur

The University of Texas, Arlington, 2020

Supervising Professor: Daniel W. Armstrong

This thesis contributes to advancing liquid and gas chromatography by introducing new stationary phases for HPLC and a new hyphenated GC technique. In the first section, new pH stable stationary phases based on geopolymers are presented for applications in liquid chromatography. The first-ever synthesis of micron-sized spherical particles of geopolymers, customized to be used as HPLC stationary phases, is reported. Complete material characterization of geopolymers using X-ray diffraction, scanning electron microscopy, energy dispersive spectroscopy, laser diffraction, and porosimetry is shown. The chromatographic evaluation of geopolymers is done by comparing parameters such as hydrophilicity, ion exchange selectivity, efficiency, hydrolytic stability, and pH stability with silica stationary phases. Geopolymers are successfully employed for separations of various classes of compounds using hydrophilic interaction liquid chromatography (HILIC) and normal phase chromatography. Furthermore, geopolymer monoliths are synthesized by inducing higher and interconnected porosity in their otherwise impermeable structure to advance their applications in fields like separation science, catalysis, and drug delivery. This thesis also presents chemical

modifications of original geopolymer particles to extend the applications in separation and adsorption sciences. Firstly, transition metal-free geopolymer microspheres are introduced as a second-generation geopolymer stationary phase, showcasing the improvements in the chromatographic performance (particularly peak shapes). Secondly, barium exchanged geopolymers are proposed as new HILIC stationary phases specially developed for separations of compounds with acidic functional groups like carboxylates, sulfonates, and sulfates. Thirdly, iron oxide coated geopolymer microspheres are demonstrated as cost-effective and porous adsorbents for arsenate, arsenite, monomethyl arsenate, and dimethyl arsenate.

The second section of this thesis introduces the concept of hyphenation of gas chromatography (GC) with molecular rotational resonance spectroscopy (GC-MRR). The power of MRR lies in its ability to discern the slightest change in the mass and/or molecular geometry in a molecule resulting in distinct rotational spectra. The unique abilities of the GC-MRR are demonstrated by the separation and quantification of a series of 24 isotopologues and isotopomers of five organic compounds. Natural isotopic abundances of mixtures of compounds containing chlorine, bromine, and sulfur heteroatoms are easily determined.

Table of Contents

List of Illustrations

List of Tables

Chapter 1. Introduction

Part I: Advent of geopolymers in separation science

This part describes the development of geopolymer microparticles as stationary phases for hydrophilic interaction liquid chromatography applications. Modified geopolymers have also been formulated to extend their applications in liquid chromatography and adsorption sciences.

1.1 Geopolymers

Geopolymers are X-ray amorphous inorganic polymers consisting of randomly crosslinked silica and alumina tetrahedral units [1]. The negative charge of aluminate (AlO_4) tetrahedra is compensated by alkali metal cations like K^+, Na^+, etc. Geopolymers share similarities with zeolites in terms of their fundamental framework [2]; however, geopolymers are strictly synthetic, whereas zeolites can both be found in nature or be synthesized. Also, geopolymers do not have regular micropores owing to the lack of long-range ordering. The chemical properties and microstructure of geopolymers depend on: a) composition and dissolution properties of aluminosilicate source, b) Si/Al ratio, c) amount, and type of alkali activator, d) curing temperature, and e) curing time [3, 4]. Geopolymers initially gained importance in the field of construction materials since they are considered a "green" alternative to Portland Cement [5]. However, owing to their unique physicochemical properties such as high mechanical strength, heat resistance, and chemical resistance to acids and bases [6], geopolymers are finding applications in chemistry as adsorbents for heavy metals [7], in catalysis [8], and drug delivery [9, 10].

The promising physicochemical properties of geopolymers such as pH stability, mechanical strength, and heat resistance, make them an ideal candidate for HPLC stationary phases. However,

there have been no reports on applications of geopolymers in the chromatographic sciences owing to the challenge of synthesizing geopolymer microparticles. Interestingly, since the inception of geopolymers in 1972, there is no study on the fabrication of geopolymer micron-sized spherical particles. The literature is focused on making geopolymers in block form since they are used as building materials. The monolithic block forms cannot be translated to monolithic HPLC columns due to the intrinsic low permeability of their structure. This thesis reports the first-ever synthesis of geopolymer microspheres and macroporous monoliths using water in oil emulsion technique (also referred to as reverse emulsion technique or inverse suspension polymerization). In this technique, the suspension of monomers is sustained in an immiscible liquid with the help of mechanical stirring and surfactants (or stabilizers).

1.2 Synthesis of geopolymers

The geopolymers are readily synthesized by dissolving reactive aluminosilicate precursors (e.g., metakaolin, fly ash) in a highly alkaline solution (e.g., KOH or NaOH) [1]. The viscous solution, thus formed, is cured to form a gel which finally consolidates. A new technique based on reverse emulsion templating (or inverse suspension polymerization) has been implemented in this work, to cater specifically to the requirement of developing HPLC stationary phases. In this method, a geopolymer slurry, consisting of natural metakaolin (the aluminosilicate source used in this study), KOH, fumed silica, and water, are mixed with large volumes of canola oil under constant mechanical stirring to form an inverse suspension. An interesting feature of this polymerization technique is that it does not require the addition of an external stabilizer since the highly alkaline geopolymer slurry reacts with the triglycerides in the oil to form carboxylate surfactants, which in

turn help stabilize the suspension [11]. The geopolymerization is continued for 8 hours and the microparticles thus formed are extracted into the water, washed, and dried.

The factors that affect the physical parameters such as particle size, surface area, and microstructure of the geopolymer particles lie in the synthetic conditions of the inverse suspension polymerization. It is important to optimize these physical parameters since they control the efficiency and retention characteristics of the chromatographic column, consequently affecting the resolution [12]. Equation 1.1 shows the dependence of particle size on various synthetic parameters [13].

$$d = k\,\frac{D_v \cdot R \cdot v_d \cdot \varepsilon}{D_s \cdot N \cdot v_m \cdot C_s} \qquad (1.1)$$

where d = average particle size; k = parameters such as apparatus design, type of stirrer, self-stabilization D_v = diameter of vessel; D_s= diameter of stirrer; R = volume ratio of the droplet phase to suspension medium; N = stirring speed; v_d= viscosity of the droplet phase; v_m= viscosity of the suspension medium; ε = interfacial tension between the two immiscible phases, C_s = stabilizer concentration.

According to the chromatographic theory, decreasing particle size is a useful method to increase chromatographic efficiency and thus providing better resolution. From equation 1.1, it can be inferred that the stirring speed is the most convenient way to control particle size. In this work, stirring speed and the stirring apparatus have been optimized to get smaller particle sizes, narrow particle size distributions, and large surface areas.

Herein, high purity transition metal-free geopolymers as HPLC stationary phases are also reported. The natural metakaolin contains trace transition metal impurities like Fe and Ti which are carried

forward to the final geopolymer particles. Fig. 1.1 shows the total amount of trace metals in the natural metakaolin (employed in this study).

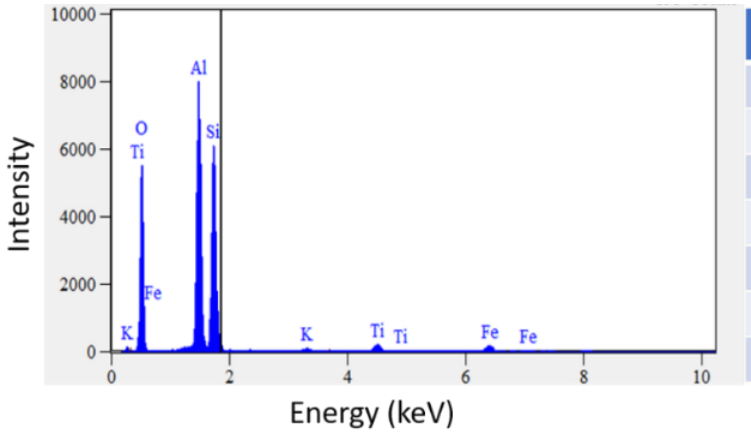

Element	Atom %
O	65.42 ±0.36
Al	16.36 ± 0.10
Si	16.81 ± 0.12
K	0.15 ± 0.03
Ti	0.58 ± 0.02
Fe	0.69 ± 0.04
Total	100.00

Fig. 1.1 EDS spectrum and corresponding quantitative elemental analysis of natural metakaolin

These transition metals are detrimental to the chromatographic performance of the stationary phase, often leading to peak tailing or no elution at all [14]. Therefore, a synthetic aluminosilicate precursor was employed to prepare geopolymers containing no trace transition metals (Chapter 4). The synthetic aluminosilicate precursor is synthesized by a simple sol-gel method [15].

This thesis also reports the fabrication of macroporosity in geopolymer monoliths. Geopolymers are intrinsically highly dense structures exhibiting low permeability [16]. Many researchers have reported the generation of additional porosity in geopolymers by using blowing agents (H_2O_2) [17], in situ saponification [18], and surfactants [19]. However, there are no reports on geopolymers with interconnected macroporosity. The interconnected macroporosity in geopolymers can advance their applications in adsorption, filtration, and separation science. In this work, we report the fabrication of interconnected macroporosity in geopolymer monoliths (ultimately increasing the permeability) by a route of the "sticky period," which occurs during inverse suspension polymerization [20]. During the sticky period, the particles can coalesce, in

the event of a collision, but cannot further re-divide because of their partial hardening (or polymerization). The monoliths with macropores were synthesized by deliberately causing the coalescence of the particles during the "sticky period".

1.3 Chromatographic aspects of geopolymers

The fundamental aim of chromatography is to achieve resolution between analytes of interest. The fundamental resolution equation (1.1) describes how the three chromatographic parameters, a) efficiency, b) selectivity c) retention factor, impacts the resolution.

$$R_s = \left(\frac{\sqrt{N}}{4}\right)\left(\frac{a-1}{\alpha}\right)\left(\frac{k_2}{1+k_2}\right) \qquad (1.2)$$

where R_s is the resolution between two peaks, 'N' is the efficiency or the plate count, 'α' is the selectivity and '*k*' is the retention factor.

Selectivity, α, plays a major role in controlling resolution, whereas efficiency, N, and the retention factor, k, play relatively smaller roles. Selectivity can be adjusted by changing the stationary phase or changing mobile phase parameters such as an organic modifier type, pH, and composition ratios. Therefore, developing new chromatographic materials is one of the most active research areas in separation science. The physicochemical features of geopolymers fulfill all the primary criteria for a new stationary phase with unique selectivities for liquid chromatography. The selectivity comparison was done with 36 other stationary phases (commercial and published) by plotting a "selectivity chart" where the x-axis plots the selectivity of cytosine /uracil, signifying hydrophilicity of the stationary phase, and the y-axis plots selectivity of BTMA/cytosine, which is taken as a measure of the ion exchange characteristic of the stationary phase (see Chapter 2 Figure 2.3). The geopolymer stationary phase occupies a remarkable position in this selectivity diagram,

demonstrating that the geopolymer stationary phase is the most hydrophilic HILIC stationary phase among 37 stationary phases in the selectivity plot. Further selectivity comparisons have been made with silica, which is the most common HPLC HILIC stationary phase, test analytes from various classes of compounds were selected; for example, aromatic acids and derivatives, nucleosides, and oxazolidinones (see Chapter 2 Figure 2.4)

Hydrolytic stability is critical for HILIC stationary phases since continuous leaching of stationary phase results in significant retention time drifts. Also, the stability of the stationary phase at high pH is a great advantage as eluent pH is one of the most powerful chromatographic parameters to control the selectivity of ionizable solutes. It's well known that silica does not have either hydrolytic stability or high pH stability [21, 22]. It has been demonstrated in this work that geopolymers show exceptional pH stability and excellent hydrolytic stability allowing for a broader range of method development chromatographic parameters.

The chromatographic evaluation of a second generation geopolymer stationary phase, which is free from transition metal impurities, is also presented. The deleterious effects of the presence of transition metals in the geopolymer stationary phase on peak shapes are highlighted (Chapter 4). The chromatographic evaluation of the new synthetic aluminosilicate based geopolymers demonstrated significant improvements in the peak shape (particularly peak tailing) for the analytes known to complex with transition metals. Further, high pH separations, mixed-mode behavior, and the use of high temperatures to tune retention and selectivity in liquid chromatography have been demonstrated.

1.4 Modified geopolymers and their applications

1.4.1 Barium geopolymer stationary phases for enhanced selectivity of polar hydrophilic analytes

Salts play a major role in HILIC retention mechanisms and alter the selectivity [23]. Geopolymers exhibit cation exchange properties due to the tetrahedral aluminate units. This thesis describes the modification of geopolymer microparticles using ion-exchange to incorporate Ba^{2+} in their structures. This has extended their applications in separations of specific classes of analytes, for example, sulfonic acids, sulfates, carboxylic acids, and phosphonic acids. Besides the chromatographic assessment of Ba^{2+} modified geopolymer stationary phase, it has also been shown that Ba^{2+} can be introduced in trace amounts in the mobile phase to impart affinity towards the analyte classes mentioned above on silica phases.

1.4.2 Iron oxide coated geopolymer microspheres for arsenic adsorption

Arsenic contamination in drinking water is a global issue having adverse effects on human and animal health. Adsorption is an inexpensive and facile method to remove arsenic from water. Iron oxides are commonly used adsorbents for arsenic removal but present the disadvantages of difficulty in separation after adsorption and intrinsic low hydraulic conductivity. Hence, a suitable, inexpensive, high surface area supporting material is imperative for adsorption applications. Until now, only two studies have been reported using geopolymer based adsorbents for arsenic adsorption. However, these studies used big, irregular low surface area geopolymer particles, and adsorption of only arsenate species have been conducted. In this thesis, iron oxide coated geopolymer microspheres (Fe-GP) have been developed as non-toxic, cost-effective, porous solid supports with the high surface area for arsenic adsorption. Geopolymer microparticles have been coated with iron using ferrous chloride solution. Iron oxide coated geopolymers have been

discussed for adsorption of four different arsenic species viz arsenate, arsenite, monomethyl arsenate and, dimethyl arsenate. The effect of parameters such as pH, contact time, initial concentration, adsorbent dosage, temperature, and competing anions have been detailed. High percent removal of ~86%, 100%, 95%, and 96% for As(III), As(V), DMA and MMA, respectively, were observed at an initial arsenic concentration of 0.5 mg/L, an adsorbent dosage of 10 g/L and in just 60 minutes.

Part II: Hyphenation of molecular rotational resonance spectroscopy with gas chromatography

This part of the thesis investigates the hyphenated technique of molecular rotational resonance spectroscopy- gas chromatography (GC-MRR) developed by coupling GC with MRR. The remarkable features of this technique, such as ultra-high resolution and exceptional chemical specificity, have been highlighted by demonstrating the separations of isotopomers and isotopologues.

1.5 Molecular rotational resonance spectroscopy

Molecular rotational resonance (MRR) spectroscopy identifies and quantifies compounds based on the compound's signature high-resolution rotational spectrum. The molecules' rotational angular momentum is quantized in the low-pressure gas phase. Equation 1.3 and 1.4 defines the moment of inertia of a molecule and describes the relationship of rotational energy levels with the moment of inertia, respectively:

$$I = \sum_i m_i r_i \qquad (1.3)$$

$$E_J = J(J+1)\frac{\hbar}{2I}, \text{ J= 0,1,2, …,} \qquad (1.4)\ *$$

*Equation 1.4 is only valid for linear and symmetric rotors and has been shown to depict the general relationship of rotational energy levels with moment of inertia

where *I* is the moment of inertia, m is mass of atom *i*, r is the distance of atom *i* from the rotational axis passing through the center of mass of the molecule, J is the angular momentum quantum number. It can be elucidated from the equations that the rotational energy levels are dependent on the moment of inertia of the molecule, which in turn is extremely sensitive to the molecule's mass and three-dimensional geometry. Even molecules with the same mass have a distinguishable rotational spectrum due to subtle differences in their structure.

Although the capabilities of MRR for chemical analysis have been known for decades, previous Fourier transform microwave spectrometers had limited measurement speed and sensitivity. However, the major developments in the field of high-speed electronics, micro- and millimeter wave components, and computational chemistry in the past few years, have contributed to using MRR as a dynamic flow-through detector [24].

1.5.1 Hyphenated GC-MRR

The on-line combination of a separation technique and a spectroscopic detection technique is referred to as "hyphenation" by Hirschfeld [25]. Recent advances in techniques such as GC-MS, LC-MS, LC-NMR, CE-MS have significantly widened applications for the analysis of a multitude of analytes. In this work, MRR has been coupled with GC as a dynamic flow-through detector. Gas chromatography helps to simplify the matrix by separating the components beforehand and avoiding possible rotational spectral overlaps. MRR delivers selective information for identification using standards or library spectra. The resolution of this technique exceeds that of NMR, FTIR, and, most importantly, high-resolution mass spectrometry.

GC-MRR has been harnessed for the separation and identification of 24 isotopologues and isotopomers of five organic solvents and determination of natural isotopic abundances of mixtures of compounds containing chlorine, bromine, and sulfur heteroatoms (Chapter 7).

1.6 Organization of the dissertation

The first section of this thesis details the development and applications of high pH stable HPLC stationary phases based on geopolymers. Chapter 2 reports the first-ever synthesis of micron-sized spherical particles of geopolymer, their complete structural characterization, and their applications in liquid chromatography. Chapter 3 details the manipulation of the original microstructure of geopolymers to weave the interconnected macroporosity in geopolymer monoliths using an intricate aspect of suspension polymerization, known as the "sticky period". Chapter 4 examines the deleterious effects of transition metals present in natural metakaolin based geopolymers on chromatographic peak shapes. This chapter also reports the synthesis of synthetic aluminosilicate precursors for the geopolymer stationary phase, which is free of metal impurities and then evaluates their chromatographic properties. Chapter 5 reports the use of barium in the mobile phase for altering the selectivity of various classes of anionic polar analytes, for example, sulfate, sulfonate, phosphate, phosphonate, and carboxylate. Also, a new stationary phase called barium exchanged geopolymers has been evaluated for separating the above-mentioned classes of compounds. In chapter 6, geopolymer microspheres modified with iron oxide have been discussed for their use in the adsorption of four environmentally toxic arsenic species viz. arsenate, arsenite, dimethyl arsenate, and monomethyl arsenate.

The second section of this thesis introduces a new hyphenated technique known as "gas chromatography- molecular rotational resonance spectroscopy" (GC-MRR). Chapter 7 discusses

the new features and applications of GC-MRR in the separation of isotopomers and isotopologues. The second section of this thesis introduces a new hyphenated technique known as “gas chromatography- molecular rotational resonance spectroscopy” (GC-MRR). Chapter 7 discusses the new features and applications of GC-MRR in the separation of isotopomers and isotopologues.

1.7 References

[1] J. Davidovits, Geopolymer chemistry and applications, Geopolymer Institute2008.

[2] J.L. Provis, G.C. Lukey, J.S. van Deventer, Do geopolymers actually contain nanocrystalline zeolites? A reexamination of existing results, Chemistry of materials, 17 (2005) 3075-3085.

[3] H. Rasouli, F. Golestani-Fard, A. Mirhabibi, G. Nasab, K. Mackenzie, M. Shahraki, Fabrication and properties of microporous metakaolin-based geopolymer bodies with polylactic acid (PLA) fibers as pore generators, Ceramics International, 41 (2015) 7872-7880.

[4] E. Papa, V. Medri, P. Benito, A. Vaccari, S. Bugani, J. Jaroszewicz, E. Landi, Insights into the macroporosity of freeze-cast hierarchical geopolymers, RSC advances, 6 (2016) 24635-24644.

[5] C. Shi, A.F. Jiménez, A. Palomo, New cements for the 21st century: The pursuit of an alternative to Portland cement, Cement and Concrete Research, 41 (2011) 750-763.

[6] P. Duxson, A. Fernández-Jiménez, J.L. Provis, G.C. Lukey, A. Palomo, J.S. van Deventer, Geopolymer technology: the current state of the art, Journal of materials science, 42 (2007) 2917-2933.

[7] Z. Yunsheng, S. Wei, C. Qianli, C. Lin, Synthesis and heavy metal immobilization behaviors of slag based geopolymer, Journal of hazardous materials, 143 (2007) 206-213.

[8] P. Sazama, O. Bortnovsky, J. Dědeček, Z. Tvarůžková, Z. Sobalík, Geopolymer based catalysts—new group of catalytic materials, Catalysis today, 164 (2011) 92-99.

[9] B. Cai, H. Engqvist, S. Bredenberg, Evaluation of the resistance of a geopolymer-based drug delivery system to tampering, International journal of pharmaceutics, 465 (2014) 169-174.

[10] E. Jämstorp, M. Strømme, G. Frenning, Modeling structure–function relationships for diffusive drug transport in inert porous geopolymer matrices, Journal of pharmaceutical sciences, 100 (2011) 4338-4348.

[11] F. Gunstone, The chemistry of oils and fats: sources, composition, properties and uses, John Wiley & Sons2009.

[12] D. Corradini, Handbook of HPLC, CRC Press, Boca Raton, FL 2016.

[13] R. Arshady, Suspension, emulsion, and dispersion polymerization: A methodological survey, Colloid and polymer science, 270 (1992) 717-732.

[14] M. Verzele, M. De Potter, J. Ghysels, Trace elements in HPLC silica gel, Journal of High Resolution Chromatography, 2 (1979) 151-153.

[15] M. Catauro, F. Bollino, A. Dell'Era, S.V. Ciprioti, Pure $Al_2O_3 \cdot 2SiO_2$ synthesized via a sol-gel technique as a raw material to replace metakaolin: Chemical and structural characterization and thermal behavior, Ceramics International, 42 (2016) 16303-16309.

[16] W.M. Kriven, J.L. Bell, M. Gordon, Microstructure and microchemistry of fully-reacted geopolymers and geopolymer matrix composites, Ceramic Transactions, 153 (2003).

[17] G. Masi, W.D. Rickard, L. Vickers, M.C. Bignozzi, A. Van Riessen, A comparison between different foaming methods for the synthesis of light weight geopolymers, Ceramics International, 40 (2014) 13891-13902.

[18] D. Medpelli, J.M. Seo, D.K. Seo, Geopolymer with hierarchically meso-/macroporous structures from reactive emulsion templating, Journal of the American Ceramic Society, 97 (2014) 70-73.

[19] A. Singhal, B.P. Gangwar, J. Gayathry, CTAB modified large surface area nanoporous geopolymer with high adsorption capacity for copper ion removal, Applied Clay Science, 150 (2017) 106-114.

[20] R. Arshady, A. Ledwith, Suspension polymerisation and its application to the preparation of polymer supports, Reactive Polymers, Ion Exchangers, Sorbents, 1 (1983) 159-174.

[21] Y. Wang, M.F. Wahab, Z.S. Breitbach, D.W. Armstrong, Carboxylated cyclofructan 6 as a hydrolytically stable high efficiency stationary phase for hydrophilic interaction liquid chromatography and mixed mode separations, Analytical Methods, 8 (2016) 6038-6045.

[22] H. Claessens, M. Van Straten, J. Kirkland, Effect of buffers on silica-based column stability in reversed-phase high-performance liquid chromatography, Journal of chromatography A, 728 (1996) 259-270.

[23] A.J. Alpert, Effect of salts on retention in hydrophilic interaction chromatography, Journal of chromatography A, 1538 (2018) 45-53.

[24] G.G. Brown, B.C. Dian, K.O. Douglass, S.M. Geyer, S.T. Shipman, B.H. Pate, A broadband Fourier transform microwave spectrometer based on chirped pulse excitation, Review of Scientific Instruments, 79 (2008) 053103.

[25] I. Wilson, U.T. Brinkman, Hyphenation and hypernation: the practice and prospects of multiple hyphenation, Journal of chromatography A, 1000 (2003) 325-356.

Chapter 2. Geopolymers as a new class of high pH stable supports with different chromatographic selectivity

2.1 Abstract

Geopolymers belong to an interesting class of X-ray amorphous polycondensed alumino-silicate ceramic solids. The high mechanical strength, chemical stability in basic conditions and water insolubility make geopolymers a unique solid support in separation science. This work describes a new straight forward synthetic procedure for making spherical porous geopolymer particles with high surface area which are amenable for chromatographic purposes. In-depth physicochemical evaluation of geopolymers is conducted via particle size distribution, porosity measurements, X-ray diffraction, pH titration, energy dispersive spectroscopy and compared with silica, titania, and zirconia. Chromatographic selectivity shows that the surface chemistry of geopolymers has strong hydrophilic and electrostatic character, which makes it different from 36 chromatographic columns. Hydrophilic interaction liquid chromatography in columns packed with geopolymer particles shows different selectivity than silica with excellent peak shapes. Phosphate or fluoride additives are not required as they are for zirconia or titania phase.

2.2 Introduction

The reaction of solid aluminosilicates with highly concentrated alkali solutions yields an interesting class of inorganic polymeric ceramic materials referred to as geopolymers [1]. The resulting solids are essentially X-ray amorphous polycondensed solids consisting of a polymeric network of Si-O-Al bonds (Figure 2.S1) with varying Si:Al ratios. Geopolymers and zeolites both consist of a polymeric Si–O–Al frameworks [2], but the fundamental difference between the two is the long-range order, i.e., zeolites are X-ray crystalline materials [3-5]. The geopolymer three-

dimensional polymer network mainly comprises of tetrahedrally coordinated Si^{4+} and Al^{3+} [6-8]. The overall negative charge results from the bridging oxygens in the aluminate tetrahedron and is balanced by alkali metal counter ions, more commonly K^+ or Na^+, but other multivalent cations can be present [7]. Nanometer-scale porous aluminosilicate clusters have been observed in transmission electron micrographs of geopolymer gels [9, 10]. However, the size and micro-arrangement of these clusters are responsible for the long-range ordering of the final geopolymer composite [11]. Geopolymers have received significant attention in construction and environmental engineering as they exhibit excellent mechanical properties such as high compression strength, heat resistance, and chemical resistance[1, 2, 11].

The promising physicochemical features of geopolymers (*vide supra*) fulfill all the primary criteria for a new stationary phase for liquid chromatography [12]. Additionally, a new chemically stable, geopolymer stationary phase should offer: (a) unique/different selectivity compared to existing phases (b) superior chromatographic properties such as stability at elevated pHs and figures of merit such as efficiency and (c) reproducible synthesis. Silica based supports are broadly accessible and practical for most traditional separation modes including hydrophilic interaction liquid chromatography (HILIC), despite its very well-known narrow pH working window of 3-7. A recent study showed that bare silica, which is a popular HILIC phase, has very high bleed even with mild mobile phases consisting of acetonitrile and buffers [13]. The hydrolytic stability of HILIC phases has been extensively investigated by several groups [13-16]. As a result, alternative chromatographic materials have been proposed such as zirconia, carbon clad zirconia, titania and porous graphitic carbon, along with polymeric materials coated onto silica [17]. These materials that have met with partial success, e.g., zirconia and titania have very strong Lewis acid sites, requiring fluoride or phosphate containing mobile phases to quench these sites [18]. Similarly,

chemically modified porous graphitic carbon or polymer coated supports for HILIC offers lower efficiency than silica despite their very different selectivity features [14].

In this work, we synthesize and propose an aluminosilicate geopolymer as a new material for chromatography and evaluate its chromatographic properties in HILIC, normal phase, and ion chromatography. Given the hydrophilic nature of geopolymers, these materials are very promising for HILIC applications as HILIC is one of the fastest growing techniques for the separation of highly to moderately polar compounds that cannot be easily separated in the reversed phase chromatography mode [15, 19-24]. Usually, in HILIC mode, polar stationary phase, and organic-rich aqueous mobile phase is an essential requirement [25]. Polar surfaces are also beneficial in multi-modal chromatography. The geopolymer stationary phase is attractive as a stationary phase due to its excellent hydrolytic stability and hydrophilic/polar character. Effective applications of alkaline pH stable geopolymers in HPLC have not been reported to the best of our knowledge. In this work, we report the first efficient and simple synthetic route to obtain porous spherical geopolymer particles with a high surface area and reproducible surface chemistry. Its hydrolytic stability and selectivity are evaluated and compared to silica gel.

2.3 Experimental

2.3.1 Materials

Metakaolin was purchased from Advanced Cement Technologies, Blaine, WA, USA and used without further treatment. Submicron-sized (0.007 μm) fumed silica (fused and branched) was obtained from Sigma-Aldrich, St. Louis, MO, USA. Canola oil was obtained from J.M. Smucker Company, Orrville, Ohio, USA. Porous polystyrene/divinylbenzene polymer resins (PolyRP 10/300) were purchased from Sepax Technologies (Newark, DE). All reagents and solvents for

synthesis were purchased from Sigma-Aldrich, St. Louise, MO, USA. Ultra-purified water (Millipore, Billerica, MA, USA) was utilized throughout the synthesis and chromatography experiments. All analytes and solvents used in chromatography experiments were obtained from Sig-ma-Aldrich, St. Louis, MO, USA.

2.3.2 Synthesis of Metakaolin Geopolymer Stationary Phases

2.3.2.1 Synthesis of Porous Geopolymer Particles

The activator solution was prepared in high-density polyethylene (HDEP) beaker by dissolving KOH and fumed silica in water. The required amount of metakaolin was then added to the activator solution to obtain initial geopolymer composition where Si: Al: K molar ratio is 2:1:2. Three approaches were tested for the synthesis of geopolymer material. The details of monolithic structures and alternative approaches for particle synthesis such as particle templating is also outlined in the Supporting Information.

Water in oil emulsion (reverse emulsion) templating technique.

Water in oil emulsion was prepared by mixing appropriate volumes of canola oil and aqueous geopolymer mixture to maintain oil to aqueous volume ratio 25:1 in an HDEP beaker. Overhead stirrer with a three-blade propeller (Talboys 101, Troemner, Thorofare, NJ) was utilized in emulsion preparation. The shear rate of 4000 rpm was provided at ambient temperature for 8-72 hours to complete the geopolymerization process. The particles were then extracted into the water via hexane and water solvent extraction. Particles were washed with MeOH, hexane, EtOH, and required amount of water (until the filtrate was neutral pH). The particles were cured in an incubator (I2400 incubator shaker, New Brunswick Scientific, Edison, NJ) at 60 °C for 48 hours.

Particles were sintered in a muffle furnace (Sentry 2.0, Oriton Ceramic Foundation, Westerville, OH) at different temperatures (400 - 800 °C) in an air atmosphere.

2.3.2.2 Characterization of Geopolymer Particles and Monoliths

Particles and monolith morphology were characterized using scanning electron microscopy (Hitachi S-3000N Variable Pressure SEM, Hitachi High-Technologies Science America, Inc., Northridge, CA, USA). Shimadzu SALD-7101 laser diffraction particle size analyzer (Shimadzu Scientific Instruments, Columbia, MD, USA) was used to determine average particle size and particle size distribution. BET specific surface area and pore size were measured using Tristar II 3020 (Micromeritics, Norcross, GA, USA). Elemental composition of the geopolymer particles was analyzed using X-ray energy dispersion spectroscopy (Shimadzu EDX-7000, Shimadzu Scientific Instruments, Columbia, MD, USA.) The amorphous nature of the geopolymer material was examined using powder X-ray diffraction method (Shimadzu MAXima X XRD-7000 X-ray diffractometer, Shimadzu Scientific Instruments, Columbia, MD, USA).

2.4 Results and Discussion

2.4.1. Synthetic Aspects of Geopolymer Particles

The geopolymerization reaction is a polycondensation process. Reverse emulsion polymerization is the principal technique used in this work to synthesize geopolymer particles as shown schematically in Figure 2.S1(a-g). Aqueous alkaline (with KOH) aluminosilicate solution droplets are dispersed in a continuous oil phase to obtain a reverse emulsion. The partial hydrolysis of oil produces potassium salts of fatty acids, resulting in a surfactant system. The surfactant stabilizes

the water-in-oil emulsion (see Experimental and Figure 2.S1g) The synthesis protocol resulted in reproducible particle morphologies and surface chemistries. More than 20 batches were prepared as replicates, and the chromatographic parameters were reproducible (Figure 2.S2)

As noted in the experimental, shear rate and the experiment setup were intentionally chosen to generate turbulence in the reaction mixture and control particle size. After the desired reaction time, particles are extracted into water, and the fatty acid carboxylates and glycerol were readily removed from the system as they are water soluble. The amount of base in the geopolymer reaction mixture is crucial since the rate of saponification in the system is controlled by the amount of free base. Excess or inadequate amounts of the base resulted in irregularly shaped particles and broad particle size distributions (results not shown). Curing of particles was carried out at 60 °C to obtain optimum physical and mechanical properties [26, 27]. Curing at elevated temperatures other than ambient temperature accelerates the geopolymerization reaction while improving the compressive strength and surface area by increasing the mesoporosity [26]. On the basis of our own observations and the literature sintering at high temperatures (400 °C – 800 °C) sometimes results in microcracks (size range of a few microns [28]) , a small degree of compressive strength loss [29, 30], and reduction of particle size. The formation of micro cracks was not observed when slow temperature ramps (e.g., 2 °C/min) are utilized (Data not shown). Further heating can result in crystalline material such as leucite and kalsilite [31]. Reduction of particle size due to thermal shrinkage is advantageous in chromatography as theoretical plates are inversely proportional to the particle diameter at the van Deemter minimum. Additionally, potassium geopolymer was chosen over sodium geopolymer because potassium geopolymer shows less mechanical strength degradation after exposing to high temperatures [28].

2.4.2. Characterization of Synthetic Geopolymer Particles and Monolithic Materials

The synthesis, curing and sintering temperature should ensure that the material remains X-ray amorphous (compared to zeolites). Secondly, particle shape and size distribution are critical parameters for any chromatographic support. Scanning electron micrographs (Figure 2.1a) showed that particles are spherical. Irregular particles do not pack as well in slurry packing procedures. Hence spherical particles are preferred [32]. The surface roughness of the particles was also observed in scanning electron micrographs as shown in Figure 2.S3

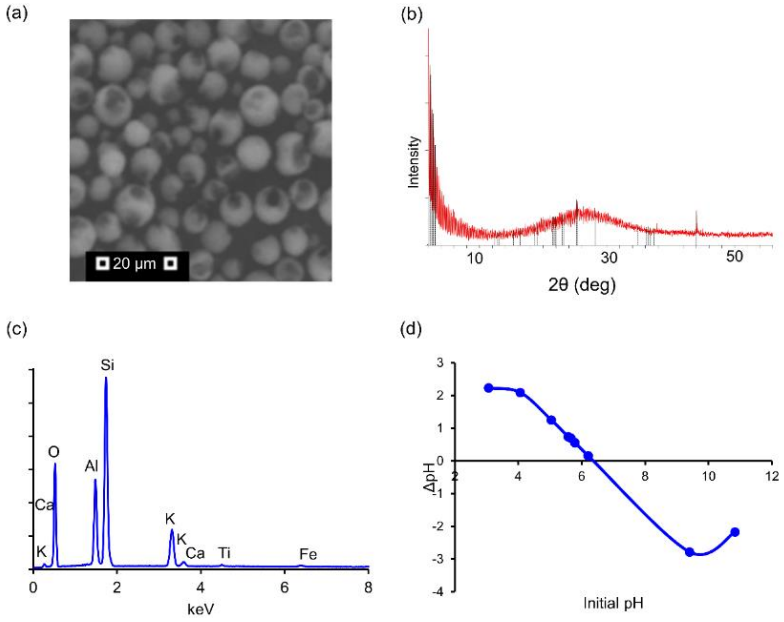

Figure 2.1 Characterization of geopolymer particles (a) Scanning electron microscopy (b) Powder X-ray diffraction patterns (c) Energy dispersive spectroscopy (Peak identity (element) is mentioned next to the peak) (d) Surface charge of the geopolymer stationary phase (pH_{pzc} by pH drift method in water)

Laser diffraction particle size distribution (PSD) data (Figure 2.S5) showed average particle size of 6.1 µm and D90/D10 of 2.9 after a de-fining procedure in water. The relationship between particle size distribution and column efficiency is still subject to debate [33]. Nevertheless, it appears that narrower the particle size distribution, better the efficiency [33]. The RSD of geopolymer PSD was calculated to be 7.6% resulting acceptable packing material. Comparatively, RSD as high as ≈ 20% has been reported for state of the art fully porous regular silica particles [34].

Geopolymerization was confirmed by powder X-ray diffraction analysis (Figure 2.1b). The broad 2θ peak around 28º is a characteristic feature of metakaolin based geopolymers indicating amorphous nature [35-37]. Note the absence of any other crystalline peaks in the XRD. It is very common that the crystalline form of the metal oxides (e.g., ZrO_2, TiO_2) are employed when they are utilized as chromatographic stationary phases [18, 38]. In contrast, one of the unique features of geopolymer stationary phase is that it can be recognized as a non-silica, completely amorphous HPLC stationary phase. Many commercial silica phases are often partially crystalline [39]. A detailed X-ray diffraction study showed that the degree of crystallinity positively correlated with pore-size in many cases such as titania and zirconia [39]. However, this statement should not be over-generalized since hydrothermal treatment history and calcination temperature are not disclosed for commercial phases. The dispersive energy spectrum (Figure 2.1c) indicates that potassium has been successfully incorporated into the geopolymer matrix (Kα 3.3 eV). Trace metal impurities were observed in final geopolymers which also were found in the starting material (For quantitative results, see Table 2.S1). Figure 2.1.d shows the pH of the point of zero charge. It will be discussed in detail in later sections.

Compared to the surface area of commercially available or laboratory synthesized metal oxide HPLC stationary phases, the specific surface area of geopolymers is very promising. For titania and alumina phases, ≈ 50 - 150 m^2/g specific area have been reported [40, 41]. For zirconia even less, specific surface area (≈ 30 m^2/g) has been reported by manufacturers. Despite the excellent chemical stability, these metal oxide stationary phases were unable to produce satisfactory chromatographic retention due to the limited specific surface area. Geopolymer particles produced 385 m^2/g BET specific surface area, the highest among the existing metal oxide containing HPLC stationary phases. BJH (Barrett-Joyner-Halenda) average pore size was measured to be 35 Å. On the other hand, the geopolymer specific surface area is comparable with a specific surface area of commercially available fully porous silica (200 – 450 m^2/g). A new support/stationary phase should be able to withstand high pressures encountered in modern liquid chromatography instruments (400 bar above). Systematic studies on column packing [32] showed geopolymer particles as a mechanically stable material. Multiple columns lengths (5, 10, 15 cm) were packed at 10,000-11,000 psi, and no peak shape distortion due to column settling or extensive pressure build-up was observed throughout the entire process and subsequent usage. Using toluene as the probe molecule and pure ACN as the mobile phase, 53000 plates per meter column efficiency and reduced plate height of 3.1 were observed. Comparatively, optimally packed 10 µm fully porous silica resulted in similar efficiencies. For some acidic compounds, i.e., ketoprofen 20% increased efficiency was observed with geopolymer stationary phase compared to 10 µm fully porous silica stationary phases. These studies show that geopolymers can sustain the pressures encountered in HPLC. To make prototype monolithic structures of geopolymers, the so-called sticky period phenomenon was employed. During the initial phase of geopolymerization when emulsions lack stabilizers and are exposed to extreme shear stress, the cohesion forces cause droplets to coagulate

and form polymer aggregates. This phenomenon is informally known as the “sticky state” [42]. The growth of the water-in-oil emulsion prepared as described in the Experimental section was monitored carefully (scanning electron microscopy) to trace the experimental “sticky state” [42]. Centrifugation of the emulsion brought the sticky particles close enough to promote self-assembly of the monolithic structure of the geopolymer. The “necks” formed in between the neighboring sticky particles resulted in the rigid monolithic skeleton as shown in Figure 2.S4. A prototype geopolymer monolith was made by connecting two 2 cm x 0.46 cm i.d. columns in HILIC mode.

2.4.3. High pH Stability of Geopolymer Stationary Phase in HILIC Mode

Hydrolytic stability is the Achilles heel of a majority of HILIC phases, especially at high pH. Extensive studies have highlighted this issue with different HILIC chemistries [14-16, 43]. Retention time drift is one of the significant problems in HILIC because of continuous leaching of silica and /or ligands. The leaching of bonded phases on HILIC is postulated as follows: The polar surface of HILIC stationary phase promotes the adsorption of the water layer. Silica has a propensity to dissolve in pure water (0.01 to 0.012%), and the siloxane linkage (Si-O-Si) is prone to hydrolysis and form silanols [15]. Basic conditions can be harmful to silica owing to the formation of water-soluble silicates. The presence of silicates has been observed via a silicomolybdate test in silica columns with various pH buffers [44]. With state of the art silica SPP, we reported a % retention time drift in 30 hours with a “mild” mobile phase consisting of 75% ACN and 25% buffer at (aqueous) pH of 6.8 [15]. One of the unique features of the geopolymer stationary phase is excellent pH and hydrolytic stability as shown in Figure 2.2.

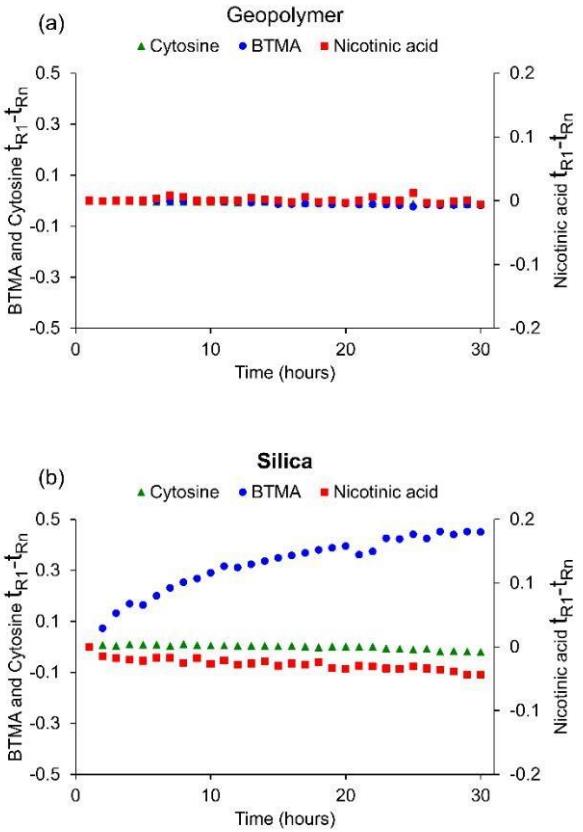

Figure 2.2 Ultra-high stability of the geopolymer stationary phase at extreme high pH compared to silica, (a) Geopolymer (b) Silica, mobile phase – ACN/25 mM NH4OAc pH 10 (80/20), 0.425 mL/min, column – 3 mm ID x 100 mm. The pH was adjusted with aqueous ammonia. Detection at 220 nm

The hydrolytic and pH stability test was conducted at pH 10 for 30 hours with three probes. The capability of a stationary phase to operate in a broad range of pH is highly desirable as it ultimately allows one to optimize separations freely using mobile phase pH. Probes were chosen in such way that it allowed examining the retention behavior of neutral, negative, and positive charge analytes on the geopolymer stationary phase [15]. Nicotinic acid is negatively charged at this operating pH and the cationic species, BTMA is positively charged at all pHs. Cytosine is the hydrophilic neutral probe. Figure 2.2 plots the value of retention - original retention time vs. time (hours). Over the

designated time span, the geopolymer stationary phase did not show in any significant drift in retention times for the test analytes (Figure 2.2a). According to both Davidovits and Barbosa geopolymer network model, the oxygen atoms are mainly bonded to other non-hydrogen atoms, thus limiting the number of free surface silanol groups [4, 44-46]. Furthermore, geopolymers are known to have exceedingly low water solubility [47, 48].

The hydrolytic stability of silica and geopolymer stationary phases can be further quantitatively represented and compared when retention time drift (retention time of nth injection – retention time of the first injection) is plotted against time or column volumes passed through the column (Figure 2.2 and Figure 2.S7). The slopes of the retention time curves can indicate the stability. Ideally, a stationary phase should show a slope of zero (perfectly horizontal). For geopolymer stationary phase, the slope values are nearly zero (Table 2.S2) indicating negligible drift. The opposite behavior of nicotinic acid and BTMA is observed universally on modified and unmodified silica [15]. This trend is attributable on silica to the formation of Si-OH groups, which increase the cation exchange behavior of silica with time. The neutral (uncharged) analyte, cytosine showed negligible retention time drift both on the silica stationary phase and the geopolymer stationary phase (See Table 2.S2).

However, the retention time drift is more significant for charged analytes as expected if the retention is being affected by the charged state of the surface. Note that retention time drift of nicotinic acid is not significant compared to BTMA as nicotinic acid has a smaller retention factor. The retention time drift per hour for BTMA on fully porous silica stationary phase is significantly high compared to the geopolymer stationary phase (See Figure 2.2). Nicotinic acid also exhibits nearly 14 times greater retention time drift per hour, under these conditions, compared to geopolymer. At pH 10, the silica stationary phase shows sequential deterioration within the

experimental period as expected. The effect is most noticeable with positively charged species, BTMA (Figure 2.2b).

2.4.4 Selectivity Comparison and Surface Charge Properties of Geopolymers

For any new stationary phase, it is essential to explore the nature of the stationary phase compared to other existing stationary phases to understand selectivity, stability, and method optimization. To date, a large number of HILIC stationary phases are available with a wide range of hydrophilicity and ion exchange capabilities. Based on the data of Irgum, Lucy, and our own studies, a simple selectivity chart has been constructed to examine hydrophilicity and ion ex-change capabilities of available stationary phases (Figure 2.3) [14, 15, 49, 50]. The compiled data allowed us to compare geopolymer particles with 36 commercial (and published) stationary phases. The diagram shows clustering of different classes of stationary phases. The traditional reverse phase media appears on the left, and more polar phases on the right. This data is visualized graphically in the "selectivity chart." The x-axis plots the selectivity of cytosine /uracil indicating hydrophilicity of the stationary phase. The y-axis consists of selectivity of BTMA/cytosine, which is taken as a measure of the ion exchange characteristics of the stationary phase. The choice of BTMA/cytosine pair has been made on the basis of previous data for more than 30 columns used for selectivity comparison [15, 49, 50]. Geopolymer phases showed less propensity as cation exchange media, than silica phases, but more than that of zwitterionic phases (Figure 2.3). The geopolymer stationary phase occupies in a unique position of this selectivity chart showing that geopolymer stationary phase is the most hydrophilic HILIC stationary phase among all those in the selectivity plot.

To further understand the retention mechanism of (an) analyte/s of interest on the geopolymer stationary phase, it is essential to understand the fundamental interactions of the stationary phase with the analyte.

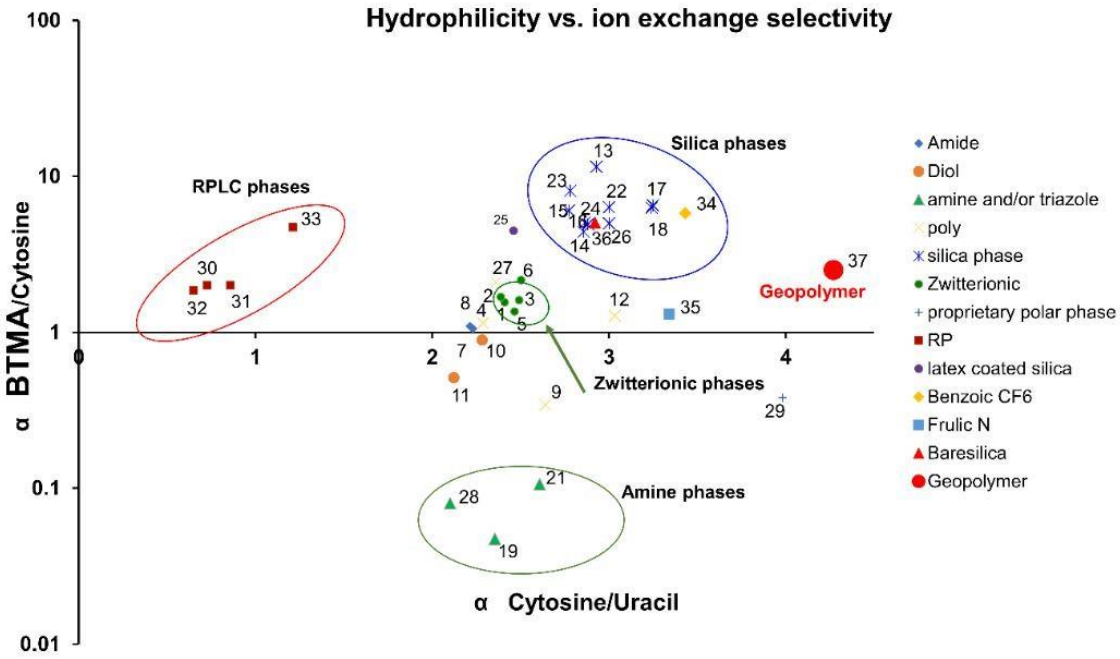

Figure 2.3. Hydrophilicity and ion exchange selectivity of geopolymer stationary phase com-pared to other stationary phase chemistries. Mobile phase Acetonitrile/25 mM NH_4OAc (80/20), Flow rate 0.50 mL/min, detection at 254 nm. The key to actual points is provided in Table 2.3.

The selectivity chart (Figure 2.3) employed an ACN buffer mixture. However, the concept of surface charge is more meaningful in purely aqueous media. This type of understanding is helpful for rationalizing the behavior of ionizable analytes (acids and bases) and simple ions. The pH of the surface where the net charge of the solid surface of interest is zero is known as pH of the point of zero charge (pH_{PZC}) [51] . The pH_{PZC} is a good indicator of the charge of the surface of the stationary phase. The salt addition method was used to determine pH_{PZC} of geopolymer stationary

phase following the experimental procedures reported in the literature [51]. The pH_{PZC} of geopolymer stationary phase was found to be 6.4 (Figure 2.1d) implying that when pH < 6.4, the stationary phase is positively charged and when pH > 6.4, the stationary phase is negatively charged. The pH_{PZC} of silica is reported as ~ 3 in the literature [52, 53].

2.4.5 Chromatographic Assessment of the Geopolymer Phases

2.4.5.1 Geopolymer as a HILIC Stationary Phase

With the promising selectivity and surface charge properties observed in the selectivity chart and surface charge studies, geopolymers have appeared to have promise when utilized as a HILC phase. To be useful as a HILIC phase, the geopolymer surface must be "wettable" by water to form a surface water layer [14]. HILIC has always been recognized as mass spectrometry friendly chromatography mode. This is not necessarily the case with alternative high pH stable metal oxides (TiO2, ZrO2,) based stationary phases which are operated in HILIC. These phases invariably require fluoride or phosphate buffer additives in the mobile phase due to the presence of active Lewis acid sites. This is especially true for carboxylic acids which can adsorb strongly on titania surfaces [54]. Carboxylic acids are known to show extremely long retention times, and poor plate counts on zirconia and titania with acetate buffers [54]. Many drug molecules and their synthetic precursors have a carboxylic acid group. Ketoprofen, acetylmandelic acid and indoprofen are small acidic molecules of pharmaceutical interest are used as synthetic precursors. All three were baseline separated (Figure 2.10a) on a geopolymer stationary phase with no significant tailing or fronting at pH 8.0. The USP tailing factor for ketoprofen, acetylmandelic acid and indoprofen were found to be 1.16, 1.09, 1.15 respectively. On the other hand, indoprofen eluted before acetylmandelic acid on silica stationary phase but not the geopolymer (Figure 2.4a). Also, note

that ketoprofen and indoprofen have only partial separations on silica under optimized mobile phase conditions. Thymidine, adenine, and uridine belong to the class of nucleosides. As shown in Figure 2.4b, adenine elutes before uridine on the geopolymer stationary phase with the resolution of 2.35 where on silica stationary phase retention order is switched and resolution is lowered (resolution – 1.35) under similar mobile phase composition. On both stationary phases, adenine, thymine and uridine were separated. Having inverse retention order is beneficial especially in quantitation when the first peak is tailing. As a general trend, the silica gel stationary phase showed lower retention times compared to the geopolymer stationary phase under identical mobile phase conditions. One of the reasons for this observation could be the higher hydrophilicity of the geopolymer stationary phase. Therefore, geopolymer stationary phase can be recognized as a promising new material for the separation of very hydrophilic compounds that cannot be easily separated on commonly existing HILIC phases. The selectivity of geopolymers clearly indicates that retention/ partitioning is not solely due to an adsorbed water layer (otherwise all HILIC separations would have similar selectivity on silica and geopolymer phases) [19]. The nature of the stationary phase chemistry also is vital since HILIC is essentially a multi-mode retention mechanism which also involves hydrogen bonding, dipole-dipole interactions, and ionic interactions [15, 19, 21].

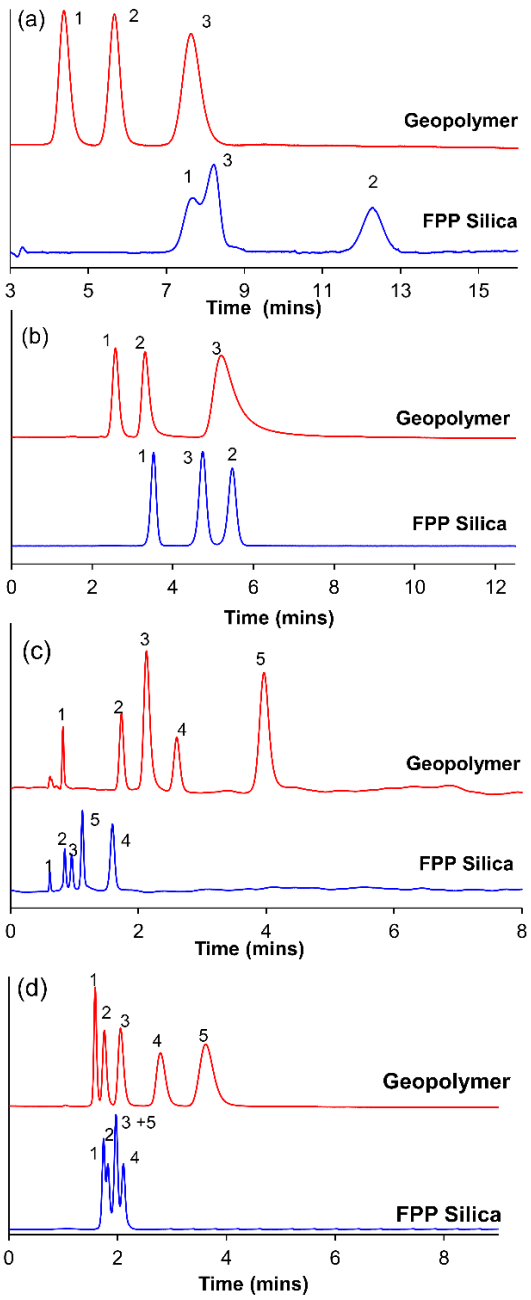

Figure 2.4 HILIC selectivity comparison of geopolymer stationary phase and silica (a) separation of aromatic acids and derivatives, analytes – 1. ketoprofen 2. acetylmandelic acid 3. indoprofen, mobile phase – ACN/25 mM NH_4COOH pH 8.0 (92/8), 0.425 mL/min, on geopolymer, ACN/100 mM NH_4OAc (92/8) on silica columns – 3 mm ID x 150 mm. detection at 220 nm (b) Separation of nucleic acid bases and nucleosides, analytes – 1. thymidine 2. adenine 3. uridine, mobile phase

– ACN/100 mM NH_4OAc (87/13), 0.425 mL/min, columns – 3 mm ID x 150 mm. detection at 254 nm (c) Inorganic anion separation, analytes – 1. iodide 2. nitrate 3. azide 4. bromide 5. nitrite, mobile phase - ACN/50 mM NH_4COOH pH 4.0 (91/9), 1.00 mL/min, columns – 3 mm ID x 150 mm. detection at 200 nm (d) analytes – 1. methyl-3-Boc-2,2-dimethyl-4-oxazolidine-carboxylate 2. 4-isopropyl-5,5-diphenyl-2-oxazolidinone 3. 4-(diphenylmethyl)-2-oxazolidinone 4. 4-isopropyl-2-oxazolidinone 5. (1H-Indol-3-ylmethyl)-2-oxazolidinone, mobile phase – ACN/100 mM NH_4OAc (90/10), 0.425 mL/min, column – 3 mm ID x 150 mm, detection at 220 nm

Analysis of inorganic ions is generally accomplished using ion-exchange and ion chromatography. HILIC has offered an alternative by using acetonitrile and buffers to separate simple in-organic ions. Based on the surface charge properties, it is expected that geopolymers, like zeolites, should display interactions with ionic analytes. A mixture of five UV detectable anions, iodide, nitrate, azide, bromide, and nitrite were baseline separated using a geopolymer stationary phase and isocratic conditions within 4 minutes (Figure 2.4c). Comparatively, on silica stationary phase the same mixture was separated within 2 minutes under the same conditions, but with different selectivity and low resolution. Recently, it was demonstrated that anions (e.g., iodide and bromide) could be separated using a multi-step gradient on 2.7 µm bare silica superficially porous particles. However, these authors did not test azide ion and nitrite-nitrate pair. Additionally, the anion selectivity of geopolymers is different from the majority of commercial ion chromatography phases (latex coated sulfonated anion exchangers), where the iodide invariably has large retention factors and broad peak shapes. This observation (Figure 2.4c) implies different retention modes on geopolymers vs. latex coated polymers [17]. Most likely the separation of the halides is based on different hydration levels. Indeed, this is the case with iodide ion which is least hydrated among the halogens [55]. On the geopolymer stationary phase, bromide showed higher retention than

azide anion. However, on silica, the opposite selectivity was observed. A unique selectivity for inorganic anions is observed on geopolymers compared to commercially available divinylbenzene particle based strong cation or anion exchange ion chromatography phases and other metal oxide based stationary phases such as alumina [56-58].

To further understand the retention behavior of ions Figure 2.S8 shows the chromatographic behavior of two UV absorbing inorganic anions, namely iodide and nitrate on a geopolymer stationary phase at different pHs in the HILIC mode. The retention of iodide and nitrate were evaluated at three preadjusted pH values (4.0, 6.4, 10.0) of the aqueous ammonium acetate portion of the mobile phase. The highest retention time and selectivity were observed at pH of 4 which is below the "pure aqueous" pH_{PZC}, as expected (given the surface should be positively charged. So as the pH of the aqueous portion of the mobile phase increases to 10, retention times decreased, indicating that high pH can be used to decrease analysis times and optimize many separations, provided the stationary phase is stable.

Oxazolidinones are an essential class of antibacterial compounds against gram-positive organisms [59]. They are neutral and structurally very closely related. Since oxazolidinones are very polar, HILIC is an excellent tool to separate them with reasonable retention and selectivity. Five oxazolidinones, methyl-3-Boc-2,2-dimethyl-4-oxazolidinecarboxylate,4-isopropyl-5,5-diphenyl-2-oxazolidinone, 4-(diphenylmethyl)-2-oxazolidinone, 4-isopropyl-2-oxazolidinone, and (1H-Indol-3-ylmethyl)-2-oxazolidinone have been baseline separated on geopolymer stationary phase where none of them was completely separated on 10 µm FPP silica phase (Figure 2.4d). The optimized separation of oxazolidinones on 10 µm FPP is shown in the Figure 2.4d. Also (1H-Indol-3-ylmethyl)-2-oxazolidinone and 4-isopropyl-2-oxazolidinone show elution order inversion on silica stationary phase. 4-(diphenylmethyl)-2-oxazolidinone and (1H-Indol-3-ylmethyl)-2-

oxazolidinone are baseline resolved on geopolymer stationary phase with α = 3.8. In contrast, they coelute on the silica stationary phase.

2.4.5.2 Geopolymers as a Normal Phase Stationary Phase

Normal phase and HILIC share a common property in terms of requiring a polar adsorbent. The advantage of normal phase over RPLC is its power to separate structural isomers since the adsorption mechanism in normal phase is sensitive to structural changes [60]. As a result, normal phase chromatography holds its potential in petroleum analysis and shape selective separations. As shown in Figure 2.5 excellent selectivity for structural isomers has been obtained. Nitrobenzene, 2-nitroaniline, 3-nitroaniline, and 4-nitroaniline can be baseline separated on geopolymer stationary phase within 2 minutes.

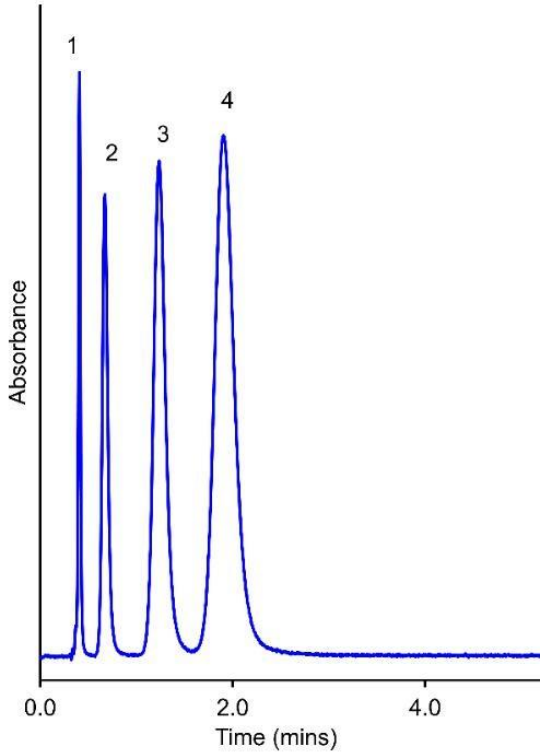

Figure 2.5 Structural isomers separation on geopolymer stationary phase in normal phase chromatography mode, analytes – 1. nitrobenzene 2. o-nitroaniline 3. m-nitroaniline 4. p-

nitroaniline, mobile phase - Hexane/Ethanol (84/16), 1.425 mL/ min, column – 3 mm ID x 100 mm, detection at 254 nm

2.5 Conclusions

Geopolymers were shown to be promising new materials for liquid chromatography. The aluminosilicate geopolymer is a high-pH stable stationary phase with negligible retention time drift even at pH 10 in the HILIC mode. Reverse emulsion polymerization and resin templating techniques were successfully utilized to synthesize metakaolin geopolymer particles with reproducible surface chemistry. Geopolymer stationary phases are effective HILIC phases for the separation of remarkably hydrophilic analytes. Geopolymer stationary phase can be designated as the most hydrophilic HILIC stationary phase existing to date. Ultrahigh hydrolytic and pH stability of the stationary phase is another attractive feature of the geopolymer stationary phase. This exceptional pH stability and excellent hydrophilicity ultimately facilitate method optimization flexibility allowing one to obtain best separations possible. Unique selectivities for a broad range of analytes was observed on geopolymer stationary phases compared to the most common chromatographic stationary phase, silica. A unique selectivity for inorganic ions was produced by geopolymer stationary phase compared to most of the existing ion chromatography stationary phases. Also, geopolymer stationary phase can be successfully utilized in the separation of structural isomers in normal phase chromatography mode.

2.6 References

[1] J. Davidovits, Geopolymers: inorganic polymeric new materials, Journal of Thermal Analysis and calorimetry, 37 (1991) 1633-1656.

[2] P. Duxson, A. Fernández-Jiménez, J.L. Provis, G.C. Lukey, A. Palomo, J.S. van Deventer, Geopolymer technology: the current state of the art, Journal of materials science, 42 (2007) 2917-2933.

[3] M.L. Granizo, S. Alonso, M.T. Blanco-Varela, A. Palomo, Alkaline activation of metakaolin: effect of calcium hydroxide in the products of reaction, Journal of the American Ceramic Society, 85 (2002) 225-231.

[4] V.F. Barbosa, K.J. MacKenzie, C. Thaumaturgo, Synthesis and characterisation of materials based on inorganic polymers of alumina and silica: sodium polysialate polymers, International Journal of Inorganic Materials, 2 (2000) 309-317.

[5] S. Alonso, A. Palomo, Calorimetric study of alkaline activation of calcium hydroxide–metakaolin solid mixtures, Cement and Concrete Research, 31 (2001) 25-30.

[6] G. Biscan, H. Hojaji, D.L. Melmeth, T. Pham, H. Zhang, Geopolymeric particles, fibers, shaped articles and methods of manufacture, Google Patents, 2013.

[7] D. Medpelli, J.M. Seo, D.K. Seo, Geopolymer with hierarchically meso-/macroporous structures from reactive emulsion templating, Journal of the American Ceramic Society, 97 (2014) 70-73.

[8] J. Davidovits, Geopolymers and geopolymeric materials, Journal of thermal analysis, 35 (1989) 429-441.

[9] P. Duxson, J.L. Provis, G.C. Lukey, S.W. Mallicoat, W.M. Kriven, J.S. Van Deventer, Understanding the relationship between geopolymer composition, microstructure and mechanical properties, Colloids and Surfaces A: Physicochemical and Engineering Aspects, 269 (2005) 47-58.

[10] W.M. Kriven, J.L. Bell, M. Gordon, Microstructure and microchemistry of fully-reacted geopolymers and geopolymer matrix composites, Ceramic Transactions, 153 (2003).

[11] W.M. Kriven, INORGANIC POLYSIALATES OR" GEOPOLYMERS", American Ceramics Society Bulletin, 89 (2010) 31-34.

[12] M. Alzeer, R.A. Keyzers, K.J. MacKenzie, Inorganic polymers as novel chromatographic stationary phase media, Ceramics International, 40 (2014) 3553-3560.

[13] K. Qian, Y. Peng, F. Zhang, B. Yang, X. Liang, Preparation of a low bleeding polar stationary phase for hydrophilic interaction liquid chromatography, Talanta, (2018).

[14] M.F. Wahab, M.E. Ibrahim, C.A. Lucy, Carboxylate modified porous graphitic carbon: a new class of hydrophilic interaction liquid chromatography phases, Analytical chemistry, 85 (2013) 5684-5691.

[15] Y. Wang, M.F. Wahab, Z.S. Breitbach, D.W. Armstrong, Carboxylated cyclofructan 6 as a hydrolytically stable high efficiency stationary phase for hydrophilic interaction liquid chromatography and mixed mode separations, Analytical Methods, 8 (2016) 6038-6045.

[16] M.E. Ibrahim, M.F. Wahab, C.A. Lucy, Hybrid carbon nanoparticles modified core–shell silica: A high efficiency carbon-based phase for hydrophilic interaction liquid chromatography, Analytica Chimica Acta, 820 (2014) 187-194.

[17] M.F. Wahab, C.A. Pohl, C.A. Lucy, Ion chromatography on carbon clad zirconia modified by diazonium chemistry and functionalized latex particles, Analyst, 136 (2011) 3113-3120.

[18] J. Nawrocki, C. Dunlap, A. McCormick, P. Carr, Part I. Chromatography using ultra-stable metal oxide-based stationary phases for HPLC, Journal of chromatography A, 1028 (2004) 1-30.

[19] C. Wang, C. Jiang, D.W. Armstrong, Considerations on HILIC and polar organic solvent-based separations: Use of cyclodextrin and macrocyclic glycopetide stationary phases, Journal of Separation Science, 31 (2008) 1980-1990.

[20] B. Buszewski, S. Noga, Hydrophilic interaction liquid chromatography (HILIC)—a powerful separation technique, Analytical and bioanalytical chemistry, 402 (2012) 231-247.

[21] Y. Guo, Recent progress in the fundamental understanding of hydrophilic interaction chromatography (HILIC), Analyst, 140 (2015) 6452-6466.

[22] R.M. Wimalasinghe, C.A. Weatherly, Z.S. Breitbach, D.W. Armstrong, Hydroxypropyl beta cyclodextrin bonded superficially porous particle-based HILIC stationary phases, Journal of Liquid Chromatography & Related Technologies, 39 (2016) 459-464.

[23] R.M. Wimalasinghe, Z.S. Breitbach, J.T. Lee, D.W. Armstrong, Separation of peptides on superficially porous particle based macrocyclic glycopeptide liquid chromatography stationary phases: consideration of fast separations, Analytical and bioanalytical chemistry, 409 (2017) 2437-2447.

[24] M.F. Wahab, R.M. Wimalasinghe, Y. Wang, C.L. Barhate, D.C. Patel, D.W. Armstrong, Salient Sub-Second Separations, Analytical chemistry, 88 (2016) 8821-8826.

[25] A.J. Alpert, Hydrophilic-interaction chromatography for the separation of peptides, nucleic acids and other polar compounds, Journal of chromatography A, 499 (1990) 177-196.

[26] M. Muñiz-Villarreal, A. Manzano-Ramírez, S. Sampieri-Bulbarela, J.R. Gasca-Tirado, J. Reyes-Araiza, J. Rubio-Ávalos, J. Pérez-Bueno, L. Apatiga, A. Zaldivar-Cadena, V. Amigó-Borrás, The effect of temperature on the geopolymerization process of a metakaolin-based geopolymer, Mater. Lett., 65 (2011) 995-998.

[27] S. Alonso, A. Palomo, Alkaline activation of metakaolin and calcium hydroxide mixtures: influence of temperature, activator concentration and solids ratio, Materials Letters, 47 (2001) 55-62.

[28] D.L. Kong, J.G. Sanjayan, K. Sagoe-Crentsil, Factors affecting the performance of metakaolin geopolymers exposed to elevated temperatures, J. Mater. Sci., 43 (2008) 824-831.

[29] D.L. Kong, J.G. Sanjayan, K. Sagoe-Crentsil, Comparative performance of geopolymers made with metakaolin and fly ash after exposure to elevated temperatures, Cement and Concrete Research, 37 (2007) 1583-1589.

[30] P. Duxson, G.C. Lukey, J.S. van Deventer, Thermal evolution of metakaolin geopolymers: Part 1–Physical evolution, Journal of Non-Crystalline Solids, 352 (2006) 5541-5555.

[31] P. He, D. Jia, M. Wang, Y. Zhou, Thermal evolution and crystallization kinetics of potassium-based geopolymer, Ceramics International, 37 (2011) 59-63.

[32] M.F. Wahab, D.C. Patel, R.M. Wimalasinghe, D.W. Armstrong, Fundamental and Practical Insights on the Packing of Modern High-Efficiency Analytical and Capillary Columns, Analytical chemistry, 89 (2017) 8177-8191.

[33] F. Gritti, D.S. Bell, G. Guiochon, Particle size distribution and column efficiency. An ongoing debate revived with 1.9 μm Titan-C 18 particles, Journal of chromatography A, 1355 (2014) 179-192.

[34] F. Gritti, G. Guiochon, The rationale for the optimum efficiency of columns packed with new 1.9 μm fully porous Titan-C 18 particles—A detailed investigation of the intra-particle diffusivity, Journal of chromatography A, 1355 (2014) 164-178.

[35] Z. Zhang, H. Wang, J.L. Provis, F. Bullen, A. Reid, Y. Zhu, Quantitative kinetic and structural analysis of geopolymers. Part 1. The activation of metakaolin with sodium hydroxide, Thermochimica acta, 539 (2012) 23-33.

[36] H. Wang, H. Li, F. Yan, Synthesis and mechanical properties of metakaolinite-based geopolymer, Colloids Surf Physicochem Eng Aspects, 268 (2005) 1-6.

[37] T. Skorina, Ion exchange in amorphous alkali-activated aluminosilicates: Potassium based geopolymers, Applied Clay Science, 87 (2014) 205-211.

[38] C. Laurent, H. Billiet, L. De Galan, On the use of alumina in HPLC with aqueous mobile phases at extreme pH, Chromatographia, 17 (1983) 253-258.

[39] A. Kurganov, U. Trüdinger, T. Isaeva, K. Unger, Native and modified alumina, titania and zirconia in normal and reversed-phase high-performance liquid chromatography, Chromatographia, 42 (1996) 217-222.

[40] J.J. Pesek, J.E. Sandoval, M. Su, New alumina-based stationary phases for high-performance liquid chromatography: synthesis by olefin hydrosilation on a silicon hydride-modified alumina intermediate, Journal of chromatography A, 630 (1993) 95-103.

[41] C. Jaroniec, M. Jaroniec, M. Kruk, Comparative studies of structural and surface properties of porous inorganic oxides used in liquid chromatography, Journal of chromatography A, 797 (1998) 93-102.

[42] H. Warson, C.A. Finch, Applications of Synthetic Resin Latices, Latices in Diverse Applications, John Wiley & Sons2001.

[43] J.E. O'Gara, B.A. Alden, C.A. Gendreau, P.C. Iraneta, T.H. Walter, Dependence of cyano bonded phase hydrolytic stability on ligand structure and solution pH, Journal of chromatography A, 893 (2000) 245-251.

[44] H. Claessens, M. Van Straten, J. Kirkland, Effect of buffers on silica-based column stability in reversed-phase high-performance liquid chromatography, Journal of chromatography A, 728 (1996) 259-270.

[45] J.J. Kirkland, M. Van Straten, H. Claessens, High pH mobile phase effects on silica-based reversed-phase high-performance liquid chromatographic columns, Journal of chromatography A, 691 (1995) 3-19.

[46] H. Claessens, M. Van Straten, C. Cramers, M. Jezierska, B. Buszewski, Comparative study of test methods for reversed-phase columns for high-performance liquid chromatography, Journal of chromatography A, 826 (1998) 135-156.

[47] T. Ejaz, A.G. Jones, P. Graham, Solubility of zeolite A and its amorphous precursor under synthesis conditions, J. Chem. Eng. Data, 44 (1999) 574-576.

[48] H.A. Gasteiger, W.J. Frederick, R.C. Streisel, Solubility of aluminosilicates in alkaline solutions and a thermodynamic equilibrium model, Ind. Eng. Chem. Res., 31 (1992) 1183-1190.

[49] M.E. Ibrahim, Y. Liu, C.A. Lucy, A simple graphical representation of selectivity in hydrophilic interaction liquid chromatography, Journal of chromatography A, 1260 (2012) 126-131.

[50] N.P. Dinh, T. Jonsson, K. Irgum, Probing the interaction mode in hydrophilic interaction chromatography, Journal of chromatography A, 1218 (2011) 5880-5891.

[51] T. Mahmood, M.T. Saddique, A. Naeem, P. Westerhoff, S. Mustafa, A. Alum, Comparison of different methods for the point of zero charge determination of NiO, Industrial & Engineering Chemistry Research, 50 (2011) 10017-10023.

[52] J. Nawrocki, M. Rigney, A. McCormick, P. Carr, Chemistry of zirconia and its use in chromatography, Journal of chromatography A, 657 (1993) 229-282.

[53] F. Unob, B. Wongsiri, N. Phaeon, M. Puanngam, J. Shiowatana, Reuse of waste silica as adsorbent for metal removal by iron oxide modification, Journal of hazardous materials, 142 (2007) 455-462.

[54] T. Zhou, C.A. Lucy, Separation of carboxylates by hydrophilic interaction liquid chromatography on titania, Journal of chromatography A, 1217 (2010) 82-88.

[55] P.A. Bergstroem, J. Lindgren, O. Kristiansson, An IR study of the hydration of perchlorate, nitrate, iodide, bromide, chloride and sulfate anions in aqueous solution, The Journal of Physical Chemistry, 95 (1991) 8575-8580.

[56] C.A. Lucy, M.F. Wahab, Advances in high-speed and high-resolution ion chromatography, LC GC North America, 31 (2013) 38-42.

[57] C. Pohl, Recent developments in ion-exchange columns for ion chromatography, LC GC North America, 31 (2013) 16-22.

[58] G.L. Schmitt, D.J. Pietrzyk, Liquid chromatographic separation of inorganic anions on an alumina column, Analytical chemistry, 57 (1985) 2247-2253.

[59] D.L. Shinabarger, K.R. Marotti, R.W. Murray, A.H. Lin, E.P. Melchior, S.M. Swaney, D.S. Dunyak, W.F. Demyan, J.M. Buysse, Mechanism of action of oxazolidinones: effects of linezolid and eperezolid on translation reactions, Antimicrobial agents and chemotherapy, 41 (1997) 2132-2136.

[60] T. Zhang, D.J. Creek, M.P. Barrett, G. Blackburn, D.G. Watson, Evaluation of coupling reversed phase, aqueous normal phase, and hydrophilic interaction liquid chromatography with Orbitrap mass spectrometry for metabolomic studies of human urine, Analytical chemistry, 84 (2012) 1994-2001.

2.7 Supporting Information

2.7.1 Synthesis of geopolymer stationary phases

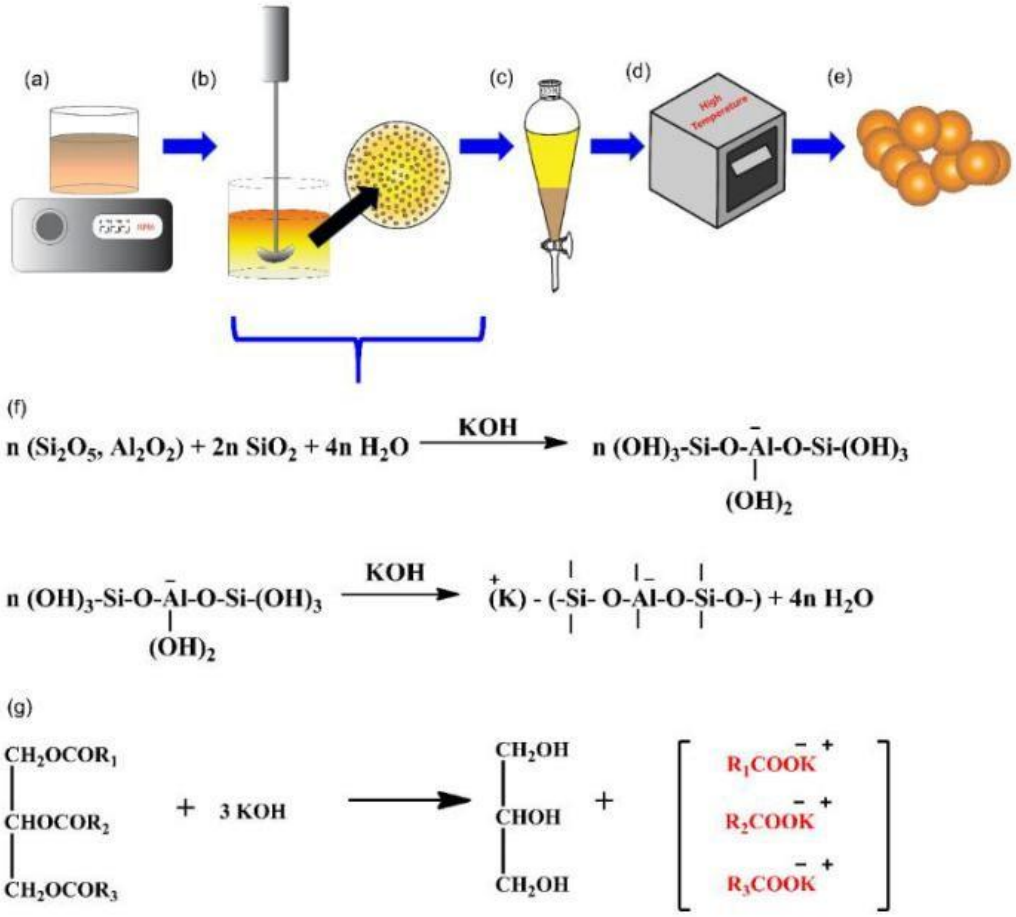

Figure 2.S1 Schematic representation of geopolymer particle synthesis protocol (a) Geopolymer reaction mixture preparation (b) High speed stirring of geopolymer reaction mixture and canola oil to obtain water in oil emulsion (c) Isolation of particles - Hexane-water solvent extraction (d) Particles sintering at elevated temperatures in a furnace (e) Sintered geopolymer particles. Reaction schemes for geopolymer particle synthesis (f) Geopolymerization reaction (g) Production of ionic surfactant by saponification reaction

2.7.2 Alternative Geopolymer Particle Synthesis Approach

Polymer resin templating technique – Polymer resins were dispersed in hexane and wetted with Span 80 by stirring (Corning PC 420-D, Corning, NY, USA) and ultra-sonication (Aquasonic 250 Hz, VWR, Radnor, PA, USA) for 30 minutes. Then wetted resins were filtered and extracted. Wetted resins were suspended in geopolymer reaction mixture and stirred (Corning PC 420-D, Corning, NY, USA) followed by sonication (Aquasonic 250 Hz, VWR, Radnor, PA, USA) for 30 minutes to fill pores with geopolymer reaction mixture. Resins were then isolated by centrifugation followed by filtration. Then curing was carried out at 60 °C in an incubator (I2400 incubator shaker, New Brunswick Scientific, Edison, NJ). Finally, the resin was burnt out at 800 °C in Sentry 2.0 furnace (Oriton Ceramic Foundation, Westerville, OH) and particles were isolated.

2.7.3 Geopolymer Monolith Synthesis

The geopolymer monolith was synthesized using an unconventional route of the "sticky period" during "suspension polymerization" [1]. The sticky period is defined as the period in which partially polymerized droplets cannot re-divide, but coalescence can still occur. This coagulation of particles has been deliberately brought about by bringing the particles in proximity using centrifugation. Eventually, the curing leads to the formation of connecting necks between particles, fabricating the monolithic structure.

A potassium silicate solution was prepared by dissolving 3.30 g of potassium hydroxide and 3.00 g of fumed silica in 7.59 mL deionized water. The mixture was stirred for 30 minutes at room temperature. Then, 6.25 g of metakaolin was added and stirred for five minutes. The resulting homogeneous slurry was then added to 700 mL of soybean oil (Crisco® Pure Vegetable Oil) with stirring at 5000 rpm (Talboys overhead mixer was used). The fractions were taken out from the

reaction mixture during the sticky period (between 3rd and 4th hour, in these synthetic conditions) and put in a polycarbonate tube. The filled tube was then centrifuged for 2 minutes to settle the solid particles at the bottom, and the oil was decanted. This process was repeated until the mold was filled. The curing of geopolymer was done at 60 °C for 24 hours during which time the particles fused forming a monolith. The monolith was removed from the mold and sintered at 500 °C in an air atmosphere for 4 hours at 2 °C/min ramp to burn off all the organics. The monolith was cladded inside 200 mm x 4.6 mm ID stainless steel column using epoxy resin. The chromatography was performed after equilibrating the column with mobile phase. The optimization of synthetic conditions for monolith continued to be a subject of future studies in our laboratory.

2.7.4 Chromatographic Setup for Stationary Phase Evaluation

Geopolymer particles were slurry packed into empty stainless-steel columns using an air-driven high-pressure pump (Haskel International Inc., Burbank, CA, USA). Dispersed slurries produced the best results as stated in the literature [2]. All chromatography experiments were run using an Agilent 1200 series HPLC instrument (Agilent Technologies, Santa Clara, CA, USA). The instrument was equipped with an UV-visible diode array detector, temperature-controlled column compartment, auto-sampler, quaternary pump, and a degasser. The Agilent ChemStation version B.01.03 under the Microsoft Windows XP operating system environment was utilized to control the instrument.

2.7.5 Batch to batch reproducibility of geopolymers

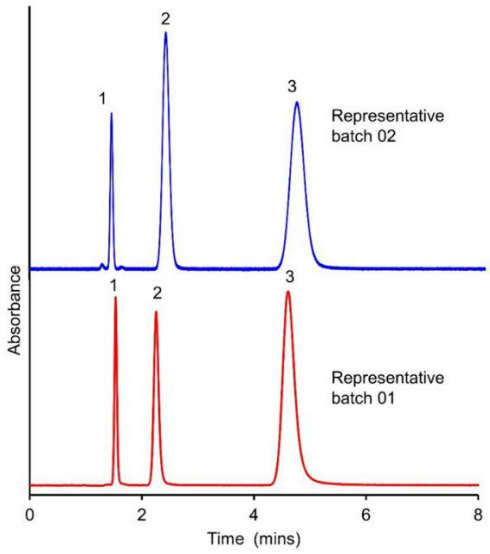

Figure 2.S2 Batch to batch chromatographic reproducibility of geopolymer stationary phase. Analytes – 1. Acetone (dead time marker) 2. Uracil 3. Cytosine, mobile phase – ACN/ 25 mM NH4OAC (80/20), 0.425 mL per min, column – 3 mm ID x 150 mm, detection at 254 nm

2.7.6 Scanning electron micrographs of metakaolin geopolymer particles and monolith

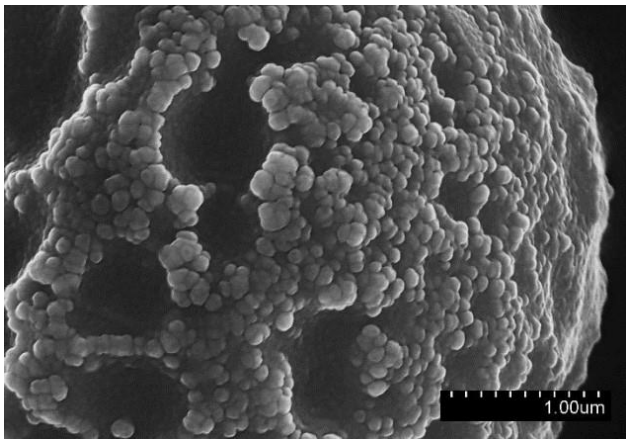

Figure 2.S3 Surface structure of a metakaolin geopolymer particle

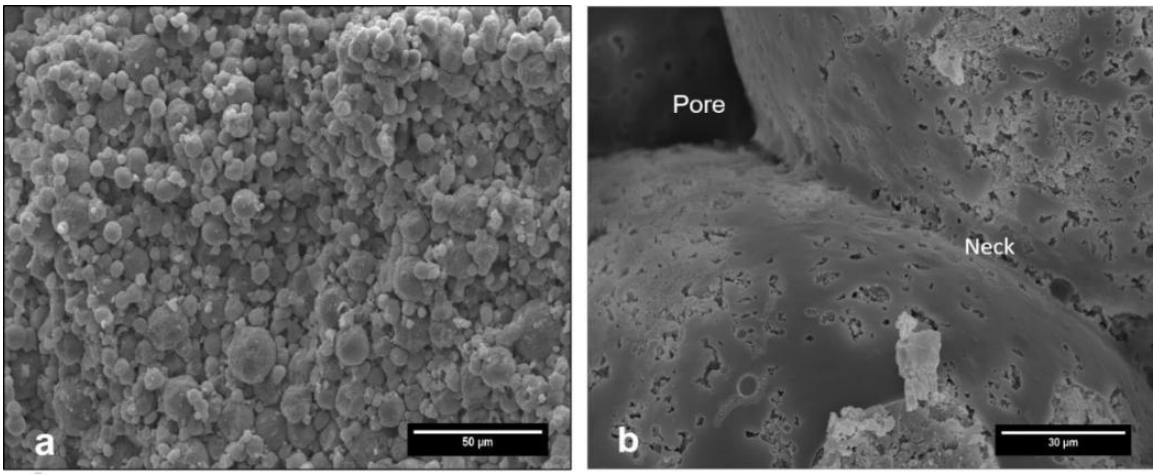

Figure 2.S4 (a) Cross-sectional image of geopolymer monolith (b) SEM image showing the neck and pore formation between 2 particles

2.7.7 Elemental composition of geopolymer particles

Table 2.S1 Elemental composition comparison of geopolymer particles and metakaolin (starting material) as weight percentage by EDS

Element	**Weight %**	
	Metakaolin	**Geopolymer**
O	54.95	52.43
Al	20.42	10.74
Si	22.42	28.06
K	0.16	7.52
Ca	0.06	0.12
Ti	0.89	0.46
Fe	1.10	0.68
Total	**100.00**	**100.00**

2.7.8 Laser diffraction particle size distribution

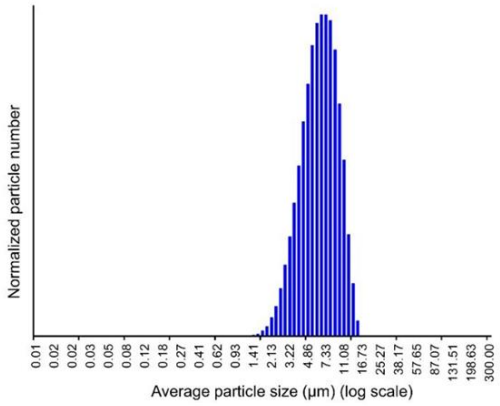

Figure 2.S5 Laser diffraction particle size distribution of geopolymer microparticles

2.7.9 Chromatographic separations on geopolymer monolith

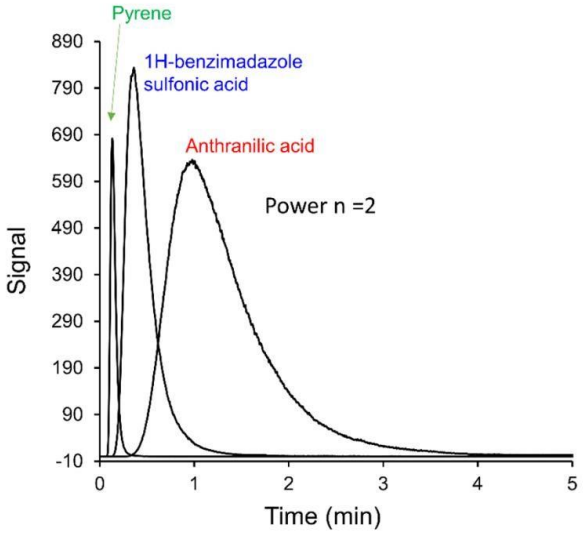

Figure 2.S6 Chromatograms of 1) Pyrene 2) 1-H Benzimidazole-2-sulfonic acid 3) Anthranilic acid at a flow rate of 1 mL min^{-1}. Mobile Phase: 95 % Acetonitrile 5% 5 mM Ammonium formate adjusted to pH 10.50. Column: 2 x (20 x 4.6 mm ID) monolith coupled. Injection volume= 0.1 µL, UV detection at 220 nm. Overlaid individual chromatogram plotted after applying power law (n =2) on individual chromatograms [3].

2.7.10 Hydrolytic stability data interpretation

Hydrolytic stability of the geopolymer stationary phase at elevated pH was examined and qualitatively and quantitatively compared with fully porous commercially available silica. Retention time drift over the time is represented as $\Delta t_R = t_{Rn} - \Delta t_{R1}$ (Where tR1 is the retention time of the first injection, and t_{Rn} is the retention time of the nth injection). The linear trend line was obtained (Microsoft office excel 16 version 1711) for each data set, and slopes ware quantitatively compared. Table 2.S2 shows the calculation of slope ratios of hydrolytic stability data sets. Hydrolytic stability can also be represented based on column volumes passed through the column as represented in Figure 2.S7.

Table 2.S2 Slopes of the stability data sets and quantitative comparison of slopes.

Analyte	**Geopolymer**		**Silica**		**| mSi/mGP |**
	Slope - (mGP)	**Standard error of slope**	**Slope - (mSi)**	**Standard error of slope**	
Nicotinic acid	-7.5E-05	8.0E-05	-9.5E-04	8.6E-05	1.3E+01
Cytosine	-4.7E-04	2.3E-05	-8.3E-04	9.5E-05	1.8E+00
BTMA	-7.6E-04	4.9E-05	1.3E-02	8.8E-04	1.7E+01

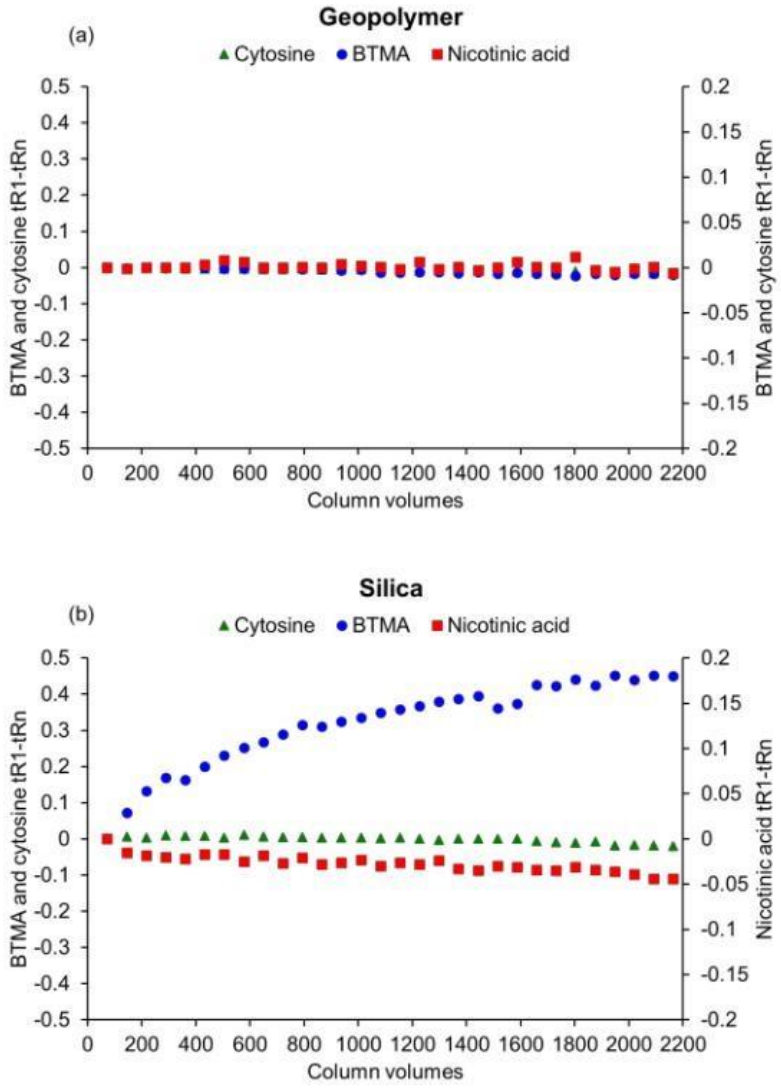

Figure 2.S7 Comparison of hydrolytic stability of (a) geopolymer stationary phase and (b) 10 µm fully porous silica stationary phase based on column volumes. (t_{R1} is the retention time of the first injection, and t_{Rn} is any nth injection after the first injection.)

2.7.11 Selectivity chart data interpretation

The selectivity plot was constructed based on information provided in literature and our experimental data [4-6].

Table 2.S3 Selectivity chart data interpretation

Stationary phase type	Column ID	Description
Zwitterionic	1	ZIC-HILIC 100x4.6, 5µm, 200Å
Zwitterionic	2	ZIC-HILIC 150x4.6, 3.5µm, 200Å
Zwitterionic	3	ZIC-HILIC 150x4.6, 3.5µm, 100Å
Poly	4	ZIC-pHILIC 50x4.6, 5µm, ??Å
Zwitterionic	5	Nucleodur 100x4.6, 5µm, 100Å
Zwitterionic	6	Shiseido 100x4.6, 5µm, 100Å
Amide	7	Tosoh Amide 80 100x4.6, 5µm
Amide	8	Tosoh Amide 80 50x4.6, 3µm
poly	9	PolyHYDROXYETHYL A 100x4.6, 5µm, 100Å
Diol	10	LiChrospher Diol 100x4, 5µm, 100Å
Diol	11	Luna 5u HILIC 100x4.6, 5µm (514356-6)
Poly	12	PolySULFOETHYL A 100x4.6, 5µm, 100Å
Si	13	Chromolith SI 100x4.6, 5µm, 200Å
Si	14	Atlantis HILIC SILICA 100x4.6, 5µm, 200Å
Si	15	Purospher SI 100x4, 5µm,
Si	16	LiChrospher SI 100x4, 5µm, 100Å
Si	17	LiChrospher SI 100x4, 5µm, 60Å
Si-C	18	Cogent Silica-C 100x4.6, 4µm
NH2	19	LiChrospher NH2 100x4, 5µm, 100Å
NH2	20	Purospher NH2 100x4, 5µm, 100Å
NH2	21	Tosoh NH2 50x4.6, 3µm
Si	22	Atlantis HILIC Silica 50×1.0mm, 3µm, 100Å
Si	23	Onyx monolithic Si 100×4.6mm, 2µm, 130Å
Si	24	Agilent ZORBAX HILIC plus 100×4.6mm, 3.5µm 95Å

Si	25	AS9-sc Si monolith 80
Si	26	Agilent ZORBAX RRHD HILIC PLUS 100×3mm, 1.8µm, 95Å
Poly-Si	27	Acclaim Trinity P1, 150×3mm, 3µm
NH2	28	Cosmosil 150×4.6mm, 5µm, 120Å
Proprietary polar phase	29	Acclaim HILIC-10 150×4.6mm, 3µm, 120Å
RP	30	Agilent Eclipse XDB-C18 150×4.6mm, 5µm, 80Å
RP	31	Waters Xbridge C18 150×4.6mm, 5µm,
RP	32	YMC Pro C18 150×2.0mm, 3µm,120Å
RP	33	ZORBAX SB-C18 150×4.6mm, 3.5µm
	34	Benzoic CF6
	35	Frulic N
	36	baresilica
	37	**Geopolymer**

2.7.12 Retention behavior of inorganic anions at different pH

Retention behavior of two inorganic anions were observed under three different pHs.

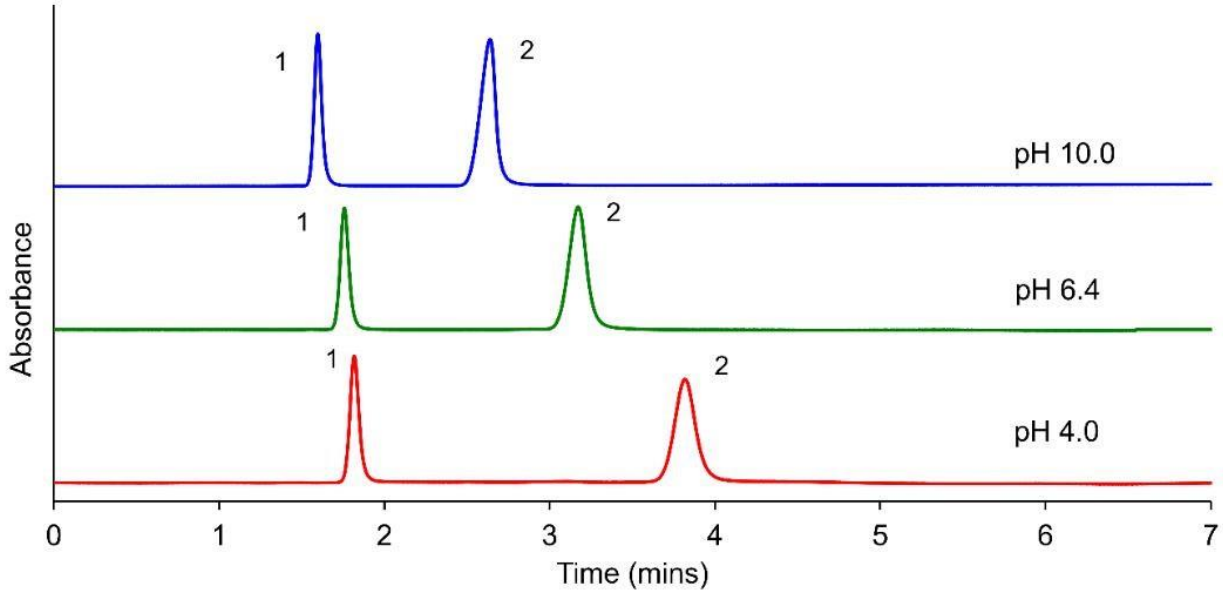

Figure 2.S8 Effect of the stationary phase surface charge on electrostatic interactions in HILIC mode, analytes - 1. iodide 2. nitrate, mobile phase - ACN/100 mM NH_4COOH (91/9), 0.425 mL/min, column – 3 mm ID x 150 mm

2.7.13 References for Supporting Information

[1] R. Arshady, A. Ledwith, Suspension polymerisation and its application to the preparation of polymer supports, Reactive Polymers, Ion Exchangers, Sorbents, 1 (1983) 159-174.

[2] M.F. Wahab, D.C. Patel, R.M. Wimalasinghe, D.W. Armstrong, Fundamental and Practical Insights on the Packing of Modern High-Efficiency Analytical and Capillary Columns, Analytical chemistry, 89 (2017) 8177-8191.

[3] P.K. Dasgupta, Y. Chen, C.A. Serrano, G. Guiochon, H. Liu, J.N. Fairchild, R.A. Shalliker, Black box linearization for greater linear dynamic range: the effect of power transforms on the representation of data, Analytical chemistry, 82 (2010) 10143-10150.

[4] M.E. Ibrahim, Y. Liu, C.A. Lucy, A simple graphical representation of selectivity in hydrophilic interaction liquid chromatography, Journal of chromatography A, 1260 (2012) 126-131.

[5] Y. Wang, M.F. Wahab, Z.S. Breitbach, D.W. Armstrong, Carboxylated cyclofructan 6 as a hydrolytically stable high efficiency stationary phase for hydrophilic interaction liquid chromatography and mixed mode separations, Analytical Methods, 8 (2016) 6038-6045.

[6] N.P. Dinh, T. Jonsson, K. Irgum, Probing the interaction mode in hydrophilic interaction chromatography, Journal of chromatography A, 1218 (2011) 5880-5891.

Chapter 3. Fabrication of interconnected macroporosity in geopolymers via inverse suspension polymerization

3.1 Abstract

A new approach to fabricate geopolymer monoliths with interconnected macroporosity and a permeable structure is presented. This was achieved using an unconventional route of inverse suspension polymerization in which the aqueous geopolymer slurry consisting of potassium hydroxide, fumed silica, and natural metakaolin was dispersed in a continuous phase of soybean oil. The geopolymer monolith was synthesized by taking advantage of the so-called "sticky period" that occurs during inverse suspension polymerization. During this period, individual droplets can coalesce but cannot re-divide because of the partially polymerized matrix. We deliberately brought the partially polymerized geopolymer particles in proximity during sticky period to fuse the particles. Hence this method, termed as "sticky period particle fusion," helped to form a monolithic structure with inter-particle spacing as macropores which resulted in high permeability. The sticky period was observed to depend on synthesis conditions such as stirring speed, temperature, and viscosity of continuous phase which in turn helped to tune the surface and pore properties of geopolymer monoliths. The BET surface area up to 67 m^2/g and total pore volumes of 0.4 cm^3/g from pycnometry were obtained.

3.2 Introduction

Geopolymers are ceramic-like inorganic polymers synthesized from reactive aluminosilicate precursors (e.g., metakaolin, fly ash, etc.) and alkali solutions [1]. Geopolymers are finding various applications as construction materials [2], adsorbents for heavy metals [3], in catalysis [4], separation science [5], etc. Intrinsically, geopolymers are mesoporous, but they are highly dense structures exhibiting low permeability [6]. The induction of higher and interconnected porosity in geopolymers can advance their utility particularly in adsorption, filtration, and separation applications. There are various reported methods to generate additional porosity in geopolymers, for example, by using blowing agents (H_2O_2) [7], in situ saponification [8], and surfactants [9]. However, there are no reports on geopolymers with interconnected macroporosity. Here, we report the fabrication of interconnected macroporosity in geopolymer monoliths, which in turn boosts the permeability.

The geopolymer monoliths were synthesized using inverse suspension polymerization, which is used for the synthesis of a vast number of organic polymers [10]. In this method, suspension of monomers is sustained in an immiscible liquid using mechanical stirring and surfactants/stabilizers. The droplets containing monomers act as individual mini reactors in which polymerization proceeds. In the initial phase, there is a dynamic equilibrium between coalescence and re-division of the droplets [10]. But after certain time, the droplets can coalesce, in the event of a collision, but cannot further re-divide because of partial hardening of droplets. This is termed the "*sticky period*" [10]. Although the sticky period is considered a serious side effect in the particle synthesis as it leads to coagulation, we used this feature to advantage. The monoliths of geopolymers were fabricated by coalescing the droplets during the sticky period by bringing them in proximity using centrifugation.

3.3 Experimental Procedure

3.3.1 Synthesis

A potassium silicate solution was prepared by mixing 2.80 g of KOH (Millipore Sigma, MO, USA) and 3.00 g fumed silica (Millipore Sigma, MO, USA) in 7.59 mL of deionized water. Then, 6.25 g of metakaolin (Advanced cement technologies, WA, USA) was added to the solution. The resulting geopolymer slurry was added to 700 mL of soybean oil (Crisco® Pure Vegetable Oil) dropwise under stirring at room temperature. An overhead stirrer with a three-blade propeller (Talboys 101, Troemner, Thorofare, NJ) was used. As geopolymer slurry is highly alkaline, it reacts with the triglycerides in the oil to form carboxylate surfactants which in turn help stabilizing the suspension [11]. This hypothesis was also supported by the fact that, when geopolymer slurry was suspended in paraffin oil, the suspension could not be sustained. The sticky period was tracked using scanning electron microscopy. For this purpose, fractions were pipetted out from the suspension in polypropylene cylindrical molds (100 x 4.6 mm i.d.). The oil was decanted, and this process was repeated few times to completely fill the molds with dispersed phase. The molds were kept at 60 ºC for 24 hours for curing of the geopolymer (Relative humidity was not controlled during curing). The fractions were taken every hour or so, and above process was repeated. After curing, the solidified fractions were washed using boiling water. This step was particularly useful for eliminating the fractions obtained after the sticky period was over, as those fractions disintegrate into the particles. The rest of the fractions were sintered at 550 ºC for 4 hours at a ramp rate of 2 ºC/min to remove the organics from the monoliths. A standard monolithic sample (GS0) was also prepared by bulk geopolymerization for comparison with monoliths prepared by "sticky period particle fusion" method. For this, KOH, fumed silica, water and metakaolin (using

the amounts previously mentioned) were mixed and the slurry was transferred to the mold. The slurry was then cured at 60 ºC for 24 hours and sintered at 550 ºC for 4 hours.

3.3.2 Characterization

The scanning electron microscopy (SEM) images of silver coated samples were acquired using Hitachi S-4800 II Field Emission SEM (FE-SEM) under a high vacuum and acceleration voltage of 20kV. A dilute slurry of finely ground geopolymer samples in ethanol was made and placed on the copper grid for transmission electron microscopy (TEM). The TEM images were obtained using Hitachi H-9500 High-resolution Transmission Microscope under a high vacuum and acceleration voltage of 300 kV. The elemental composition of geopolymer samples was investigated by energy dispersive spectroscopy (EDS) analysis using EDAX EDS system attached to SEM. The Fourier transform-infrared spectroscopy (FTIR) was done using Thermo Nicolet 6700 FTIR Spectrometer, from 600 cm^{-1} to 4000 cm^{-1}. The X-ray diffraction pattern was obtained by using Bruker D8 Advance X-ray diffractometer. The Brunauer–Emmett–Teller (BET) surface area analysis was performed using Micrometrics ASAP 2020 Porosimeter. The samples were first degassed at 90 ºC for 24 hours to remove any adsorbed species. The total pore volumes were determined by pycnometery using DI water at 25 ºC and ambient pressure.[8] The Cannon-Fenske Routine Viscometer was used to measure the viscosity of oil at different temperatures.

3.4 Results and Discussion

The variation in the sticky period and pore properties of samples synthesized at different synthesis conditions are shown in Table 3.1.

Table 3.1 Sticky period determination and pore properties for different synthesis conditions

Sample	Stirring speed (rpm)	Temperature (ºC)	Kinematic Viscosity[¥] of soybean oil	External agents added	Sticky period[¶] (hours)	BET Surface Area (m^2/g)	Pore volume[§] (cm^3/g)	Total Pore volume[ǂ] (cm^3/g)
GS0	N/A	N/A	N/A	N/A	N/A	10.67	0.012	0.053
GS1	2000	23	71.81	N/A	12-13	29.89	0.089	0.152
GS2	3000	23	71.81	N/A	12-13	31.42	0.092	0.220
GS3	4000	23	71.81	N/A	12-13	40.65	0.110	0.302
GS4	5000	33	48.72	N/A	3-4	47.58	0.094	0.356
GS5	6000	39	40.64	N/A	1-2	48.25	0.095	0.391
GS6	5000	33	48.72	SDS	3-4	66.72	0.153	0.401

[¥]From viscometer

[¶]From SEM Analysis

[§]BJH desorption pore volume from pores less than 300 nm

[ǂ]From water pycnometery

FE-SEM was used to determine the sticky period for each sample. Fig. 3.1 illustrates the FE-SEM images of fractions taken at different times for sample GS4. The images were taken after curing, washing, and sintering the samples. The fraction taken at the second hour, denoted as GS4-2, (Fig. 3.1a) shows no particle formation and is similar to standard bulk geopolymer GS0 (Fig. 3.S3), i.e., a highly dense structure with no macro-pores. The FE-SEM image of the aliquot taken at the third hour (GS4-3) shows individual particles well fused to each other (Fig. 3.1b). The formation of necks and macro-pores can be seen in the magnified image of GS4-3 (Fig. 3.1d). The size of macropores ranged from approximately 1-5 µm for sample GS4-3 (measured using SEM). Hence a highly interconnected macroporous monolithic structure was formed with interparticulate spacing serving as macropores.

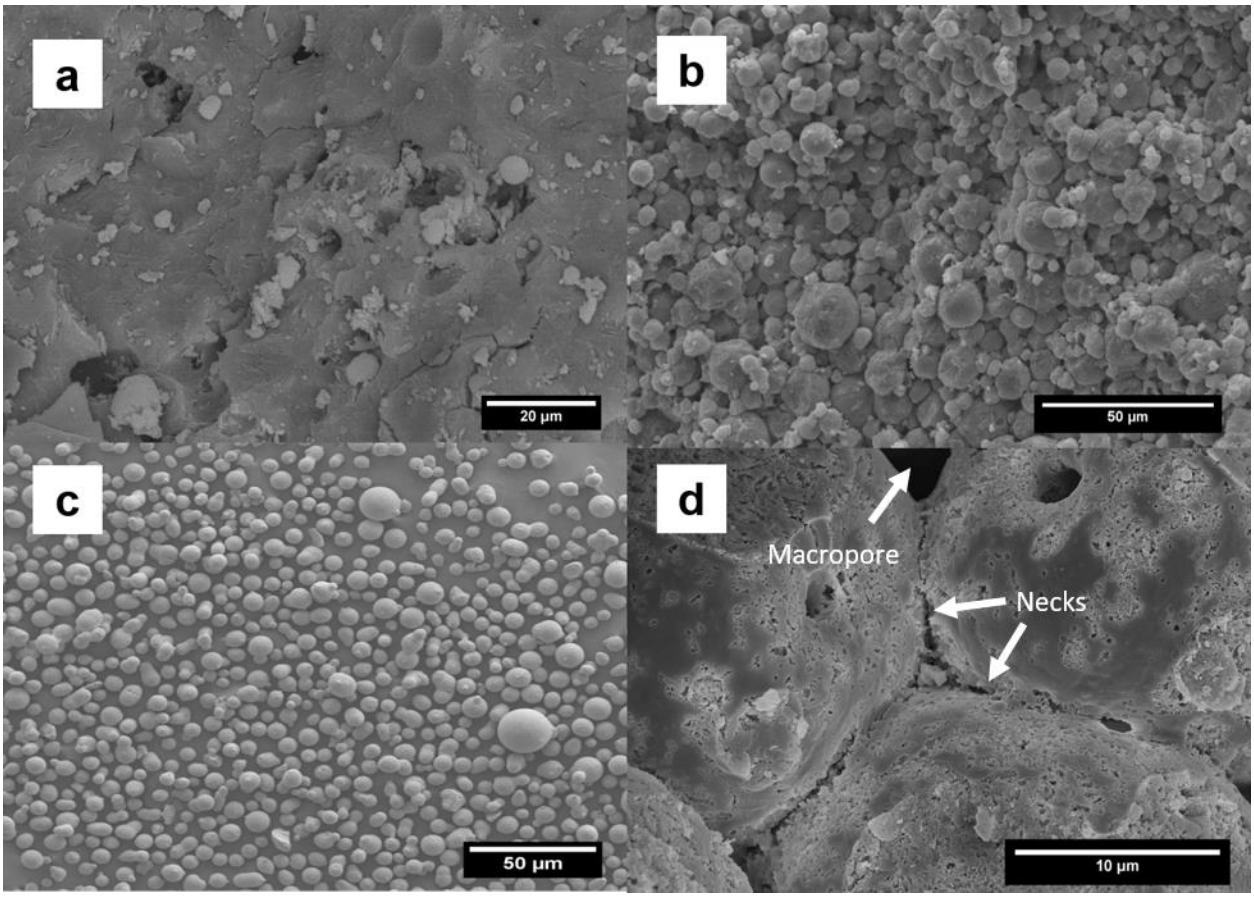

Fig. 3.1: Field emission-scanning electron microscopy images of sample GS4. a) aliquot taken at 2nd hour (GS4-2) b) aliquot taken at 3rd hour (GS4-3) c) aliquot taken at 5th hour (GS4-5) d) magnified image of GS4-3

Finally, the sample taken at the fifth hour (GS4-5) shows the full-fledged particles, concluding the end of the sticky period (Fig. 3.1c). The TEM image (Fig. 3.S4) shows the internal mesoporous structure of an individual geopolymer particle in sample GS4-3. The gel-like structure can be observed in which particles are attached to each other.

The XRD analysis of GS4-3 shows the characteristic amorphous hump of geopolymers between the 2θ value of 25-30º hence confirming the formation of geopolymers (Fig. 3.S1)[12]. The final composition of GS4-3 as measured by EDS was Si/Al/K molar ratio 2:1:1. (Fig. 3.S5). The FTIR

spectrum of GS4-3 (Figure 3.S2) shows the characteristic geopolymer bands, located between 900 and 1100 cm^{-1}, attributed to asymmetric stretching of Si-O or Al-O [3]. The bands at 600 cm^{-1} and 700 cm^{-1} correspond to Al-O-Si stretching vibrations and bending vibrations respectively [13].

3.4.1 Effect of synthesis conditions

As the stirring speed increases, the temperature inside the reactor increases because some part of the mechanical energy dissipates as heat. It has been shown previously that reaction rate of geopolymerization increases with increase in temperature [14]. The consequences of the temperature increase can be seen in the time period for the arrival of the sticky period. The sticky period of geopolymer synthesized at 6000 rpm, whose reactor temperature reached 39 ºC, occurred just in one hour. In contrast, the sticky period of the samples synthesized at 2000, 3000 and 4000 rpm, in which temperature is 23 ºC, does not start until the twelfth hour. Therefore, the reaction times, in inverse suspension polymerization, decrease with higher stirring speed.

The SEM image analysis (Fig. 3.S6- 3.S10) shows that, as the stirring speed increases, the particle size of the fused particles decreases. This is because as the stirring speed increase, the energy input to break the dispersed droplets increases and hence the droplet size decreases [15]. Also, it is known that viscosity of the continuous phase has an effect on the final particle size in suspension polymerization [15]. If the viscosity is high, the probability of the droplet coalescence decreases, therefore yielding a smaller particle size. However, as the stirring speed increases, the temperature also increases and hence the viscosity decreases. Thus, the end particle size is the result of a trade-off between these physical parameters.

Previously, surfactants have been shown to increase the surface area of geopolymers [8]. The surface area of all the samples prepared by “sticky period particle fusion” is higher than that of the

bulk geopolymer GS0, which can be attributed to *in situ* surfactant formation. 20 mg of an anionic surfactant, sodium dodecyl sulfate (SDS), was added to the geopolymer slurry to see its effect on the surface area (Table 3.1). This additional surfactant can help in stabilizing the suspension as well as the air trapped inside the geopolymer matrix, hence increasing the mesoporosity and surface area [8]. As can be seen from the Table 3.1, GS6, synthesized by adding external surfactant, has relatively higher surface area than the sample without added external surfactants (GS4).

The pore volume from nitrogen adsorption measurements and total pore volume from pycnometry also shows an increasing trend with an increase in stirring speed. The increase in total pore volume is more prominent implying larger increase in macroporosity than mesoporosity. The high permeability of these geopolymer monoliths has been shown by using them as monolithic chromatographic solid supports [5]. The geopolymers synthesized by bulk geopolymerization or by a reactive emulsion template technique [8] could not be used as chromatographic monolithic columns because of the lack of macropores and the predominant closed pores and hence exerted back pressures of more than 400 MPa (column dimensions: 5 cm x 4.6 mm i.d., mobile phase: methanol, flow rate: 1 mL/min), which is an upper limit for back pressure for most of the modern HPLC instruments. In contrast, the monoliths prepared by "sticky period particle fusion" gave the back pressure of only 70 MPa under the same chromatographic conditions (for 4.6 mm x 5 cm column made by GS4-3). The drastic dip in back pressure indicates the presence of a more permeable structure for the geopolymers. The chromatography has been discussed in the paper [5].

3.5 Conclusions

The fabrication of interconnected macroporosity and permeability in the geopolymer monoliths using "sticky period particle fusion" has been successfully shown. Fusing particles taken during

the sticky period, a solid structure with interparticle spacing as macroporosity can be produced. Moreover, it has been demonstrated that the sticky period depends on the synthetic conditions of the reaction, particularly on the stirring speed and temperature. The conditions also affect the pore properties like surface area and pore volume. Hence the structure and the physical properties can be manipulated using different conditions. The optimization of the reaction conditions and geopolymer composition to get the specific structural features like high permeability, high surface area, and uniform pore structure is still under investigation in our laboratory. This simple and unique method can be applied for synthesis of other materials.

3.6 References

[1] J. Davidovits, Geopolymer chemistry and applications, Geopolymer Institute2008.

[2] B. Singh, G. Ishwarya, M. Gupta, S. Bhattacharyya, Geopolymer concrete: A review of some recent developments, Construction and Building Materials, 85 (2015) 78-90.

[3] Z. Yunsheng, S. Wei, C. Qianli, C. Lin, Synthesis and heavy metal immobilization behaviors of slag based geopolymer, Journal of hazardous materials, 143 (2007) 206-213.

[4] P. Sazama, O. Bortnovsky, J. Dědeček, Z. Tvarůžková, Z. Sobalík, Geopolymer based catalysts—new group of catalytic materials, Catalysis today, 164 (2011) 92-99.

[5] R.M. Wimalasinghe, C.A. Weatherly, M.F. Wahab, N. Thakur, D.W. Armstrong, Geopolymers as a New Class of High pH Stable Supports with Different Chromatographic Selectivity, Analytical chemistry, 90 (2018) 8139-8146.

[6] W.M. Kriven, J.L. Bell, M. Gordon, Microstructure and microchemistry of fully-reacted geopolymers and geopolymer matrix composites, Ceramic Transactions, 153 (2003).

[7] G. Masi, W.D. Rickard, L. Vickers, M.C. Bignozzi, A. Van Riessen, A comparison between different foaming methods for the synthesis of light weight geopolymers, Ceramics International, 40 (2014) 13891-13902.

[8] D. Medpelli, J.M. Seo, D.K. Seo, Geopolymer with hierarchically meso-/macroporous structures from reactive emulsion templating, Journal of the American Ceramic Society, 97 (2014) 70-73.

[9] A. Singhal, B.P. Gangwar, J. Gayathry, CTAB modified large surface area nanoporous geopolymer with high adsorption capacity for copper ion removal, Applied Clay Science, 150 (2017) 106-114.

[10] R. Arshady, A. Ledwith, Suspension polymerisation and its application to the preparation of polymer supports, Reactive Polymers, Ion Exchangers, Sorbents, 1 (1983) 159-174.

[11] F. Gunstone, The chemistry of oils and fats: sources, composition, properties and uses, John Wiley & Sons2009.

[12] J. Davidovits, Geopolymers: inorganic polymeric new materials, Journal of Thermal Analysis and calorimetry, 37 (1991) 1633-1656.

[13] L. Chen, Z. Wang, Y. Wang, J. Feng, Preparation and Properties of Alkali Activated Metakaolin-Based Geopolymer, Materials, 9 (2016) 767.

[14] P. Rovnaník, Effect of curing temperature on the development of hard structure of metakaolin-based geopolymer, Construction and Building Materials, 24 (2010) 1176-1183.

[15] R. Arshady, Suspension, emulsion, and dispersion polymerization: A methodological survey, Colloid and polymer science, 270 (1992) 717-732.

3.7 Supporting Information

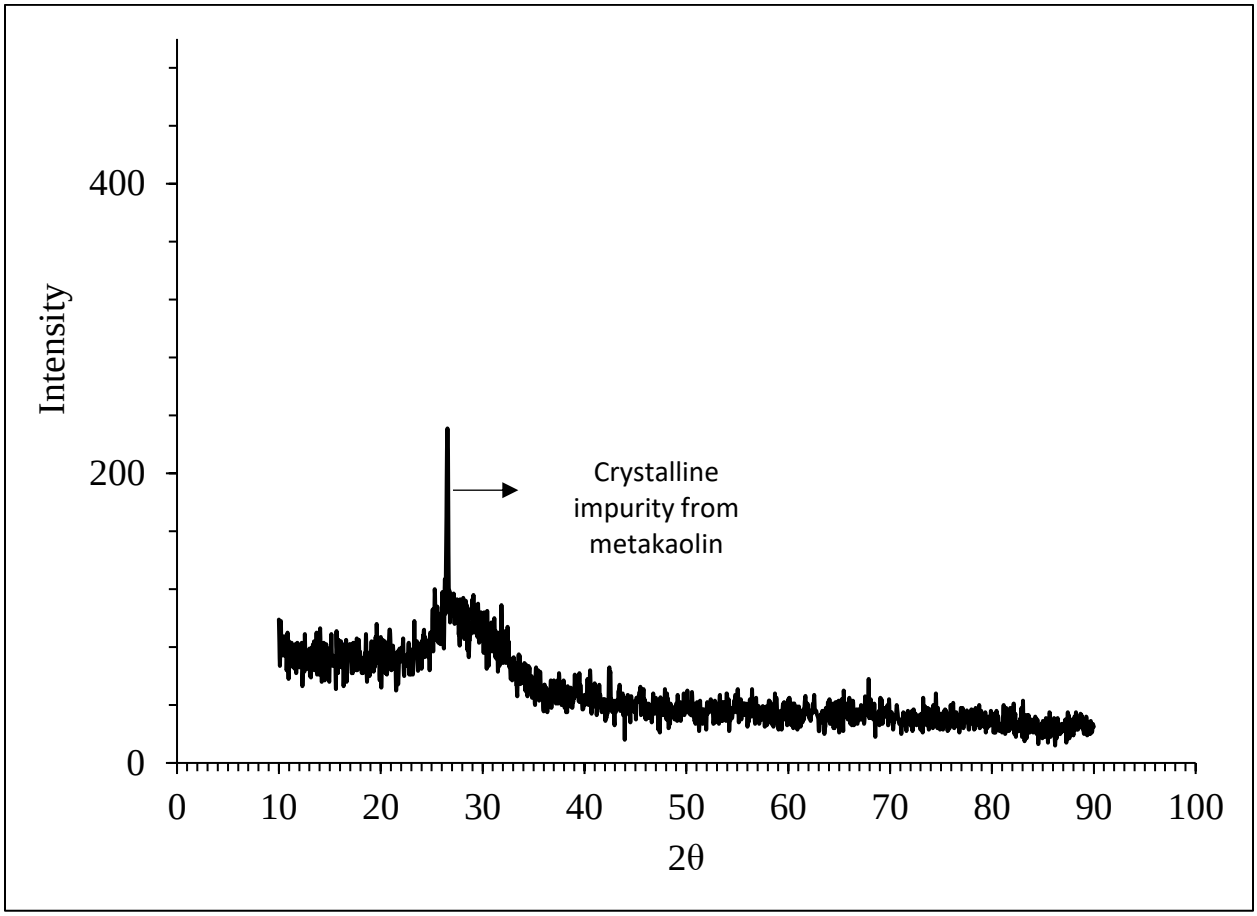

Fig. 3.S1: Cu Kα X-ray diffractogram of sample GS4-3.

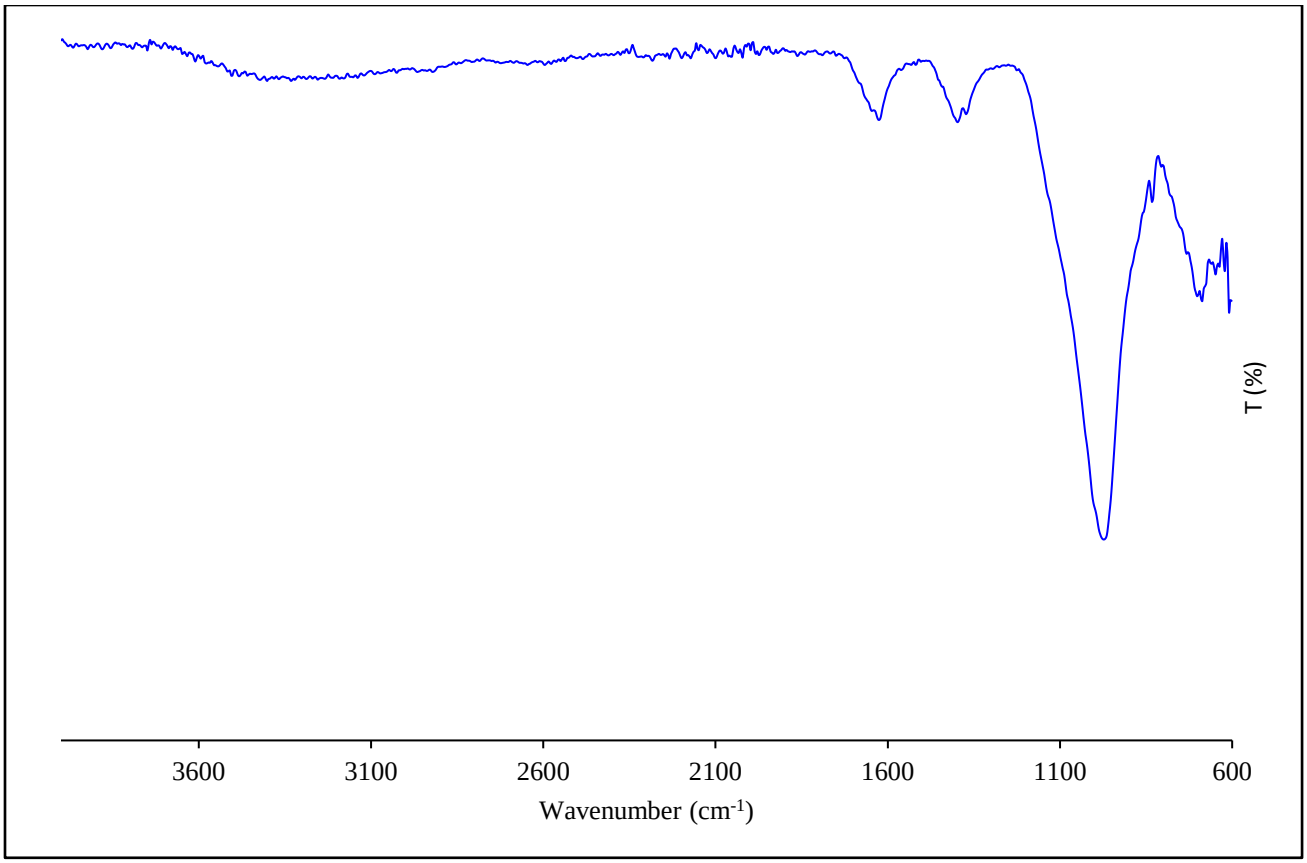

Fig. 3.S2: FTIR of sample GS4-3.

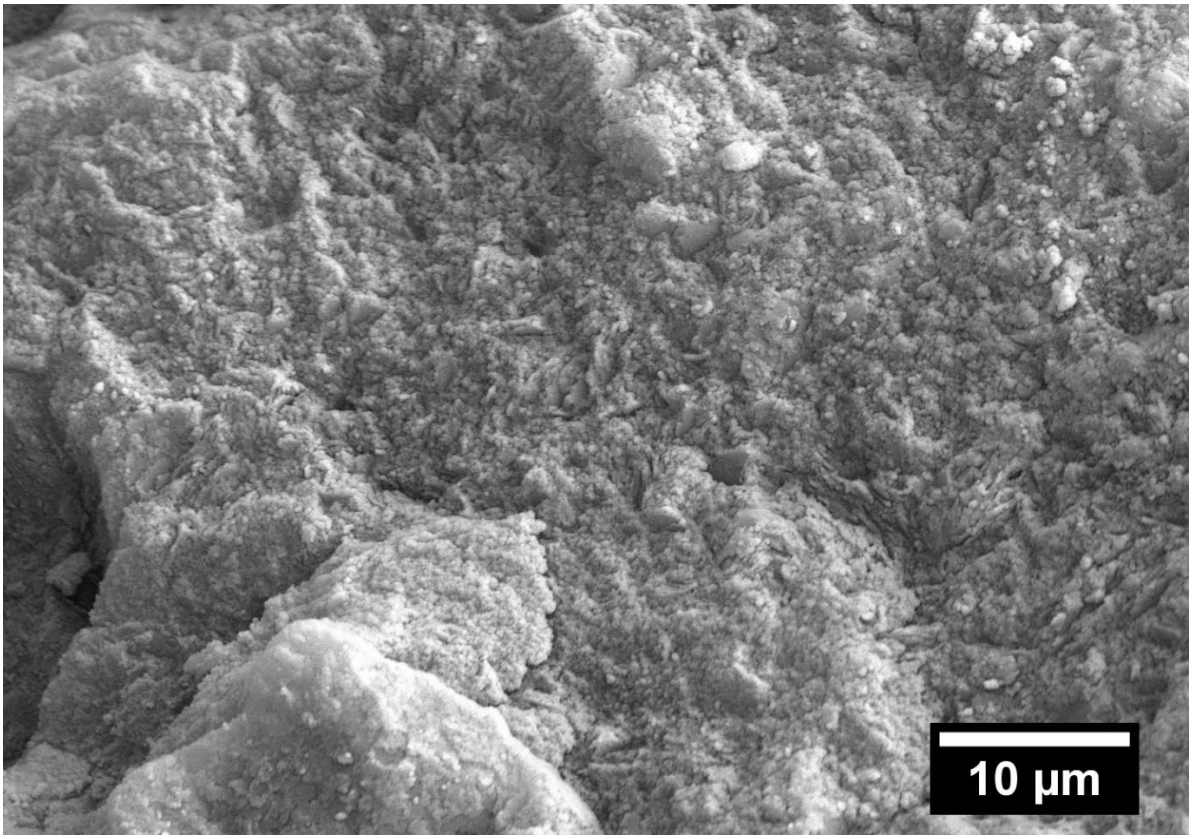

Fig. 3.S3: FE-SEM image of sample GS0 (Standard bulk geopolymer). See experimental for synthesis details.

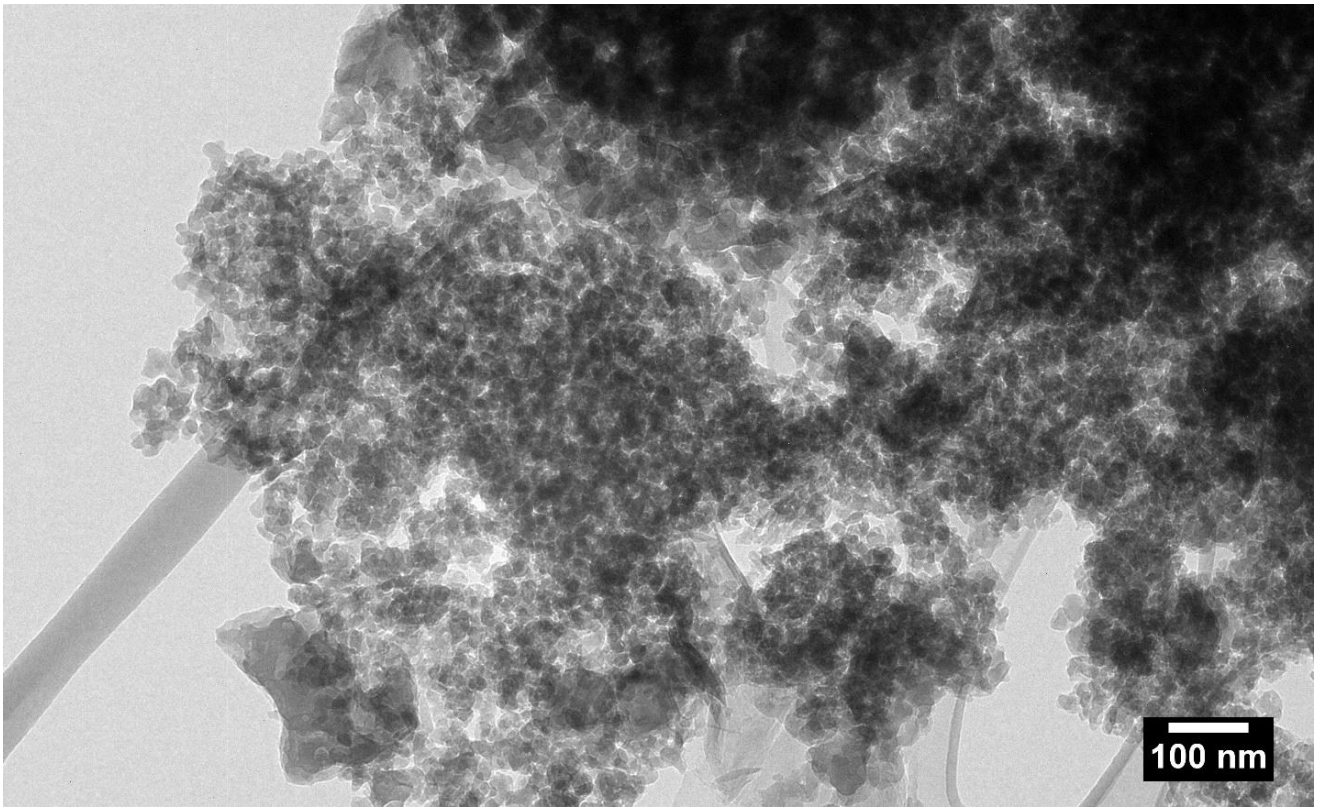

Fig. 3.S4: Bright field TEM image of a single particle of GS4-3. This shows the internal mesoporous structure of the individual geopolymer particle.

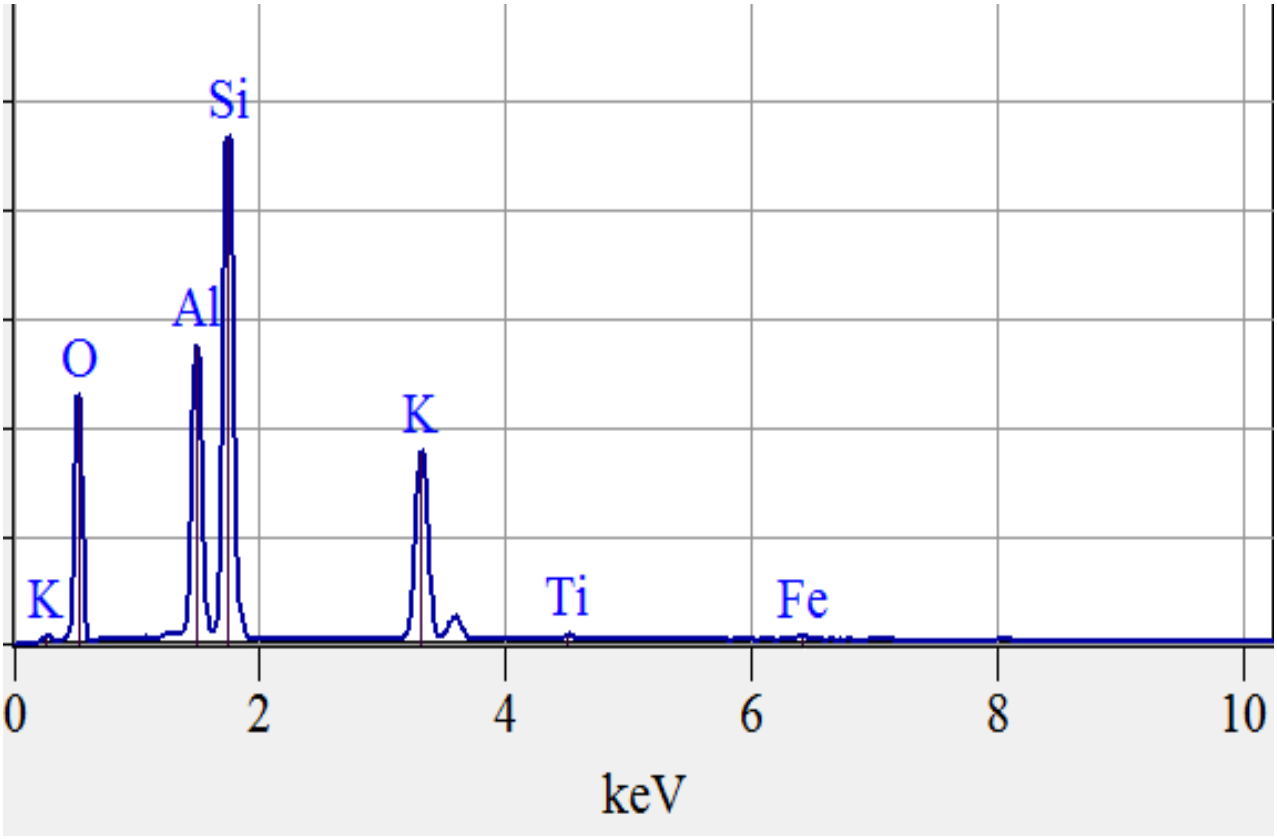

Fig. 3.S5: EDS spectrum of GS4-3.

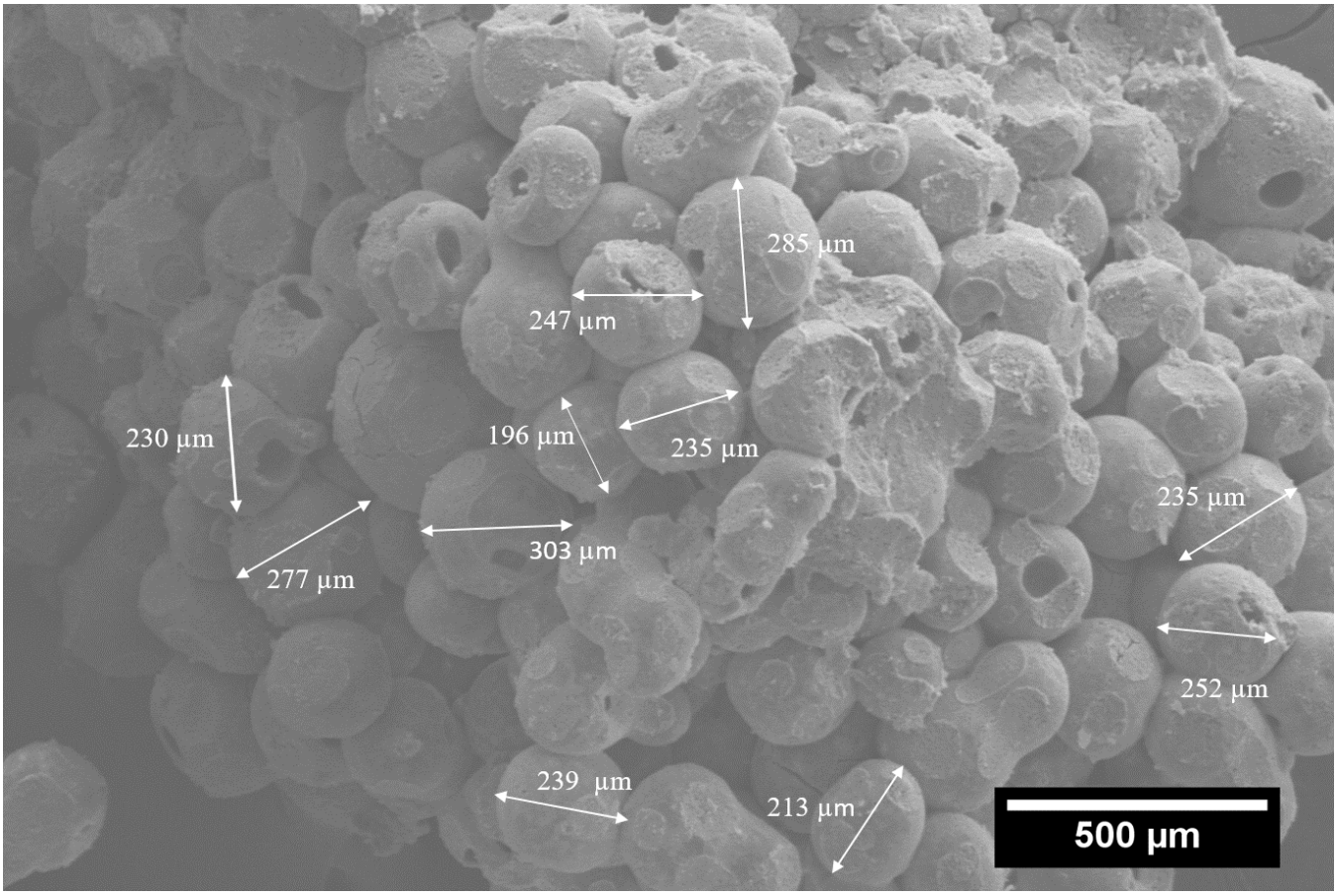

Fig. 3.S6: FE-SEM image of GS1 monolith formed during sticky period (stirring speed of 2000 rpm).

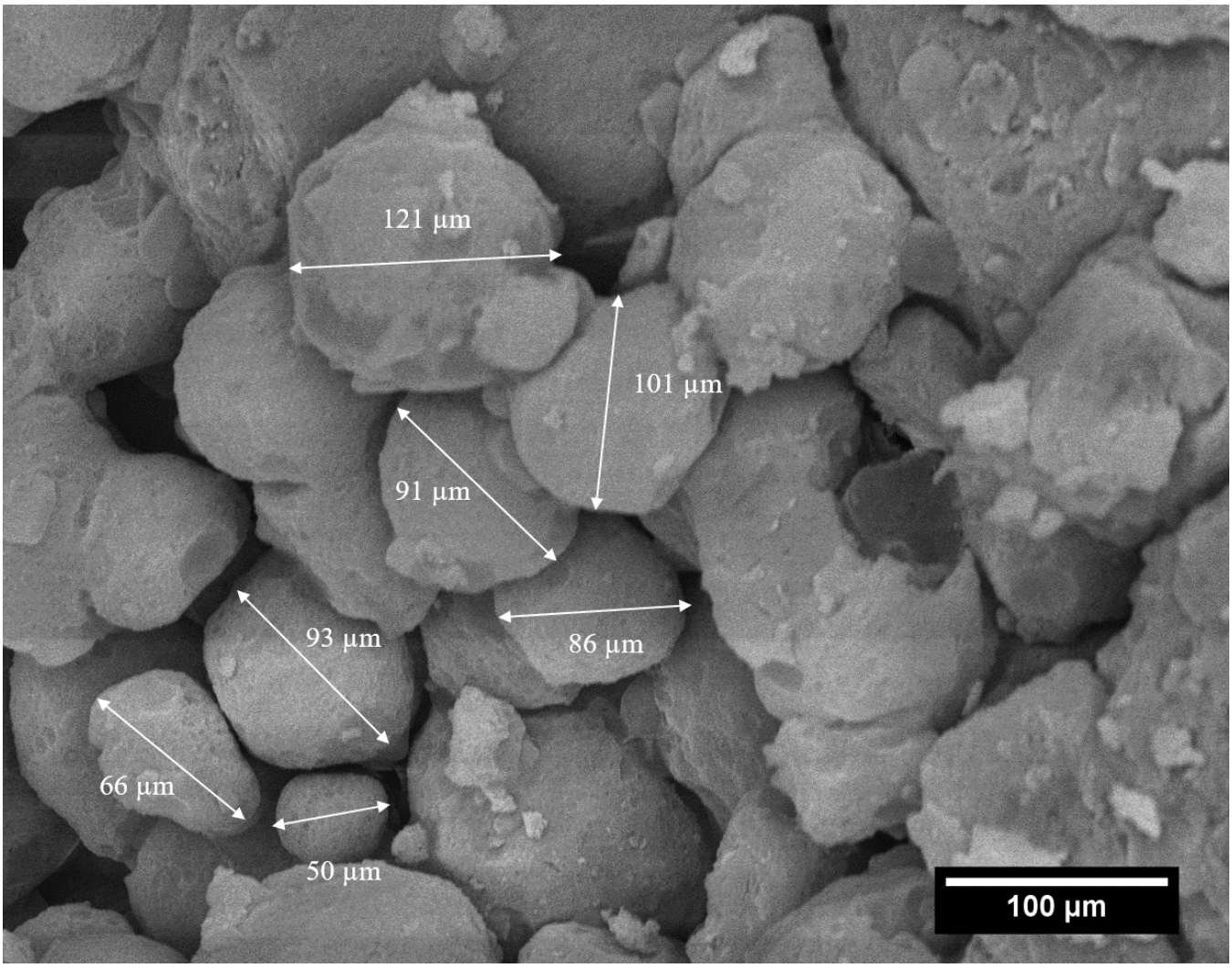

Fig. 3.S7: FE-SEM image of GS2 monolith formed during sticky period (stirring speed of 3000 rpm).

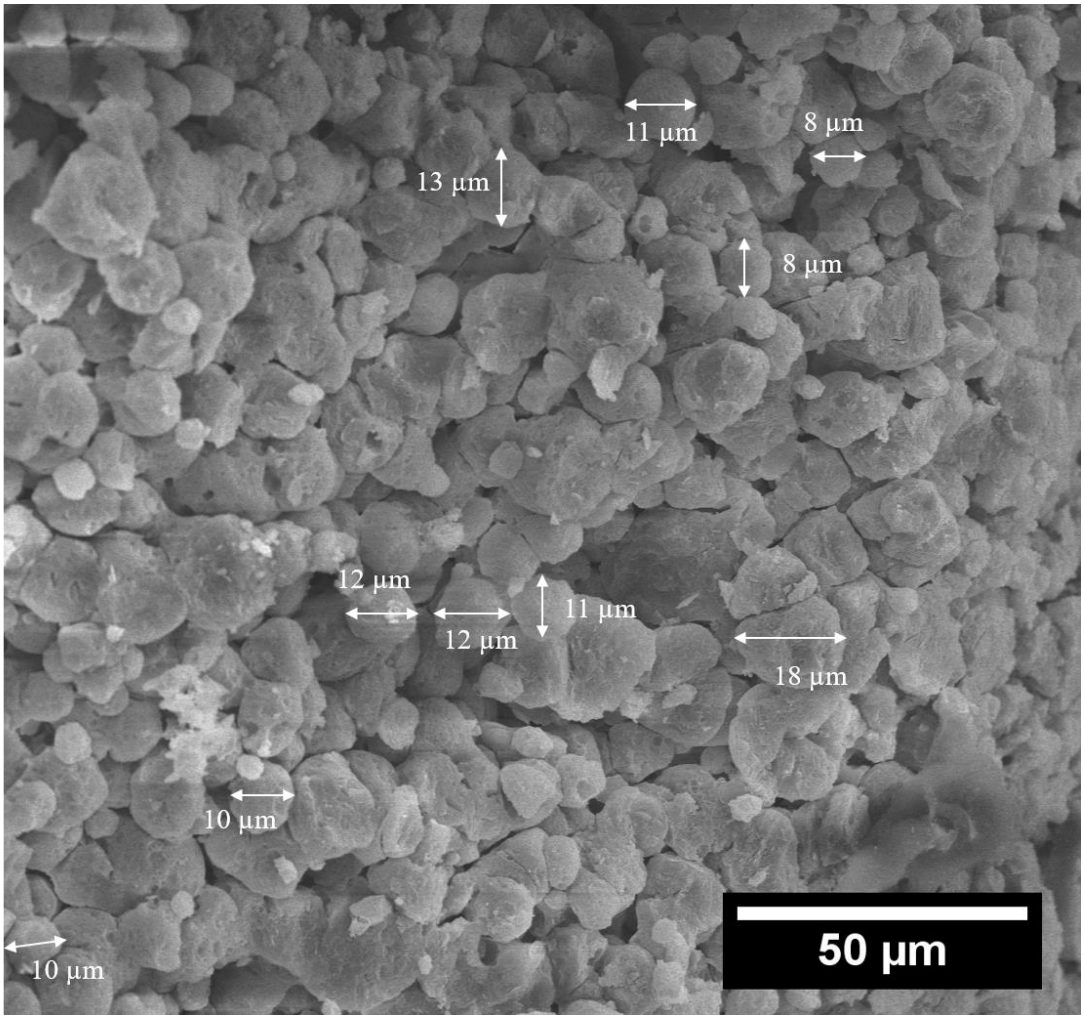

Fig. 3.S8: FE-SEM image of GS3 monolith formed during sticky period (stirring speed of 4000 rpm).

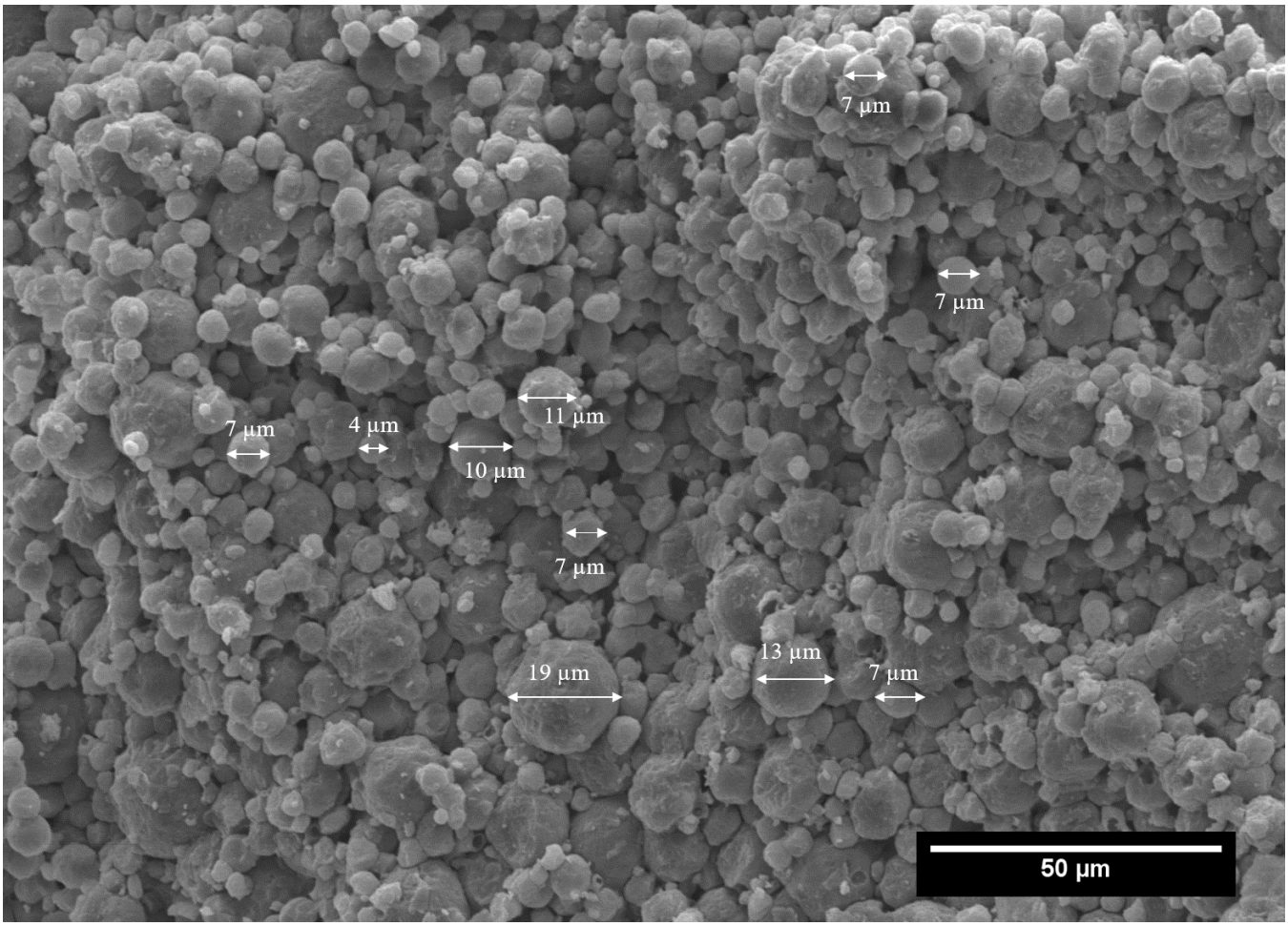

Fig.3.S9: FE-SEM image of GS4 monolith formed during sticky period (stirring speed of 5000 rpm).

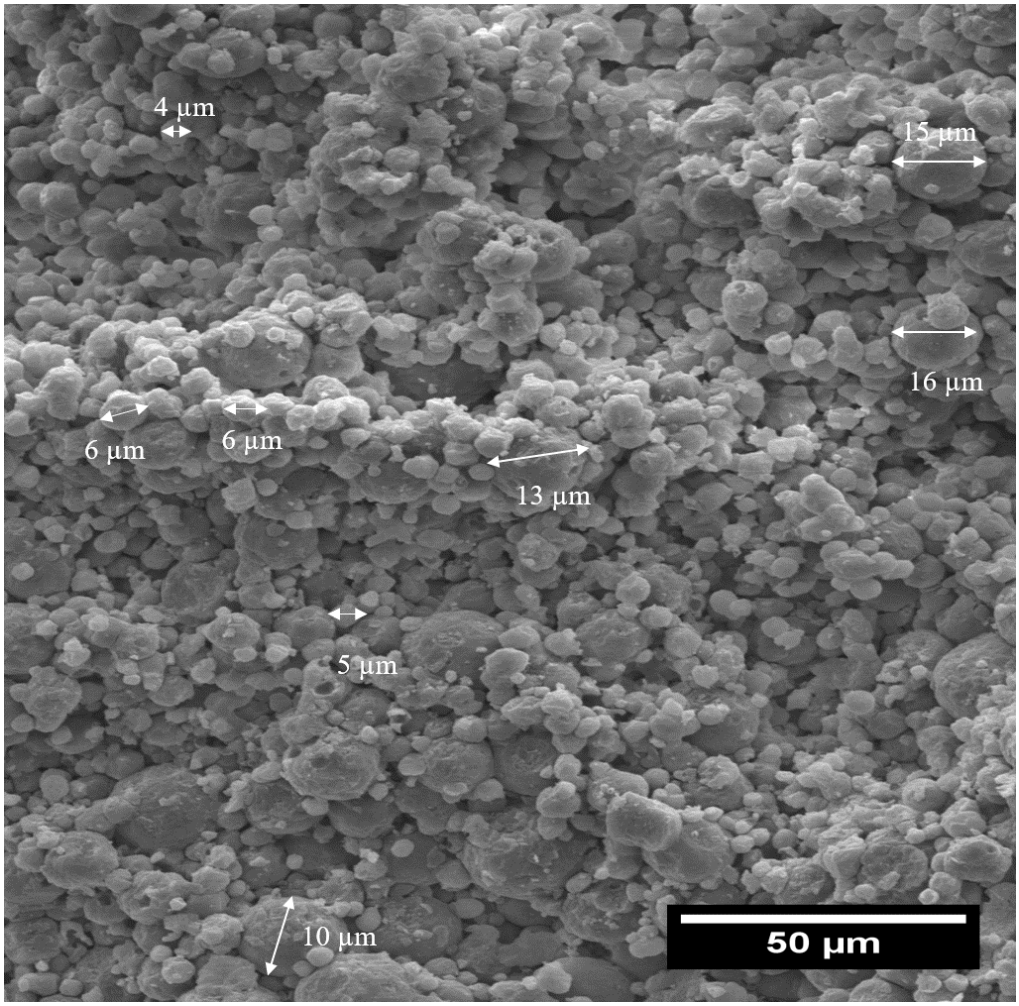

Fig.3.S10: FE-SEM image of GS5 monolith formed during sticky period (stirring speed of 6000 rpm).

3.4.1 Degree of geopolymerization

Qualitative tests including a “boiling water test” and a “freeze/thaw cycles test” [1] were done to help make sure if the geopolymers formed here were fully condensed or not. According to these tests, non-fully condensed geopolymers are sensitive to water and can undergo swelling or total destruction. All the samples in this study, maintained their structural integrity after undergoing these severe tests.

3.4.2 References for Supporting Information

1. Davidovits J. Geopolymer chemistry and applications: Geopolymer Institute; 2008.

Chapter 4. Synthetic aluminosilicate based geopolymers – Second generation geopolymer HPLC stationary phases

4.1 Abstract

A survey of existing stationary phases classified by the United States Pharmacopeia reveals that 120 groups of chromatographic supports mostly utilize silica-silane chemistry, polymeric materials along with some niche metal oxides. In this work, the synthesis and characterization of transition-metal free geopolymers as a new class of stationary phases for hydrophilic interaction liquid chromatography and normal phase separations is reported. The geopolymers were synthesized by reaction of synthetic aluminosilicate with potassium silicate (fumed silica dissolved in KOH) in a water-in-oil emulsion. For comparative purposes of peak shapes, a geopolymer from natural metakaolin was also synthesized. The geopolymers were examined by X-ray diffraction, energy dispersive spectroscopy, laser diffraction, and N_2-adsorption isotherms. This two-step approach gives spherical microparticles with surface area and pore size comparable to silica phases (150 m^2/g and 120 Å respectively). Both synthetic aluminosilicates based and natural metakaolin based geopolymers occupy a unique "spot" in the HILIC selectivity chart when compared to 36 HILIC phases. An additional promising feature of geopolymers is high pH and temperature stability which are used to tune selectivity for small polar analytes. High pH separations are shown with carboxylic acids. Geopolymers also show mixed mode behavior in retention with ion-exchange properties in purely aqueous mobile phases. The separation of derivatized sugars is demonstrated and compared with porous graphitic carbon (Hypercarb^{TM}) as another pH-stable phase.

4.2 Introduction

A survey of more than 120 United States Pharmacopeia (USP) classes of columns overemphasizes the need of different chromatographic supports in challenging separations in HPLC [1]. A clear trend is that the majority of listed columns show silica-silane chemistry, followed by polymeric stationary phases and some niche materials such as titania, zirconia and porous graphitic carbon. Thus, one of the active research areas in separation science is to develop new materials to provide new and orthogonal selectivity in one and two-dimensional chromatography respectively. The fundamental resolution equation, $R_s = [N^{1/2}/4][(\alpha-1)/\alpha][k_2/(1+k_2)]$, shows maximum dependency on the selectivity, α, whereas efficiency *N* and retention factor *k* play relatively a smaller role. In this work new materials known as geopolymers are examined. They consist of an amorphous network of inorganic aluminosilicate chains with a monovalent/divalent counter cation. Geopolymers have gained extensive popularity due to their versatile properties like mechanical strength, thermal stability and chemical resistance in materials engineering [2, 3]. They are conveniently prepared by the reaction of metakaolin/aluminosilicate with a highly alkaline silicate solution. Only two reports exist on the chromatographic evaluation of geopolymers, so far, in the extensive literature on HPLC [4, 5]. Recently, natural metakaolin based geopolymer was shown to be a promising stationary phase for liquid chromatography especially for hydrophilic interaction liquid chromatography (HILIC) when compared with silica [5]. The geopolymers have high pH stability and different selectivity from a majority of traditional column chemistries used in chromatography today [5].

The major shortcoming encountered during the chromatographic evaluation of natural metakaolin based geopolymer in our previous study was the distorted peak shapes and peak tailing for certain types of analytes, especially those with coordinating capability. The energy dispersive

spectroscopy (EDS) data showed the presence of a small amounts of iron and titanium in the geopolymer particles [5]. These transition metals could be a possible underlying cause for the observed peak asymmetries. The detrimental effects of the presence of metal impurities in stationary phases, on chromatographic performance, are well known in silica gel-based supports [6, 7]. The coordination between the metal ions held in a solid matrix and adsorbed analytes is due to the interaction between an electron acceptor (Lewis acid) and an electron donor (Lewis base). These trace impurities give rise to secondary interactions leading to an additional mode of retention and causes the analyte peak to tail and broaden simultaneously- often a compound may not elute at all. Such sites are also referred to as, "tail-producing sites" [8].

The precursors used in the synthesis of geopolymers (metakaolin, fly ash, blast furnace, etc.[9]) often contain traces of metal oxide impurities (e.g., Fe_2O_3, TiO_2, CaO, MgO and Na_2O) along with aluminum silicates [10]. Metakaolin is a good candidate for general geopolymer research due to its relative purity and chemical composition consistency [11]. However, from a chromatographer's perspective, natural metakaolin still contains an appreciable amount of metal oxide impurities. The source of impurities is the precursor of metakaolin- "kaolin" itself. Chemical weathering, hydrothermal processes, and solfatara alterations are responsible for the formation of kaolins [12]. These processes impart a different level of transition metal oxide impurities to kaolins depending on their formation age and location [13]. Also, crystalline impurities like quartz, muscovite, etc. are often found in kaolins [13]. These impurities are present during dehydroxylation of kaolin to form metakaolin at 750 ℃. The crystalline impurities do not take part in geopolymerization reactions and hence are present as unreacted fillers in the geopolymer matrix [14]. The presence and variability of various impurities is a setback for the use of metakaolin derived from natural kaolin, as a precursor for geopolymer stationary phases.

The current study presents the chromatographic evaluation of the first geopolymer synthesized using entirely synthetic aluminosilicate precursor to overcome the drawbacks of using natural metakaolin. We show that under the proposed synthetic scheme, spherical and porous geopolymers particles can be made reproducibly and conveniently. The chromatographic performance is compared with natural metakaolin geopolymer and another highly pH stable stationary phase known as Hypercarb^{TM}. Further, this work explicates the fundamental chromatographic properties of geopolymers synthesized using new synthetic raw material and shows its applications as a new HILIC phase.

4.3 Materials and methods

4.3.1 Chemicals and reagents

Tetraethylorthosilicate (TEOS), aluminum nitrate nonahydrate (ANN), fumed silica (CAS no. 112945-52-5), and potassium hydroxide was purchased from Millipore Sigma (MO, U.S.A.). Metakaolin was obtained from Advanced Cement Technologies (WA, U.S.A.). All solvents including hexane and acetonitrile were HPLC grade and purchased from EMD (Gibbstown, NJ, U.S.A.). Milli-Q water purification system (Millipore, Billerica, MA, U.S.A.) was employed to purify water. Ammonium acetate, ammonium hydroxide (ACS reagent, 28-30 % on NH_3 basis), acetic acid, ethylenediamine acetic acid (EDTA) and all analytes were obtained from Sigma–Aldrich (Milwaukee, WI, U.S.A.).

4.3.2 Apparatus and instrument

Hitachi S-4800 II Field Emission SEM (FE-SEM) was used to take SEM images under a high vacuum and acceleration voltage of 20 kV. The geopolymer particles were coated with a thin

conductive layer of silver using CrC-100 sputtering system before acquiring scanning electron microscopy (SEM) images. An EDAX EDS system on FE-SEM was used to do elemental analysis without coating. The X-Ray diffraction pattern was obtained by using Shimadzu MAXima X XRD-7000 X-ray diffractometer. Shimadzu SALD-7101 laser diffraction particle size analyzer was used to determine particle size and particle size distribution. The Brunauer–Emmett–Teller (BET) surface area analysis was performed using Micrometrics ASAP 2020 Porosimeter. The samples were first degassed at 90 ºC for 24 hours to remove any adsorbed species from the samples. An Agilent 1200 HPLC series system (Agilent Technologies, Palo Alto, CA) was used for all LC separations which consist of 1200 diode array detector (DAD), a quaternary pump, thermostat, and an autosampler. The wavelengths of UV detection were set at 220, 230, 254 and 280 nm for detection and identification of the analytes. The mobile phases were degassed prior to analysis by ultrasonication under vacuum. All LC separations were done using the isocratic method and at room temperature unless specified. The LC data acquisition was done using Agilent Chemstation software (Rev. B.03.02 [341])

4.3.3 Synthesis

4.3.3.1 Synthesis of $Al_2O_3.2SiO_2$ powders

The synthesis of $Al_2O_3.2SiO_2$ powder was done according to the sol-gel methods, the chemistry of which has been described in earlier reports [15, 16]. Aluminum nitrate nonahydrate, ANN, was dissolved in a mixture of water and ethanol in a 250 mL Erlenmeyer flask. Then, TEOS was added slowly and dropwise in the ANN solution. The flask was put in an oil bath maintained at 70 ºC until a gel was formed. The gel was then dried at 110 ºC for 1 hour. Finally, the gel was calcined to yield powders at 750 ºC using a ramp rate of 5 ºC/min for 2 hours (Paragon controlled by Sentry

2.0 Microprocessor). The oven atmosphere was not controlled. The powders were crushed using a mortar and pestle for further use in the geopolymerization reaction.

4.3.3.2 Synthesis of synthetic aluminosilicate based geopolymer microparticles

The totally synthetic aluminosilicate based geopolymer (Syn-GP) microparticles were synthesized by generating an inverse suspension of aqueous geopolymer slurry in canola oil[5, 17]. The geopolymer slurry was prepared by dissolving 5.18 g of potassium hydroxide, 3.30 g of fumed silica and 6.17 g of synthetic $Al_2O_3.2SiO_2$ powders in 12.5 mL of deionized water. The amounts were selected such that the Si/Al/K initial molar ratio was 2:1:2. The aqueous slurry was then added in a large volume (400 mL) of canola oil under mechanical stirring in a 500 mL polypropylene beaker. An overhead stirrer consisting of the three-blade propeller (Talboys 101, Troemner, Thorofare, NJ, U.S.A.) was used. The stirring speed was maintained at 5000 rpm. The geopolymerization reaction was continued for 24 hours at room temperature. The particles thus formed, were extracted in water. The particles were washed using hexane, methanol, and water to remove excess oil and surfactants. The particles were then calcined at 500 ºC for 4 hours using a ramp rate of 2 ºC/min. The multiple batches of the Syn-GP particles were found to be reproducible using EDS based atomic ratios. The batch to batch reproducibility of geopolymer particles has been shown in our previous work [5]. The de-fining of the particles was done using water to remove large particles and fines. The natural metakaolin based geopolymers (NM-GP) were also synthesized using the above procedure for allowing chromatographic comparison with synthetic geopolymers.

4.3.3.3 Packing

The dried clean particles were packed in 10 cm x 3 mm i.d. column (Shepard Inc.) using dispersed slurry techniques at 0 – 10,000 or 11,000 psi using Haskel pneumatic pump with methanol as a push solvent.

4.4 Results and discussions

4.4.1 Synthesis and Characterization of synthetic metakaolin geopolymer

This work aims to introduce a new class of geopolymers, synthesized using fully synthetic aluminosilicate precursor, with different selectivity in liquid chromatography. The geopolymers were synthesized by reacting synthetic aluminosilicate with aqueous potassium silicate in an oil suspension. As the geopolymer slurry has excess KOH, it reacts with the triglycerides in the canola oil to form soaps. The soaps assist in stabilizing water-in-oil (W/O) suspensions of particles, where each aqueous droplet acts as a mini-reactor for geopolymerization. Spherical microparticles are formed as a result. Before the new phase can be used in HPLC, it is imperative to fundamentally assess their physical properties such as shape, particle size, particle size distribution, surface area and, pore size. These physical parameters control the efficiency and retention characteristics of the chromatographic column, ultimately affecting the resolution [18]. The scanning electron microscopy image (Figure 4.1A) of the synthesized and defined Syn-GP particles clearly demonstrates the spherical shape of particles. By optimizing the stirring speed, stirrer height, vessel shape and the amount of oil in the vessel, one can avoid the formation of broken particles or particles with large cavities as were seen in scanning electron micrographs in preliminary experiments [19]. The key observation was that the stirring arrangement should provide turbulence free mixing of aqueous geopolymer droplets and canola oil. Modern HPLC demands spherical and smaller particle sizes because the irregular shape and large diameter particles can lead to sizeable

interstitial space in the column bed and are prone to flow mal-distribution [20]. Moreover, column packing science favors the use of spherical particles for analytical chromatography to form a random close packing [21]. Stirring speed is the most convenient way to manipulate the particle size. The radical effects of stirring speed on particle size have been reported previously [17]. In the current study, the shear rate of 5000 rpm was employed to get the smallest spherical particle sizes. It was also observed that using excessive speeds led to frictional heating of the reaction mixture and consequently led to coagulation.

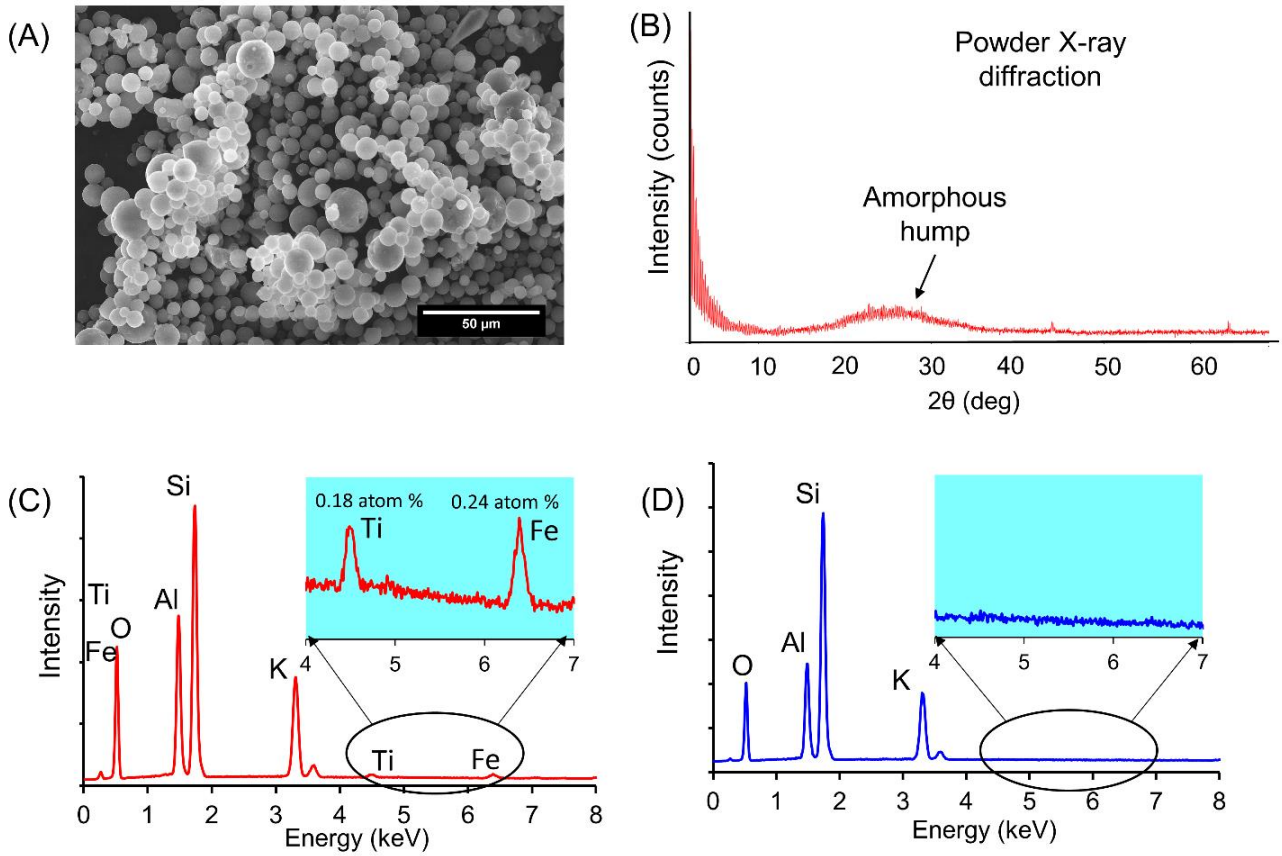

Figure 4.1 Physicochemical characterization of aluminosilicate geopolymers A) Scanning electron micrographs of Syn-GP B) XRD pattern of Syn-GP C) Energy dispersive spectrum of NM-GP D) Energy dispersive spectrum of Syn-GP. The elemental analysis shows the absence of Fe and Ti in Syn-GP

Laser diffraction particle size distribution data showed the median diameter to be 5.1 µm (See Figure 4.S1). The current particle size distribution is rather broad as compared to commercial stationary phases and further research is on-going to reduce the particle size distribution. The Brunauer-Emmett-Taylor (BET) surface area and Brunauer-Joyner-Halenda (BJH) desorption pore size of de-fined Syn-GP particles were 150 m^2/g and 120 Å respectively. The BET analysis (Figure 4.S3) showed the characteristic hysteresis loop of Type IV isotherm indicating the presence of a mesoporous structure [22]. The hysteresis loop is of Type H1 [23]. The pore shape is most likely cylindrical, as interpreted from the BET isotherm [24]. The magnified SEM image of a single synthetic particle captured at high magnification (x 30k) is shown in Figure 4.S2. The pore size distribution ranges from approximately 6-20 nm (Figure 4.S4). The high surface area and adequate pore size increase the retention of the analytes. Generally, smaller pore sizes infer higher surface areas, but it is also important that pores should be easily accessible by the analytes. The pore size of 60-150 Å is desirable for small molecules, and is comparable to fully porous silica and superficially porous particles [25]. The BET surface area and BJH desorption pore size of defined NM-GP synthesized in this study for comparison with Syn-GP were 183 m^2/g and 63 Å. The formation of geopolymers using synthetic aluminosilicate is confirmed by the characteristic amorphous hump between the 2θ value of 25-30º shown in Figure 4.1B [2]. Also, note that the absence of crystalline impurities in the final product according to XRD data.

The energy dispersive spectrum of NM-GP shown in Figure 4.1C, visibly indicates the presence of the transition metal impurities, Fe and Ti in NM-GP (potential Lewis acid sites). It should be noted that EDS can be considered as a bulk technique as its typical sampling depth can reach 5000 Å and can increase on increasing the accelerating voltage (as 30 kV was used here) [26]. Hence, the quantitative data pertains to much deeper layers than just surface analysis, unlike X-ray

photoelectron spectroscopy. The lower limit of detection (LOD) for SEM-EDS is approximately 0.08 wt% [27]. EDS determined 0.18 atom % and 0.24 atom% of Fe and Ti (which corresponded to 0.66 wt% and 0.42% of Fe and Ti respectively) in NM-GP. The EDS spectrum of Syn-GP (Figure 4.1D) shows that transition metals are absent or are below the LOD in Syn-GP for this method.

The packing of the particles into a stable bed is another crucial step to assess the chromatographic performance of the new stationary phase. Unlike silica-based phases, geopolymer particles posed significant challenges as most combinations of organic solvents could not stabilize the suspension. Finally, a viscous solvent medium was chosen consisting of methanol and 2-ethyl-1-hexanol (among >10 solvent systems studied) which also dispersed the particles and kept the particles suspended. Since the mechanical stability of the packed bed is also essential, the geopolymer was packed at 11,000 psi. The optimum slurry concentration in this study was found to be 30% for Syn-GP and 35% for NM-GP. The efficiency of 30,000 per meter was achieved for both Syn-GP and NM-GP columns, using toluene as a probe molecule. The efficiencies needed to be similar in this study because the peak shape discrepancies should not arise from the packing. The mechanical strength of the Syn-GP and NM-GP was assessed by packing the particles in an HPLC column at 11000 psi and subsequently unpacking the column. The SEM of the particles acquired after unpacking the column showed no signs of breakage.

4.4.2 Effect of trace transition metals on the chromatographic performance of geopolymers

The separation of benzene, phenol, resorcinol, and phloroglucinol on NM-GP and Syn-GP is shown in Figure 4.2. The chromatograms highlight the better chromatographic performance of Syn-GP as compared to NM-GP under identical conditions. The USP tailing factors of benzene,

phenol, and resorcinol on NM-GP are 1.81, 2.41 and 3.16 respectively. The tailing factor of phloroglucinol could not be determined because of the extensive peak tailing which led to almost nine minutes wide peak. Peak tailing under linear conditions is observed due to the presence of more than one interaction sites [28], hence leading to mixed retention mechanism (see Section 3.3.2). Phenolic compounds are known to form complexes with transition metals especially Fe and Ti. This complex formation can lead to slow mass transfer kinetics on secondary transition metals sites in the case of NM-GP. On the other hand, the USP tailing factor of benzene, phenol, resorcinol and phloroglucinol on synthetic geopolymer were 1.80, 1.50, 1.75 and 1.96 respectively. The relatively low tailing factors in case of Syn-GP can be directly attributed to the absence of the undesirable secondary interactions.

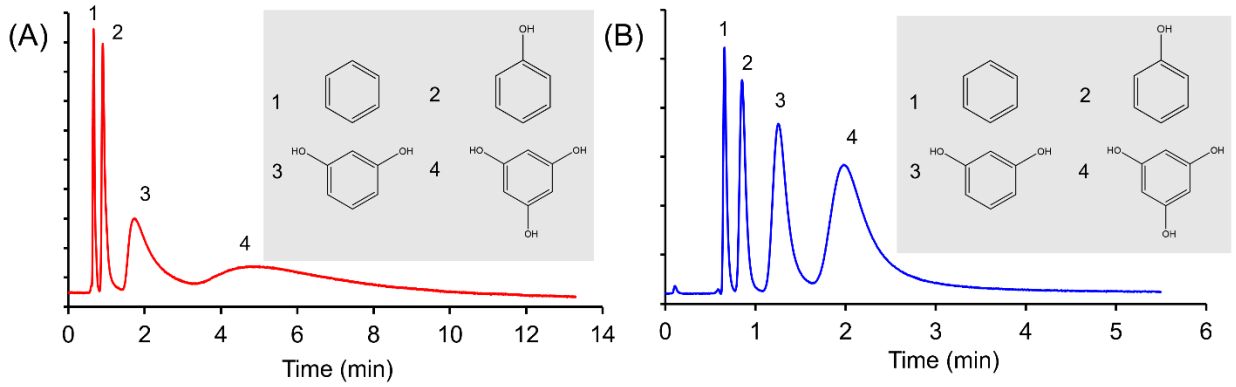

Figure 4.2 Effects of transition metals on peak shape of phenols. Separation of 1) benzene 2) phenol 3) resorcinol 4) phloroglucinol on A) NM-GP B) Syn-GP. Column dimensions: 10 cm x 3 mm i.d., mobile phase: 80/20 hexane/ethanol, flow rate: 0.80 mL/min, UV detection at 220 nm

To verify the above observation, a chromatographic experiment was designed based on a simple proposition. If transition metals are the real cause of peak tailing, then masking these interaction

sites would lead to symmetrical peak shapes as analytes will not interact with the metals. For this purpose, ethylenediaminetetraacetic acid (EDTA) was tested as a mobile phase additive to quench undesirable active sites. EDTA is a well-known chelating agent which readily forms coordination complexes with metal ions with large formation constants [29]. The formation constants (log K_f) for Fe^{2+}-EDTA and Ti^{3+}-EDTA is 14.3 and 21.3 respectively [29]. A chelating analyte, 2-hydroxybenzoic acid was chosen for this experiment. A HILIC mobile phase comprising of 90/10 ACN/100 mM NH_4OAc (pH=10) was used so that EDTA can be solubilized. Figure 4.3A shows the peak tailing observed for 2-hydroxybenzoic acid on NM-GP.

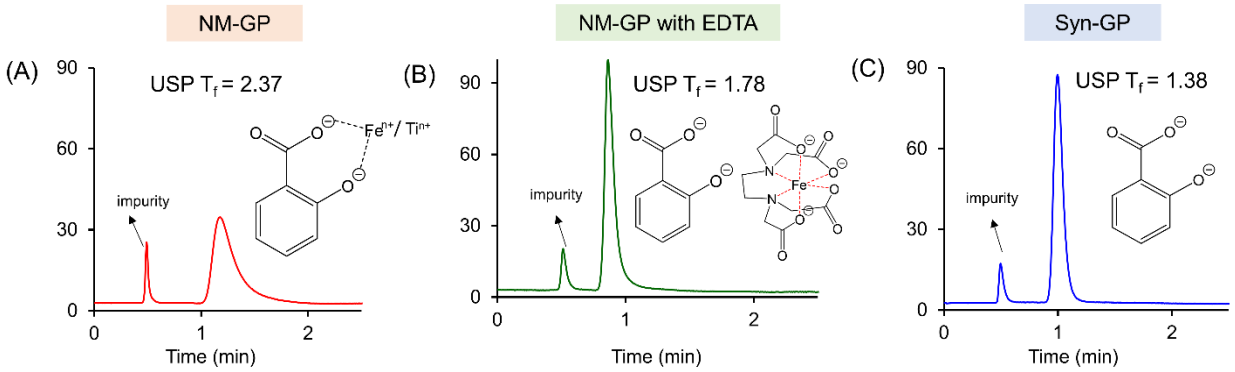

Figure 4.3 Illustration of peak shape differences of 2-hydroxy benzoic acid with and without EDTA as additive. A) Column: NM-GP, mobile phase: 90/10 ACN/100mM NH_4OAc pH= 10 B) Column: NM-GP, mobile phase: 90/10 ACN/100mM NH_4OAc, pH= 10 with 0.5 mM EDTA C) Column: Syn-GP mobile phase: 90/10 ACN/100mM NH_4OAc, pH= 10. Column dimensions: 10 cm x 3 mm i.d., flow rate 0.850 mL/min, UV detection at 220 nm

The USP tailing factor was 2.37. The peak tailing reduced substantially and the USP tailing factor reduced to 1.78 when EDTA was added to the mobile phase (Figure 4.3B). This shows that EDTA is sequestering the transition metal sites; hence analyte does not get the chance to interact with the

metals. EDTA will bind preferably to metals rather than 2- hydroxybenzoic acid as EDTA is hexadentate, and 2-hydroxybenzoic acid is bidentate. It should also be noted that peak tailing deteriorates the sensitivity. The analysis on Syn-GP gave similar results as in the case, where EDTA concealed the metals in NM-GP (Figure 4.3C). In this case, the USP tailing factor was 1.38. This straightforward experiment proved that the origin of peak tailing in NM-GP is indeed from the presence of transition metals.

4.4.3 Investigation of selectivity properties of synthetic aluminosilicate based geopolymers

4.4.3.1 Selectivity in HILIC mode

As stated earlier, the goal was to develop geopolymer using synthetic aluminosilicates as a stationary phase with different selectivity. It was desired that separations were carried in HILIC mode since this material was hydrophilic and pH stable (*vide infra*) whereas silica-based HILIC phases are notorious for dissolution and bleeding issues. To semi-quantitatively assess the "hydrophilicity" and "electrostatic" character of stationary phases, we employed the Irgum-Lucy graphical approach to classify stationary phases based on the selectivity of cytosine/uracil on the x-axis and benzyl trimethylammonium chloride/cytosine pair on the y-axis- [30, 31]. The y-axis is plotted on a log-10 scale to show the grouping, whereas the x-axis is on a linear scale. In Figure 4.4, we compare 35 stationary phases with the synthetic aluminosilicate based geopolymers. It is clear from the comparative data the Syn-GP has a separate position in the HILIC chart, i.e., it has hydrophilic character as well as ion-exchange character, which is good for mixed mode chromatography. The ion-exchange and mixed mode character are further probed below.

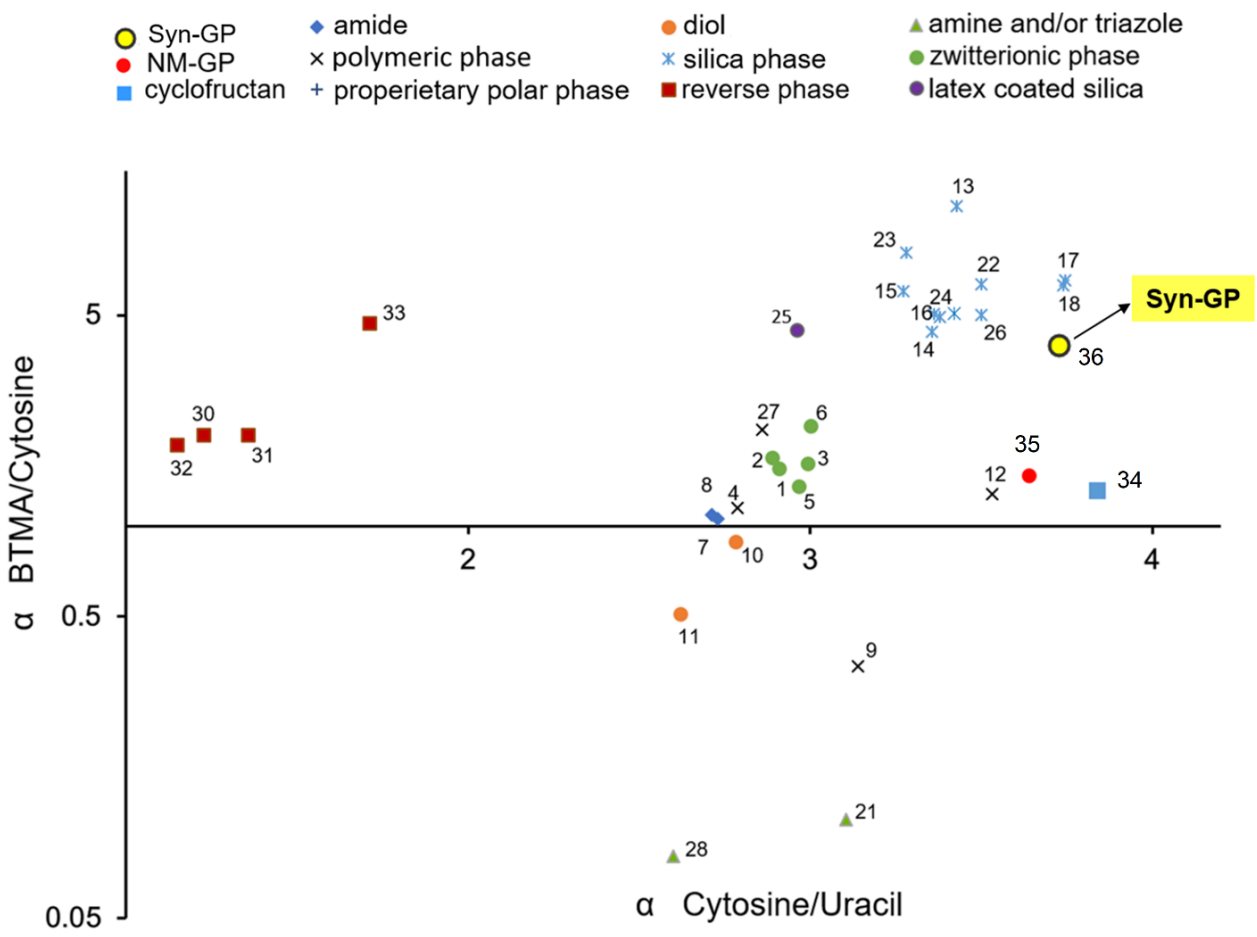

Figure 4.4 Hydrophilicity and ion-exchange selectivity of Syn-GP compared to other stationary phases chemistries. Column dimensions: 10 cm x 3 mm i.d., mobile phase: 80/20 ACN/25 mM NH_4OAc, flow rate: 0.425 mL/min, UV detection at 254 nm. The names of the stationary phases and their characteristics are provided in supporting information, Table 4.S1, and references [30, 31]

4.4.3.2 Ion-exchange and mixed mode behavior

Based on the information provided by the HILIC selectivity chart, the Syn-GP has mixed-mode character. The theory of liquid-liquid partitioning due to the immobilized water layer on polar

stationary phases in HILIC is often quoted [32]. Besides the presence of water layer available for partitioning, other interactions like hydrogen bonding, ion exchange interactions, hydrophilic and hydrophobic interactions are also present between the analyte and the surface of the stationary phase. This essentially makes an Syn-GP a promising mixed mode HPLC support. Underivatized surfaces of HILIC stationary phases such as that of titania and zirconia, always show this mixed mode retention mechanism, often phosphate and fluoride salts are needed as mobile phase additives to sequester Lewis acid sites [33, 34]. A similar investigation for probing the retention characteristics of the Syn-GP was carried out by judiciously choosing a neutral, negatively and positively charged analytes (uridine, 4-aminobenzoic acid, and benzyl trimethylammonium chloride). The retention factor was studied as a function of acetonitrile content with a fixed total aqueous buffer concentration. Figure 4.5 summarizes the results. The neutral molecule, uridine, and the negatively charged molecules, 4-aminobenzoic acid, showed no retention at low ACN percentage and their relative retention increased very rapidly with an increase in ACN content. BTMA was employed to probe the electrostatic character of newly developed HILIC phases [5]. The BTMA probe, with its permanently positive charge showed an interesting U-shaped curve, i.e., it showed very large k values in the water rich mobile phase buffer as well as at high ACN %. The geopolymers can undergo ion-exchange processes, as is known for small inorganic ions [35], the retention in pure aqueous medium was ascribed to a pure ion-exchange process. To further confirm this hypothesis, a log k- log [NH_4^+] plot was made without ACN. As per the ion-exchange theory, a linear relationship indicates an ion-exchange mechanism and the slope magnitude indicates the charge of the analyte [36, 37]. In the case of BTMA, the slope of the curve is -1.05 with a correlation coefficient value of 0.9997, strongly supporting the ion-exchange behavior of a singly charged cation (quaternary amine in this case). This mixed mode retention is often beneficial

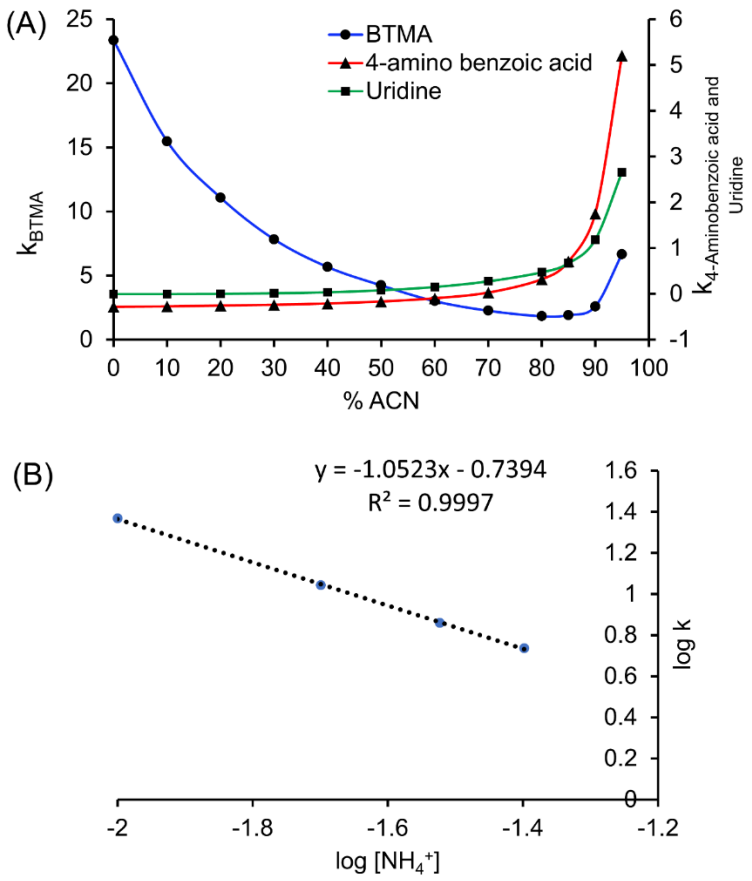

Figure 4.5 A) Retention characteristics of Syn-GP as a function of ACN concentration. B) Plot of log (retention factor k) vs. log [NH_4^+]

for imparting unique selectivity characteristics and in cases where the set of analytes have a wide range of polarities and charges (cations, anions and, neutrals).

4.4.4 High pH applications on synthetic aluminosilicate based geopolymers

It was recently demonstrated in our previous study that natural metakaolin based geopolymer phases are water and base stable supports [5]. In the current work, we tested the Syn-GP column for hydrolytic and high pH stability and developed an application showing the exploitation of pH

as a chromatographic parameter to tune selectivity and resolution. Eluent pH is the next most powerful chromatographic parameter to control the selectivity of ionizable solutes, after the altering stationary phase and solvents. Figure 4.6A compares the separation of 7 acidic analytes at a pH of 6.8 and 10.0.

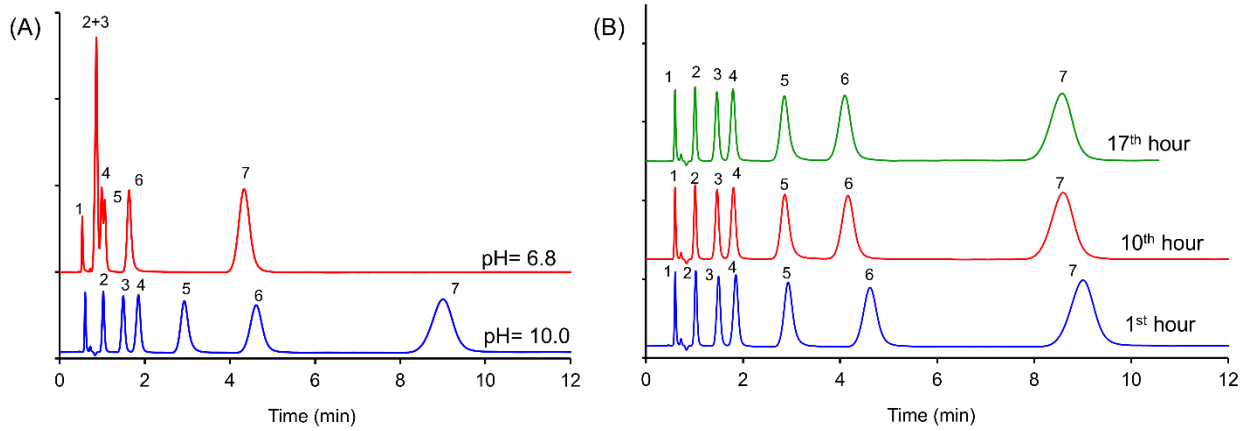

Figure 4.6 A) Separation of acidic analytes at high pH. 1) hydroxy naphthoic acid 2) nitro benzoic acid 3) benzoic acid 4) indole acrylic acid 5) 4-hydroxyphenylacetic acid 6) diphenic acid 7) 3-sulfobenzoic acid on Syn-GP at pH 6.8 and 10.0. Column dimensions: 10 cm x 3 mm i.d., mobile phase: 90/10 ACN/ 25mM NH_4OAc, flow rate: 0.85 mL/min, UV detection at 220 nm. B) Demonstration of high pH stability of Syn-GP. Column dimensions: 10 cm x 3 mm ID, mobile phase: 90/10 ACN/ 25mM NH_4OAc pH=10.0., flow rate: 0.85 mL/min, UV detection at 220 nm.

The mixture was baseline separated at pH 10.0, but the neutral pH led to complete co-elution of benzoic acid and 4-nitrobenzoic acid and partial separation of indole acrylic acid and 4-hydroxyphenyl acetic acid. In this case, prior knowledge of the pK_a of an analyte can help to control the state of the analyte which in turn, controls the retention as the chemistry of the analyte completely changes. At high pH, acidic analytes generally exist as negatively charged entities. Since in HILIC, hydrophilicity is one of the criterions for retention and it is well known that ionized

species are more hydrophilic than their neutral counterparts, the retention increases along with ionic strength effects. As can be seen clearly, the retention relatively increased for the mixture of acids at pH 10 as compared to pH 6.8, hence ultimately altering the resolution. The differences in retention for reverse phase liquid chromatography (RPLC) and HILIC do not surprisingly show opposite trends. In RPLC, acidic analytes are well retained at low pH (in neutral form) and basic analytes are retained at high pH (in neutral form). Conversely, in HILIC acidic analytes are expected to retain at high pH and basic analytes are retained in low pH.

Long term chemical stability is a critical parameter for a chromatographic stationary phase. Low hydrolytic and pH stability are serious shortcomings of various HILIC stationary phase chemistries [5, 38]. Silica, the most widely used support, is well known for its drawbacks of hydrolytic and high pH instability. Also, the dissolution of silica occurs at much faster rates at high pH and in highly aqueous systems [39]. This instability of silica in HILIC mode was demonstrated in our previous work [40]. This causes significant retention time drift and loss in column efficiency over time. Eventually, the continuous exposure to high pH leads to the destruction of the silica bed, rendering the column unusable. Figure 4.6B illustrates the stability of the Syn-GP column against continuous aggressive high pH-10 mobile phase. The mixture of acids was injected for every 30 minutes for 17 hours without recycling the mobile phase. The retention times did not show any significant drift in retention times which indicates the ruggedness of the Syn-GP phase under high pH conditions. This study has also been done in our previous study for NM-GP particles [5].

4.4.5 Comparison of Geopolymers with Porous Graphitic Carbon for Its Retention of Polar Compounds

Whenever a new stationary phase is proposed, it is imperative to compare its selectivity and figures of merit with already available materials. As shown earlier, one of the main features of geopolymers is their resistance to pH. Porous graphitic carbon (PGC) is another material which can be used at all pHs and it is inert to most solvents like geopolymers [41]. PGC consists of sheets of extremely pure graphite with a porous structure and spherical shape formed by pyrolyzing polymers embedded in silica (which is later dissolved) [42]. PGC has been referred to as a superhydrophobic stationary phase as compared to C18 because it requires more acetonitrile to elute hydrophobic compounds. On the other hand, it retains polar compounds with excellent selectivity by an effect termed as the polar retention effect on graphite (PREG) [42]. It is postulated that traces of oxygen functional groups on the surface (phenolic, carboxylic, quinones) are perhaps responsible for these effects [38]. PGC is commercially known as Hypercarb. In Figure 4.7, the new geopolymer phase Syn-GP is compared with 3 μm fully porous particles under optimized conditions for both column chemistries to provide a fair comparison. Hypercarb was operated in reversed phase mode and geopolymer was operated in HILIC mode. Three derivatized sugars, benzylidene-D-threitol, phenyl-β-D-galactopyranoside and 4-nitrophenyl-β-maltoside, were chosen as probes. Initially PGC was also tested in the HILIC mode and as expected, it could not separate all three derivatized sugars, given its hydrophobic nature. However, the reversed phase mode separated all three derivatized sugars with very high resolution. Syn-GP, on the other hand, needed HILIC mode. As it can be seen, Syn-GP and Hypercarb have permuted 1-2-3 vs. 2-1-3 peaks. Therefore, both Hypercarb and Syn-GP could form an orthogonal set. An interesting fact is that the larger sugar molecule with more hydroxyl group was eluted last for both phases. This is

for completely different reasons. More hydroxyl groups in HILIC means more retention whereas it is the p-nitrophenyl group that forms a strong π-π interactions in PGC. Such type of orthogonal selectivity would definitely be useful in two-dimensional liquid chromatography.

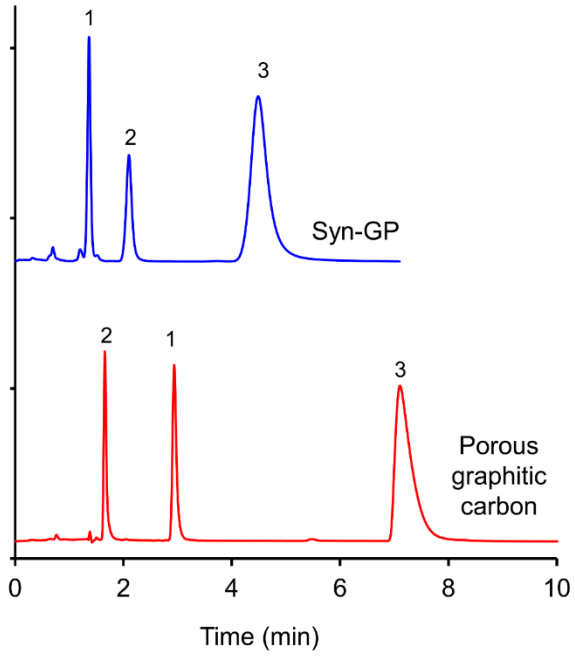

Figure 4.7 Comparison of porous graphitic carbon (Hypercarb) with Syn-GP. Analytes: 1) (+)-2,3-O-Benzylidene-D-threitol 2) phenyl-β-D-galactopyranoside 3) 4-nitrophenyl-β-maltoside. Column dimensions: 10 cm x 3 mm, mobile phase: 90/10 ACN/H_2O, pH= 6.8, flow rate: 0.425 mL/min, UV detection at 220 nm

The high pH stability of Syn-GP can be applied in case of separation of underivatized sugars. Anomerization of underivatized sugars often presents the problem of split peaks, which complicates the chromatographic analysis [43]. One of the solutions to obtain singlet peaks is increasing the mutarotation reaction rate by base or acid catalysis. Base catalysis has been shown to remove the anomeric doublets effectively as compared to acid catalysis, in case of silica support

[43]. However, silica runs a risk of alkaline degradation. Hence, in the case of Syn-GP, the base stability can be rewarding. Since the sugars used in our analysis are derivatized at anomeric carbon, there was no need to employ high pH to prevent anomerization of sugars. Nevertheless, Syn-GP was also able to separate the sugars at pH 11 (data not shown).

Besides selectivity, column efficiency is also important for a new phase. The peaks were modeled as an exponentially modified Gaussian to account for the tailing and reflect the true column performance. Moment analysis was done for the three peaks using PeakFit^{TM}. The efficiency of phenyl-β-D-galactopyranoside, (+)-2,3-*O*-Benzylidene-D-threitol and 4-nitrophenyl-β-maltoside are 3480, 5076, 1044 plates respectively on 10 cm column with 3 μm particles. Note that the Gaussian efficiencies on Hypercarb were 6000, 8100, and 3300 respectively. The median particle size of Syn-GP is 5.1 μm. The efficiency from second moments of (+)-2,3-*O*-Benzylidene-D-threitol, phenyl-β-D-galactopyranoside and 4-nitrophenyl-β-maltoside were 2400, 1700, 600 respectively. The asymmetry for Hypercarb and Syn-GP are both under 2, which is a requirement for USP and accurate quantitation. This compares very well with the efficiency of Hypercarb except for the middle peak. Further work would be undertaken to reduce the particle size of Syn-GP with uniform particle size distribution.

4.4.6 Selectivity change with temperature

Thermal stability of a stationary phase is advantageous in high-temperature chromatography applications [44, 45]. Column temperature can be used to tune retention and selectivity in liquid chromatography based on thermodynamic considerations [44]. The effects of temperature have been seen to be more pronounced in the case of polar and ionizable molecules [46]. Hence temperature can play a very important role in optimizing separations in the case of HILIC as it is

designed for polar/ionizable analytes. Silica is the most common solid support available in a wide range of particle sizes and pore sizes. However, the long-term thermal stability of silica is not adequate for high-temperature chromatographic applications. At room temperature and neutral pH, silica column shows drift due to finite solubility of silica. Solubility of silica is expected to with an increase in temperature. Metal oxide phases like zirconia, titania and alumina are known for their thermal stability. Geopolymers have been shown to be thermally stable at least up to 800 ℃ just like other metal oxide phases [47]. Above this temperature, geopolymers generally start transitioning to crystalline materials. Figure 4.8 shows the change in selectivity of a wide range of analytes with a change in temperature.

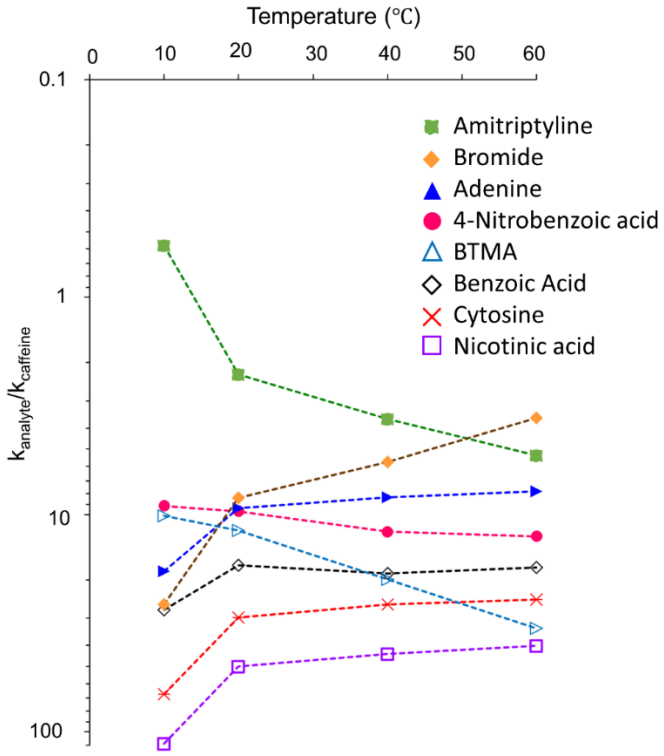

Figure 4.8 Plot of temperature vs. α (with respect to caffeine). Column: Syn-GP. Mobile phase: 90/10 ACN/ 15 mM NH_4OAc, pH= 6.8. Column dimensions: 10 cm x 3 mm, flow rate: 0.425 mL/min, UV detection at 220 nm

For this study, small neutral molecules, acids, bases, and inorganic ions were chosen. Four different temperatures at 10 ℃, 20 ℃, 40 ℃, and 60 ℃ were monitored at neutral pH. The temperature was not raised above 60 ℃ because the boiling point of acetonitrile is 82 ℃ (bubbles form in the detector). The α with respect to caffeine was plotted against temperature. As expected, for most of the analytes, alpha decreased with an increase in temperature. It is postulated that the partition coefficient will decrease as a function of temperature. Additionally, peak shape improvement was observed. For instance, the peak efficiency of nicotinic acid was 1904 at 10 ℃ while it increased to 2300 at 60 ℃. Similarly, the peak efficiency of cytosine increased from 1999 at 10 ℃ to 2440 at 60 ℃. Benzyltrimethyl ammonium chloride (BTMA) presented an interesting case as its selectivity (α) was observed to increase with an increase in temperature. Interestingly, even though retention of BTMA increased with increase in temperature, the efficiency did not change drastically like other probes. On the contrary, the peak efficiency of BTMA was 2554 at 10 ℃ while it increased to 2716 at 60 ℃. The C term (mass transfer coefficient) in the van Deemter equation decreases significantly as the temperature is increased [45]. It has been previously shown that most of this decrease arises from the solute's diffusion coefficient rather than solute's retention factor [45]. Amitrypline, a tertiary amine, also showed the same behavior. The chromatographic thermal stability of Syn-GP was assessed by a hysteresis study. The chromatography on Syn-GP column was first performed at 20 ℃, then at 60 ℃ and then again at 20 ℃. No drifts in the retention times of the analytes was observed. Also, Syn-GP did not show any swelling (marked by high back pressure), unlike polymer phases at high temperatures, rather the back pressure decreased due to the decrease in viscosity of the mobile phase at high temperature. Therefore, it also opens the avenue of fast separations by using high flow rates without compromising the bed quality.

4.5 Conclusions

A new pH and temperature stable synthetic aluminosilicate based geopolymer has been introduced as a stationary phase for liquid chromatography. Extensive characterization by X-ray diffraction, laser diffraction, energy dispersive spectroscopy, BET and BJH was done to thoroughly investigate the potential of geopolymers in separation science. By eliminating traces of Fe and Ti impurities, considerable peak shape improvements were observed. It was demonstrated that a transition metal free geopolymer particles can be reproducibly prepared in a two-step process by polycondensation of synthetic aluminosilicates in a highly alkaline medium. The microparticles are mechanically stable for high pressure chromatographic purposes. Additionally, the synthetic aluminosilicates based geopolymers extend the pH window as compared to traditional stationary phases based on silica. The complementary selectivity with another base stable material (porous graphitic carbon) for sugars shows the promise of new support 2-dimensional liquid chromatography.

4.6 References

[1] USP Chromatographic Columns, https://www.uspchromcolumns.com/chrom/display (requires user registration, accessed 21st June 2019)

[2] J. Davidovits, Geopolymers: inorganic polymeric new materials, Journal of Thermal Analysis and calorimetry, 37 (1991) 1633-1656.

[3] B. Singh, G. Ishwarya, M. Gupta, S. Bhattacharyya, Geopolymer concrete: A review of some recent developments, Construction and building materials, 85 (2015) 78-90.

[4] M. Alzeer, R.A. Keyzers, K.J. MacKenzie, Inorganic polymers as novel chromatographic stationary phase media, Ceramics International, 40 (2014) 3553-3560.

[5] R.M. Wimalasinghe, C.A. Weatherly, M.F. Wahab, N. Thakur, D.W. Armstrong, Geopolymers as a New Class of High pH Stable Supports with Different Chromatographic Selectivity, Analytical Chemistry, 90 (2018) 8139-8146.

[6] M. Verzele, M. De Potter, J. Ghysels, Trace elements in HPLC silica gel, Journal of High Resolution Chromatography, 2 (1979) 151-153.

[7] J. Nawrocki, Silica surface controversies, strong adsorption sites, their blockage and removal. Part I, Chromatographia, 31 (1991) 177-192.

[8] J.C. Giddings, Kinetic Origin of Tailing in Chromatography, Analytical Chemistry, 35 (1963) 1999-2002.

[9] L. Vickers, A. van Riessen, W.D.A. Rickard, Precursors and Additives for Geopolymer Synthesis, Fire-Resistant Geopolymers: Role of Fibres and Fillers to Enhance Thermal Properties, Springer Singapore, Singapore, 2015, pp. 17-37.

[10] P. Duxson, A. Fernández-Jiménez, J.L. Provis, G.C. Lukey, A. Palomo, J.S. van Deventer, Geopolymer technology: the current state of the art, Journal of materials science, 42 (2007) 2917-2933.

[11] A. Autef, E. Joussein, A. Poulesquen, G. Gasgnier, S. Pronier, I. Sobrados, J. Sanz, S. Rossignol, Influence of metakaolin purities on potassium geopolymer formulation: the existence of several networks, Journal of colloid and interface science, 408 (2013) 43-53.

[12] J. Adams, J. Hooper, A. Gil, Clays, Encyclopedia of Materials: Science and Technology (Second Edition), (2001) 1236-1242.

[13] M. Gougazeh, Removal of iron and titanium contaminants from Jordanian Kaolins by using chemical leaching, Journal of Taibah University for Science, 12 (2018) 247-254.

[14] J. He, J. Zhang, Y. Yu, G. Zhang, The strength and microstructure of two geopolymers derived from metakaolin and red mud-fly ash admixture: a comparative study, Construction and building materials, 30 (2012) 80-91.

[15] M. Catauro, F. Bollino, A. Dell'Era, S.V. Ciprioti, Pure $Al_2O_3 \cdot 2SiO_2$ synthesized via a sol-gel technique as a raw material to replace metakaolin: Chemical and structural characterization and thermal behavior, Ceramics International, 42 (2016) 16303-16309.

[16] G. Zheng, X. Cui, D. Huang, J. Pang, G. Mo, S. Yu, Z. Tong, Alkali-activation reactivity of chemosynthetic Al_2O_3–$2SiO_2$ powders and their ^{27}Al and ^{29}Si magic-angle spinning nuclear magnetic resonance spectra, Particuology, 22 (2015) 151-156.

[17] N. Thakur, C.A. Weatherly, R.M. Wimalasinghe, D.W. Armstrong, Fabrication of interconnected macroporosity in geopolymers via inverse suspension polymerization., Journal of American Ceramic Society, 102 (2019) 4405-4409.

[18] D. Corradini, Handbook of HPLC, CRC Press, Boca Raton, FL 2016.

[19] R. Arshady, Suspension, emulsion, and dispersion polymerization: A methodological survey, Colloid and polymer science, 270 (1992) 717-732.

[20] D.T.T. Nguyen, D. Guillarme, S. Rudaz, J.L. Veuthey, Fast analysis in liquid chromatography using small particle size and high pressure, Journal of Separation Science, 29 (2006) 1836-1848.

[21] M.F. Wahab, D.C. Patel, R.M. Wimalasinghe, D.W. Armstrong, Fundamental and practical insights on the packing of modern high-efficiency analytical and capillary columns, Analytical chemistry, 89 (2017) 8177-8191.

[22] J.B. Condon, Surface area and porosity determinations by physisorption: measurements and theory, Elsevier, Amsterdam, Netherlands 2006.

[23] M. Thommes, K. Kaneko, A.V. Neimark, J.P. Olivier, F. Rodriguez-Reinoso, J. Rouquerol, K.S. Sing, Physisorption of gases, with special reference to the evaluation of surface area and pore size distribution (IUPAC Technical Report), Pure and Applied Chemistry, 87 (2015) 1051-1069.

[24] B. Xue, J. Zhang, X. Tang, C. Yang, Q. Chen, X. Man, W. Dang, Micro-pore Structure and Gas Accumulation Characteristics of Shale in the Longmaxi Formation, Northwest Guizhou, Petroleum Research, 1 (2016) 191-204.

[25] J.W. Dolan, Problems with large molecules separations, LCGC North America, Volume 32 Number 4 (2014).

[26] S. Ebnesajjad, Surface and material characterization techniques, Handbook of Adhesives and Surface Preparation, Elsevier, Oxford UK 2011, pp. 31-48.

[27] S.J.B. Reed, Electron microprobe analysis and scanning electron microscopy in geology, Cambridge University Press, Cambridge, UK 2005.

[28] T. Fornstedt, G. Zhong, G. Guiochon, Peak tailing and mass transfer kinetics in linear chromatography, Journal of Chromatography A, 741 (1996) 1-12.

[29] D.C. Harris, Quantitative chemical analysis, Macmillan, NY, USA 2010.

[30] M.E. Ibrahim, Y. Liu, C.A. Lucy, A simple graphical representation of selectivity in hydrophilic interaction liquid chromatography, Journal of Chromatography A, 1260 (2012) 126-131.

[31] N.P. Dinh, T. Jonsson, K. Irgum, Probing the interaction mode in hydrophilic interaction chromatography, Journal of Chromatography A, 1218 (2011) 5880-5891.

[32] N.P. Dinh, T. Jonsson, K. Irgum, Water uptake on polar stationary phases under conditions for hydrophilic interaction chromatography and its relation to solute retention, Journal of Chromatography A, 1320 (2013) 33-47.

[33] R. Kučera, P. Kovaříková, M. Klivický, J. Klimeš, The retention behaviour of polar compounds on zirconia based stationary phases under hydrophilic interaction liquid chromatography conditions, Journal of Chromatography A, 1218 (2011) 6981-6986.

[34] T. Zhou, C.A. Lucy, Separation of carboxylates by hydrophilic interaction liquid chromatography on titania, Journal of Chromatography A, 1217 (2010) 82-88.

[35] S.J. O'Connor, K.J. MacKenzie, M.E. Smith, J.V. Hanna, Ion exchange in the charge-balancing sites of aluminosilicate inorganic polymers, Journal of Materials Chemistry, 20 (2010) 10234-10240.

[36] M.F. Wahab, J.K. Anderson, M. Abdelrady, C.A. Lucy, Peak distortion effects in analytical ion chromatography, Analytical chemistry, 86 (2013) 559-566.

[37] C. Liang, C.A. Lucy, Characterization of ion chromatography columns based on hydrophobicity and hydroxide eluent strength, Journal of Chromatography A, 1217 (2010) 8154-8160.

[38] M.F. Wahab, M.E. Ibrahim, C.A. Lucy, Carboxylate modified porous graphitic carbon: a new class of hydrophilic interaction liquid chromatography phases, Analytical chemistry, 85 (2013) 5684-5691.

[39] J. Kirkland, J. Henderson, J. DeStefano, M. Van Straten, H. Claessens, Stability of silica-based, endcapped columns with pH 7 and 11 mobile phases for reversed-phase high-performance liquid chromatography, Journal of Chromatography A, 762 (1997) 97-112.

[40] Y. Wang, M.F. Wahab, Z.S. Breitbach, D.W. Armstrong, Carboxylated cyclofructan 6 as a hydrolytically stable high efficiency stationary phase for hydrophilic interaction liquid chromatography and mixed mode separations, Analytical Methods, 8 (2016) 6038-6045.

[41] M. Gilbert, J. Knox, B. Kaur, Porous glassy carbon, a new columns packing material for gas chromatography and high-performance liquid chromatography, Chromatographia, 16 (1982) 138-146.

[42] J.H. Knox, B. Kaur, G.R. Millward, Structure and performance of porous graphitic carbon in liquid chromatography, Journal of Chromatography A, 352 (1986) 3-25.

[43] L.T. Verhaar, B. Kuster, H. Claessens, Retention behaviour of carbohydrate oligomers in reversed-phase chromatography, Journal of Chromatography A, 284 (1984) 1-11.

[44] T. Greibrokk, T. Andersen, High-temperature liquid chromatography, Journal of Chromatography A, 1000 (2003) 743-755.

[45] B. Yan, J. Zhao, J.S. Brown, J. Blackwell, P.W. Carr, High-temperature ultrafast liquid chromatography, Analytical chemistry, 72 (2000) 1253-1262.

[46] J.W. Dolan, Temperature selectivity in reversed-phase high performance liquid chromatography, Journal of Chromatography A, 965 (2002) 195-205.

[47] D. Hardjito, M. Tsen, Strength and thermal stability of fly ash-based geopolymer mortar, The 3rd International Conference-ACF/VCA, 2008, pp. 144-150.

4.7 Supporting Information

File Name	SGP			Meas Date	18/11/26 15:06:11
Sample ID	SGP		Sample No.	1	
Comment					

Median D	5.094	Mean V	3.705
Modal D	8.131	Std Dev	0.422

10%D(μm)	20%D(μm)	30%D(μm)	40%D(μm)	50%D(μm)	60%D(μm)	70%D(μm)	80%D(μm)	90%D(μm)
0.964	1.348	1.778	2.462	5.094	6.649	7.961	9.413	11.428

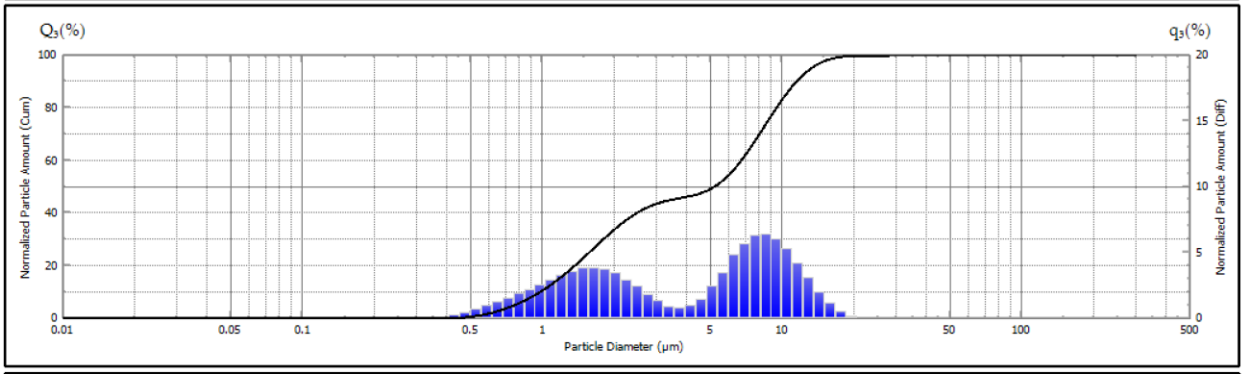

Figure 4.S1 Laser diffraction particle size distribution of synthetic aluminosilicate based geopolymer in water

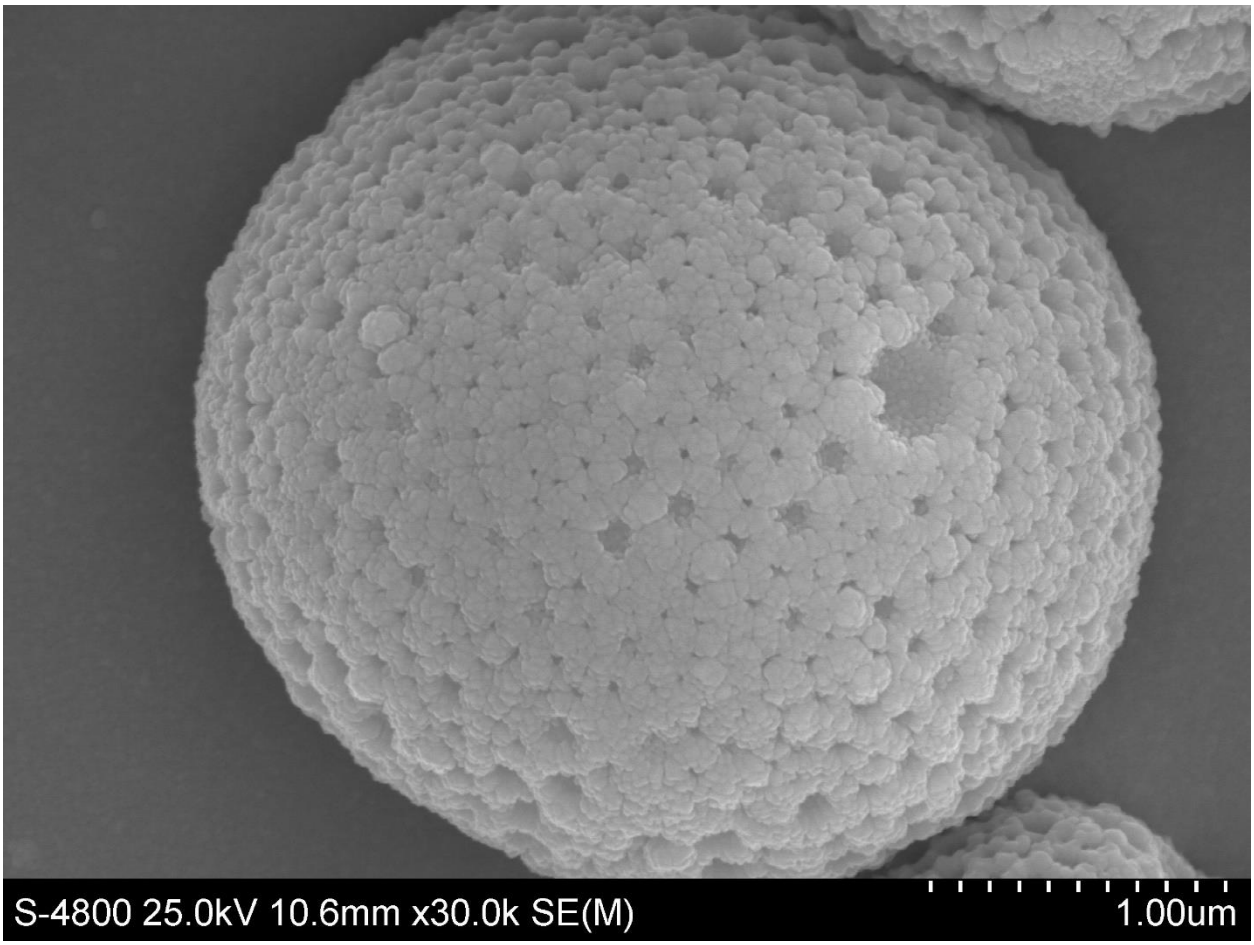

Figure 4.S2 High magnification (x30k) scanning electron micrograph of synthetic aluminosilicate based geopolymer microparticle

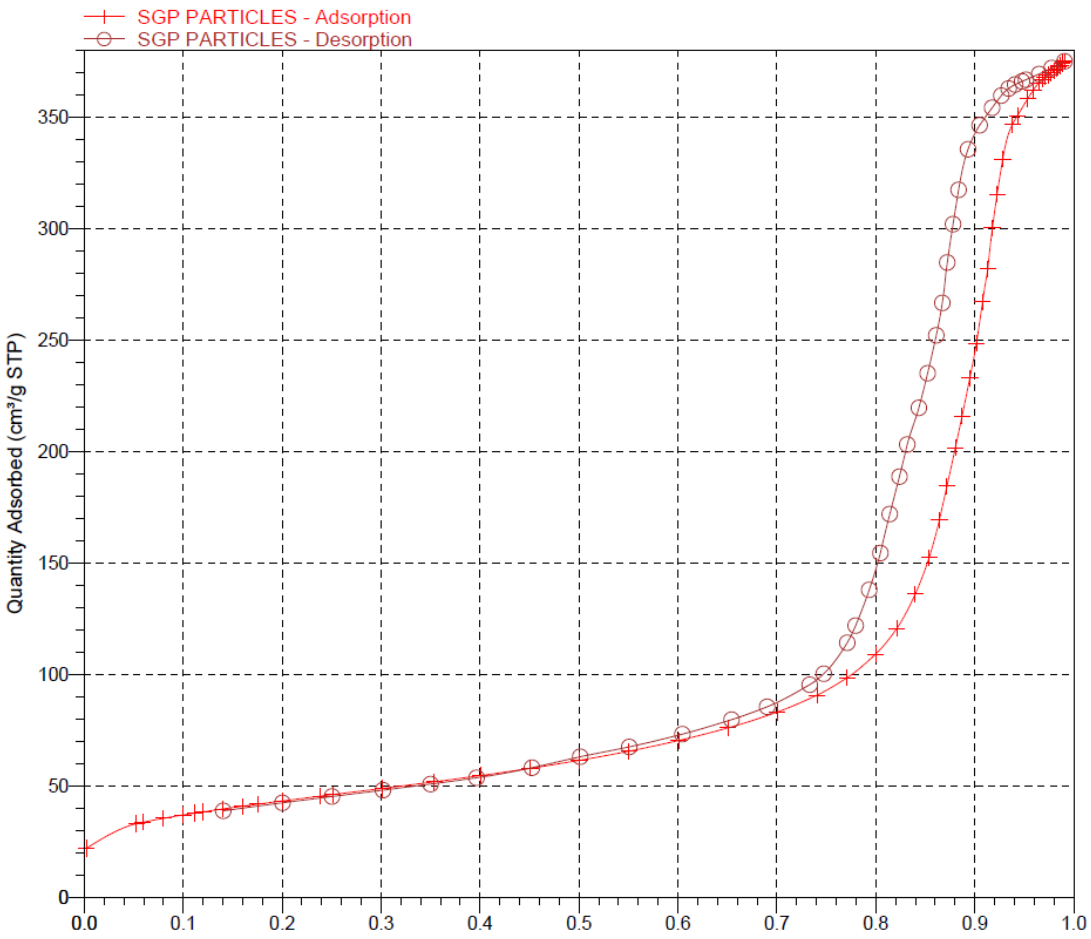

Figure 4.S3 Brunauer-Emmett-Teller isotherm of synthetic aluminosilicate based geopolymer microparticles.

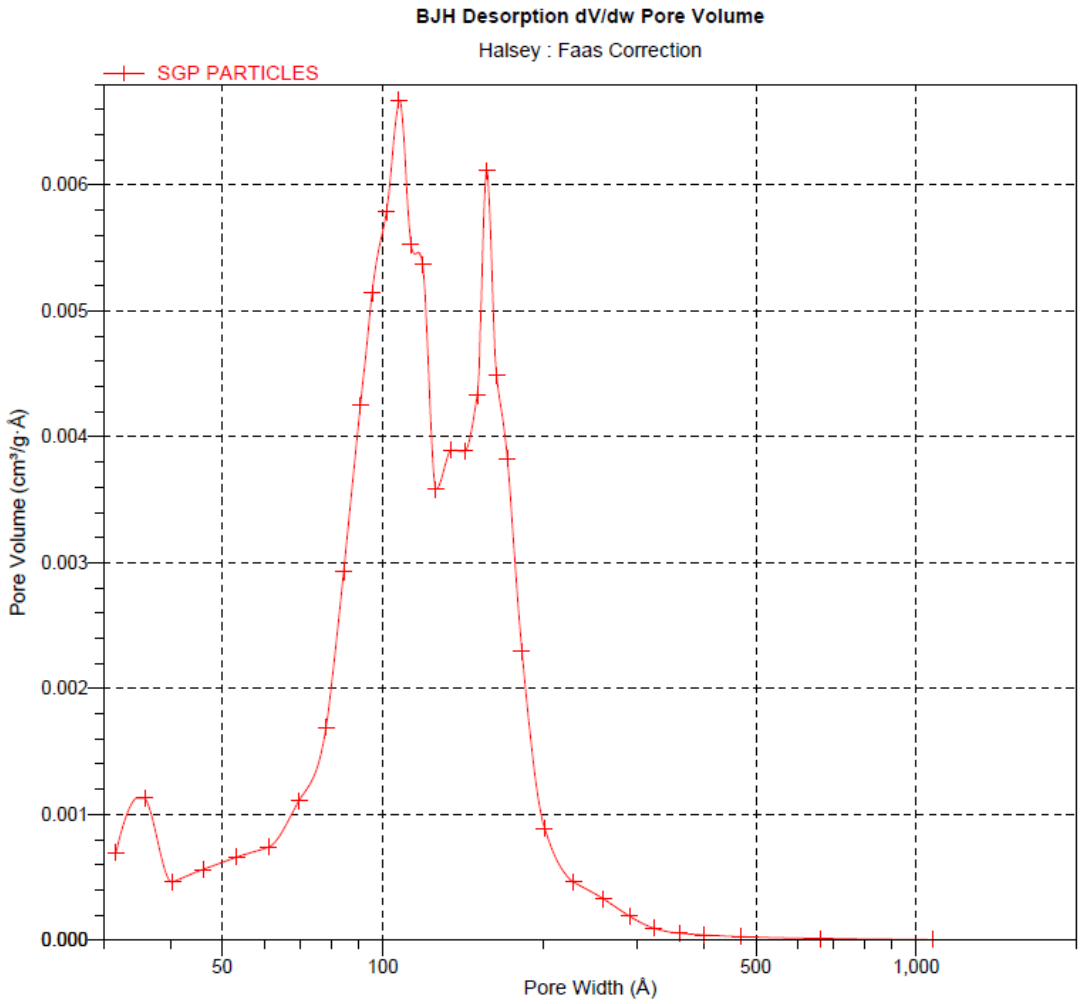

Figure 4.S4 BJH desorption pore size distribution curve of synthetic aluminosilicate based geopolymer microparticles.

4.7.1 Selectivity chart data interpretation

The selectivity plot was constructed based on information provided in literature and our experimental data.

Table 4.S1 Selectivity chart data interpretation

Stationary phase type	Column ID	Description
Zwitterionic	1	ZIC-HILIC 100x4.6, 5µm, 200Å
Zwitterionic	2	ZIC-HILIC 150x4.6, 3.5µm, 200Å
Zwitterionic	3	ZIC-HILIC 150x4.6, 3.5µm, 100Å
Poly	4	ZIC-pHILIC 50x4.6, 5µm, ??Å
Zwitterionic	5	Nucleodur 100x4.6, 5µm, 100Å
Zwitterionic	6	Shiseido 100x4.6, 5µm, 100Å
Amide	7	Tosoh Amide 80 100x4.6, 5µm
Amide	8	Tosoh Amide 80 50x4.6, 3µm
poly	9	PolyHYDROXYETHYL A 100x4.6, 5µm, 100Å
Diol	10	LiChrospher Diol 100x4, 5µm, 100Å
Diol	11	Luna 5u HILIC 100x4.6, 5µm (514356-6)
Poly	12	PolySULFOETHYL A 100x4.6, 5µm, 100Å
Si	13	Chromolith SI 100x4.6, 5µm, 200Å
Si	14	Atlantis HILIC SILICA 100x4.6, 5µm, 200Å
Si	15	Purospher SI 100x4, 5µm, ??
Si	16	LiChrospher SI 100x4, 5µm, 100Å
Si	17	LiChrospher SI 100x4, 5µm, 60Å
Si-C	18	Cogent Silica-C 100x4.6, 4µm
NH2	19	LiChrospher NH2 100x4, 5µm, 100Å
NH2	20	Purospher NH2 100x4, 5µm, 100Å
NH2	21	Tosoh NH2 50x4.6, 3µm
Si	22	Atlantis HILIC Silica 50×1.0mm, 3µm, 100Å
Si	23	Onyx monolithic Si 100×4.6mm, 2µm, 130Å
Si	24	Agilent ZORBAX HILIC plus 100×4.6mm, 3.5µm 95Å
Si	25	AS9-sc Si monolith 80*
Si	26	Agilent ZORBAX RRHD HILIC PLUS 100×3mm, 1.8µm, 95Å
poly	27	Acclaim Trinity P1, 150×3mm, 3µm
NH2	28	Cosmosil 150×4.6mm, 5µm, 120Å
Proprietary polar phase	29	Acclaim HILIC-10 150×4.6mm, 3µm, 120Å
RP	30	Agilent Eclipse XDB-C18 150×4.6mm, 5µm, 80Å
RP	31	Waters Xbridge C18 150×4.6mm, 5µm,

RP	32	YMC Pro C18 150×2.0mm, 3µm,120Å
RP	33	ZORBAX SB-C18 150×4.6mm, 3.5µm
Cyclofructan	**34**	**Frulic N**
Geopolymer	**35**	**NM-GP**
Geopolymer	**36**	**Syn-GP**

Chapter 5. Enhancing the selectivity of polar hydrophilic analytes with a low concentration of barium ions in the mobile phase using geopolymers and silica supports

5.1 Abstract

Charged analytes such as organic sulfonic acids, sulfates, carboxylates, and phosphates are often analyzed by hydrophilic interaction liquid chromatography (HILIC). In many cases, these analytes do not show any selectivity and elute near the dead time using the conventional acetonitrile-ammonium acetate buffers. In this work, we introduce a powerful selectivity enhancing technique by using a trace amount of Ba^{2+} ion in the mobile phase as a general approach for HILIC with UV-Vis detection. Silica and a newly developed material called geopolymers are used as stationary phases. Geopolymers are X-ray amorphous aluminosilicate inorganic polymers with cation exchange properties. Barium exchanged geopolymers (Ba-NM-GP) are synthesized from metakaolin based geopolymer. Thorough characterization of Ba-NM-GP is reported using scanning electron microscopy (SEM), energy dispersive spectroscopy (EDS), Brunauer-Emmett-Teller (BET) surface area analyzer and laser diffraction particle size distribution analyzer for the determination of their shape, size, porosity, surface area and particle size distribution respectively. It is demonstrated that in the absence of barium, baseline separations of sulfonates, carboxylates, and phosphates is not possible, whereas, in the presence of Ba^{2+} in the mobile phase, these analytes are easily separated. Barium perchlorate is suggested as an additive for it is UV transparent, and it has practically an unlimited solubility in acetonitrile.

5.2 Introduction

Hydrophilic interaction liquid chromatography (HILIC) has become a standard technique for separating small polar and hydrophilic molecules. Although it was well known that sugars increase their retention with increasing acetonitrile content on a hydrophilic phase, this general technique was not named until 1990 [1, 2]. A survey of current reviews and articles on HILIC reveals that there are only limited classes of polar stationary phases and even lesser number of solvents which can be utilized successfully in the HILIC mode due to UV cut-off issues [3-6]. Fortunately, chromatographic selectivity can be dramatically varied by two independent parameters *viz*. stationary phase chemistry, and mobile phase composition. The choice of altering the composition of the latter is practically the most convenient and economical approach when dealing with challenging separations. The role of salts in HILIC mobile phases cannot be overemphasized because the nature of salts is known to modify the retention and reverse elution orders of charged analytes- even neutral molecules are also "modestly" affected by the nature of kosmotropic and chaotropic ions of the Hoffmeister series [7]. Currently, ammonium salts are almost exclusively used in the HILIC mode [3, 4], because a majority of the salts of group I and II elements become insoluble in a high concentration of acetonitrile [4]. Due to the limited studies of salt effect in HILIC eluents, a recent study addressed the role of salts in mobile phases in great detail by showing the importance of various inorganic and organic salts which are soluble in acetonitrile [7]. Various salts such as triethylammonium sulfate, triethylammonium perchlorate, lithium, sodium, cesium, and magnesium methyl phosphonates were employed to better understand their role in the retention of neutral molecules and peptides [7].

To date, relatively few studies exist which utilize barium salts in the mobile phase. Carr et al. used Ba^{2+} salts in reversed phase chromatography to block silanol activity in order to improve the peak

shapes of amines [8]. They concluded that long-chain alkylamines, e.g., octylamine, are better silanol blocking agents than barium ions. A recent investigation evaluated the effect of different cations in the mobile phase, including Ba^{2+} ion on the retention of amines and dipeptides on silica and amide stationary phases in the HILIC mode [9]. The authors found that the Ba^{2+} salt additive produced the highest retention and provided different selectivity, especially for dipeptides [9]. A similar approach was used with Ba^{2+} ion in the mobile phase for the separation of carbohydrates with improved peak shapes by the use of anion-exchange chromatography [10]. Dramatic effects of Ba^{2+} salts have been shown in chiral chromatography using native cyclofructans [11]. Native cyclofructan has negligible chiral selectivity towards enantiomers; however, when an isopropyl group cyclofructan based stationary phase is exposed to barium salts in the eluent, enantiomeric sulfonate and phosphonate functionalized molecules are easily resolved [11]. This chiral recognition property originated because cyclofructan binds Ba^{2+} more strongly than other metal cations [12].

The goal of this work is to introduce a new selectivity altering technique in HILIC mode by utilizing the affinity of barium ions towards carboxylate, phosphate, phosphonate, sulfonate, and sulfate functional groups. Also, a new material called barium exchanged "geopolymer" is introduced as a chromatographic stationary phase. Geopolymers are inorganic polymers formed by polycondensing aluminosilicates under highly alkaline conditions [13-15]. Tetrahedral aluminate units in geopolymers give rise to negative charges which are balanced by alkali metal cations like Na^+ or K^+. Geopolymers are usually synthesized with Na^+ and K^+ as counterions because only NaOH and KOH have high solubilities in water. These cations can later be replaced with other cations like NH_4^+, Ag^+, Zn^{2+}, Cu^{2+}, Ba^{2+}, etc., using ion exchange techniques [16, 17]. Herein, we report a convenient synthesis approach for making geopolymers with Ba^{2+} ions. The

natural metakaolin based geopolymer (NM-GP) particles were further ion-exchanged under optimized conditions with Ba^{2+} ions, and the physicochemical properties of the barium "exchanged" natural metakaolin based geopolymers (Ba-NM-GP) particles are examined for chromatographic purposes. Comparison is provided with a bare, fully porous silica.

5.3 Materials and methods

5.3.1 Chemicals

Metakaolin was purchased from Advanced Cement Technologies, Blaine, WA, U.S.A. The 10 µm fully porous silica particles (Daisogel, lot number 100701TSP) were purchased from Daisogel Co. Osaka, Japan. Pure canola oil of Crisco brand was obtained from Walmart, TX, USA. Reagent grade barium perchlorate trihydrate salt was purchased from Alfa Aesar, U.S.A. Fumed silica, anhydrous barium acetate, and barium chloride dihydrate salt were purchased from Sigma-Aldrich, St. Louis, MO, U.S.A. All solvents used for the synthesis and chromatographic purposes and all the analytes, e.g., sulfonic acids, carboxylic acids, organic sulfates, and organic phosphates, were obtained from Sigma-Aldrich, St. Louis, MO, USA. Ultra-purified water (Millipore, 18.2 MΩ) was used throughout the experiment.

5.3.2 Synthesis of barium exchanged natural metakaolin based geopolymer (Ba-NM-GP) stationary phase

Ba-NM-GP particles were obtained from NM-GP particles by the ion-exchange process. NM-GP particles were synthesized by mixing metakaolin, fumed silica, and KOH in a specific molar ratio Si/Al/K 2:1:2 [13]. Fumed silica mass of 6.6 gram was dissolved in 10.37 gram of KOH in 25 mL

of water and mixed for 20 min. Then, 12.34 gram of metakaolin was added to the mixture and stirred for five more minutes using a magnetic stirrer bar. The total mixture was further stirred in water to oil (W/O) emulsion ratio of 1:18 using overhead stirrer with three-blade propellers (Talboys 101, NJ, U.S.A.). Mixing was done for 8 hours for geopolymerization at a stirring speed of 5000 rpm in polypropylene beaker containing 450 mL of canola oil. After synthesis, the geopolymer particles were extracted in the water phase. The particles were washed with methanol, hexanes, and water to remove the oil and surfactants. Clean NM-GP particles were dried in an oven at 110 ºC for two hours. Dried NM-GP particles were calcined at 500 ºC for 4 hours with the temperature ramp of 2 ºC/min. Particles were then de-fined for smaller sized particles using water as a dispersant.

A new approach was developed to obtain the maximum ion exchange of Ba^{2+} in NM-GP particles. The cleaned NM-GP particles were packed in 5 x 0.21 cm i.d. column to assess the extent of ion-exchange of Ba^{2+} at different times. The packed column was exposed to 0.2 M $BaCl_2$ aqueous solution at 60 ºC using HPLC instrument. Agilent HPLC instrument 1100 series was used with a flow rate of 0.5 mL/min. Barium exchange was done in NM-GP for different time periods to optimize ion-exchange. Particles were washed with ultrapure water after ion-exchange for 2 hours at the same flow rate. The column was extruded, and Ba-NM-GP particles were again washed with DI water and dried in an incubator at 60 ºC for 24 h and characterized. Final ion exchange was carried out in 25 cm x 0.46 cm in a column for 72 h using the same procedure as above to get approximately 2.5 gram of Ba-NM-GP particles.

5.3.3 Column Packing

Ba-NM-GP columns and fully porous 10 µm silica particles columns were packed by slurry packing procedure using 10 cm x 0.3 cm stainless steel hardware. The solvent composition of 80% methanol and 20% iso-octanol was used for packing of Ba-NM-GP with a slurry concentration of 35%. The 25% slurry composition was used for the packing of silica particles using isopropanol and cyclohexanol mixture. Haskel pneumatic pump was used for packing at high pressure at 10,000 psi [18]. The efficiency obtained for the Ba-NM-GP was 32,000/m plates, and silica was 30,000/m plates. The bare silica column after packing was conditioned with ACN-0.5 mM $Ba(OAc)_2$ solution for 90 min before performing chromatography.

5.3.4 Instrumentation and Procedure

Geopolymers (NM-GP and Ba-NM-GP) were characterized by using scanning electron microscopy (SEM), energy dispersive spectroscopy (EDS), X-ray diffraction analyzer (XRD), laser diffraction analyzer (LDS) and Brunauer-Emmett-Teller (BET) surface area analyzer. Hitachi S-4800 II Field Emission SEM (FE-SEM) was used for acquiring the images of particles under high vacuum condition using high acceleration voltage of 30 kV. EDS was used for the elemental analysis of geopolymer particles before and after the ion exchange process. The X-ray diffraction analysis was performed for the analysis of Ba-NM-GP particles by using Shimadzu Maxima XRD-7000 X-ray diffractometer. Particle size distribution was obtained using Shimadzu SALD-7101 laser diffraction particle size analyzer. In addition, BET surface area analysis was carried out using a Micromeritics Tristar II 3020 instrument for the surface area and pore size determination of geopolymer particles. Degassing of the geopolymer particles was performed to remove any adsorbed species for 24 h at 90 ºC before surface area analysis. The chromatographic evaluation

was done using the Agilent HPLC 1100 Series system with a binary pump, autosampler, and ultraviolet diode array as the detector. Chromatograms were collected at 220 nm, 254 nm, and 280 nm. The separations were done in isocratic HILIC mode.

The solubility of barium perchlorate ($Ba(ClO_4)_2.3H_2O$) in acetonitrile was also studied by adding barium perchlorate salt in 50 mL of acetonitrile solvent until a syrupy solution was formed. The solution was left for 24 hours at room temperature to settle, and excess of solid salts were removed by the decantation. The 5 mL of that solution was taken, and the solvent was evaporated using rotavapor. The remaining salt was recovered and dried for one day at 30 ℃.

5.4 Results and Discussion

5.4.1 Characterization of barium exchanged geopolymer

The principle behind natural metakaolin geopolymer (NM-GP) stationary phase synthesis using KOH fumed silica, metakaolin, and water-in-oil W/O emulsion has been reported previously [13]. The goal here was to replace the K^+ counterion with Ba^{2+} ion to alter the selectivity of NM-GP. The limited solubility of $Ba(OH)_2$ in water [19] and formation of insoluble barium soaps in oil prohibit the direct synthesis of a geopolymer with barium ions. Therefore, an ion-exchange technique was chosen for the synthesis of barium exchanged geopolymer particles. It should be noted that Ba^{2+} ions have a comparable size with K^+ ions [20]. An SEM image obtained of Ba-NM-GP particles confirmed the formation of spherical particles (Figure 5.1) which are preferred for modern column packings [18, 21] rather than irregularly shaped particles. EDS was performed on NM-GP and Ba-NM-GP particles and provided information on the elemental composition of the geopolymer and thus the extent of ion exchange as shown in Table 5.1. The spectra are shown in Figure 5.S1 (Supporting Information). The results clearly indicated successful ion exchange of

K^+ ion with Ba^{2+}. The data obtained from the BET surface area and BJH analysis are also tabulated in Table 5.1.

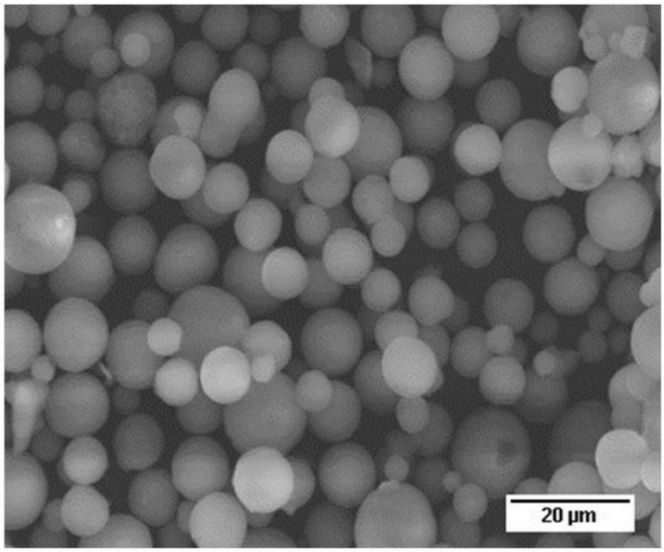

Figure 5.1: Scanning electron microscopy of barium exchanged natural metakaolin based geopolymer particles (Ba-NM-GP).

Table 5.1: Energy dispersive spectrum (EDS) analysis and surface characteristics of NM-GP and Ba-NM-GP

Element	***EDS data***	
	Atom % (NM-GP)	**Atom % (Ba-NM-GP)**
Oxygen	67.50 ± 0.51	68.30 ± 0.51
Aluminum	8.92 ± 0.09	9.82 ± 0.11
Silicon	17.73 ± 0.11	18.09 ± 0.13
Potassium	5.30 ± 0.05	0.90 ± 0.04
Barium	Not detectable	2.60 ± 0.04
Iron	0.31 ± 0.02	0.29 ± 0.04
Titanium	0.24 ± 0.03	Not detectable

Surface Characteristics			
BET surface area (NM-GP)	**BJH desorption pore size (NM-GP)**	**BET surface area (Ba-NM-GP)**	**BJH desorption pore size (Ba-NM-GP)**
214 m^2/g	45 Å	151 m^2/g	50 Å

The surface area of the barium exchanged geopolymer decreases by 29%, but the pore size and pore volume of NM-GP and Ba-NM-GP remain comparable. The BET surface area analysis also indicates the "mesoporous" structure of Ba-NM-GP, which is consistent with our previously reported geopolymer stationary phase [13, 22]. The average particle size obtained for Ba-NM-GP particles was ~ 10 µm with an overall distribution of 5 µm to 16 µm by laser diffraction analyzer (Supplementary information Figure 5.S2). The broad hump obtained in between 25 to 35 degree of 2θ value in x-axis by XRD confirms the characteristic amorphous structure of Ba-NM-GP, which is similar to the XRD pattern as that of NM-GP [13] (Supporting information, Figure 5.S3). The mechanical strength of particles was checked by packing, extruding, and repacking the material again. The particles were packed with the high pressure up to 10,000 psi and extruded, and the particles analyzed in SEM were found to be intact.

5.4.2 Optimization of barium exchange in geopolymer

Preliminary experiments with the ion-exchange of barium on NM-GP showed that the extent of ion exchange by Ba^{2+} is slow unlike the typical cation exchange process on polymeric sulfonated ion-exchange resins [23]. Figure 5.2 displays the atom % of Ba^{2+} exchanged with the K^{+} present in the geopolymer at different times intervals up to 72 h. The y-axis on the left side represents Ba/Al atom percent ratio, whereas y-axis on the right side shows the K/Al atom percent ratio. The plot indicates that the amount of Ba^{2+} exchange was rapid until 12 h and was slower afterward as indicated by the plateau at ~ 40 h and 72 h. Maximum Ba^{2+} exchange of 83% was obtained at 72 h. The divalent cations will need two proximate aluminate sites to satisfy the valency of barium. This could be a likely reason for the small amounts of remaining potassium which may be bound to single or more isolated monovalent sites.

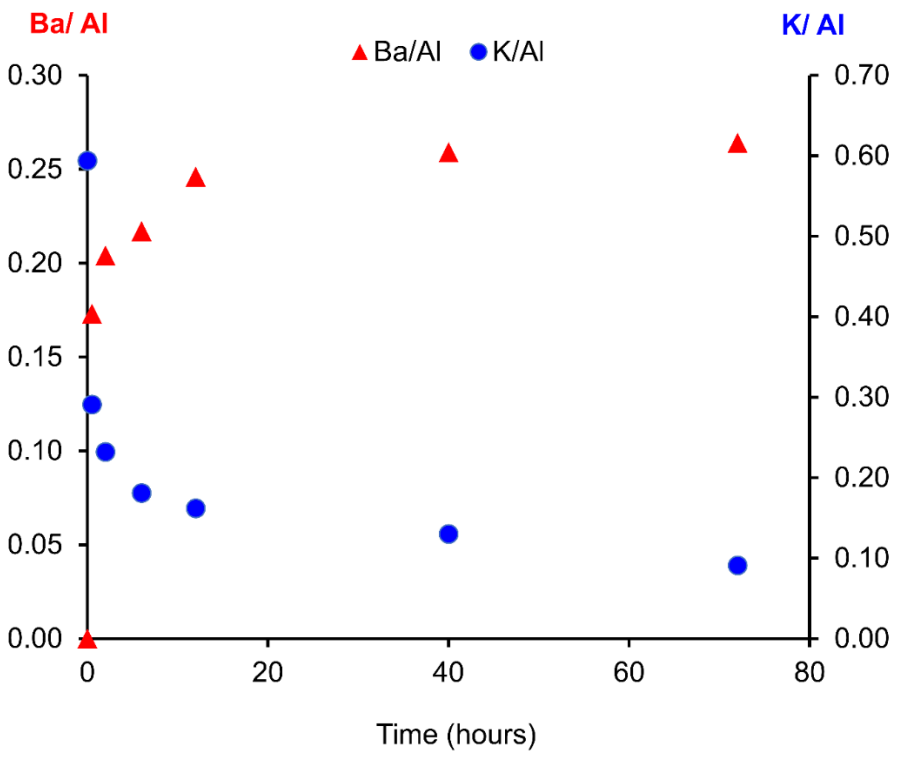

Figure 5.2: Ion exchange of barium ion with potassium ion on natural metakaolin based geopolymer. Atomic percent ratio of Ba/Al vs. K/Al is shown as a function of time using EDS.

5.4.3 Effect of ammonium buffer on Ba-NM-GP stationary phase

Buffers and additives are generally used in HILIC to alter selectivities and retention characteristics of charged analytes [24]. The addition of buffer or additive to the mobile phase is known to disrupt analyte electrostatic interactions and often decrease the peak asymmetry by minimizing undesired secondary interactions [25]. The effects of an ammonium acetate buffer on Ba-NM-GP stationary phase was studied to assess how quickly retention times changed with ammonium ions in the mobile phase. Four analytes containing a sulfate, amine and a phosphate functional group were chosen. The HILIC eluent containing 0.5 mM NH4OAc was pumped through the Ba-NM-GP for 90 min. Figure 5.3 shows the initial retention times of four analytes (90 min of pre-equilibration), and a separation after 300 min.

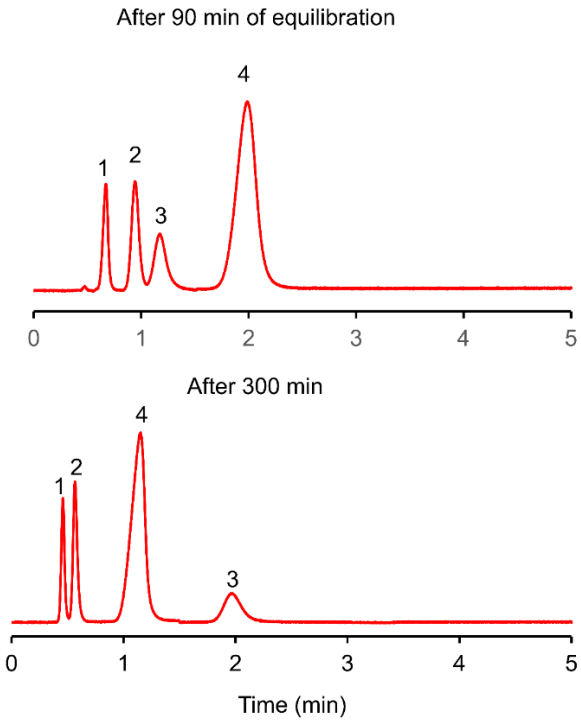

Figure 5.3: Variation of retention time after repetitive injections of various types of analytes on Ba-NM-GP with ammonium acetate in the mobile phase. Column dimension: 10 cm x 0.3 cm i.d., solvent system: 85% ACN-15% H2O with 0.5 mM NH4OAc (total), flow rate: 1 mL/min, detection at 220nm, Analytes: (1) potassium 4-nitrophenyl sulfate (2) potassium 3-indoxyl sulfate (3) 2-amino imidazole sulfate (4) dibenzyl phosphate

As expected, 4-nitrophenyl sulfate and 3-indoxyl sulfate, began to merge due to the loss of barium ions from the stationary phase surface. The same trend was observed with dibenzyl phosphate. On the contrary, 2-aminoimidazole retention increased. The pKa of 2-aminoimidazolium ion is 8.46 [26]. The 2-amino group does not have a major effect on the imidazole structure, because the pKa of imidazole is 7.0. The basic amino group just shifts the pKa values by 1.5 units. The higher affinity of 2-aminoimidazolium ion towards the geopolymer is consistent with the trend seen on polymeric cation exchangers [27] as well as aluminosilicates [28]. It is well known that the general affinity of the cation exchanger with cations follows the elution order: monovalent cations << monovalent organic cations [27]. Clearly, the ammonium ions slowly ion exchange with Ba2+ ions in the stationary phase and alter the chromatographic retention and the

associated ammonium counterions such as acetate and perchlorate do not play a major role in the retention of these molecules. To negate this problem, a small amount of barium ion must be present in the solution in order to maintain the constancy of retention times on Ba-NM-GP (vide infra).

5.4.4 Effect of barium perchlorate concentration on the separation of anionic analytes

Both Ba(ClO4)2 and Ba(OAc)2 were tested as mobile phase additives to optimize the separation of sulfates, sulfonates, carboxylates, and phosphates on Ba-NM-GP. However, the low solubility of $Ba(OAc)_2$ in an acetonitrile + water mobile phase (with 90% ACN and 10% H2O, a 0.5mM solution can be made) limited the attempts to optimize the effect of $Ba(OAc)_2$ concentration. However, another salt, $Ba(ClO4)_2$, has a higher solubility in both water and organic solvents [29] with excellent UV transparency down to 200 nm [30]. The solubility of $Ba(ClO_4)_2$ in pure ACN was determined and found to be approximately 83 g/100 mL. The concentration of $Ba(ClO_4)_2$ was varied from 0.5-30 mM for 90/10 acetonitrile/water mixture. The results are shown in Figure 5.4. As shown, the greatest retention and usually the best separation were observed at 0.5 mM $Ba(ClO_4)_2$ for all the analytes. The retention factors of all analytes decreased with increasing $Ba(ClO_4)_2$ concentration. The same data can be visualized by linear log k – log $[Ba^{2+}]$ plots for each analyte shown along with the corresponding equations and R2 values in Figure 5.S4.

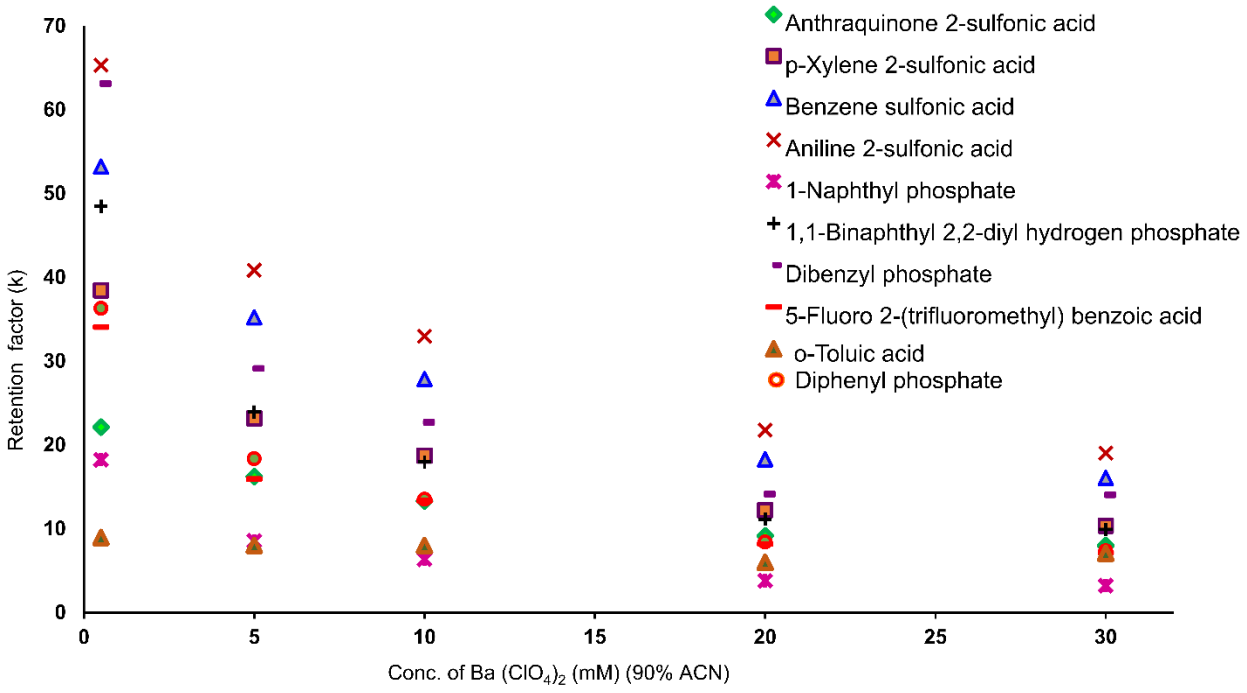

Figure 5.4: A plot of retention factor (k) of different analytes (see inset) as a function of the concentration of $Ba(ClO_4)_2$ in 90% ACN-10% H2O, on a Ba-NM-GP. The concentration of $Ba(ClO_4)_2$ is the total concentration. Column dimension: 10 cm x 0.3 cm i.d., flow rate: 1 mL/min, detection at 220 nm.

Analytes like anthraquinone -2-sulfonic acid, 5-fluoro-2-(trifluoromethyl) phenylacetic acid and o-toluic acid coelute at higher concentrations of $Ba(ClO_4)_2$. Changes in selectivity were observed as well at higher concentration of $Ba(ClO_4)_2$. Similarly, Figure 5.5 shows the corresponding representative chromatograms of the selected compounds from Figure 5.4 (an amine, sulfate, sulfonic acids, phosphates, and carboxylic acids). Clearly, in the absence of the $Ba(ClO_4)_2$ salt in the mobile phase, peaks display fronting, and tailing (Figure 5.5A). At 0.5 mM $Ba(ClO_4)_2$, all the analytes are baseline separated, whereas at higher concentrations of $Ba(ClO_4)_2$, there was a loss of resolution.

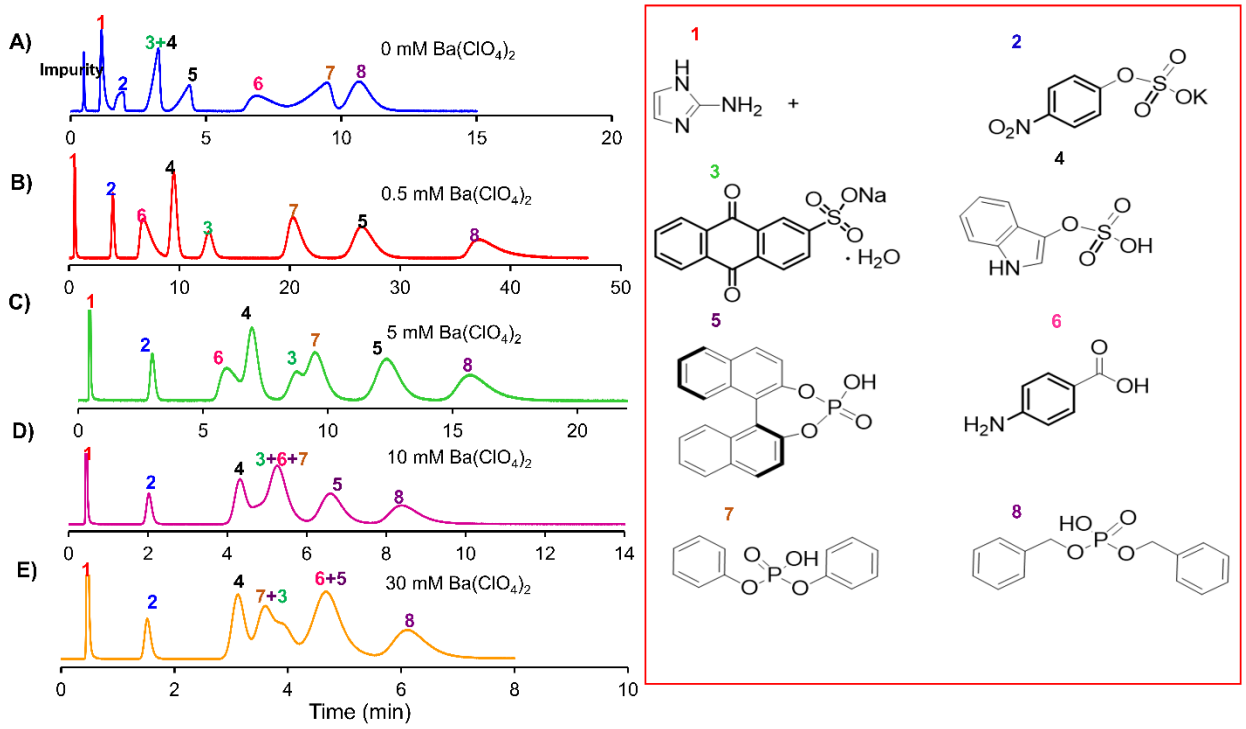

Figure 5.5: Separation of 8 different types analytes with different concentrations of barium perchlorate salt in mobile phase on a Ba-NM-GP. Column dimension: 10 cm x 0.3 cm i.d., solvent system: 90% ACN-10% H_2O, flow rate: 1mL/min, detection at 220 nm, (A) Without mobile phase additives, (B) 0.5 mM of $Ba(ClO_4)_2$ (total), (C) 5 mM $Ba(ClO_4)_2$ (total), (D) 10 mM $Ba(ClO_4)_2$ (total), (E) 30 mM $Ba(ClO_4)_2$ (total), elution order: (1) 2-amino imidazole, (2) 4-nitrophenyl sulfate potassium salt, (3) anthraquinone 2-sulfonic acid, (4) 3-indoxyl sulfate potassium salt, (5) 1,1-binaphthyl 2,2-diyl hydrogen phosphate, (6) 4-amino benzoic acid, (7) diphenyl phosphate, (8) dibenzyl phosphate

Again retention times decreased significantly from approximately 40 minutes for 0.5 mM $Ba(ClO_4)_2$ to 7 minutes for 30 mM $Ba(ClO_4)_2$. The analytes were also tested at 100 mM concentration of $Ba(ClO_4)_2$, and maximum retention of 6 min was found for o-toluic acid with most of the compounds coeluting. The main reason behind decreasing retention with an increase in $Ba(ClO_4)_2$ concentration could be due to the increasing eluent strength of the mobile phase on the Ba-NM-GP. The presence of a higher concentration of Ba^{2+} cations in the mobile phase decreases the interaction of analytes with Ba^{2+} ions on the stationary phase leading to a decrease in the retention of analytes. The optimum concentration of $Ba(ClO_4)_2$ was found

to be 0.5 mM in this study. Hence, the lower solubility of $Ba(OAc)_2$ is not a major issue since it is also soluble at 0.5 mM.

5.4.5 The effect of barium ions on the separation of organic sulfonates on silica and Ba-NM-GP

Silica gel is a popular HILIC phase with modest cation exchange capacities, due to the presence of silanols. Similarly, geopolymers have cation exchange properties due to the tetrahedral aluminate units. Consequently, both barium exchanged geopolymer (Ba-NM-GP) and silica were examined for their ability to separate five highly polar organic sulfonic acids. In Figure 5.6 (A&B), we show the control experiments on silica using ammonium acetate and perchlorate. It is evident in both cases that ammonium ion, acetate and perchlorate ion play no role in the separation (analytes elute near the void time). However, as barium is introduced in the mobile as an acetate salt or a perchlorate salt, separation of sulfonates occurs with excellent peak shapes on bare silica Figure 5.6 (C&D). Baseline separation was observed for all five analytes except benzene sulfonic acid and aniline 2-sulfonic acid (Resolution (Rs)=1.4). As a control for geopolymers, we used natural metakaolin based geopolymer (NM-GP) to see if the aluminosilicate network can retain sulfonic acids in HILIC mode with ammonium acetate and perchlorate. No separation occurs, as shown in Figure 5.6 (E&F). When Ba-NM-GP is used as a stationary phase with a trace amount of barium acetate or perchlorate, we obtain baseline resolution of all five sulfonic acids as shown

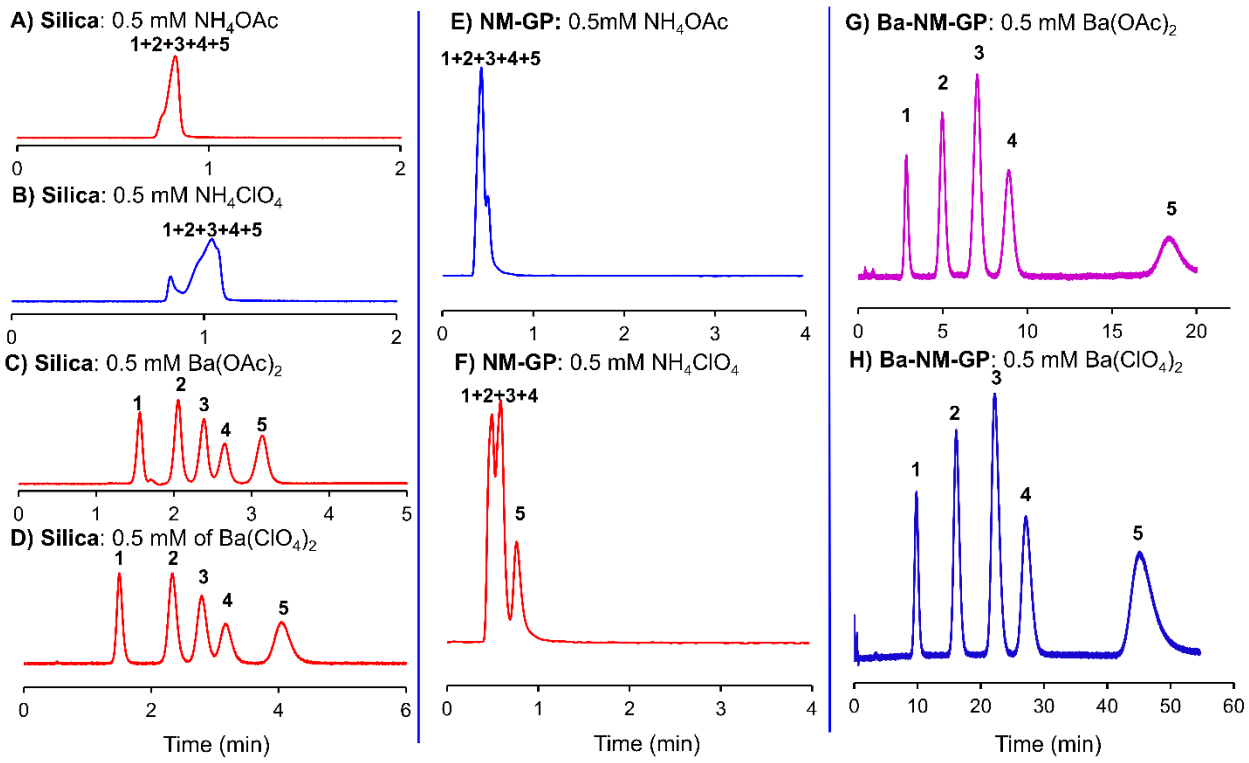

Figure 5.6. HILIC selectivity comparison of five sulfonic acids on silica, NM-GP, and Ba-NM-GP, columns (10 cm x 0.3 cm), solvent system: 90% ACN-10% H_2O , (A) silica with 0.5 mM of NH_4OAc (total), flow rate: 0.425 mL/min, (B) silica with 0.5 mM of NH_4ClO_4 (total), flow rate: 0.425 mL/min, (C) silica with 0.5 mM $Ba(OAc)_2$ (total), flow rate: 1 mL/min, (D) silica with 0.5 mM $Ba(ClO_4)_2$ (total), flow rate: 1 mL/min, (E) NM-GP column with 0.5 mM of NH_4OAc (total), flow rate: 1 mL/min, (F) NM-GP column with 0.5 mM of NH_4ClO_4 (total) (G) Ba-NM-GP column with 0.5 mM $Ba(OAc)_2$ (total), flow rate: 1 mL/min, (H) Ba-NM-GP column with 0.5 mM $Ba(ClO_4)_2$ (total), flow rate: 1 mL/min, detection at 220 nm. Analytes (1) anthraquinone 2-sulfonic acid, (2) p-xylene 2-sulfonic acid, (3) benzene sulfonic acid, (4) aniline 2-sulfonic acid, (5) 4-hydroxy benzene sulfonic acid

in Figure 5.6 (G&H). The resolution of these acids on Ba-NM-GP is better than the silica column of the same dimension (Rs > 1.5). It was noted with the use of barium perchlorate, retention times were significantly higher than when using the corresponding barium acetate salt, as shown in this section as well as later sections. From the ranking on the Hoffmeister series perchlorate ion lies on the highly chaotropic

side, whereas acetate ion is considered a kosmotropic anion [31]. Chaotropic ions are known as hydrogen bond breakers in water. In general, if the analyte is being retained via hydrogen bonding, the presence of chaotropic ions should cause the analyte to elute earlier. However, sulfonic acids retention time dramatically increases in the presence of perchlorate, thus ruling out any hydrogen bonding mediated retention. Unlike the polymeric ion-exchangers, the geopolymer is a rigid monovalent cation exchanger. If we compare the elution strength of barium acetate with barium perchlorate, in each case, it is clear that the latter is a weaker eluent than the former. Interestingly, isopropyl group functionalized cyclofructan show similar effects (retention increase) with barium perchlorate as compared barium acetate in the mobile phase [11]. Regardless of the mode of chromatography, barium perchlorate increases the retention time in chiral chromatography [11] and in these experiments. The ion-pairing effects of perchlorate have been well documented in reversed phase HPLC [32] but not in other modes of chromatography, where the presence of perchlorate ion increases the retention of analytes. It should be noted that the elution order is not altered in case of silica and Ba-NM-GP, confirming that it is only barium which is causing the separation. The counterions are simply tuning the retention time of analytes.

5.4.6 Enhanced selectivity of barium towards analytes bearing carboxylate groups

Comparative chromatographic HILIC separations of a mixture of five different carboxylic acids (indoline-2-carboxylic acid, 5-fluoro-2(trifluoromethyl)phenylacetic acid, trans-cinnamic acid, benzoic acid, 4-hydroxybenzoic acid) are shown in Figure 5.7(A-H).

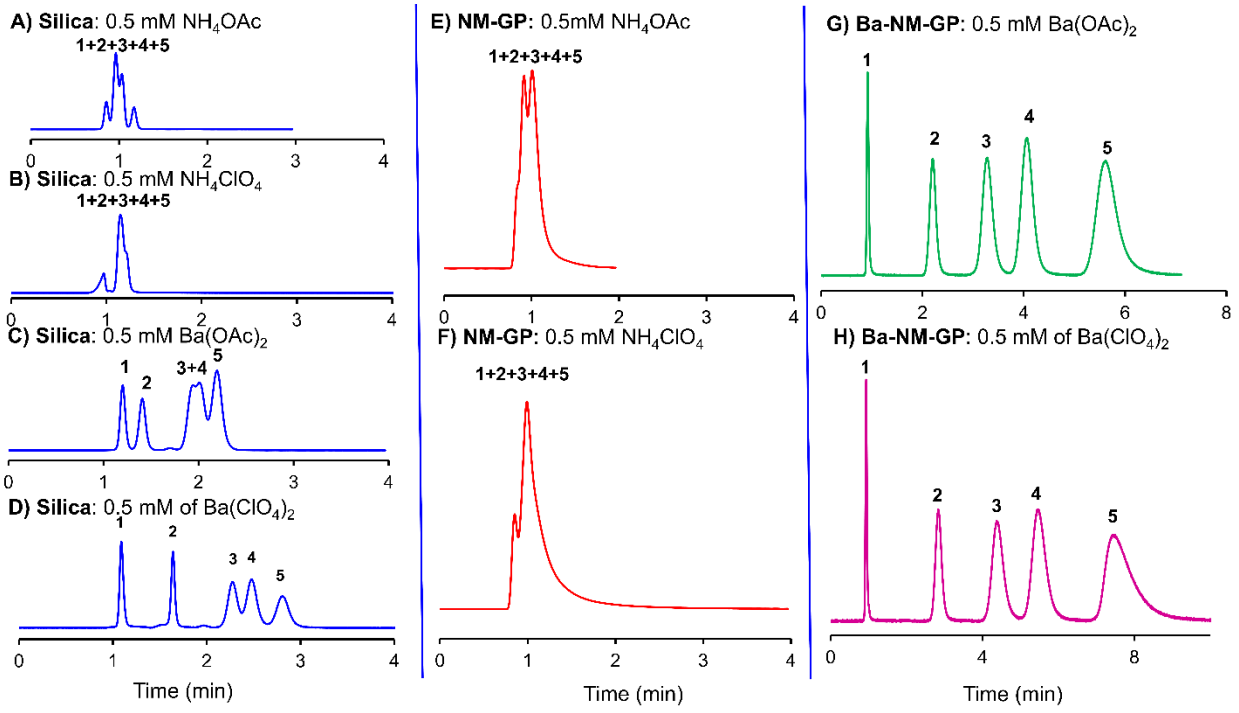

Figure 5.7 HILIC selectivity comparison of five carboxylic acids on silica, NM-GP, Ba-NM-GP columns (10 cm x 0.3 cm), solvent system: 75% ACN-25% H_2O, flow rate: 0.425 mL/min, (A) silica with 0.5 mM of NH4OAc, (B) silica column with 0.5 mM NH_4ClO_4 (total), (C) silica column with 0.5 mM $Ba(OAc)_2$ (total), (D) silica column with 0.5 mM $Ba(ClO_4)$(total), (E). NM-GP column with 0.5 mM NH_4OAc (total), (F) NM-GP column with 0.5 mM NH_4ClO_4 (total), (G) Ba-NM-GP column with 0.5 mM $Ba(OAc)_2$ (total), (H) Ba-NM-GP column with 0.5 mM of $Ba(ClO_4)_2$(total), detection at 220 nm. Analytes: (1) indoline 2-carboxylic acid, (2) 5-fluoro 2(trifluoromethyl) phenyl acetic acid, (3) trans-cinnamic acid, (4) benzoic acid, (5) 4-hydroxy benzoic acid.

The control work was done using a silica column with 0.5 mM NH_4ClO_4 and NH_4OAc in the mobile phase which showed the coelution of analytes near to the dead time, as shown in Figure 5.7(A&B). This behavior is the same as that of sulfonic acids in the absence of barium ion. When Ba^{2+} is added in the mobile phase as acetate and perchlorate salts, the carboxylates begin to separate although not all of them are baseline (Figure 5.7(C&D); in this case, barium perchlorate outperforms barium acetate. As a control, natural geopolymer shows no selectivity for carboxylic acids as they eluted near the dead time (Figure 5.7(E&F).

Best results are achieved by using Ba-NM-GP where all the carboxylic acids separate with a resolution > 1.5 (Figure 5.7(G&H)). In contrast with sulfonic acids, the perchlorate counterion slightly increases the separation window from 7 min to 9 min for carboxylates. It should be noted that the elution order is not altered.

5.4.7 Affinity of Ba2+ towards the organic phosphates

Further evaluation of silica and Ba-NM-GP was carried out by using a mixture of organic phosphates due to the affinity of barium towards phosphate ion [11]. Five analytes were chosen: tris-p-nitrophenylphosphate, 1-naphthyl phosphate, diphenyl phosphate, 1,1-binaphthyl 2,2-diyl hydrogen phosphate and dibenzyl phosphate. Corresponding chromatograms are shown in Figure 5.8(A&B) using bare silica with barium acetate and barium perchlorate. Using 90% ACN, bare silica can resolve all four phosphates except the pair of diphenyl phosphate and 1,1-binaphthyl 2,2-diyl hydrogen phosphate. Using the combination of perchlorate with barium is again seen to be beneficial. When Ba-NM-GP is used as a stationary phase, all five organophosphates can be baseline resolved when barium perchlorate is used. Compare Figure 5.8(C&D). In each case, whether it is silica or a geopolymer, the barium perchlorate additive shows a superior selectivity enhancement. Overall, the results showed the effectiveness of Ba2+ ions as the mobile phase additive for baseline separation of phosphates mixture using both Ba-NM-GP and silica column.

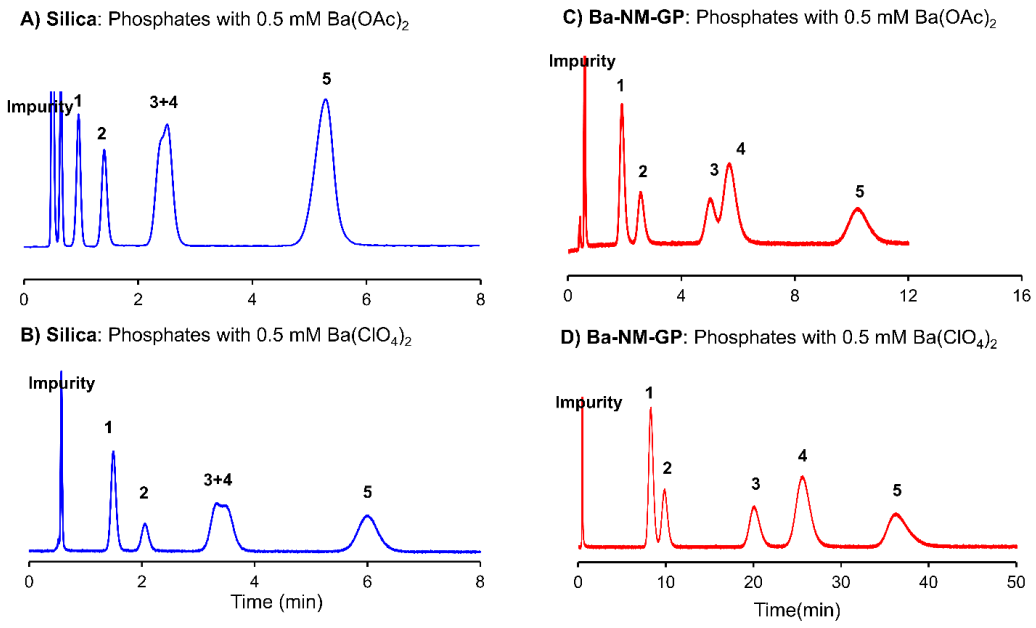

Figure 5.8 HILIC selectivity comparison of a mixture of five organic phosphates on silica and Ba-NM-GP (10 cm x 0.3 cm), solvent system: 90% ACN-10% H2O, flow rate: 1 mL/min, (A) silica column with 0.5 mM of $Ba(OAc)_2$, (B) silica column with 0.5 mM of $Ba(ClO_4)_2$, (C) Ba-NM-GP column with 0.5 mM $Ba(OAc)_2$ (total), (D) Ba-NM-GP column with 0.5 mM $Ba(ClO_4)_2$ (total), detection at 220 nm, Analytes (1) tris-p-nitrophenyl phosphate, (2) 1-naphthyl phosphate, (3) diphenyl phosphate, (4) 1,1-binaphthyl 2,2-diyl hydrogen phosphate, (5) dibenzyl phosphate.

5.4.8 Separation of structural isomers

Mixtures of structural isomers can sometimes pose challenges in chromatography [34]. Presence of Ba2+ ions in the stationary phase or mobile phase can have a different affinity to the anionic functional group at the ortho, meta, and para position of aromatic compounds due to steric effects [35]. In Figure 5.9, using 0.5 mM $Ba(ClO_4)_2$ in the ACN/H2O mixture baseline separation was observed for the following three sets of isomeric acids namely (a) 2-amino 1-naphthalene sulfonic acid and 5-amino 2-naphthalene sulfonic acid, (b) 2-hydroxybenzoic acid and 4-hydroxybenzoic acid, and (c) 2-aminobenzoic acid and 4-aminobenzoic acid on both silica as well as Ba-NM-GP stationary phases with the same elution order.

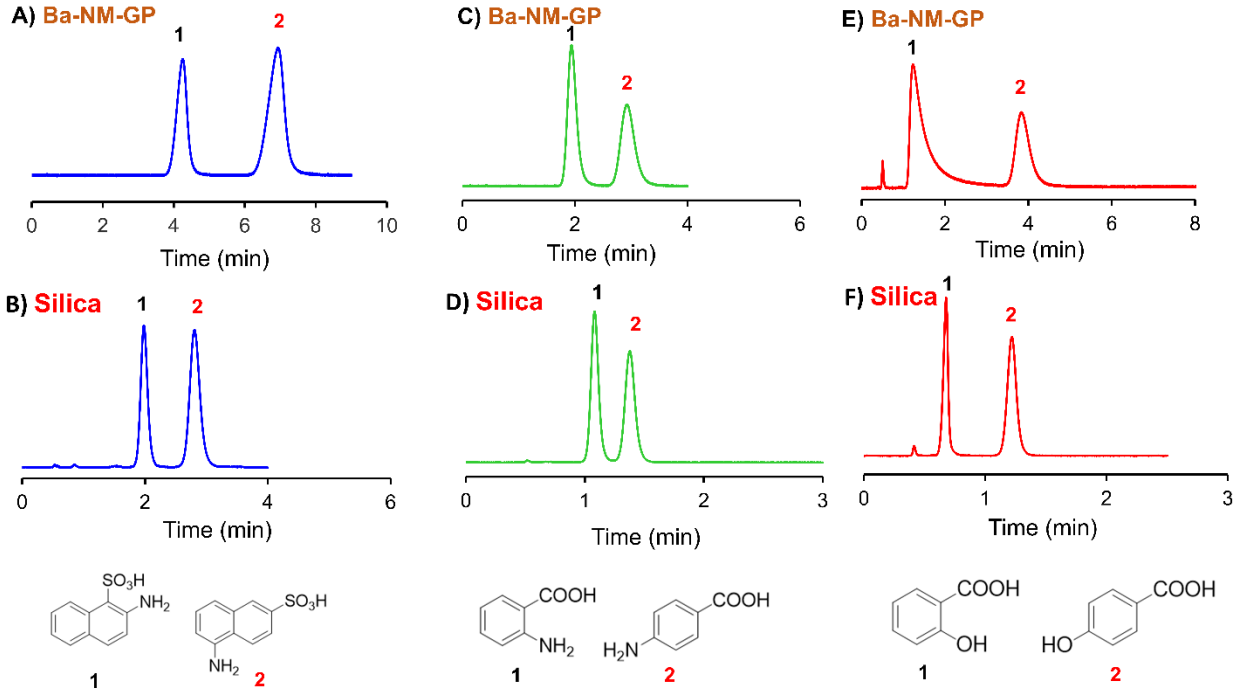

Figure 5.9: Separation of structural isomers on a Ba-NM-GP and silica columns (10 cm x 0.3 cm), flow rate: 1mL/min, (A) mixture of 2-amino 1-naphthalein sulfonic acid and 5-amino 2-naphthalein sulfonic acid on Ba-NM-GP, 90% ACN-10% H_2O with 0.5 mM $Ba(ClO_4)_2$, (B) a mixture of 2-amino 1-naphthalein sulfonic acid and 5-amino 2-naphthalein sulfonic acid, on silica, 90% ACN-10% H_2O with 0.5 mM $Ba(ClO_4)_2$, (C) mixture of 2-amino benzoic acid and 4-amino benzoic acid on Ba-NM-GP, 75% ACN-25% H_2O with 0.5 mM $Ba(ClO_4)_2$, (D) mixture of 2-amino benzoic acid and 4-amino benzoic acid on silica, 75% ACN-25% H_2O with 0.5 mM of $Ba(ClO_4)_2$, (E) mixture of 2-hydroxy benzoic acid and 4-hydroxy benzoic acid on Ba-NM-GP, 75% ACN with 0.5 mM $Ba(ClO_4)_2$, (F) mixture of 2-hydroxy benzoic acid and 4-hydroxy benzoic acid on silica, 75% ACN-25% H_2O with 0.5 mM $Ba(ClO_4)_2$, detection at 220 nm.

5.5 Conclusions

In this work, we proposed a new facile approach for altering the selectivity of various classes of anionic polar analytes containing the following functional groups: sulfate, sulfonate, phosphate, phosphonate, and carboxylate. This technique is compatible with UV-Vis detection. A trace amount of barium ions in an acetonitrile-water mobile phase can drastically change the elution behavior compounds with acidic functional groups. Besides providing examples on silica, a new stationary phase called barium exchanged geopolymer was proposed to expand the choice of HILIC stationary phases. Chromatographers can also tune the retention of the analyte by choosing appropriate counterions such as acetate or perchlorate with barium. Barium perchlorate offers an additional advantage that it is highly soluble in HILIC friendly mobile phases (acetonitrile) thereby eliminating any issues related to precipitation. Conversely, barium acetate has minimal solubility in organic solvents. The use of barium in the mobile phase is a general technique which can be employed on any HILIC stationary phase to impart affinity towards the analyte classes mentioned above. The addition of barium in the mobile phase can potentially give us an orthogonal selectivity to the same column chemistry in two-dimensional chromatography.

5.6 References

[1] D.W. Armstrong, H.L. Jin, Evaluation of the liquid chromatographic separation of monosaccharides, disaccharides, trisaccharides, tetrasaccharides, deoxysaccharides and sugar alcohols with stable cyclodextrin bonded phase columns, J. Chrom. A 462 (1989) 219-232.

[2] A.J. Alpert, Hydrophilic-interaction chromatography for the separation of peptides, nucleic acids and other polar compounds, J. Chrom. A 499 (1990) 177-196.

[3] B. Buszewski, S. Noga, Hydrophilic interaction liquid chromatography (HILIC)—a powerful separation technique, Anal. Bioanal. Chem. 402(1) (2012) 231-247.

[4] P.J. Boersema, S. Mohammed, A.J. Heck, Hydrophilic interaction liquid chromatography (HILIC) in proteomics, Anal. Bioanal. Chem. 391(1) (2008) 151-159.

[5] M.F. Wahab, M.E. Ibrahim, C.A. Lucy, Carboxylate modified porous graphitic carbon: a new class of hydrophilic interaction liquid chromatography phases, Anal. Chem. 85(12) (2013) 5684-5691.

[6] N.P. Dinh, T. Jonsson, K. Irgum, Probing the interaction mode in hydrophilic interaction chromatography, J. Chrom. A 1218(35) (2011) 5880-5891.

[7] A.J. Alpert, Effect of salts on retention in hydrophilic interaction chromatography, J. Chrom. A 1538 (2018) 45-53.

[8] M. Reta, P.W. Carr, Comparative study of divalent metals and amines as silanol-blocking agents in reversed-phase liquid chromatography, J. Chrom. A 855(1) (1999) 121-127.

[9] K. Kalíková, M. Boublík, G. Kučerová, P. Kozlík, The effect of buffer concentration and cation type in the mobile phase on retention of amino acids and dipeptides in hydrophilic interaction liquid chromatography, Chem. Pap. 72(1) (2018) 139-147.

[10] T.R. Cataldi, C. Campa, G. Margiotta, S.A. Bufo, Role of barium ions in the anion-exchange chromatographic separation of carbohydrates with pulsed amperometric detection, Anal. Chem. 70(18) (1998) 3940-3945.

[11] J.P. Smuts, X.-Q. Hao, Z. Han, C. Parpia, M.J. Krische, D.W. Armstrong, Enantiomeric separations of chiral sulfonic and phosphoric acids with barium-doped cyclofructan selectors via an ion interaction mechanism, Anal. Chem. 86(2) (2013) 1282-1290.

[12] Y.-C. Na, N.L. Padivitage, M.K. Dissanayake, D.W. Armstrong, Binding characteristics of native cyclofructan 6 and its derivatives with metal ions, Supramol. Chem. 26(10-12) (2014) 705-713.

[13] R.M. Wimalasinghe, C.A. Weatherly, M.F. Wahab, N. Thakur, D.W. Armstrong, Geopolymers as a New Class of High pH Stable Supports with Different Chromatographic Selectivity, Anal. Chem. 90(13) (2018) 8139-8146.

[14] P. Duxson, A. Fernández-Jiménez, J.L. Provis, G.C. Lukey, A. Palomo, J.S. van Deventer, Geopolymer technology: the current state of the art, J. Mater. Sci. 42(9) (2007) 2917-2933.

[15] N. Thakur, C.A. Weatherly, R.M. Wimalasinghe, D.W. Armstrong, Fabrication of interconnected macroporosity in geopolymers via inverse suspension polymerization, J. Am. Ceram. Soc. 102(8) (2019) 4405-4409.

[16] S.J. O'Connor, K.J. MacKenzie, M.E. Smith, J.V. Hanna, Ion exchange in the charge-balancing sites of aluminosilicate inorganic polymers, J. Mater. Chem. 20(45) (2010) 10234-10240.

[17] Y. Ge, X. Cui, C. Liao, Z. Li, Facile fabrication of green geopolymer/alginate hybrid spheres for efficient removal of Cu (II) in water: batch and column studies, Chem. Eng. J. 311 (2017) 126-134.

[18] M.F. Wahab, D.C. Patel, R.M. Wimalasinghe, D.W. Armstrong, Fundamental and practical insights on the packing of modern high-efficiency analytical and capillary columns, Anal. Chem. 89(16) (2017) 8177-8191.

[19] W.F. Whitmore, M. Lauro, Metallic Soaps—Their Uses, Preparation, and Properties, Ind. Eng. Chem. 22(6) (1930) 646-649.

[20] M. Jurado-Vargas, M. Oliguín, E. Erdóñez-Regil, M. Miménez-Reyes, n. chemistry, Ion exchange of radium and barium in zeolites, J. Radioanal. Nucl. Chem. Art 218(2) (1997) 153-156.

[21] D.T.T. Nguyen, D. Guillarme, S. Rudaz, J.L. Veuthey, Fast analysis in liquid chromatography using small particle size and high pressure, J. Sep. Sci. 29(12) (2006) 1836-1848.

[22] J.B. Condon, Surface area and porosity determinations by physisorption: measurements and theory, Elsevier, Amsterdam, Netherlands 2006.

[23] D. Reichenberg, Properties of ion-exchange resins in relation to their structure. III. Kinetics of exchange, J. Am. Chem. Soc. 75(3) (1953) 589-597.

[24] J.C. Heaton, J.J. Russell, T. Underwood, R. Boughtflower, D.V. McCalley, Comparison of peak shape in hydrophilic interaction chromatography using acidic salt buffers and simple acid solutions, J. Chrom. A 1347 (2014) 39-48.

[25] A.J. Alpert, Electrostatic repulsion hydrophilic interaction chromatography for isocratic separation of charged solutes and selective isolation of phosphopeptides, Anal. Chem. 80(1) (2008) 62-76.

[26] B.T. Storey, W.W. Sullivan, C.L. Moyer, The pKa Values of Some 2-Aminomidazolium Ions, J. Org. Chem. 29(10) (1964) 3118-3120.

[27] A. Rahman, N.E. Hoffman, Retention of Organic Cations in Ion Exchange Chromatography, J. Chrom. Sci. 28(4) (1990) 157-161.

[28] D. Vasudevan, T.A. Arey, D.R. Dickstein, M.H. Newman, T.Y. Zhang, H.M. Kinnear, M.M. Bader, Nonlinearity of Cationic Aromatic Amine Sorption to Aluminosilicates and Soils: Role of Intermolecular Cation−π Interactions, Environ. Sci. Technol. 47(24) (2013) 14119-14127.

[29] H. Willard, G.F. Smith, The perchlorates of the alkali and alkaline earth metals and ammonium. Their solubility in water and other solvents J. Am. Chem. Soc. 45(2) (1923) 286-297.

[30] V.R. Weidner, R. Mavrodineanu, K.D. Mielenz, R.A. Velapoldi, K.L. Eckerle, B. Adams, Spectral Transmittance Characteristics of Holmium Oxide in Perchloric Acid Solution, J. Res. Natl. Bur. Stand. 90(2) (1985) 115-125.

[31] P. Lo Nostro, B.W. Ninham, Hofmeister phenomena: an update on ion specificity in biology, Chem. Rev. 112(4) (2012) 2286-2322.

[32] M. Shibue, C.T. Mant, R.S. Hodges, The perchlorate anion is more effective than the trifluoroacetate anion as an ion-pairing reagent for reversed-phase chromatography of peptides, J. Chrom. A 1080(1) (2005) 49-57.

[33] P.K. Martinelango, J.L. Anderson, P.K. Dasgupta, D.W. Armstrong, R.S. Al-Horr, R.W. Slingsby, Gas-Phase Ion Association Provides Increased Selectivity and Sensitivity for Measuring Perchlorate by Mass Spectrometry, Anal. Chem. 77(15) (2005) 4829-4835.

[34] L.-F. Yao, H.-B. He, Y.-Q. Feng, S.-L. Da, HPLC separation of positional isomers on a dodecylamine-N, N-dimethylenephosphonic acid modified zirconia stationary phase, Talanta 64(1) (2004) 244-251.

[35] X. Zheng, X. Zhang, N.S. Schocker, R.S. Renslow, D.J. Orton, J. Khamsi, R.A. Ashmus, I.C. Almeida, K. Tang, C.E. Costello, R.D. Smith, K. Michael, E.S. Baker, Enhancing glycan isomer separations with metal ions and positive and negative polarity ion mobility spectrometry-mass spectrometry analyses, Anal. Bioanal. Chem. 409(2) (2017) 467-476.

5.7 Supporting Information

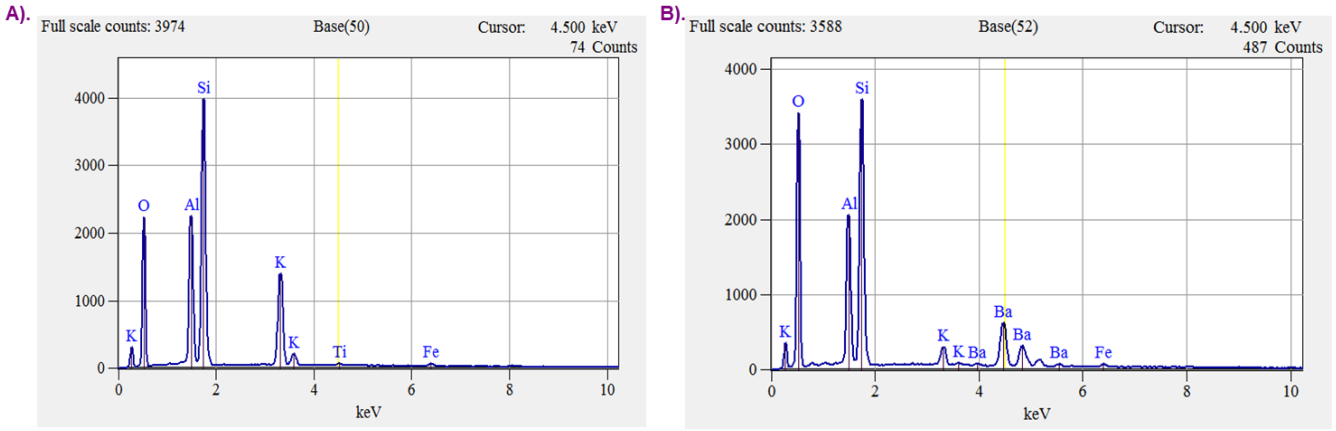

Figure 5.S1: Energy dispersive spectroscopy data of geopolymer particles before and after Ba^{2+} exchange A). EDS report of metakaolin based geopolymer particles before ion exchange (MN-GP) B). EDS report of Ba-NM-GP particles after ion exchange with $BaCl_2$.

10 %D(μm)	20 %D(μm)	30 %D(μm)	40 %D(μm)	50 %D(μm)	60 %D(μm)	70 %D(μm)	80 %D(μm)	90 %D(μm)
0.647	5.105	6.516	7.697	8.824	10.054	11.509	13.407	16.592

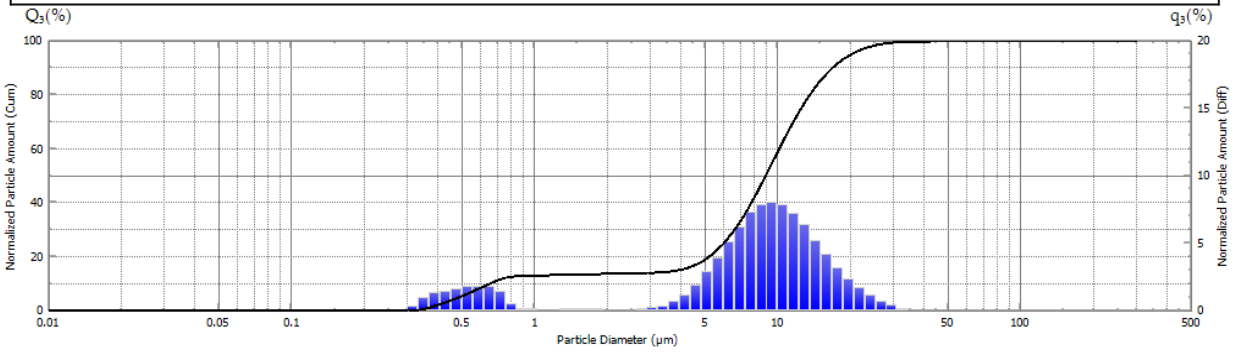

Figure 5.S2: Particles size distribution of Ba-NM-GP by laser diffraction particle size analyzer

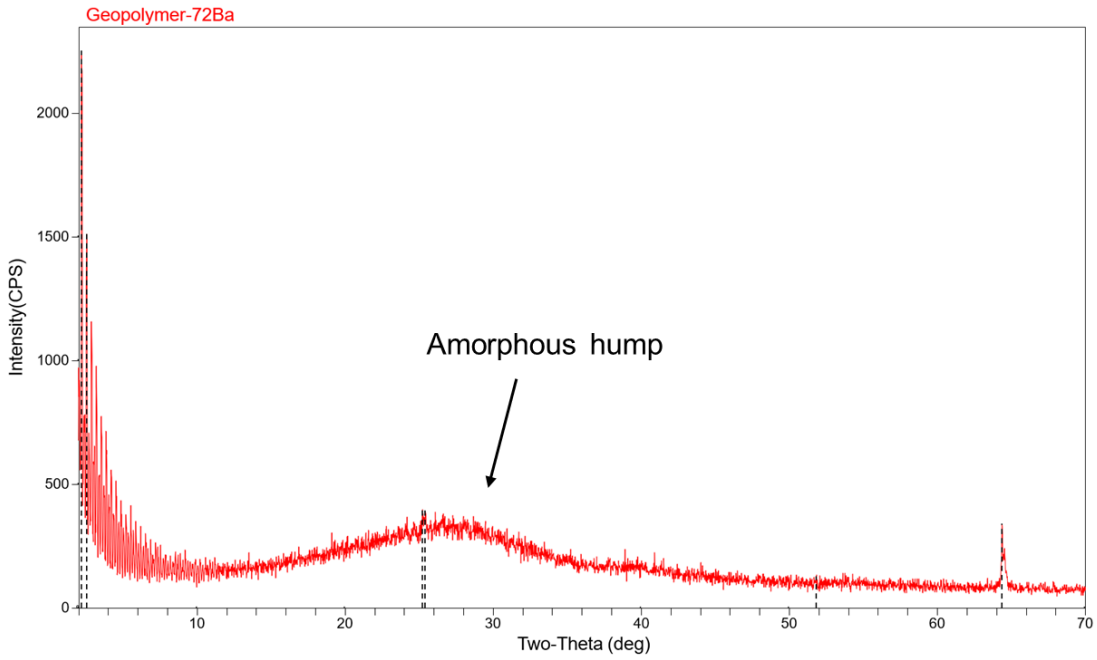

Figure 5.S3: X-rays diffraction pattern (XRD) of Ba-NM-GP particles showing the amorphous structure of geopolymer

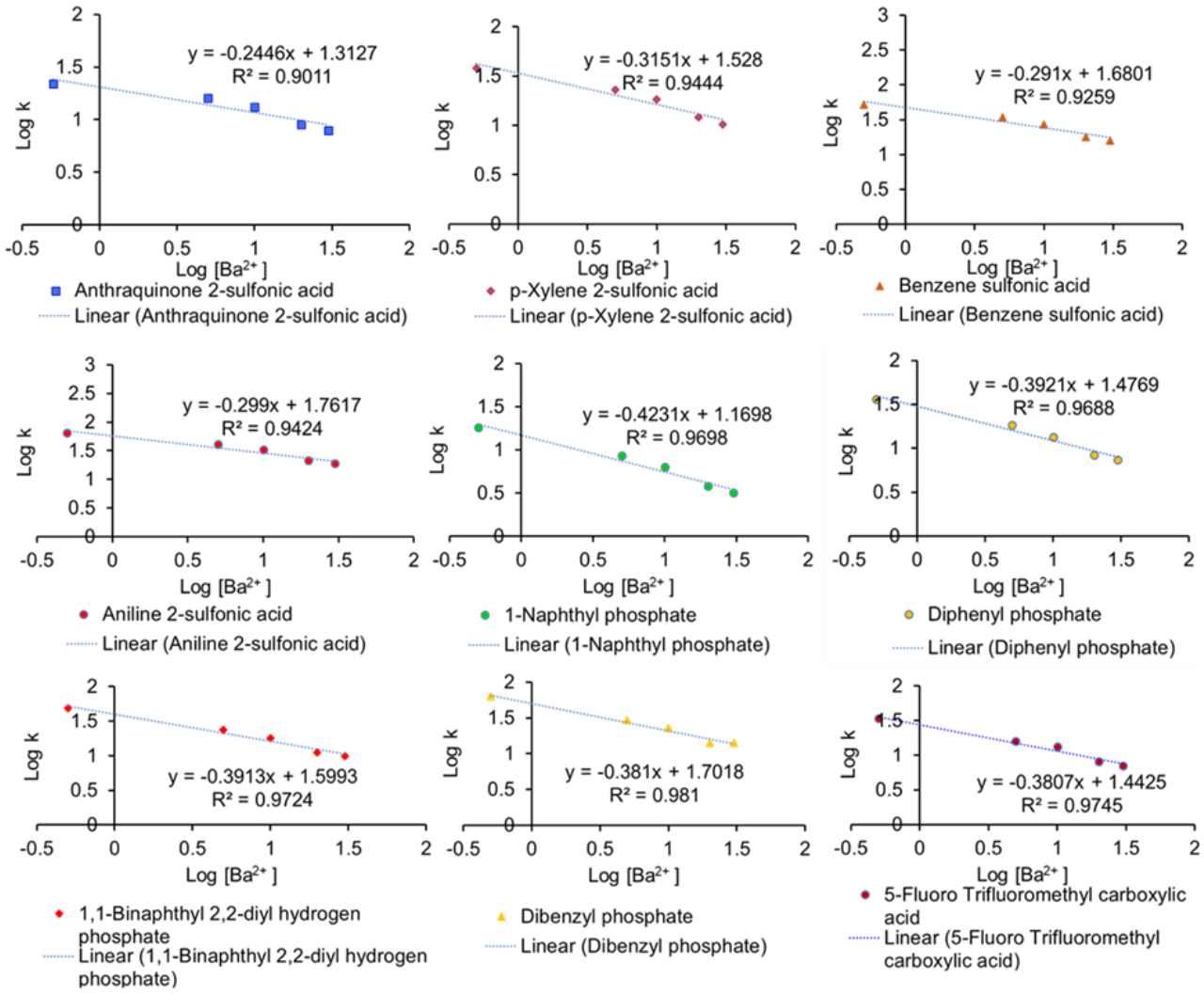

Figure 5.S4: A plot of retention factor (k) of different analytes (see inset) as a function of concentration of $Ba(ClO_4)_2$ in 90% ACN-10% H_2O, on a Ba-NM-GP. The concentration of $Ba(ClO_4)_2$ is the total concentration. Column dimension: 10 cm x 0.3 cm i.d., flow rate: 1 mL/min, detection at 220 nm

Chapter 6. Arsenic sequestration by iron oxide coated geopolymer microspheres

6.1 Abstract

A green, low-cost adsorbent based on geopolymer "microspheres" is reported for the first time for arsenic adsorption. A simple two-step process involves synthesizing geopolymer microspheres by inverse suspension polymerization and impregnating them with iron oxide. Low hydraulic conductivity of fine iron oxide powders demands the use of suitable support materials. Iron oxide modified geopolymer microparticles synthesized here, are small, spherical, porous, mechanically, and chemically stable, have high surface area of 270 m^2/g and can be easily separated from water after adsorption is complete. A comprehensive adsorption study was conducted by employing environmentally critical arsenic species, viz. As(III), As(V), monomethyl arsenate and dimethyl arsenate. The role of contact time, initial arsenic concentration, temperature, adsorbent dosage, pH and competing ions was evaluated. Highest arsenic adsorption was observed at iron content of 20 wt%. High percent removal of ~86%, 100%, 95% and 96% for As(III), As(V), DMA and MMA respectively, were observed at initial arsenic concentration of 0.5 mg/L, an adsorbent dosage of 10 g/L and in just 60 minutes. Low pH favored adsorption of As(V), monomethyl arsenate and dimethyl arsenate while high pH favored adsorption of As(III). The applicability of the novel adsorbent in column mode, its high regeneration capacity and, facile, green, and cheap production are few of its advantages. Moreover, unmodified geopolymer microspheres introduced here can be employed as adsorbents for other toxic heavy metals such as Pb, Cd and Hg.

6.2 Introduction

Arsenic toxicity is considered a serious global health issue affecting millions of people worldwide. Arsenic occurs naturally in groundwater as well as due to human activities like smelting of arsenic ores, mining, combustion of fossil fuels, and pesticide applications [1, 2]. There are more than 500 types of naturally occurring minerals that are responsible for arsenic release in water [2]. Humans are exposed to arsenic by directly drinking contaminated water, using contaminated water for food preparation or irrigation of food crops. Arsenic exists in inorganic forms such as arsenites [As(III)] and arsenates [As(V)] as well as in organic forms such as methylated forms of arsenic and organoarsenicals. Methylated forms of arsenic such as monomethyl arsenate (MMA) and dimethyl arsenate (DMA) were utilized as pesticides and herbicides [3]. Relative to organic species, inorganic arsenic species are highly toxic, known to cause skin cancer [4], cardiovascular diseases [4], adverse pregnancy outcomes [5], infant mortality [5], and have a negative impact on cognitive development [6]. Though monomethyl arsenate and dimethyl arsenate are relatively less toxic than [As(III)] and [As(V)], they can pose a higher threat if reduced to monomethyl arsenite and dimethyl arsenite [7]. Natural waters in Bangladesh and India have been reported to have arsenic concentrations of > 50 µg/L [8]. The highest concentration of arsenic at 11500 mg/L has been reported in Argentina [9]. The current WHO-recommended limit of arsenic in drinking water is 10 µg/L[10].

The most effective solution for preventing arsenic toxicity in humans and animals is having a safe water supply. There are a multitude of techniques by which arsenic can be removed from water, for example, coagulation, oxidation and precipitation, reverse osmosis, and electro-dialysis [11, 12]. The sophisticated instrumentation, high cost of processing and decreased effectiveness at removing low levels of arsenic concentration in water renders these processes to be less desirable

[12]. In contrast, adsorption technology is simple, safe, inexpensive, does not require sophisticated instrumentation, and thus can be used in small household devices as well as large-scale treatment facilities [12]. The common adsorbents for arsenic removal from water are activated carbon [13], iron oxide [11], titanium dioxide [14], etc. [12]. Iron oxides are frequently used as adsorbents because they are environmentally friendly and have low production costs. However most iron oxides exist as fine powders, and their separation from aqueous solution after adsorption is difficult [11]. Moreover, these cannot be transferred to column-based methods because of poor hydraulic conductivity. Therefore facile, green, porous, and cost-effective support materials for coating iron oxides are necessary to increase the surface area and hydraulic conductivity. Moreover, it is crucial to make iron oxide coating permanent and stable on the supports to get regenerability and avoid leaching of iron in water.

The current study reports a new, porous, and inexpensive iron oxide-based adsorbent on a geopolymer support. Geopolymers are inorganic polymers prepared by using reactive aluminosilicate precursors (for example, metakaolin, fly ash etc.) with alkali solutions [15]. Geopolymers are garnering attention due to their high mechanical strength, fire resistance, high pH stability and reputation as a “green” environmentally friendly material [16, 17]. Although mainly used as construction materials, geopolymers are finding applications in catalysis [18], separation science [17, 19, 20] and as adsorbents. They have been reported as adsorbents for various heavy metals such as lead, nickel, cadmium, mercury, copper, cesium, etc. and dyes like methylene blue, and crystal violet [21-25]. To date, only two studies have been reported using modified geopolymers as adsorbents for arsenate [24, 26]. However, these studies used large, low-surface area irregular geopolymer particles formed by crushing the monoliths to study only the limited adsorption of As(V). Unfortunately, the adsorption of other important arsenic species such

as As(III), and organic arsenic species like monomethyl arsenate and dimethyl arsenate were not investigated.

In the current study, spherical and porous geopolymer microparticles have been employed for adsorption of two inorganic arsenic species viz. As(III) and As(V) and two organic arsenic species viz. DMA and MMA. Geopolymers are negatively charged due to the presence of AlO_4^- tetrahedra in its structure, which is balanced by extra-framework cations such as Na^+ or K^+. Therefore, geopolymers can be directly used as an adsorbent for cations. To utilize geopolymers for adsorption of oxyanions like arsenate and arsenite, these need to be modified. Hence geopolymers were impregnated with iron oxide (Fe-GP). The adsorption studies have been performed to elucidate the role of different parameters such as pH, temperature, adsorbent dosage amount, contact time, and competing ions.

6.3 Materials and Methods

6.3.1 Materials

Fumed silica (CAS:112945-52-5), potassium hydroxide, iron (II) chloride tetrahydrate, sodium arsenite, potassium arsenate, and dimethylarsinic acid were purchased from Millipore Sigma (MO, U.S.A.). Monosodium acid methane arsonate sesquihydrate was purchased from Chem Service (PA, U.S.A). Metakaolin was obtained from Advanced Cement Technologies (WA, U.S.A.). Crisco® Pure Canola Oil was obtained from Walmart, USA. Milli-Q water purification system (Millipore, Billerica, MA, U.S.A.) was employed to purify water. The stock solutions (100 mg/L of elemental arsenic) of each arsenic species were prepared by dissolving an appropriate amount of the above-mentioned arsenic chemicals in DI water. The working solutions were prepared by successive dilutions with DI water. All chemicals were used without further purification.

6.3.2 Synthesis of iron oxide coated geopolymers

Figure 6.1a shows a schematic for the synthesis of iron oxide-coated geopolymer microspheres (Fe-GP). Geopolymer microspheres were synthesized using inverse suspension polymerization, as reported previously by our laboratory [17, 19, 27]. Briefly, geopolymer slurry was made by mixing 6.6 g of fumed silica, 10.37 g of potassium hydroxide, 12.34 g of metakaolin in 20 mL of DI water. The initial geopolymer composition was kept fixed at Si/ Al/ K molar ratio of 2:1:2. The slurry was suspended in a large amount (400 mL) of canola oil under mechanical stirring (6000 rpm) in a 600 mL polypropylene beaker. An overhead stirrer consisting of the three-blade propeller (Talboys 101, Troemner, Thorofare, NJ, U.S.A.) was employed.

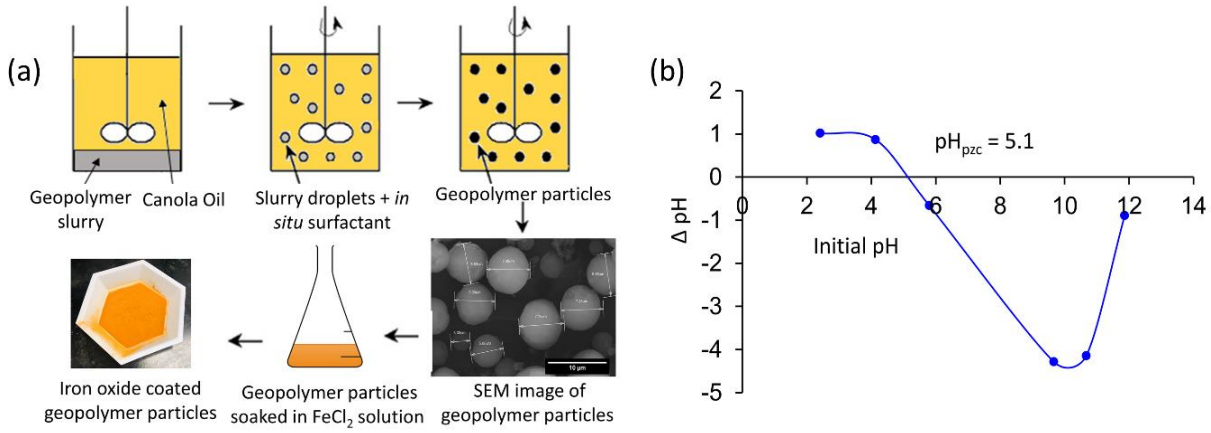

Figure 6.1 (a) Synthesis of iron oxide coated geopolymer particles (Fe-GP) (b) pHpzc of Fe-GP particles.

The geopolymerization reaction was completed in eight hours. The spherical geopolymer microparticles were extracted in water using a separatory funnel and further washed with hexane, methanol, and water to remove excess oil and surfactants. The microparticles were calcined at 500

℃ for 4 hours at the rate of 2 ℃/min. The large particles (> 500 μm) were removed by defining using water.

The geopolymer microparticles (30 g in each 250 mL Erlenmeyer flask) were then immersed in 200 mL of 0.1 M iron (II) chloride tetrahydrate and stirred in an incubator shaker at 300 rpm for 15 days. Iron (II) chloride solution was replaced with fresh iron (II) chloride solution every day. The iron-oxide coated particles thus formed were washed with DI water several times and then dried in an oven at 100 ℃. The particles were further used for adsorption experiments. The point of zero charge (pH_{pzc}) of Fe-GP is shown in Figure 6.1b and was determined by the pH drift method [17].

6.3.3 Material characterization

SEM images were acquired under a high vacuum and acceleration voltage of 20 kV using Hitachi S-4800 II Field Emission SEM (FE-SEM). The Fe-GP microspheres were coated *with a thin conductive layer of silver using CrC-100 sputtering system before doing* scanning electron microscopy. The iron wt % of iron-oxide coated geopolymer microspheres was analyzed using an EDAX EDS system on a Hitachi S-4800 II Field Emission FE-SEM without coating. The particle size and particle size distribution were determined by Shimadzu SALD-7101 laser diffraction particle size analyzer. A micrometrics ASAP 2020 Porosimeter was employed for Brunauer–Emmett–Teller (BET) surface area analysis. The samples were first degassed at 90 ºC for 24 hours to remove any adsorbed species from the samples. The X-Ray Diffraction pattern was acquired by using Shimadzu MAXima X XRD-7000 X-ray diffractometer. The Fourier transform- infrared spectroscopy (FTIR) was carried out using Thermo Nicolet 6700 FTIR Spectrometer, from 600 cm^{-1} to 4000 cm^{-1}. Thermogravimetric analysis was performed using Shimadzu TGA-51

Thermogravimetric Analyzer. Samples (~3 mg) were placed in the platinum pans and heated in a nitrogen atmosphere at 10 °C min^{-1} from 25 °C to 900 °C. Shimadzu ICPE-9800 inductively coupled plasma- optical emission spectrometer (ICP-OES) was used to analyze elemental arsenic concentrations before and after adsorption studies. The samples were acidified with 2% nitric acid before analyses. The data was collected at wavelength of 193.759 nm. The quality assurance of ICP-OES data was done by monitoring relative standard deviation of the intensity readings for each sample. The RSD ranged from ~0.1-15% for all sample readings and are shown for calibration points for each arsenic species in Table S1.

6.3.4 Adsorption experiments

Batch experiments were carried out to determine the degree of adsorption for four arsenic species on the Fe-GP. Various factors affecting adsorption viz, pH, dose of adsorbent, contact time, temperature, and competing ions, were studied. Adsorption experiments were performed in 20 mL cylindrical vials containing 10 mL aqueous arsenic solution. The desired dosage of Fe-GP adsorbent was added to the vials and shaken at 400 rpm in a temperature-controlled incubator shaker. Preliminary adsorption experiments were performed at 100, 200, 300 and 400 rpm to determine the effect of shaking speed on arsenic percent removal (data not shown). The increase in percent removal was observed with increase in shaking speed. Hence, 400 rpm was used in all the further adsorption experiments. After adsorption, the suspension was filtered using 0.22 µm syringe filter. The filtrate was acidified using 2% nitric acid. The concentration of elemental arsenic left in the filtrate was then determined by ICP-OES.

The quantity of arsenic adsorbed by Fe-GP was determined using the following equation:

$$q = \frac{(C_0 - C_e)}{m} \times V \quad (6.1)$$

where q is the quantity of arsenic adsorbed by Fe-GP ($mg_{As}/g_{Fe\text{-}GP}$), C_0 is the initial concentration of arsenic (mg/L), C_e is the equilibrium arsenic concentration (mg/L), m is the mass of Fe-GP adsorbent (g) and V is the volume of the solution (L). The adsorption efficiency/percent removal (%) was determined by the following equation:

$$\text{Adsorption efficiency } (\%) = \frac{(C_0 - C_e)}{C_0} \times 100 \quad (6.2)$$

For the determination of equilibrium times and kinetic studies, 0.1 g of Fe-GP particles were added to 10 mL of the desired arsenic species at three different initial concentrations, viz. 0.5, 5 and 10 mg/L at 298 K and sampled at intervals ranging from 1 min to 17 hours.

The adsorption isotherm plots were constructed at three different temperatures viz. 298 K, 308 K, 318 K by adding 0.1 g of Fe-GP particles to 10 mL of arsenic species for 60 minutes.

The effect of adsorbent dosage on the uptake of different arsenic species was determined by adding the varying amounts of Fe-GP from 20 mg to 200 mg to 10 mL of the desired arsenic species for 1 min at 298 K.

The effect of pH on adsorption was studied by adjusting the pH using 0.1 M NaOH and 0.1 M HCl. The effect of competing ions on adsorption of arsenic species was studied for five naturally occurring ions, Cl^-, SO_4^{2-}, PO_4^{3-}, SiO_3^{2-} and HCO_3^-. The effect of competing ions on adsorption of 10 mg/L of each arsenic species was studied for two concentrations of competing ions viz. 5 mg/L and 20 mg/L for an adsorption time of 60 minutes.

Experiments were also conducted to investigate the leaching of iron from Fe-GP particles during adsorption experiments. Fe-GP particles were immersed in four different arsenic solutions at pH ranging from 2-12 for 24 hours. Concentrations of leached iron were evaluated using ICP-OES and were found to be under the limit of detection for this sensitive method. Hence it was concluded that no significant levels of Fe are leaching from Fe-GP particles.

6.3.5 Arsenic desorption

To perform desorption studies, first, the arsenic species were adsorbed by adding 0.1 g of Fe-GP in 10 mg/L of arsenic species solutions and shaken for 60 minutes at 400 rpm. After adsorption of arsenic species, the adsorbent was separated by centrifugation, washed with DI water, and dried. The filtrate was then analyzed by ICP-OES to analyze the concentration of arsenic left. The dry adsorbent containing arsenic species was then put in 10 mL of 1M NaOH solution and shaken for 60 minutes. The filtrate was then analyzed for arsenic concentration by ICP-OES.

6.4 Results and Discussion

6.4.1 Geopolymer synthesis and characterization

6.4.1.1 Optimization of iron weight percent

Preliminary experiments revealed that an increase in the iron wt% in geopolymer particles increased the percent removal of arsenic species. The amount of iron loading in the adsorbent controls the adsorption process since the removal efficiency depends on the chemical interaction of iron with arsenic species. Therefore, geopolymer particles were soaked in iron (II) chloride solution for 15 days to obtain high amounts of iron loading in the adsorbent. Fresh iron (II) chloride

solution was added every day. Figure 6.2a shows the increase in iron wt% with time. The final Fe-GP microparticles used for the adsorption studies contained 20 wt% Fe.

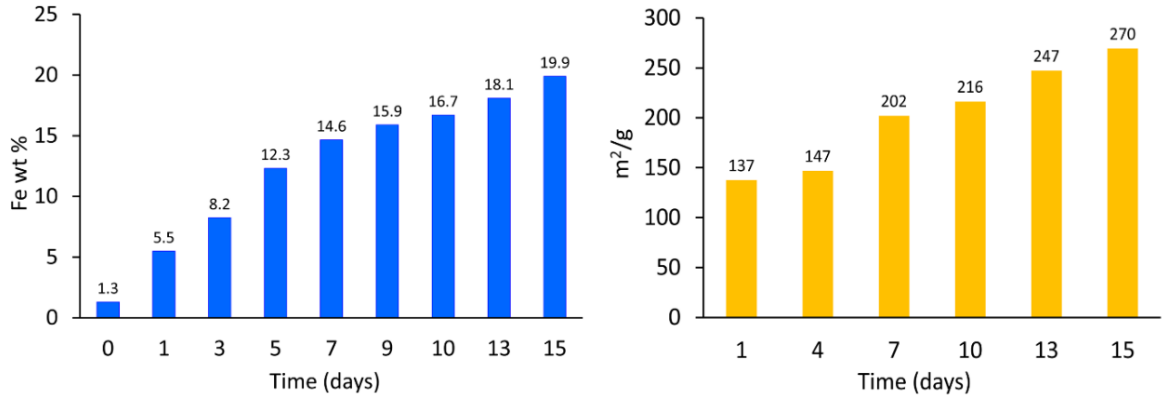

Figure 6.2 (a) EDS data showing increase in % iron with time (b) Increase in surface area of Fe-GP particles with time.

It should be noted that Fe-GP particles obtained after 16 and 17 days of iron impregnation contained approximately 22 and 24 wt% of Fe (data not shown) however, they showed a decrease in adsorption efficiency, which can be due to pore clogging and inaccessibility of arsenic species to the pores. Hence the iron adsorption period of 15 days was optimal as it provided high surface area particles while providing large enough pores to accommodate all of the studied arsenic species.

6.4.1.2 *Crystallographic studies*

Geopolymer formation was confirmed by X-ray diffraction which shows the characteristic amorphous hump between the 2θ value of 25-30º (see Figure 6.3a). Figure 6.3a shows that the coating of geopolymers with iron oxide did not change the XRD pattern and the ferric species are non-crystalline. Hence it can be concluded that hydrous ferric oxides have formed during coating process [26].

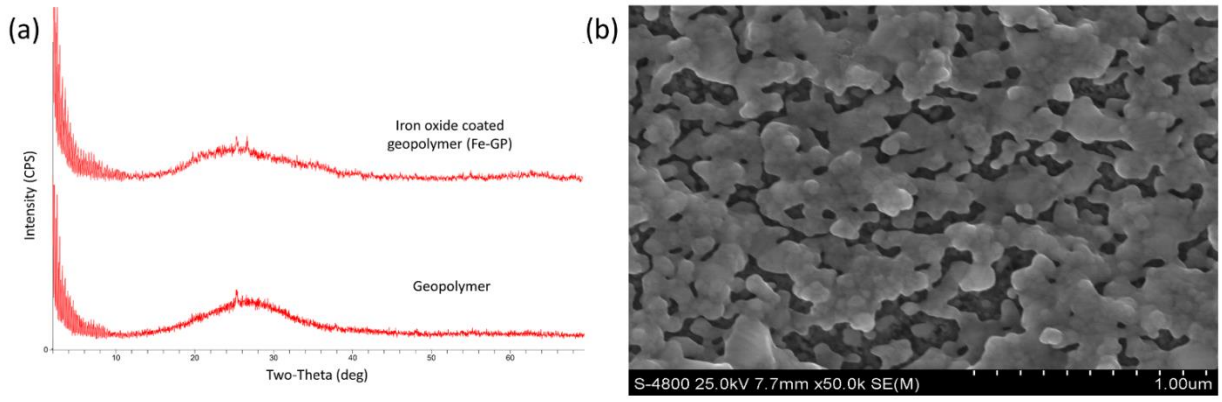

Figure 6.3 (a) XRD diffraction pattern of geopolymer and iron-oxide coated geopolymer (Fe-GP). (b) Field Emission-Scanning Electron Microscopy image showing interconnected pore network of final Fe-GP microsphere used in adsorption studies.

There was no significant change (no appearance of crystalline structure) found in XRD pattern after 90 days showing that the Fe-GP adsorbent is physically and chemically stable (data not shown).

6.4.1.3 *TGA studies*

The structural weight losses are depicted in Figure 6.4a and 6.4b by TG curves of the original geopolymer and Fe-GP respectively. The weight loss of ~ 6% below 200 ℃ is due to dehydration of aluminosilicate gels of the geopolymer (see Figure 6.4a). The loosely bound water is removed first, followed by water bound to extra framework cations (K^+). The second thermal degradation of ~2.3 % between 700-900 ℃ can be attributed to removal of surface hydroxyl groups and formation of Si-O-Si bonds [28]. Comparing TG curve of Fe-GP (Figure 6.4b) with original geopolymer, it can be noted that there is greater weight loss below 200 ℃ (~ 10%) which implies more adsorbed water in case of the Fe-GP. From TGA, it can also be concluded that the coated

iron oxide compound is thermodynamically stable as a very small amount of weight loss is observed which is due to the evaporation of physically bound water.

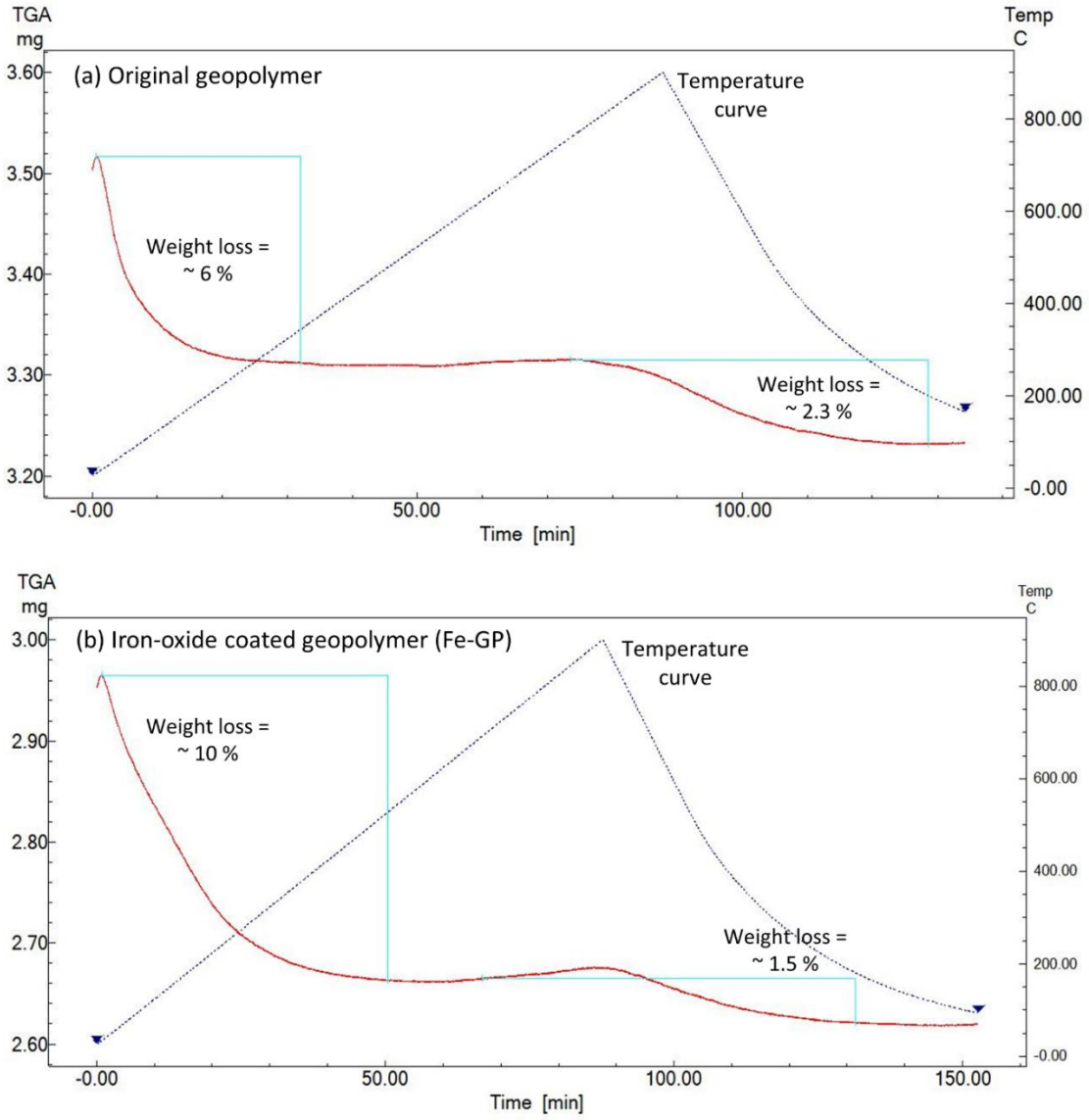

Figure 6.4: TG curve of (a) original geopolymer (b) iron-oxide coated geopolymer (Fe-GP)

6.4.1.4 FTIR studies

FTIR spectrum of original geopolymer (Figure 6.S1) showed characteristic peaks around 980 and 600 cm^{-1} corresponding to Si-O-Si/Al-O-Si asymmetric stretching and bending vibration [29]. Broad peaks around 3400 and 1600 cm^{-1} are associated with adsorbed water stretching and bending vibrations. Compared to the original geopolymer, a peak shift from 3438 to 3262 cm^{-1} and 1644 to 1622 cm^{-1} can be seen in the FTIR spectrum of the Fe-GP (Figure 6.S2). This can be attributed to the fact that adsorbed water is bound in iron in Fe-GP and the bond length of OH changes depending upon how tightly the water molecules are bound. Also, the peaks at 3262 cm^{-1} and 1622 cm^{-1} are more intense as compared to the original geopolymer which can be due to presence of more adsorbed water and surface hydroxyl groups. This observation is in line with greater weight loss seen for Fe-GP in TGA as compared to the original geopolymer. The characteristic peaks of the geopolymer, associated with Si-O-Al/ Si-O-Si also shifted slightly due to change in local environment of the geopolymer framework as potassium ions partially exchange with ferric/ferrous ions.

6.4.1.5 Morphological analysis

In addition to characterizing the chemical nature of a new adsorbent, it is also imperative to assess the physical parameters such as surface area, pore size, particle shape, and particle size distribution. The physical properties of Fe-GP adsorbent such as their morphology, mean size, surface area, and pore width were measured by scanning electron microscope, laser diffraction particle size analyzer, and a porosimeter. Spherical shape, small particle size, high surface area, adequate porosity and adequate accessibility to pores are essential in improving the adsorption efficiency of any adsorbent. Geopolymers are usually synthesized in monolithic forms since they are primarily used in construction materials. Both monoliths and irregular geopolymer particles (made by

crushing and sieving monoliths) have been reported as an adsorbent [26, 30]. However, these materials do not possess high surface areas, they have low intrinsic permeability and have an irregular particle shape. This work overcomes these disadvantages by introducing spherical geopolymer porous microparticles as adsorbent supports. Figure 6.1a demonstrates the spherical shape of the Fe-GP particles. Figure 6.2b shows the increase in specific surface area of Fe-GP with time (as the iron loading in the Fe-GP increases). The increase in specific surface area with increase in iron wt% can be due to the precipitation of iron oxide within and on the surface of the geopolymer microparticles. The specific surface area of Fe-GP used for final adsorption studies was 270 m^2/g.

The mesoporous structure of Fe-GP is indicated by the characteristic hysteresis loop of a Type IV isotherm (see Figure 6.S3). The Barrett, Joyner, and Halenda (BJH) desorption average pore width of the original geopolymer and the Fe-GP after 15 days was 96 Å and 42 Å, respectively. This decrease in pore size shows that iron oxide particles were successfully impregnated within the pores. The BJH desorption pore volume of Fe-GP after 15 days was 0.36 cm^3/g (see supporting information, Fig 6.S4). Figure 6.3b shows the morphology of the adsorbent. The high surface area and interconnected pore network of Fe-GP satisfies the requirements of a good adsorbent. Laser diffraction particle size distribution data showed the median diameter to be 20.1 µm and size distribution ranged from ~ 4 µm to 100 µm (See Figure 6.S5).

6.4.2 Effect of contact time and initial concentration

Figure 6.5 shows the effect of contact time on the adsorption of arsenic species on the Fe-GP at three different initial arsenic concentrations (0.5, 5 and 10 mg/L). The adsorption was enhanced with increasing contact time. The adsorption of arsenic species is rapid in the first 60 minutes and

then relatively small increases were observed at longer times, finally reaching an equilibrium. It was concluded that 60 minutes of contact time was suitable for conducting further adsorption studies since the percentage of arsenic adsorption after 60 minutes increases by less than 0.1% per minute for all arsenic species. As compared to other geopolymer adsorbents which were reported to have equilibrium time from somewhere between 1 to 7 days [21, 24, 26], adsorption on Fe-GP reached equilibrium very rapidly. This can be a reflection of the enhanced surface properties of Fe-GP, as adsorbate ions will have higher surface area to interact with and can penetrate the inner pores faster. Also, the slow adsorption rate after 60 minutes suggested that intraparticle diffusion mainly controlled the latter adsorption process [31].

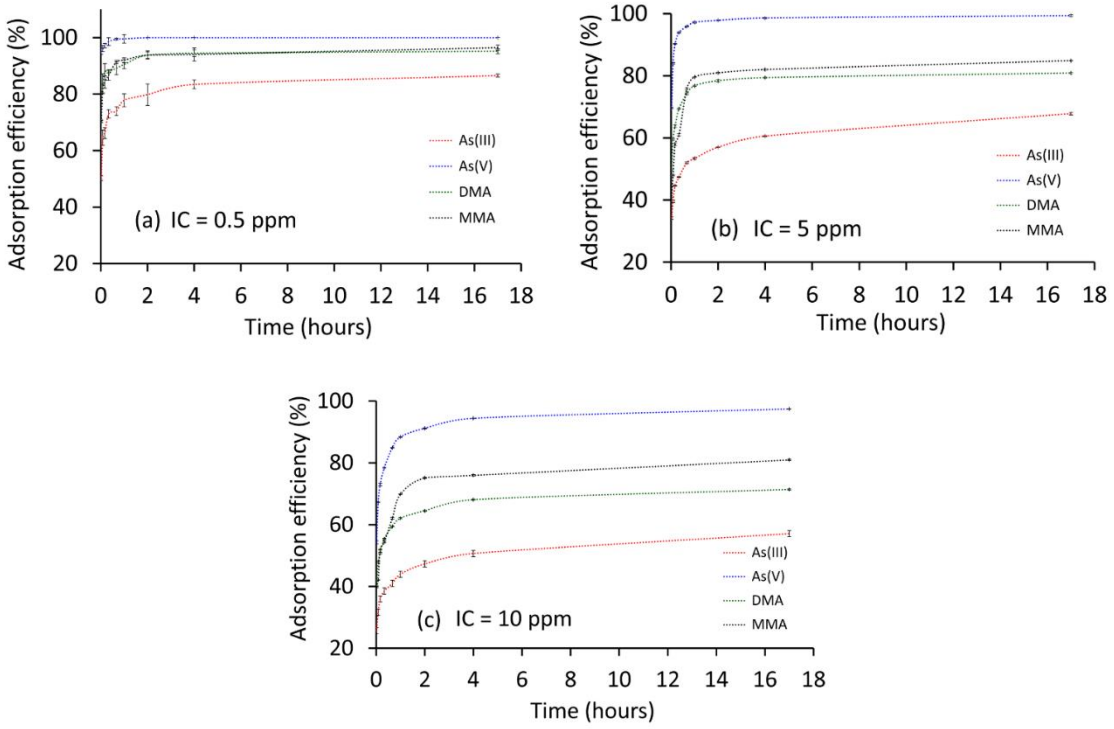

Figure 6.5 Effect of adsorption time on uptake of arsenic species by Fe-GP microspheres. Initial concentrations of arsenic species (a) 0.5 mg/L (b) 5 mg/L (c) 10 mg/L, temperature = 298 K,

volume of arsenic species solution = 10 mL, adsorbent dosage = 0.1 g, shaking rate: 400 rpm. The plots contain error bars (standard deviations) in place of markers.

The effect of initial concentration of arsenic species on adsorption process can be clearly deduced from Figure 6.5. The adsorption efficiency decreased from 86 to 57%, 100 to 97%, 95 to 71% and 96 to 81% for As(III), As(V), DMA and MMA with an increase in the initial concentration of arsenic species from 0.5 mg/L to 10 mg/L. The adsorption efficiency decreased since amount of adsorbate that can be adsorbed is fixed for a given amount of adsorbent.

The pseudo-second-order equation was applied to describe the changes in adsorption with time on Fe-GP.

$$\frac{t}{q_t} = \frac{1}{kq_e^2} + \frac{1}{q_e}t \qquad (6.3)$$

where k (g mg^{-1} min^{-1}) is the rate constant of adsorption, q_t (mg g^{-1}) and q_e (mg g^{-1}) are the adsorption capacities at time t and equilibrium time, respectively. Initial sorption rate, h (mg g^{-1} min^{-1}) can be defined as

$$h = kq_e^2 \qquad (t \to 0) \qquad (6.4)$$

h and k values can be obtained experimentally from the slope and the intercept of the linearized kinetic plots. Figure 6.6 shows the kinetic plots for all arsenic species at three different initial arsenic concentrations of 0.5, 5 and 10 mg/L. The high R^2 values (>0.999) show that kinetics of arsenic adsorption on Fe-GP fits well with the pseudo-second-order kinetic model. This indicates that overall adsorption process is controlled by chemisorption[32]. The h, k and R^2 values of arsenic species are presented in Table 6.S2. The higher the h and k values, the faster is the

adsorption [33]. The initial adsorption rate and the rate constants of adsorption are in the order of As(V) > DMA > MMA >As(III) at all initial concentrations. The rate constants decreased with increasing initial concentration of arsenic species. This implies that adsorption of arsenic on Fe-GP was slower at high adsorbate concentrations.

6.4.3 Adsorption isotherms

The two most used isotherm models for solid-liquid systems are the Langmuir isotherm and the Freundlich isotherm. The Langmuir isotherm model is based on a monolayer coverage of the adsorbate on the adsorbent which has a homogeneous surface. In contrast, the Freundlich isotherm model is an empirical model based on multilayer coverage of adsorbate onto a heterogeneous adsorbent. The Langmuir model can be written in the form;

$$\frac{C_e}{q_e} = \frac{C_e}{q_m} + \frac{1}{bq_m} \qquad (6.5)$$

The Freundlich isotherm model is expressed in the form;

$$\log q_e = \frac{1}{n}\log C_e + \log K_f \qquad (6.6)$$

where C_e is equilibrium arsenic concentration (mg/L), q_e is the quantity of arsenic adsorbed by Fe-GP at equilibrium ($mg_{As}/g_{Fe\text{-}GP}$), q_m is the maximum quantity of arsenic adsorbed by Fe-GP ($mg_{As}/g_{Fe\text{-}GP}$) and b is the Langmuir adsorption equilibrium constant. K_f and n are the Freundlich constants indicative of relative adsorption capacity of the adsorbent and intensity of adsorption process, respectively.

To calculate the maximum adsorption capacity from the Freundlich model, it is necessary to operate at a constant initial concentration of the adsorbate and variable amounts of the of adsorbent[34]. Hence, log q_m is extrapolated value of log q_e for $C_e = C_0$.

$$q_m = K_f C_0^{\frac{1}{n}} \quad (7)$$

The favorable nature of adsorption can also be expressed by dimensionless equilibrium parameter R_L:

$$R_L = \frac{1}{1+bC_0} \quad (8)$$

where C_0 is the initial concentration of adsorbate.

The equilibrium data were analyzed by Langmuir and Freundlich isotherms and the adsorption parameters are reported in Table 6.S3 and Table 6.1, respectively.

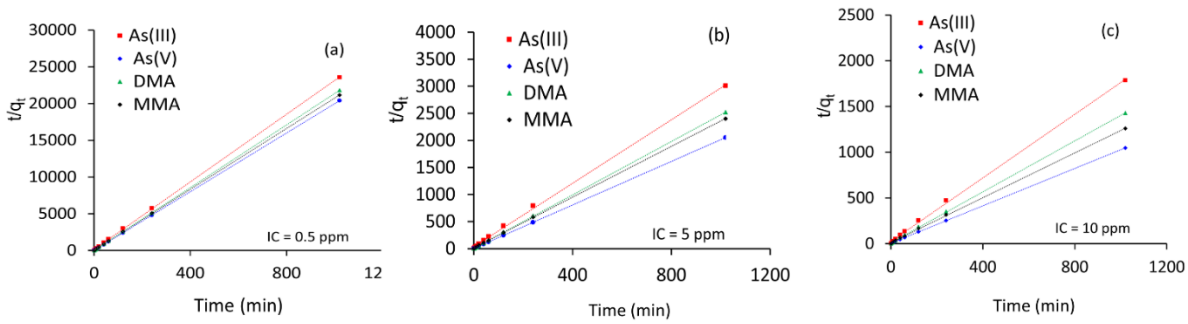

Figure 6.6 Adsorption kinetics (pseudo-second-order plots) of arsenic species on Fe-GP. Initial concentrations of arsenic species (a) 0.5 mg/L (b) 5 mg/L (c) 10 mg/L, temperature = 298 K, volume of arsenic species solution = 10 mL, adsorbent dosage = 0.1 g, shaking rate: 400 rpm. Pseudo-second-order kinetic parameters h, k and statistical parameter R^2 are presented in Table S2.

The correlation coefficients show that the adsorption of arsenic species on Fe-GP is best described by the Freundlich isotherm model indicating the heterogeneous nature of the adsorbent and a multilayer adsorption process. Figure 6.S6 shows the linearized Freundlich isotherm plots for four arsenic species at three different temperatures (298, 308 and 318 K). The n values of greater than 1 indicate strong interactions between adsorbent and adsorbate [24]. Thus, the interaction strength of different arsenic species with Fe-GP is in the order of As(V) > DMA > As(III) > MMA. The maximum adsorption capacity (q_m) from Freundlich model was found to be 614.4, 1689.6, 1076.4, 1161.7 µg/g for As(III), As(V), DMA and MMA at 298 K. Also, the increase in temperature did not show any appreciable difference in arsenic percent removal.

Table 6.1. Freundlich adsorption isotherm parameters of As(III), As(V), DMA and MMA at 298 K, 308 K, 318 K

As species (298 K)	n^a	$K_f{}^b$ ($mg^{1-1/n}\ L^{1/n}\ g^{-1}$)	$q_m{}^c$ (mg/g)	R^2
As(III)	1.62	0.1490	0.6144	0.9990
As(V)	3.59	0.8904	1.6896	0.9976
DMA	1.79	0.2968	1.0764	0.9900
MMA	0.35	0.5182	1.1617	0.9972

As species (308 K)	n^a	$K_f{}^b$ ($mg^{1-1/n}\ L^{1/n}\ g^{-1}$)	$q_m{}^c$ (mg/g)	R^2
As(III)	1.65	0.1554	0.6266	0.9992
As(V)	3.50	0.9024	1.7406	0.9988
DMA	2.35	0.3114	0.8298	0.9811
MMA	0.36	0.5145	1.1708	0.9971

As species (318 K)	n^a	$K_f{}^b$ ($mg^{1-1/n}\ L^{1/n}\ g^{-1}$)	$q_m{}^c$ (mg/g)	R^2
As(III)	1.62	0.1584	0.6541	0.9981
As(V)	3.45	0.9495	1.8518	0.9999

DMA	2.27	0.3217	0.8869	0.9790
MMA	0.36	0.5228	1.1975	0.9981

[a] n is the dimensionless Freundlich constant intensity of adsorption process

[b] K_f is the Freundlich constant indicative of relative adsorption capacity of the adsorbent

[c] q_m is the maximum quantity of arsenic adsorbed by Fe-GP ($mg_{As}/g_{Fe\text{-}GP}$)

The maximum adsorption capacity (q_m) from Langmuir model was found to be 857.4, 1513.5, 1065.6 and 1097.6 µg/g for As(III), As(V), DMA and MMA at 298 K. The type of isotherm is indicated by value of R_L, viz. irreversible ($R_L = 0$), favorable ($0 < R_L < 1$), linear ($R_L = 1$) or unfavorable ($R_L > 1$) [35]. In the current study all the R_L values are greater than 0 and less than 1, hence showing favorable adsorption.

6.4.4 Effect of dosage

The effect of adsorbent dosage on the removal of arsenic species was studied by varying the amount of Fe-GP. Figure 6.7 shows the adsorption efficiency at adsorbent dosages ranging from 20 mg to 200 mg at a volume of 10 mL and an arsenic concentration of 10 mg/L. The adsorption time was set at 1 minute so that a trend of adsorption efficiency could be observed. The adsorption efficiency increased from 12 to 63%, 13 to 80%, 19 to 84% and 18 to 82% for As(III), As(V), DMA and MMA, respectively with increased dosage amounts from 20 to 200 mg.

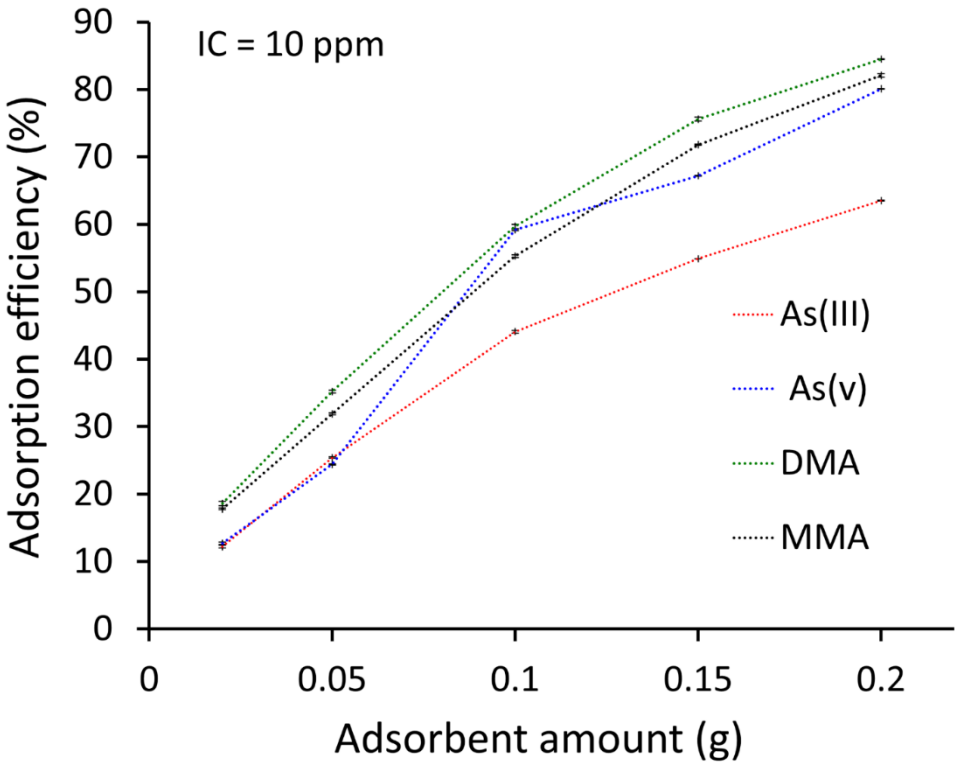

Figure 6.7 Effect of adsorbent dosage on uptake of Arsenic species by Fe-GP microspheres. Initial concentrations of arsenic species = 10 mg/L contact time = 1 minute, temperature = 298 K, volume of arsenic species solution = 10 mL, shaking rate: 400 rpm. The plots contain error bars (standard deviations) in place of markers

This is expected because as the adsorbent dosage increase, the number of adsorption sites increases. The adsorption efficiencies are different for different arsenic species owing to distinct chemical structures at given pH. As(III) shows lower removal efficiency as compared to As(V), DMA and MMA since at pH 7, As (III) exists as neutral species whereas As(V), DMA and MMA exist as ionic species. Therefore, As(V), DMA and MMA have higher electrostatic interaction with the surface of the adsorbent and consequently shows higher removal efficiency.

6.4.5 Plausible mechanism

The mechanism of arsenic adsorption on Fe-GP is explained on the basis of effect of pH and point of zero charge. pH has a great influence on adsorption efficiency of Fe-GP adsorbent. Figure 6.8 illustrates the adsorption trends of As(III), As(V), DMA and MMA on Fe-GP under different pH conditions. A high arsenic initial concentration of 10 mg/L was selected to be able to see the trends clearly. All arsenic species except As(III) showed a slight decrease in adsorption efficiency with a rise in pH to pH 10 and then a sharp decline. Highest percent removal of 99.5%, 62.7% and 80.7% were observed at an acidic pH of 2.5 for As(V), DMA and MMA. While highest percent removal of 61.4 % for As (III) was observed to be at pH of 11.5.

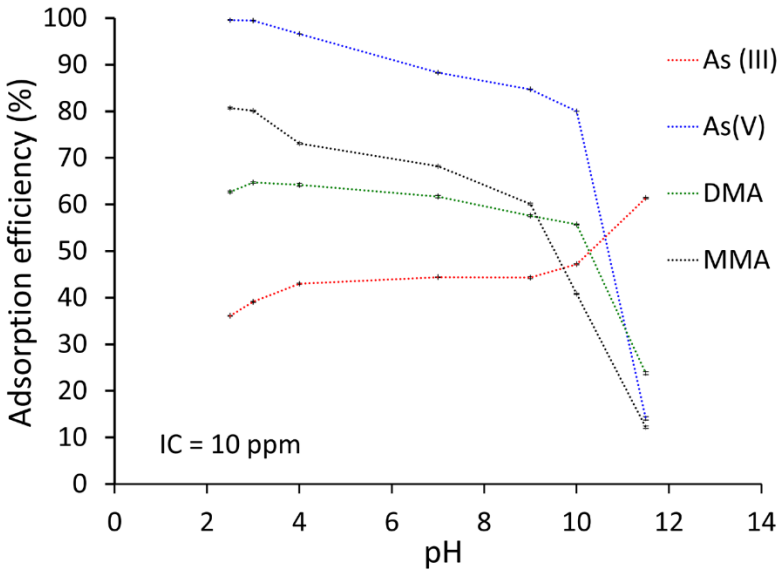

Figure 6.8 Effect of pH on uptake of Arsenic species by Fe-GP microspheres. Initial concentrations of arsenic species = 10 mg/L contact time = 60 minutes, temperature = 298 K, volume of arsenic species solution = 10 mL, adsorbent dosage = 0.1 g, shaking rate: 400 rpm. The plots contain error bars (standard deviations) in place of markers

pH affects the surface charge of adsorbent as well as the ionization of arsenic species. The pH of point of zero charge (pH_{pzc}) is a good indicator of surface charge of adsorbent material [17]. The pH_{pzc} of Fe-GP was determined to be 5.1 (Figure 6.1b) which implies that surface of adsorbent is positively charged at pH < 5.1 and is negatively charged at pH > 5.1. The surface of iron oxides acquires hydroxyl groups on exposure to water and depending on the pH of the solution the hydroxyl groups can bind or release H^+ ion [11]. The adsorption happens due to the interaction of $-OH_2^+$, -OH and $-O^-$ groups on the surface of iron oxides with ligand (O) characters on the arsenic species via surface complexation or ligand exchange processes [11].

As (V) dominantly exists as H_3AsO_4 and $H_2AsO_4^-$ in the pH range of 2-3, as $H_2AsO_4^-$ and $HAsO_4^{2-}$ in the pH range of 3-6 and as $HAsO_4^{2-}$ and AsO_4^{3-} in the pH range of 6-12 [31]. Since at lower pH, the surface of the adsorbent is positively charged due to protonation of surface hydroxyl groups, there are favorable interactions between As(V) and Fe-GP. With increasing pH, the adsorbent surface gradually becomes negatively charged and hence more unfavorable for As(V) adsorption.

As shown in Figure 6.8, adsorption of As(III) steadily increases from pH 2.5 to 7, remained almost constant from pH 7 to 10 and then abruptly increased from pH 10 to 11.5. The increase in adsorption of As(III) at high pH is not usual and to our knowledge only one study has been reported observing this trend [36]. A DFT study was reported that calculated adsorption energies for arsenic species on TiO_2 adsorbent. They concluded that for As(III) the adsorption energies are in the order of $AsO_3^{3-} > OH^- > HAsO_3^{2-} > H_2AsO_3^- > H_2O > H_3AsO_3$ [36]. Therefore AsO_3^{3-} can compete with OH^- at high pH conditions [36]. Similar reasons may explain the unusual increase in adsorption efficiency for As(III) in the current study.

DMA and MMA exist as $HAsO_2(CH_3)_2$ and $H_2AsO_3CH_3$ at low pH, and as the pH increases, these arsenic species become negatively charged in the form of $AsO_2(CH_3)_2^-$ and $HAsO_3CH_3^-$ [31, 37]. Therefore, as can be seen in Figure 6.8 the adsorption efficiency is nearly constant for DMA and MMA from pH of 2.5 to 10 and then decreased sharply until pH 11.5.

The point of zero charge has been used to elucidate the mechanism involved in arsenic adsorption on an adsorbent [38]. pH_{pzc} of Fe-GP was found to be 5.1. The pH_{pzc} of Fe-GP decreased from 5.1 to 4.3, 3.9, 4.0 and 4.0 for As(III), As(V), DMA and MMA after their adsorption at initial concentration of 10 mg/mL. The shifts in pH_{pzc} is characteristic of inner-sphere adsorption [33, 38]. In inner sphere surface complexes, there are no water molecules between the adsorbing ions and the surface. Surface of the adsorbent becomes more negatively charged as the specific adsorption of anions takes place and hence the pH_{pzc} changes. The pH_{pzc} of a metal oxide cannot be shifted by the formation of outer-sphere surface complexes since the surface charge cannot be altered by the adsorbent and the adsorbate. Therefore, it can be concluded that the arsenic species are forming inner-sphere complexes with the adsorbent which are negatively charged. The adsorption process is hence not purely electrostatic in nature.

The EDS elemental data also showed the presence of arsenic after adsorption of arsenic species on Fe-GP. Figure 6.9 shows the EDS map and spectrum for the Fe-GP before and after adsorption of As(V). The EDS data was also collected after washing the Fe-GP (with adsorbed arsenic) with water. The data showed approximately the same amount of arsenic present before and after washing implying the formation of coordination complexes with Fe-GP.

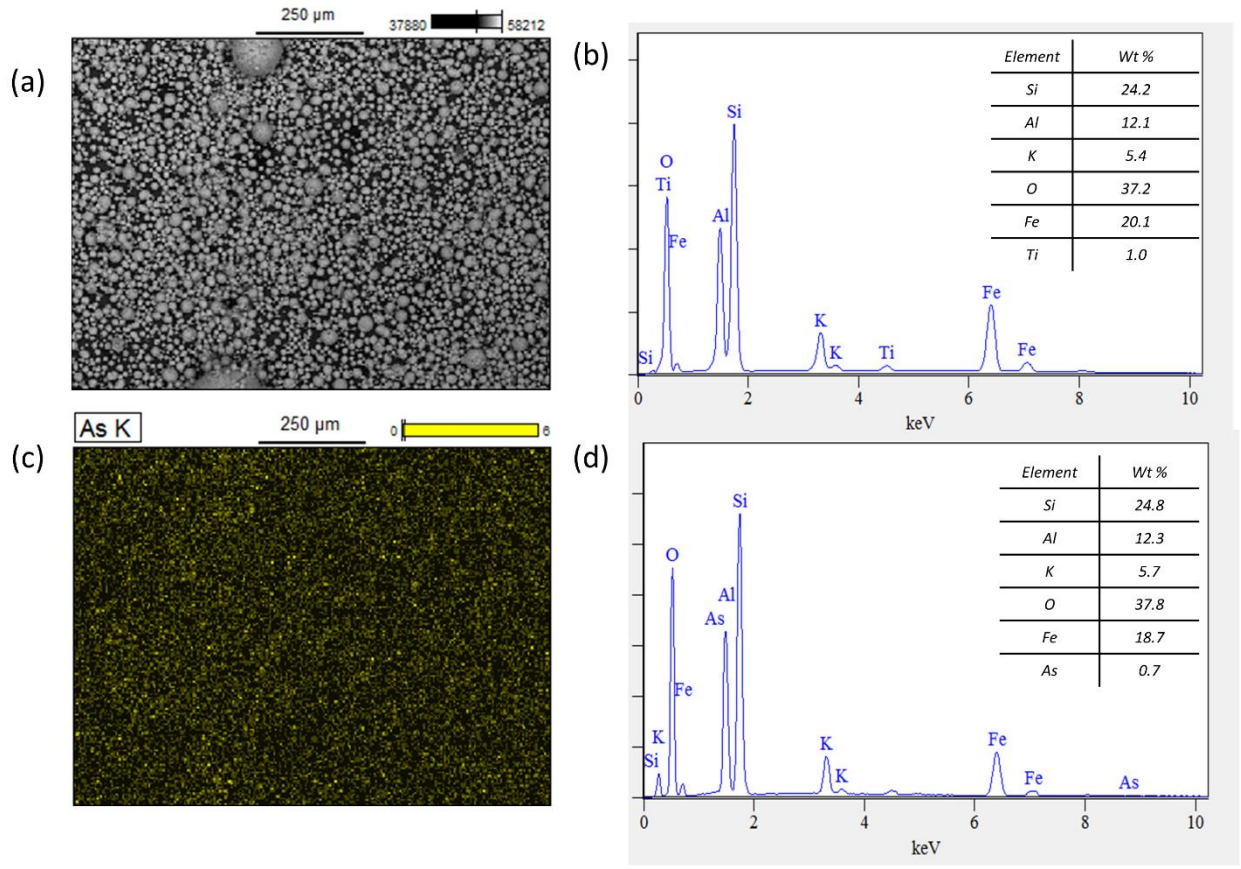

Figure 6.9 (a) and (b) EDS map and spectrum of Fe-GP adsorbent before the adsorption of As (V). (c) and (d) EDS map and spectrum of Fe-GP adsorbent after the adsorption of As (V). Initial concentrations = 10 mg/L contact time = 60 minutes, temperature = 298 K, volume of arsenic species solution = 10 mL, adsorbent dosage = 0.1 g, shaking rate= 400 rpm.

6.4.6 Effect of competing ions

Natural water is a multi-component system containing many of soluble ions like Cl^-, SO_4^{2}, NO_3^-, PO_4^{3-} etc. For instance, water in Bangladesh has been reported to have high concentrations of phosphates (0.2 to 0.3 mg/L), silicates (6-28 mg/L) and bicarbonate (50-671 mg/L) [12]. These ions can interfere with the arsenic adsorption by competing for active sites on the adsorbent [11].

Therefore, it is vital to conduct the studies which show adsorbent behavior in multi-ion systems. The influence of competing ions on arsenic adsorption is shown in Figure 6.10. A low (5 mg/L) and a high (20 mg/L) concentration of competing anions were chosen to see the influence at both extremes. As can be seen in Figure 6.10, the addition of Cl^-, SO_4^{2-}, SiO_3^{2-} and HCO_3^- do not have appreciable influence on adsorption of arsenic species. PO_4^{3-} appreciably influenced the adsorption of arsenic species on Fe-GP. The removal efficiency of As(III), As(V), DMA and MMA decreased by approximately 8, 31, 24 and 50 % respectively when the concentration of PO_4^{3-} was 20 mg/L. This decrease might be explained by the fact that PO_4^{3-} competes with arsenic as it can form inner-sphere complexes with the Fe-GP hydroxyl groups [39].

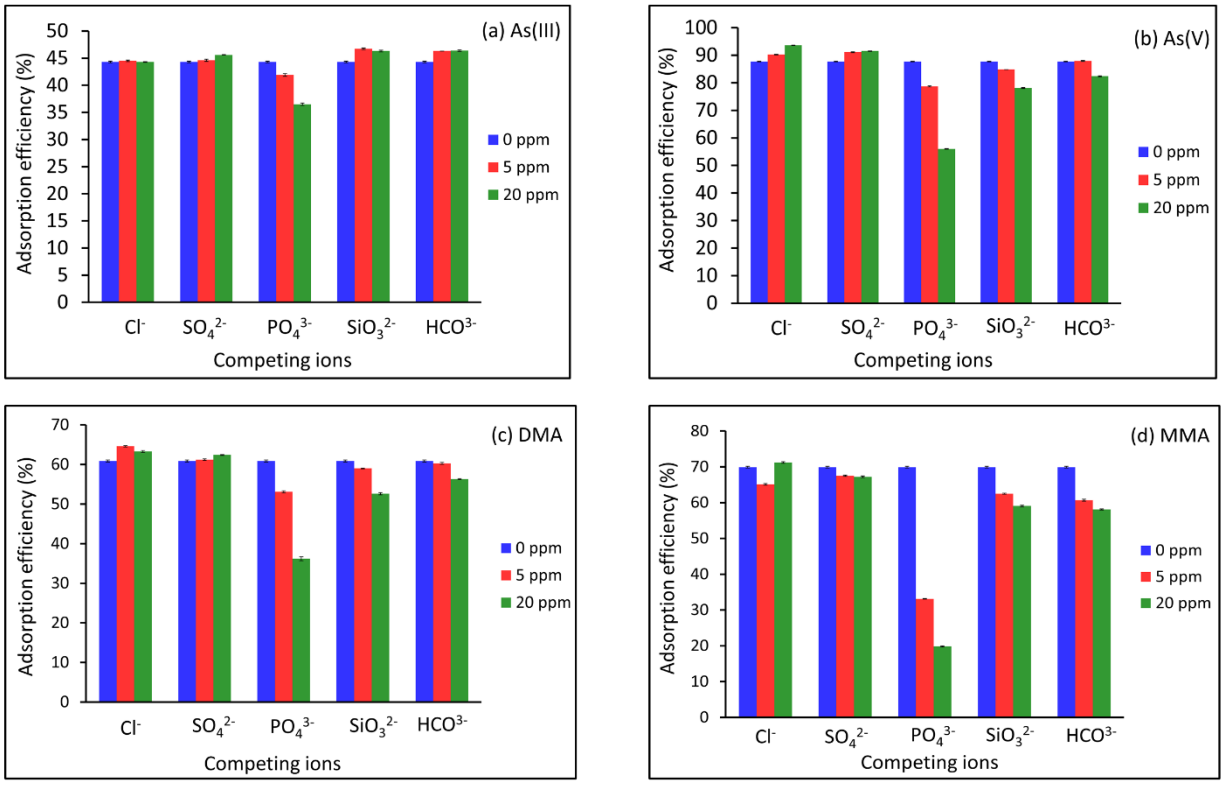

Figure 6.10 Effect of competing ions on adsorption of (a) As(III) (b) As(V) (c) DMA (d) MMA by Fe-GP microspheres. Initial concentrations of arsenic species = 10 mg/L contact time = 60

minutes, temperature = 298 K, volume of arsenic species solution = 10 mL, adsorbent dosage = 0.1 g, shaking rate= 400 rpm. Blue, red and green bars show adsorption of arsenic species in presence of 0 mg/L, 5 mg/L and 20 mg/L of competing ions respectively. The error bars represents the standard deviations.

6.4.7 Arsenic desorption

The regeneration of the adsorbent makes the adsorption process more practical and economically efficient. The ability of Fe-GP to be regenerated after adsorption of arsenic species was tested using a high pH solution of 1 M sodium hydroxide. It was observed that approximately 72%, 99%, 95%, 92% of As(III), As(V), DMA and MMA could be desorbed. High pH facilitates the desorption of arsenic species as metal oxides have a high affinity for hydroxyl ions [40]. It should be noted that even though it was observed that As(III) showed relatively high adsorption efficiency at basic conditions, the desorption using NaOH was successful owing to the fact that OH^- ion concentration is very high at the employed desorption conditions. Hence OH^- can replace arsenic species adsorbed on Fe-GP surface. The high pH stability of the geopolymer support is an important advantage and makes the regeneration of Fe-GP a practical process [17].

6.4.8 Comparison of Fe-GP with previous reported geopolymer based adsorbents

Table 6.2 compares the geopolymer based adsorbents used for arsenic removal with adsorbent reported in this study. In contrast with previous adsorbents, Fe-GP is in the form of microspheres with high surface area. Fe-GP has fastest equilibrium time of 1 hour owing to interconnected

porous structure. This study also investigated As(III), DMA and MMA in addition to As(V). The adsorption capacity for As(V) is higher as compared to previous reports.

Table 6.2. Comparison of current adsorbent with previous reported geopolymer based adsorbents for arsenic adsorption

Geopolymer based adsorbent	Morphology	Surface area (m^2/g)	Arsenic species studied	Equilibrium time (h)	Adsorption Isotherm	Adsorption Capacity	Ref.
Iron oxide-modified nanoporous geopolymers	Monoliths ground to irregular particles (425-600 µm)	73*	As(V)	72	Freundlich	950 µg/g	[26]
Fe(II)-modified geopolymer	Monoliths ground to irregular particles	107.9	As(V)	24	Freundlich	-	[24]
Iron oxide coated geopolymer microspheres	Spherical microparticles (4-100 µm)	270	As(III), As(V), DMA, MMA	1	Freundlich	As (III) = 614.4 µg/g, As (V) =1689.6 µg/g, DMA=1076.4 µg/g, MMA=1161.7 µg/g	

*Surface area of the best adsorbent reported

6.5 Conclusions

New iron oxide infused geopolymer microparticles have been introduced as adsorbents for inorganic and organic arsenic species. It was observed that adsorbent containing 20 wt% iron loading showed maximum adsorption efficiency. The isotherm study showed that the adsorption of all arsenic species was best described with the Freundlich isotherm model. The maximum adsorption capacity (q_m) from Freundlich model was found to be 614.4, 1689.6, 1076.4, 1161.7 µg/g for As(III), As(V), DMA and MMA at 298 K. It was observed that adsorption efficiency of As(V), DMA and MMA increased in acidic conditions while adsorption efficiency of As(III)

increased in basic conditions. Hence, removal efficiencies can be further enhanced by using optimum pH. The anions present in natural water like Cl^-, SO_4^{2-}, SiO_3^{2-} and HCO_3^- showed insignificant competition with arsenic species whereas PO_4^{3-} had a relative appreciable effect on arsenic adsorption. The arsenic species could be easily desorbed using sodium hydroxide hence making them available for reuse. The advantages of Fe-GP adsorbent over the geopolymer based adsorbents reported for arsenic adsorption are highlighted in Table 6.2. Additionally, it should be noted that the geopolymer microspheres, used as adsorbent supports in this study, can be used directly for adsorption of heavy metal cations such as lead, mercury, cadmium owing to their spherical particle shape, small size, enhanced porosity and surface area.

6.6 References

[1] C.A. Martinson, K. Reddy, Adsorption of arsenic (III) and arsenic (V) by cupric oxide nanoparticles, Journal of colloid and interface science, 336 (2009) 406-411.

[2] R.J. Bowell, C.N. Alpers, H.E. Jamieson, D.K. Nordstrom, J. Majzlan, The environmental geochemistry of arsenic—an overview—, Reviews in Mineralogy and Geochemistry, 79 (2014) 1-16.

[3] M. Shimizu, Y. Arai, D.L. Sparks, Multiscale assessment of methylarsenic reactivity in soil. 2. Distribution and speciation in soil, Environmental science & technology, 45 (2011) 4300-4306.

[4] S.F. Farzan, M.R. Karagas, Y. Chen, In utero and early life arsenic exposure in relation to long-term health and disease, Toxicology and applied pharmacology, 272 (2013) 384-390.

[5] R. Quansah, F.A. Armah, D.K. Essumang, I. Luginaah, E. Clarke, K. Marfoh, S.J. Cobbina, E. Nketiah-Amponsah, P.B. Namujju, S. Obiri, Association of arsenic with adverse pregnancy outcomes/infant mortality: a systematic review and meta-analysis, Environmental health perspectives, 123 (2015) 412-421.

[6] M. Tolins, M. Ruchirawat, P. Landrigan, The developmental neurotoxicity of arsenic: cognitive and behavioral consequences of early life exposure, Annals of global health, 80 (2014) 303-314.

[7] M. Shimizu, M. Ginder-Vogel, S.J. Parikh, D.L. Sparks, Molecular scale assessment of methylarsenic sorption on aluminum oxide, Environmental science & technology, 44 (2010) 612-617.

[8] S.S. Sathe, L. Goswami, C. Mahanta, L.M. Devi, Integrated factors controlling arsenic mobilization in an alluvial floodplain, Environmental Technology & Innovation, 17 (2020) 100525.

[9] K.I. Camacho, N. Pariona, A.I. Martinez, R. Castro-Rodriguez, S. Matinez-Vargas, D.L. Perry, The iron oxides as arsenic removal media from water, Iron Oxides: Structure, properties and aplications2012, pp. 189-212.

[10] https://www.who.int/news-room/fact-sheets/detail/arsenic.

[11] S.I. Siddiqui, S.A. Chaudhry, Iron oxide and its modified forms as an adsorbent for arsenic removal: A comprehensive recent advancement, Process safety and environmental Protection, 111 (2017) 592-626.

[12] D. Mohan, C.U. Pittman Jr, Arsenic removal from water/wastewater using adsorbents—a critical review, Journal of hazardous materials, 142 (2007) 1-53.

[13] C. Chuang, M. Fan, M. Xu, R. Brown, S. Sung, B. Saha, C. Huang, Adsorption of arsenic (V) by activated carbon prepared from oat hulls, Chemosphere, 61 (2005) 478-483.

[14] S. Bang, M. Patel, L. Lippincott, X. Meng, Removal of arsenic from groundwater by granular titanium dioxide adsorbent, Chemosphere, 60 (2005) 389-397.

[15] J. Davidovits, Geopolymers: inorganic polymeric new materials, Journal of Thermal Analysis and calorimetry, 37 (1991) 1633-1656.

[16] P. Duxson, A. Fernández-Jiménez, J.L. Provis, G.C. Lukey, A. Palomo, J.S. van Deventer, Geopolymer technology: the current state of the art, Journal of materials science, 42 (2007) 2917-2933.

[17] R.M. Wimalasinghe, C.A. Weatherly, M.F. Wahab, N. Thakur, D.W. Armstrong, Geopolymers as a New Class of High pH Stable Supports with Different Chromatographic Selectivity, Analytical chemistry, 90 (2018) 8139-8146.

[18] P. Sazama, O. Bortnovsky, J. Dědeček, Z. Tvarůžková, Z. Sobalík, Geopolymer based catalysts—New group of catalytic materials, Catalysis today, 164 (2011) 92-99.

[19] N. Thakur, M.F. Wahab, D.D. Khanal, D.W. Armstrong, Synthetic aluminosilicate based geopolymers–Second generation geopolymer HPLC stationary phases, Analytica Chimica Acta, 1081 (2019) 209-217.

[20] D.D. Khanal, N. Thakur, M.F. Wahab, D.W. Armstrong, Enhancing the selectivity of polar hydrophilic analytes with a low concentration of barium ions in the mobile phase using geopolymers and silica supports, Talanta, 207 (2020) 120339.

[21] L. Li, S. Wang, Z. Zhu, Geopolymeric adsorbents from fly ash for dye removal from aqueous solution, Journal of colloid and interface science, 300 (2006) 52-59.

[22] M. El Alouani, S. Alehyen, M. El Achouri, Preparation, characterization, and application of Metakaolin-based geopolymer for removal of methylene blue from aqueous solution, Journal of Chemistry, 2019 (2019).

[23] A. Maleki, Z. Hajizadeh, V. Sharifi, Z. Emdadi, A green, porous and eco-friendly magnetic geopolymer adsorbent for heavy metals removal from aqueous solutions, Journal of cleaner production, 215 (2019) 1233-1245.

[24] Q. Tian, K. Sasaki, Application of fly ash-based geopolymer for removal of cesium, strontium and arsenate from aqueous solutions: kinetic, equilibrium and mechanism analysis, Water Science and Technology, 79 (2019) 2116-2125.

[25] A. Maleki, M. Mohammad, Z. Emdadi, N. Asim, M. Azizi, J. Safaei, Adsorbent materials based on a geopolymer paste for dye removal from aqueous solutions, Arabian Journal of Chemistry, (2018).

[26] D. Medpelli, R. Sandoval, L. Sherrill, K. Hristovski, D.-K. Seo, Iron oxide-modified nanoporous geopolymers for arsenic removal from ground water, Resource-Efficient Technologies, 1 (2015) 19-27.

[27] N. Thakur, C.A. Weatherly, R.M. Wimalasinghe, D.W. Armstrong, Fabrication of interconnected macroporosity in geopolymers via inverse suspension polymerization, Journal of the American Ceramic Society, 102 (2019) 4405-4409.

[28] L.R. Caballero, M.d.D.M. Paiva, E.d.M.R. Fairbairn, R.D. Toledo Filho, Thermal, Mechanical and Microstructural Analysis of Metakaolin Based Geopolymers, Materials Research, 22 (2019).

[29] Z. Yunsheng, S. Wei, C. Qianli, C. Lin, Synthesis and heavy metal immobilization behaviors of slag based geopolymer, Journal of hazardous materials, 143 (2007) 206-213.

[30] R.M. Novais, L. Buruberri, M. Seabra, J. Labrincha, Novel porous fly-ash containing geopolymer monoliths for lead adsorption from wastewaters, Journal of hazardous materials, 318 (2016) 631-640.

[31] Q. Hu, Y. Liu, X. Gu, Y. Zhao, Adsorption behavior and mechanism of different arsenic species on mesoporous MnFe2O4 magnetic nanoparticles, Chemosphere, 181 (2017) 328-336.

[32] Y.-S. Ho, G. McKay, Pseudo-second order model for sorption processes, Process biochemistry, 34 (1999) 451-465.

[33] S. Zhang, H. Niu, Y. Cai, X. Zhao, Y. Shi, Arsenite and arsenate adsorption on coprecipitated bimetal oxide magnetic nanomaterials: MnFe2O4 and CoFe2O4, Chemical engineering journal, 158 (2010) 599-607.

[34] G.D. Halsey, The role of surface heterogeneity in adsorption, Advances in catalysis, 4 (1952) 259-269.

[35] O. Hamdaoui, E. Naffrechoux, Modeling of adsorption isotherms of phenol and chlorophenols onto granular activated carbon: Part I. Two-parameter models and equations allowing determination of thermodynamic parameters, Journal of hazardous materials, 147 (2007) 381-394.

[36] Z. Wei, K. Liang, Y. Wu, Y. Zou, J. Zuo, D.C. Arriagada, Z. Pan, G. Hu, The effect of pH on the adsorption of arsenic (III) and arsenic (V) at the TiO2 anatase [1 0 1] surface, Journal of colloid and interface science, 462 (2016) 252-259.

[37] Y.-T. Wei, Y.-M. Zheng, J.P. Chen, Uptake of methylated arsenic by a polymeric adsorbent: Process performance and adsorption chemistry, Water research, 45 (2011) 2290-2296.

[38] S. Goldberg, C.T. Johnston, Mechanisms of arsenic adsorption on amorphous oxides evaluated using macroscopic measurements, vibrational spectroscopy, and surface complexation modeling, 234 (2001) 204-216.

[39] H. Zeng, B. Fisher, D.E. Giammar, Individual and competitive adsorption of arsenate and phosphate to a high-surface-area iron oxide-based sorbent, Environmental science & technology, 42 (2008) 147-152.

[40] A. Sigdel, J. Park, H. Kwak, P.-K. Park, Arsenic removal from aqueous solutions by adsorption onto hydrous iron oxide-impregnated alginate beads, Journal of industrial and engineering chemistry, 35 (2016) 277-286.

6.7 Supporting Information

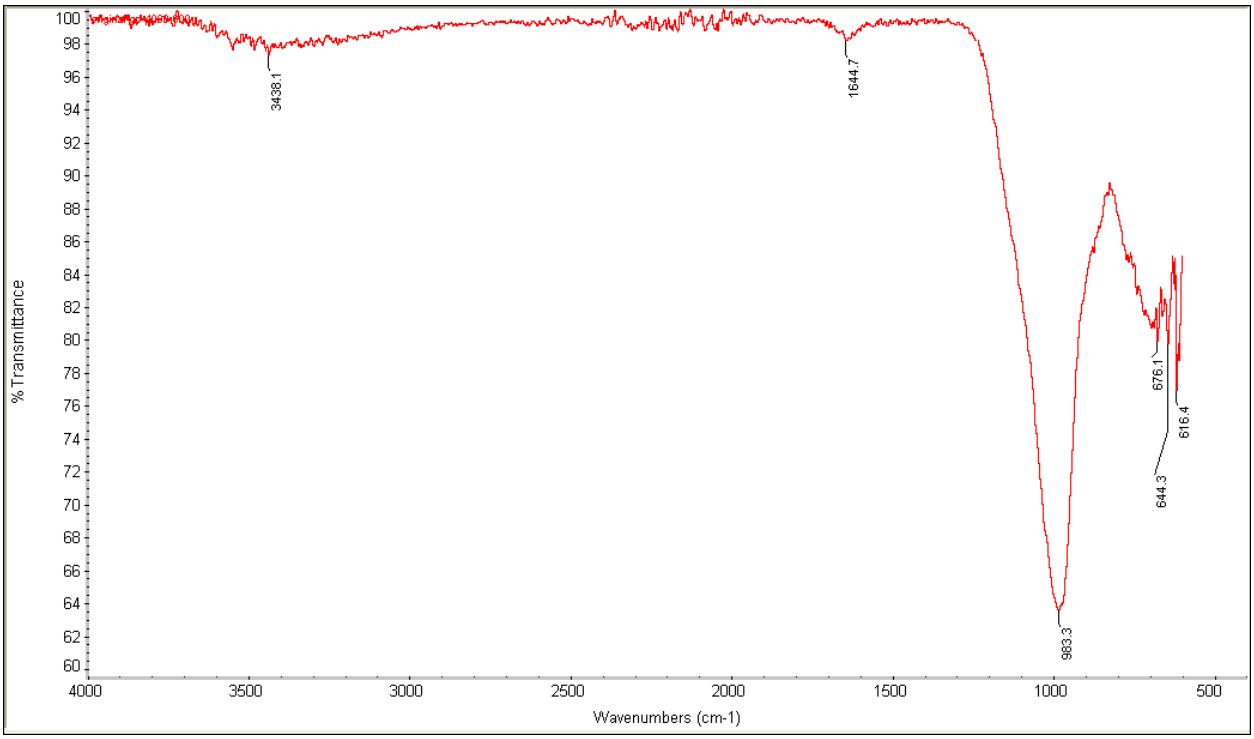

Figure 6.S1: FTIR spectrum of original geopolymer.

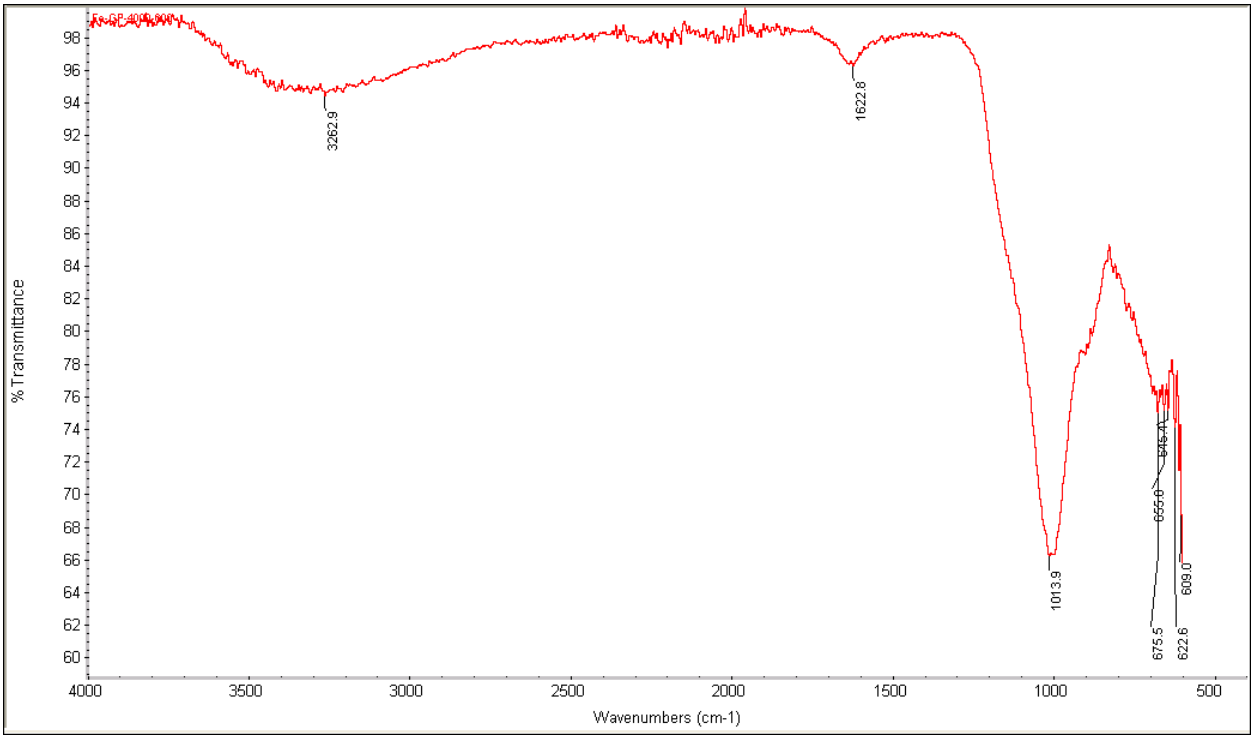

Figure 6.S2: FTIR spectrum of iron-oxide coated geopolymer (Fe-GP).

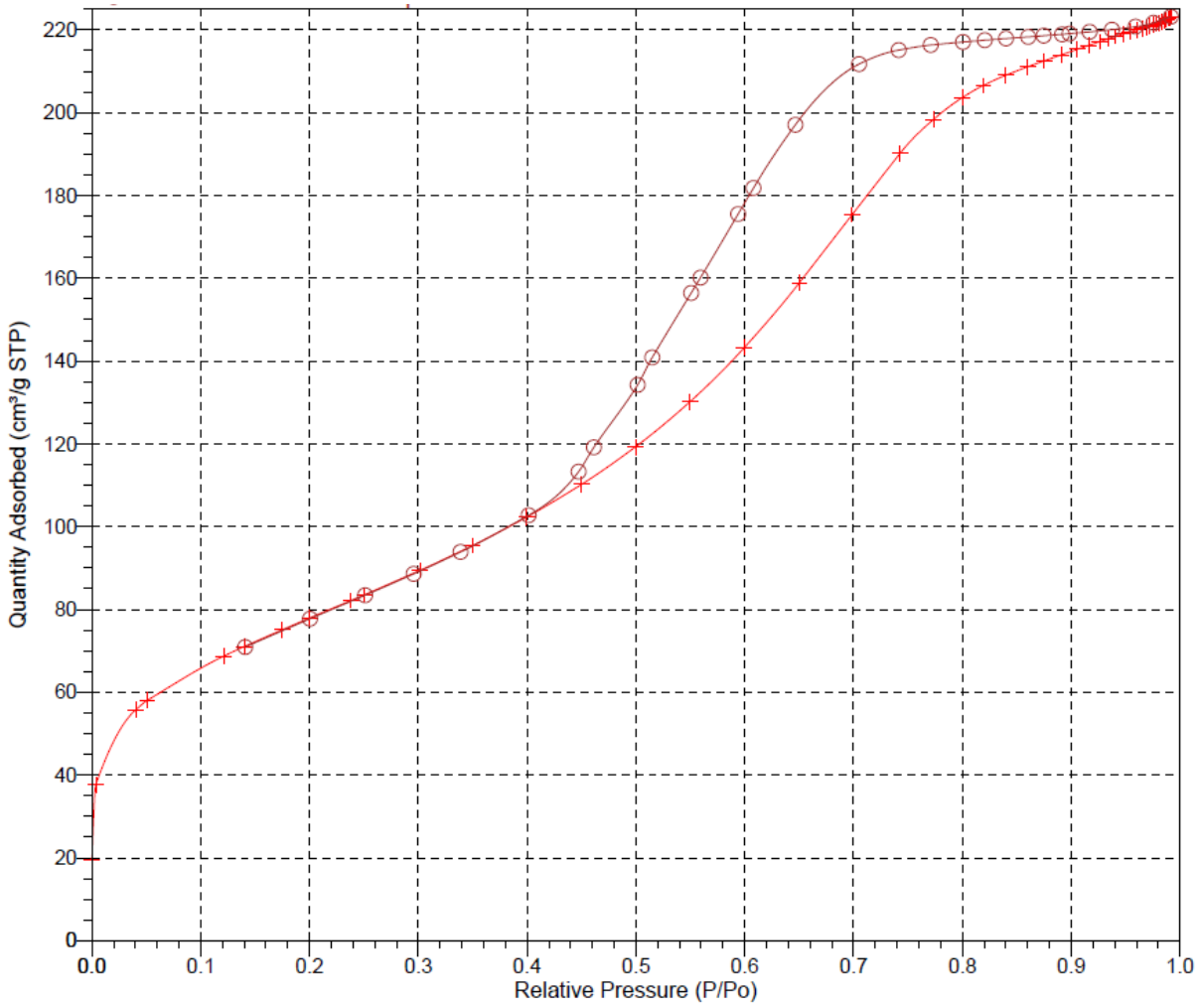

Figure 6.S3: Nitrogen sorption isotherm of final Fe-GP microspheres used in adsorption studies.

Summary Report

Surface Area

Single point surface area at P/Po = 0.301622398:	271.9478 m²/g
BET Surface Area:	269.3280 m²/g
BJH Adsorption cumulative surface area of pores between 17.000 Å and 3000.000 Å width:	305.090 m²/g
BJH Desorption cumulative surface area of pores between 17.000 Å and 3000.000 Å width:	341.4853 m²/g

Pore Volume

Single point adsorption total pore volume of pores less than 1344.162 Å width at P/Po = 0.985388054:	0.343650 cm³/g
Single point desorption total pore volume of pores less than 813.780 Å width at P/Po = 0.975621628:	0.342926 cm³/g
BJH Adsorption cumulative volume of pores between 17.000 Å and 3000.000 Å width:	0.364207 cm³/g
BJH Desorption cumulative volume of pores between 17.000 Å and 3000.000 Å width:	0.360643 cm³/g

Pore Size

Adsorption average pore width (4V/A by BET):	51.0381 Å
Desorption average pore width (4V/A by BET):	50.9306 Å
BJH Adsorption average pore width (4V/A):	47.751 Å
BJH Desorption average pore width (4V/A):	42.244 Å

Figure 6.S4: BET original data of final Fe-GP microspheres used in adsorption studies.

File Name	Fe-NMGP			Meas Date	19/10/30 08:58:21
Sample ID	Non-fired_2		Sample No.	2	
Comment	(2) Non-Fired Fe-NMGP XRD & PSD				

Median D	20.112	Mean V	20.239
Modal D	18.548	Std Dev	0.317

10%D(μm)	20%D(μm)	30%D(μm)	40%D(μm)	50%D(μm)	60%D(μm)	70%D(μm)	80%D(μm)	90%D(μm)
7.725	10.075	12.808	16.144	20.112	25.102	31.931	41.556	54.913

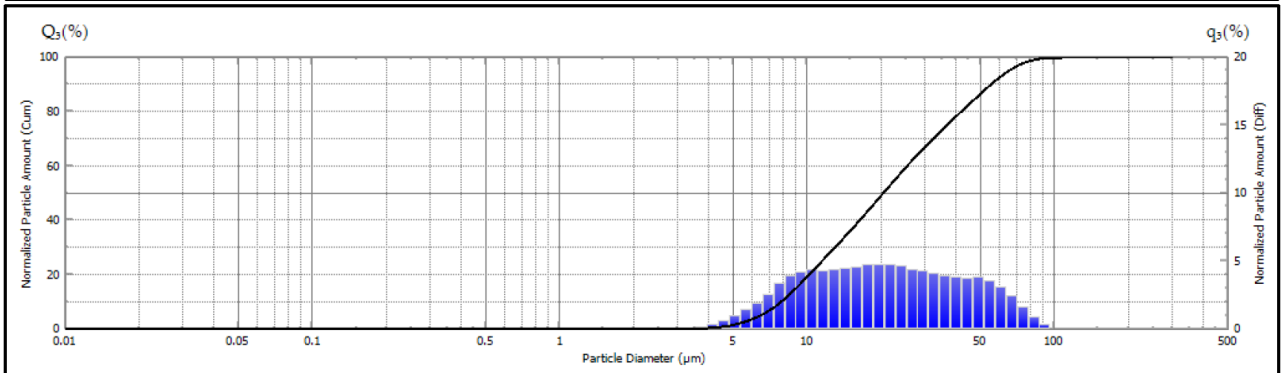

Figure 6.S5: Laser diffraction particle size distribution of Fe-GP microspheres. Nitrogen sorption isotherms.

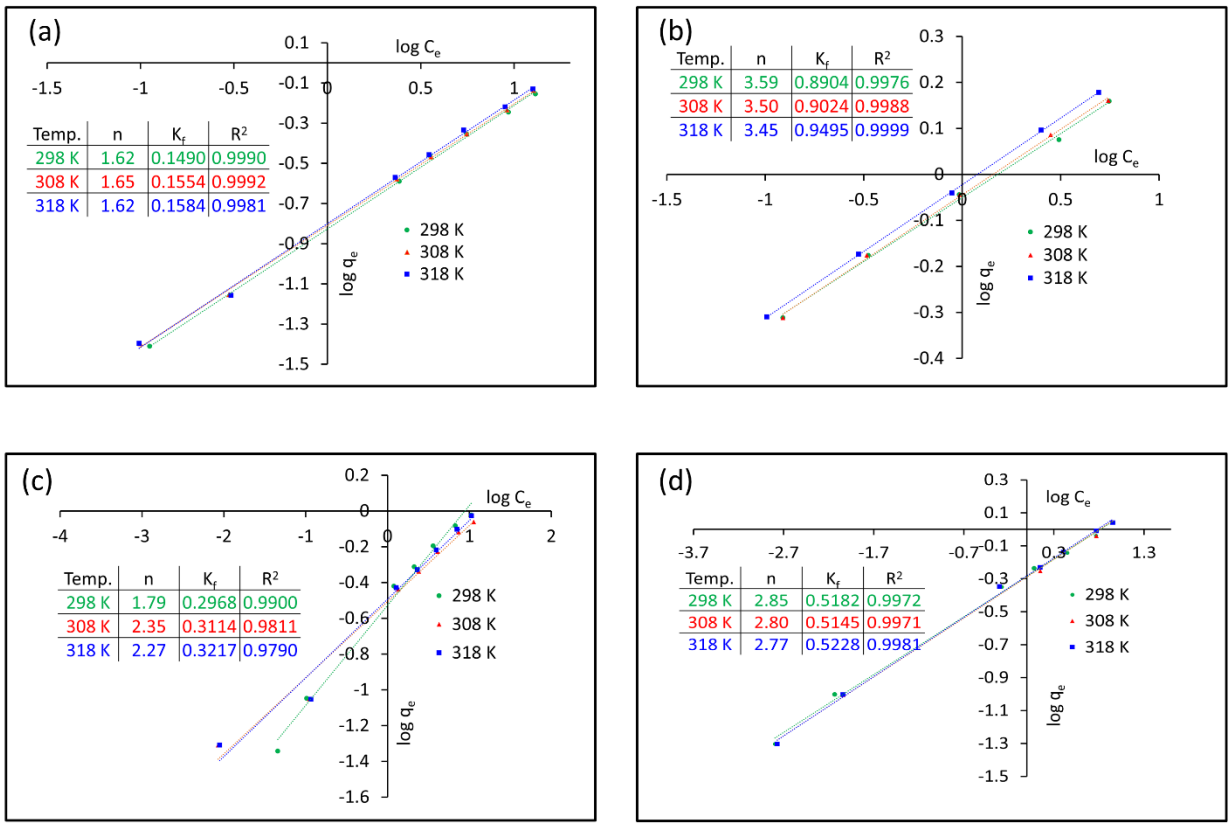

Figure 6.S6. Freundlich adsorption isotherm plots of (a) As(III) (b) As(V) (c) DMA (d) MMA on geopolymer microspheres. Initial concentrations of arsenic species = 10 mg/L contact time = 60 minutes, temperature = 298 K, volume of arsenic species solution = 10 mL, adsorbent dosage = 0.1 g, shaking rate: 400 rpm.

Table 6.S1. Relative Standard Deviation of ICP-OES data. Points taken for calibration curve for a) As(V) b) As(III) c) DMA d) MMA. As wavelength used = 193.759 nm.

a)

As (V) concentration (mg/mL)	Intensity Reading 1	Intensity Reading 2	Intensity Reading 3	Mean	SD	RSD
0.1	2.816431	2.846735	3.432467	3.032	0.33	11.45
0.5	16.47095	16.71092	16.50534	16.562	0.13	0.78
1	35.91566	37.36147	36.55679	36.611	0.72	1.98
5	179.7329	183.8942	182.1568	181.928	2.09	1.15
7	250.8723	259.7290	256.3554	255.652	4.47	1.75
10	361.4403	376.7595	365.8685	368.023	7.88	2.14

b)

As (III) concentration (mg/mL)	Intensity Reading 1	Intensity Reading 2	Intensity Reading 3	Mean	SD	RSD
0.1	2.507559	3.360054	3.030580	2.966	0.43	14.49
0.5	16.91418	17.20356	16.58065	16.899	0.31	1.84
1	34.86560	34.61864	33.98373	34.489	0.45	1.32
5	177.2112	176.1733	176.0156	176.466	0.65	0.37
7	239.5497	237.1542	238.6592	238.454	1.21	0.51
10	343.1868	341.1787	339.0532	341.140	2.07	0.61

c)

DMA concentration (mg/mL)	Intensity Reading 1	Intensity Reading 2	Intensity Reading 3	Mean	SD	RSD
0.1	3.193173	2.183899	2.833977	2.737	0.51	18.69
0.5	16.38522	16.07004	16.22924	16.228	0.16	0.97
1	35.27815	34.45830	35.05403	34.930	0.42	1.21
5	168.8922	167.4119	167.3871	167.897	0.86	0.51
7	239.2950	239.0775	239.7757	239.383	0.36	0.15
10	336.5255	336.5825	336.2659	336.458	0.17	0.05

d)

MMA concentration (mg/mL)	Intensity Reading 1	Intensity Reading 2	Intensity Reading 3	Mean	SD	RSD
0.1	4.160583	4.269856	4.405118	4.2785	0.12	2.86
0.5	22.81520	23.46026	24.08779	23.454	0.64	2.71
1	49.51766	49.46938	48.83084	49.272	0.38	0.78
5	243.5719	245.2021	244.2825	244.352	0.82	0.33
7	342.6767	345.8306	345.4862	344.664	1.73	0.50
10	477.6436	485.1030	482.7310	481.825	3.81	0.79

Table 6.S2. Pseudo second order kinetics parameters of As(III), As(V), DMA and MMA at initial arsenic concentration of 0.5, 5, 10 mg/mL

As species (10 mg/mL)	**k[a] (g mg^{-1} min^{-1})**	**h[b] (mg g^{-1} min^{-1})**	**R^2**
As(III)	0.128	0.043	0.9990
As(V)	0.206	0.197	0.9999
DMA	0.204	0.105	0.9998
MMA	0.129	0.086	0.9997

As species (5 mg/mL)	**k (g mg^{-1} min^{-1})**	**h (mg g^{-1} min^{-1})**	**R^2**
As(III)	0.245	0.028	0.9991
As(V)	1.576	0.390	1
DMA	0.819	0.135	1
MMA	0.453	0.082	0.9999

As species (0.5 mg/mL)	**k (g mg^{-1} min^{-1})**	**h (mg g^{-1} min^{-1})**	**R^2**
As(III)	4.396	0.008	0.9999
As(V)	85.794	0.215	0.9999
DMA	32.584	0.071	1
MMA	8.681	0.020	1

[a]h is the initial sorption rate

[b]k is the rate constant.

Table 6.S3. Langmuir adsorption isotherm parameters of As(III), As(V), DMA and MMA at 298 K, 308 K, 318 K

As species (298 K)	q_m[b] (mg/g)	b[c] (L/mg)	R_L[d]	R^2
As(III)	0.8574	0.2363	0.2974	0.9307
As(V)	1.5135	4.6657	0.0210	0.9883
DMA	1.0656	0.6384	0.1354	0.9743
MMA	1.0976	1.8314	0.0518	0.9697

As species (308 K)	q_m[b] (mg/g)	b[c] (L/mg)	R_L[d]	R^2
As(III)	0.8885	0.2328	0.3005	0.9067
As(V)	1.5370	4.8320	0.0203	0.9916
DMA	0.9370	0.5727	0.1487	0.9587
MMA	1.1058	1.7981	0.0527	0.9679

As species (318 K)	q_m[b] (mg/g)	b[c] (L/mg)	R_L[d]	R^2
As(III)	0.9190	0.1957	0.3382	0.9191
As(V)	1.6038	5.4515	0.0180	0.9886
DMA	1.0137	0.6117	0.1405	0.9441
MMA	1.1255	2.0062	0.0475	0.9744

[b] q_m is the maximum quantity of arsenic adsorbed by Fe-GP ($mg_{As}/g_{Fe\text{-}GP}$)

[c] b is the Langmuir adsorption equilibrium constant.

[d] R_L is the dimensionless equilibrium parameter (see eq. 8 in the manuscript)

Chapter 7. A Molecular Detection/Separations System of Singular Specificity

7.1 Abstract

We designed and demonstrated the unique abilities of the first gas chromatography – molecular rotational resonance spectrometer instrument (GC-MRR). While broadly and routinely applicable, its capabilities can exceed those of high-resolution mass spectrometry and NMR in terms of selectivity, resolution and compound identification. A series of 24 isotopologues and isotopomers of five organic compounds are separated, identified and quantified in a single run. Natural isotopic abundances of mixtures of compounds containing chlorine, bromine and sulfur heteroatoms are easily determined. MRR detection provides the added high specificity for these selective gas-phase separations. GC-MRR is shown to be ideal for compound-specific isotope analysis (CSIA). Different bacterial cultures and groundwater were shown to have contrasting isotopic selectivities for common organic compounds. The ease of such GC-MRR measurements may initiate a new era in biosynthetic/degradation and geochemical isotopic compound studies.

7.2 Introduction

Coupling high efficiency separations with highly selective detection methodologies have provided the means to a much higher degree of compound identification and with limited sample amounts. Indeed, such approaches have transformed most scientific and technical fields from genomics, proteomics and pharmaceutical science to environmental, forensics and nutritional areas among others. A prime example is the advent of electrospray ionization that effectively coupled liquid chromatography (LC) and mass spectrometry (MS) [1,2]. An equally significant earlier example was the use of MS detection with gas chromatography (GC) that allowed the analysis of complex

samples with a high degree of selectivity [3-5]. The most useful separation-detection schemes are complementary in nature. For example, isomers, including enantiomers that are indistinguishable by MS, are often easily separated by chromatography [6-9]. Troublesome matrices can be simplified or eliminated with proper separations. Conversely, compounds that coelute in chromatography are often distinguished with a selective detector. For example, isotopologues can be identified by MS but may not be separated easily [10]. There are a number of situations where even the most advanced combinations of techniques fail. This could involve simple compounds such as isotopic isomers (isotopomers) [13-14] or very complex mixtures [13,14] for example. Sample-limited cases of the aforementioned can have an increased degree of difficulty. Clearly an analytical device that would be applicable in such exceptionally challenging cases would have considerable general utility as well. In this work we demonstrate the potential of GC molecular rotational resonance spectroscopy (GC-MRR). This is done using very small amounts of sample mixtures (≤ microliters) that often cannot be effectively analyzed/characterized using any other method.

Molecular rotational resonance (MRR) spectroscopy characterizes compounds through their pure rotational angular momentum transitions in the gas phase. A molecule's rotational energy levels are quantized as stipulated by its 3-dimensional mass distribution, which also determines its moment of inertia (I). Simplistically, $I = \Sigma m_i r_i^2$, where m is the mass of atom "i" in the molecule and r_i is the distance of atom "i" from the molecule's center of mass. Molecules can be unambiguously distinguished through their principal moments of inertia in the three spatial axes, and their rotational spectra are described by a Hamiltonian that depends precisely on these quantities [15]. Given its typically numerous and extremely narrow transition lines, the high-resolution rotational spectrum is, therefore, a unique fingerprint of molecular structure.

It is well established that molecular rotational spectroscopy can provide considerable molecular information including molecular structure specificity, dipole moments, nuclear and electronic spin interactions, isomeric conformations, energy differences and more on both isolated molecules and weakly bound complexes [16-18]. Also notable is that MRR is a nondestructive technique. Transition frequencies in rotational spectroscopy are commonly measured to an accuracy of better than one part in a million, with very high resolution due to the isolated gas-phase environment, the inherently long lifetimes of rotationally excited states and other factors [19]. Such high-resolution spectra can provide structural information exceeding that of nuclear magnetic resonance (NMR) spectroscopy, Fourier transform infrared spectroscopy and importantly, high-resolution mass spectrometry (vide infra). For decades, astronomers have used high-frequency radio telescopes to identify interstellar gases by their rotational spectra, with to date over 200 molecular species identified in interstellar and circumstellar media [20,21].

While MRR, often referred to as Fourier transform microwave spectroscopy (FTMW) in the literature, has been established as a spectroscopic technique for several decades, considerable recent advances in hardware and software were necessary in order to develop spectrometers that are sufficiently sensitive and rapid (in terms of sampling frequency, data handling, etc.) to be used as a dynamic flow-through detector when coupled to modern separation devices (e.g., chromatography), while also providing accurate intensity information for quantitation. In particular, the implementation of broadband Fourier transform instrumentation in the form of chirped-pulse Fourier transform microwave (CP-FTMW) spectroscopy, somewhat analogous in operating principles to FT-NMR, is critical. MRR is employed as a broader term that encompasses both microwave and millimeter wave spectroscopic phenomena (resonance with molecular rotational transitions). A short excitation pulse (in the system used here, typically 250 ns) is

transmitted into a low-pressure sample cell (~10-2 Torr). The excited molecules then emit coherent radiation at their characteristic rotational frequencies via free induction decay (FID) for several microseconds, which are recorded in the time domain and Fourier transformed to the frequency domain. The latest chirped-pulse FT molecular rotational resonance spectrometers utilize powerful microwave and mm-wave sources, broadband active multiplier chains (AMCs), arbitrary waveform generators (AWGs), and high-speed digital electronics for both pulse generating and broadband detection. These are described in detail, elsewhere [22-26]. The term "chirp" in chirped-pulse simply refers to the fact that the frequency of the excitation pulse increases or decreases linearly with time, allowing for simultaneous detection of broad bandwidth molecular spectra and enabling the present application [27,28].

7.3 Results and Discussion

In this study, we have developed the first hyphenated GC-MRR instrument, using a 75-110 GHz MRR spectrometer (see Figure 7.S1 and experimental details in the Supporting Information) and herein demonstrate its capabilities in analyzing difficult and/or complex mixtures in a single run. This includes doing compound-specific isotope analyses (CSIA) on samples that cannot be done via any other method. Isotopic fractionation analysis and quantification are broadly important. Compound and multi-compound specific isotopic characterization provides pertinent information on many terrestrial and extraterrestrial systems, but may not be easy to obtain [10, 13, 29, 30]. Figure 7.1 (top) shows a single GC-MRR analysis of 24 isotopic species of five prevalent organic molecules as a total molecule chromatogram (TMC). Each point in the chromatogram consists of a broadband, high-resolution spectrum; in the TMC, the peak intensities of all observed transitions

are summed. The TMC indicates five dominant peaks and two small shoulders just prior to the main acetone and acetonitrile peaks (at 3.2 min and 7.6 min, respectively).

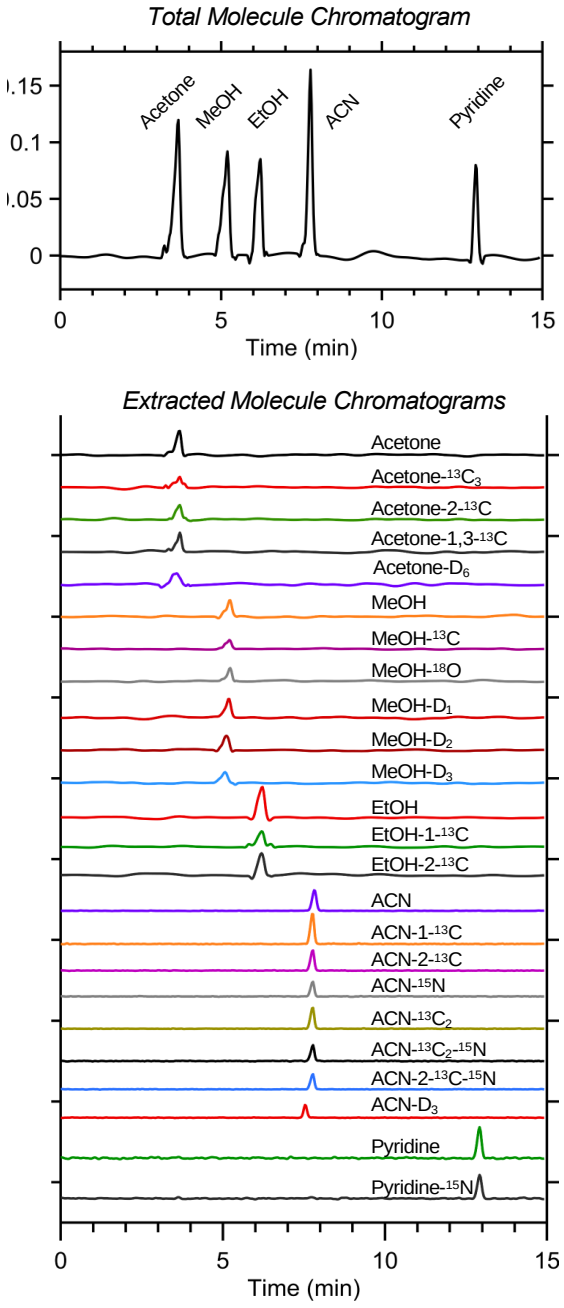

Figure 7.1 Total GC-MRR chromatogram (top, in black) of five common organic molecules. The 24 extracted molecule chromatograms showing all isotopomers and isotopologues of these

molecules are shown below in color. Each specific isotopic compound is designated next to its peak. The shorthand nomenclature is as follows: whole numbers following the compound name refer to the position(s) of the isotopic atom (e.g., both Acetone-2-^{13}C and ACN-2-^{13}C indicate that the ^{13}C atom is the second carbon of the acetone and acetonitrile respectively). The subscript number after the isotope symbol refers to the number of those isotopes in that compound (e.g., MeOH-D2 and ACN-$^{13}C2$ indicate that methanol has two deuterium substituents on its methyl group and acetonitrile has two ^{13}C isotopic atoms, respectively). See Supporting Information for experimental details.

These small, partially resolved peaks/shoulders are the totally deuterated acetone (Acetone-D6) and the triply deuterated acetonitrile (ACN-D3) which are chromatographically separated from their related co-eluted isotopologues and isotopomers (Figure 7.1). The selectivity of MRR detection further allows facile deconvolution of the TMC into 24 extracted molecule chromatograms (EMCs), one for each isotopically distinct compound. Note that isotope pattern matching/analysis [31,32] is not needed for molecular identification as all are determined directly. Molecules that have identical exact masses (e.g., H_3C-(C=O)-$^{13}CH_3$ and H_3C-(^{13}C=O)-CH_3 or $H_3{}^{13}C$-C≡N and H_3C-^{13}C≡N or $H_3{}^{13}CH_2$-OH and H_3C-$^{13}CH_2$-OH) are easily distinguished and identified due to their differences in moments of inertia. In contrast to NMR, this type of analysis is done quickly and quantitatively on complex mixtures with minute amounts of sample (*vide infra*). As can be seen (Figure 7.1), unlike with mass spectrometry, isobaric compounds pose no particular problems. Further, peak (compound) coelution does not cause signal suppression or enhancements. This is due, in major part, to the fact that MRR spectral detection is very high resolution and provides an abundance of lines highly specific to one compound even if that

compound is an isomer or an isotopologue or isotopomer of another. For example, Figure 7.2 shows the unambiguous MRR identification of acetonitrile isotopomers.

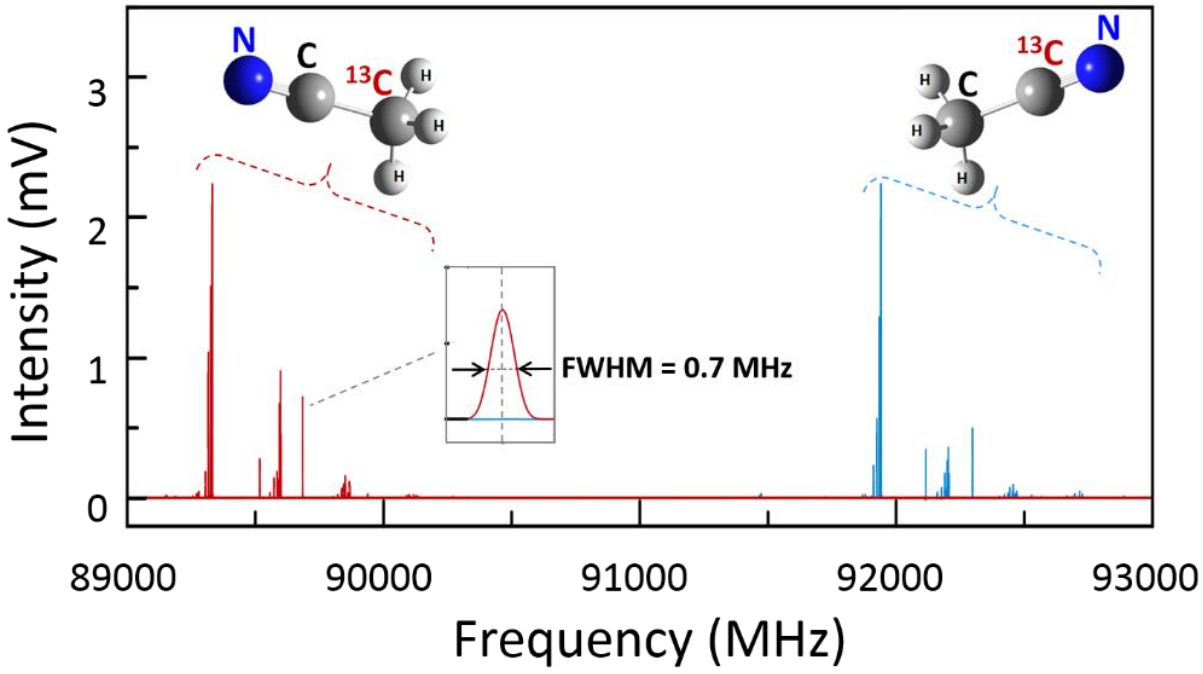

Figure 7.2 Molecular rotational resonance (MRR) spectra of two isotopomers of acetonitrile illustrating the substantial selectivity for such isobaric compounds as well as the exceedingly high resolution (sub-ppm) of the MRR spectral bands.

Also shown in Figure 7.2 inset is the full width at half maximum (FWHM) of a typical MRR line. One or more of the intense lines for each compound are selected (see Supporting Information, 7.6.2.4) for GC-MRR detection as shown in Figure 7.1 and further explored below. Also, note that selecting more lines per compound can increase the signal to noise of GC-MRR chromatograms. An additional capability (not shown) is that of performing select molecule chromatography (SMC) in which only specific narrow-band MRR transitions for a molecule, or a few molecules of interest

are monitored. By focusing the power on small portions of the spectrum rather than across the full range, the sensitivity can be increased by an order of magnitude or more [23,27]. Figure 7.3 shows the total molecule GC-MRR chromatogram for bromoethane and five heterocyclic compounds, along with isotopologue-specific extracted molecule chromatograms showing the natural isotopic abundances for bromoethane and 2-chloropyridine.

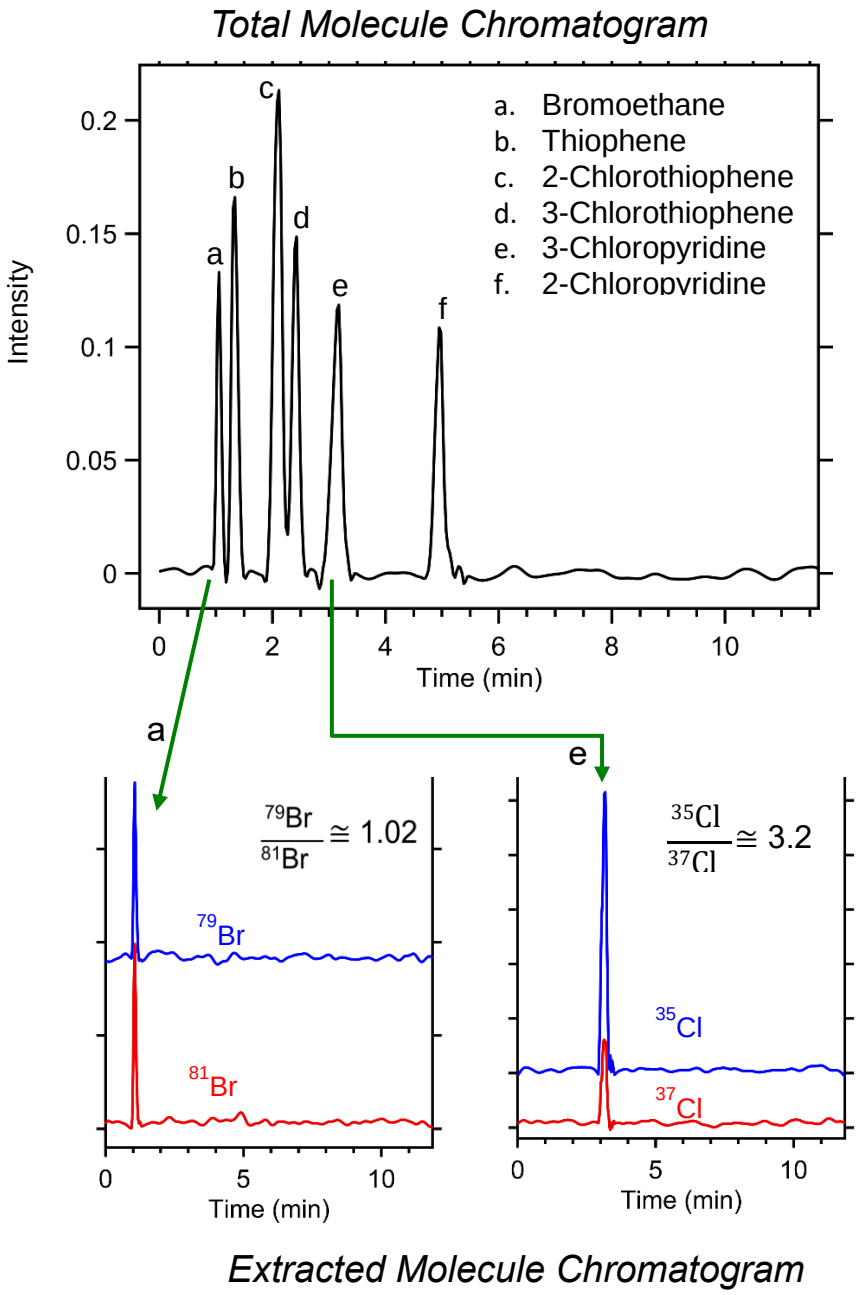

Figure 7.3 Top figure in black is the total molecule chromatogram of: a. bromoethane, b. thiophene, c. 2-chlorothiophene, d. 3-chlorothiophene, e. 3-chloropyridine and f. 2-chloropyridine. Below are two representative examples of how the natural isotopic abundances of these compounds are easily obtained via the GC-MRR extracted molecule chromatograms. The error in these ratios is +/- 3% RSD.

Integration of GC-MRR peak areas provide quantitative information for all species (see Supporting Information 7.6.2.4 and Figure 7.3). This is shown further in the data of Table 7.1.

Clearly, isotopic fractionation due to biological or other natural processes could be easily determined with very small amounts of such compounds. Indeed, compound-specific isotope analysis (CSIA) has become de rigueur in areas of environmental contamination, biodegradation, metabolomics and geochemistry, among others [13, 14, 29, 30, 33-36]. An interesting example of this involves the selective bio-depletion of a dilute sample of pyridine isotopologues. While the microbial metabolism of pyridines and other organic bases has been studied extensively [37] isotope specific studies do not exist, to our knowledge. Table 7.1 shows GC-MRR results for the biodepletion of ^{14}N and ^{15}N pyridine standards in three different microbial cultures/solutions.

Table 7.1 Selective microbial depletion of different isotopes of pyridine and acetonitrile as determined via GC-MRR.

Microbial media	Incubation Time (days)[e]	Isotopic compounds and relative concentrations (ppm)[a]				
		Pyr-^{14}N[f]	Pyr-^{15}N[f]	$^{13}CH_3CN$[g]	$CH_3{}^{13}CN$[g]	$CH_3C^{15}N$[g]
E. colib	0	500	500	500	500	500
	7	280	320	350	350	380
	14	240	270	335	345	370

B. cepaciac	0	500	500	500	500	500
	7	320	310	395	400	400
	14	300	290	390	395	395
Groundwaterd	0	500	500	500	500	500
	7	425	425	455	455	460
	14	415	415	450	450	450

a Error, RSD = ± 2.4-2.9%. Concentrations were determined by integrating the area of the chromatographic peaks (see Supporting Information 2.3-2.5).

b E. Coli incubated in nutrient broth prior to addition of pyridine or acetonitrile isotopic standards. See experimental conditions in the Supporting Information.

c B. Cepacia incubated in nutrient broth prior to addition of pyridine or acetonitrile isotopic standards. See experimental conditions in the Supporting Information.

d Groundwater obtained from Village Creek. See experimental conditions in the Supporting Information.

e All incubations were done at 37 °C. See experimental details in the Supporting Information.

f Pyr: pyridine with the indicated isotope of nitrogen.

g Acetonitrile of the indicated isotopic composition.

Both pyridine isotopologues were depleted with time in all cases. Interestingly, the E. coli culture shows selective depletion of the ^{14}N pyridine isotopologue, while B. cepacia and the groundwater do not show significant selective depletion of pyridine isotopologues. Kinetic isotope fractionation has been noted for inorganic nitrogen sources [38] and has been used to provide insight on the biotic and enzymatic hydrolysis of herbicides [29]. This particular analysis could also be accomplished by GC-isotope ratio mass spectrometry or a few other, often costly hyphenated

techniques. However, the rapid, facile study on the biodegradation of three trace level isobaric isotopomers of acetonitrile (see Table 7.1) cannot be easily accomplished with other techniques or combinations of techniques given the low amounts of isobaric and isotopic analytes in a biological matrix. This opens an entirely new area of new species for CSIA. The data in Table 7.1 shows that all acetonitrile isotopomers and pyridine isotopes are more rapidly depleted in the E. coli and B. cepacia cultures than in groundwater. However, the ^{14}N pyridine isotope and the ^{14}N acetonitrile isotopomers are selectively depleted by E. coli, but not by B. cepacia or in groundwater. More extensive studies using a greater variety of isotopic compounds and microbial cultures are currently underway and will be reported in the future.

7.4 Conclusions

In conclusion, we have shown the feasibility and potential of combining high-efficiency separations with what may be the most chemically specific form of spectroscopy. These results are exciting as they show straightforward qualitative and quantitative determinations can be done that would be difficult or impossible with other techniques or combinations of techniques. Further, the approach is simple, fast, uses very little sample and can be done on mixtures with no more than routine sample preparation. Although the focus of this work was on isotopic and isobaric compounds, it should be apparent that this is a broadly applicable technique that can be used for both common and uncommon compounds.

7.5 References

[1] S. F. Wong, C.K. Meng, J.N. Fenn, J.Phys. Chem. 1988, 92,546-550.

[2] J.B. Fenn, M. Mann, C.K. Meng, S.F. Wong, C.M. Whitehouse, Science 1989, 246, 64-70.

[3] R.S. Gohlke, Anal. Chem. 1959, 31, 535-541

[4] R.S. Gohlke, F.W. McLafferty, J. Am Soc. Mass. Spectrom 1993, 4, 367-371.

[5] R.A. Hites, Anal. Chem. 2016, 88, 6955-6961.

[6] D.W. Armstrong, T.J. Ward, R.D. Armstrong, T.E. Beesley, Science 1986, 232, 1132-1135.

[7] A. Berthod, X. Wang, K.H. Gahm, D.W. Armstrong, Geochem. Cosmochim. Acta. 1998, 62, 1619-1630.

[8] J. Huang, X. Zhang, D.W. Armstrong, Angew. Chemie. Int. Ed. 2007, 46, 9073-9077

[9] K. Huang, D.W. Armstrong, Organic Geochem. 2009, 40, 283-286.

[10] J.M. Eiler, Earth Planetary Lett. 2007, 262, 309-327.

[11] J.I. Seeman, H.V. Secor, R. Disselkamp, E.R. Bernstein, J. Chem. Soc. Chem. Commun. 1992, 713-714.

[12] B. Christensen, J. Nielsen, Metab. Eng. 1999, 1, 282-290.

[13] D.B Kell, M. Brown, H.M. Davey, W.B. Dunn, I. Spasic, S.G. Oliver, Nature Rev. Microbio. 2005, 3, 557-565.

[14] X. Huang, F.E. Regnier, Anal. Chem. 2008, 80, 107-114.

[15] W. Gordy and L.R. Cook, Microwave Molecular Spectra, 3rd Ed. John Wiley & Sons Inc.: New York, 1984.

[16] E.B. Wilson, Jr., Science 1968, 162, 59-66.

[17] B.H. Pate, Science 2011, 333, 947-948.

[18] C. Perez, J.L. Neill, M.T. Muckle, D.P. Zaleski, I. Pena, J.C. Lopez, J.L. Alonso, and B.H. Pate, Angew. Chem. Int. Ed. 2015, 127, 993-996.

[19] B.J. Harris, J.L. Neill, R.L. Pulliam, and M.T. Muckle, LC-GC 2015, 33, 18-24.

[20] E. Herbst, E.F. van Dishoeck, Annu. Rev. Astron. Astrophys. 2009, 47, 427-480.

[21] B.A. McGuire, Astrophys. J. Supp. Ser. 2018, 239, 1-48.

[22] B.J. Harris, R.L. Pulliam, J.L. Neill, M.T. Muckle, R.L. Reynolds, D.E. McDaniel, and B.H. Pate, Proc. SPIE 9101, Next-Generation Spectroscopic Technologies VII 2014, B1-B9.

[23] B.J. Harris, R.L. Pulliam, M.T. Muckle, R.L. Reynolds, B.H. Pate, Proc. SPIE 9362, Terahertz, RF, Millimeter and Submillimeter-Wave Technology and Applications VIII 2015, 1-10.

[24] G.B. Park, A.H. Steeves, K. Kuyanov-Prozument, J.L. Neill, and R.W. Field, J. Chem. Phys. 2011, 135, 024202.

[25] A.L. Steber, B.J. Harris, J.L. Neill, and B.H. Pate, J. Mol. Spectrosc. 2012, 280, 3-10.

[26] J.L. Neill, B.J. Harris, A.L. Steber, K.O. Douglass, D.F. Plusquellic, and B.H. Pate, Opt. Express 2013, 21, 19743-19749.

[27] G.G. Brown, B.C. Dian, K.O. Douglass, S.M. Geyer, S.T. Shipman, and B.H. Pate, Rev. Sci. Instrum. 2008, 79, 053103.

[28] G.B. Park and R.W. Field, J. Chem. Phys. 2016, 144, 200901.

[29] A.H. Meyer, H. Penning, M. Elsner, Environ. Sci. Technol. 2009, 43, 8079-8025.

[30] M.H. Thiemens, S. Chakraborty, G. Dominguez, Ann. Rev. Phys. Chem. 2012, 63, 155-177.

[31] P. Zhu, W. Tong, K. Alton, S. Chowdhury, Anal. Chem. 2009, 81, 5910-5917.

[32] T. Pluskal, T. Uehara, M. Yanagida, Anal. Chem. 2012, 84, 4396-4403.

[33] T.C. Schmidt, L. Zwank, M. Elsner, M. Berg, R.U. Mechenstock, S.B. Haderlein, Anal. Bioanal Chem. 2004, 378, 283-300.

[34] M. Elsner, M.A. Jochmann, T.B. Hofstetter, D. Hunkeler, A. Bernstein, T.C Schmidt, A. Shimmelmann, Anal. Bioanal. Chem. 2012, 403, 2471-2491.

[35] A. F. Charteris, T.D.J. Knowles, K. Michaelides, R.P. Evershed, Rapid Comm. Mass Spectrum. 2016, 30, 1846-1856.

[36] H. G. Close, Annu. Rev. Mar. Sci. 2019, 11, 27-56.

[37] J.-P. Kaiser, Y. Feng, J.M. Bollag, Microbiol. Rev. 1996, 60, 483-498.

[38] K. L. Casciotti, Geochim. Cosmochim. Acta 2009, 73, 2061-2076.

7.6 Supporting Information

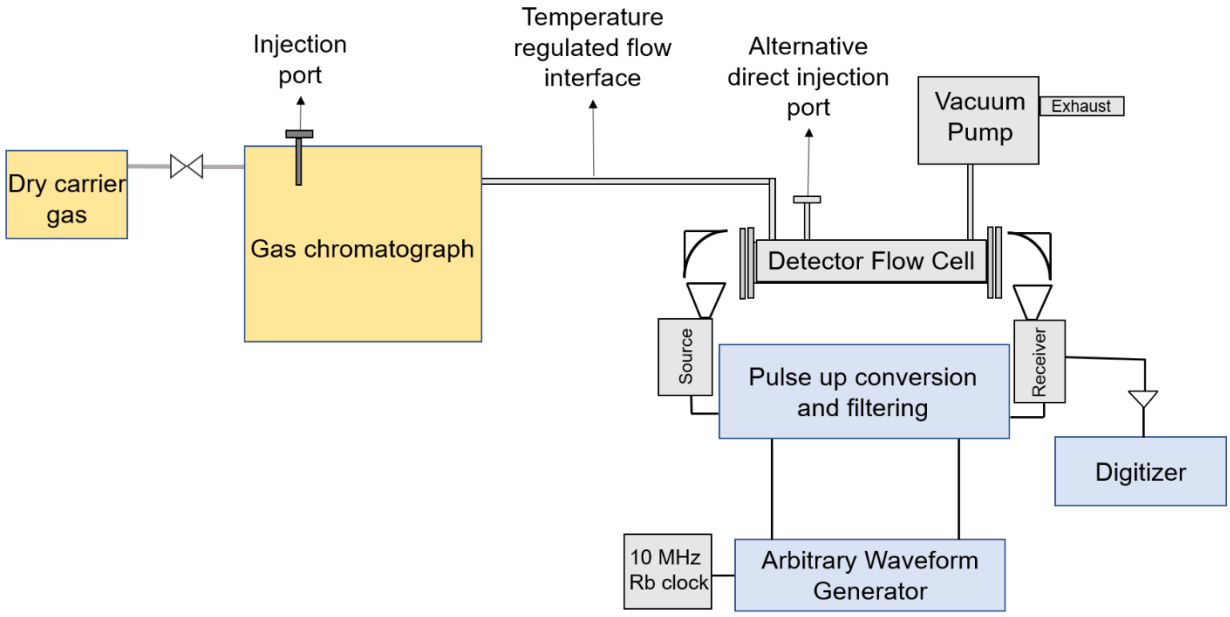

Figure 7.S1 Block diagram of GC-MRR instrument

7.6.1 Chemicals and materials

Methanol (67-56-1, 99.9%), methanol-^{13}C (14742-26-8, 99%), methanol-1-D (4206-31-9, 98%), methanol-^{18}O (5770-05-8, 95%), methan-d_2-ol (28563-35-1, 98%), methanol-D_3 (1849-29-2, 99.8%), ethanol (64-17-5, 99.9%), ethanol-1-^{13}C (14742-23-5, 99%), ethanol-2-^{13}C (14770-41-3, 99%), acetone (67-64-1, 99.9%), acetone-2-^{13}C (3881-06-9, 99.9%), acetone-1,3-$^{13}C_2$ (7217-25-6, 99.9%), acetone-$^{13}C_3$ (93628-01-4, 99%), acetone-D_6 (666-52-4, 99.9%), acetonitrile (75-05-8, 99.8%), acetonitrile-^{15}N (14149-39-4, 98%), acetonitrile-1-^{13}C (31432-55-0, 99%), acetonitrile-2-^{13}C (1722-09-4, 99%), acetonitrile-$^{13}C_2$ (1722-25-4, 99%), acetonitrile-1-^{13}C,^{15}N (14320-89-9, 99%), acetonitrile-$^{13}C_2$,^{15}N (14149-40-7, 99%), acetonitrile-d_3 (2206-26-0, 99.8%), pyridine (110-86-1, 99.8%), pyridine-^{15}N (34322-45-7, 98%), bromoethane (74-96-4, 98%), thiophene (110-02-1, 99%), 2-chlorothiophene (96-43-5, 96%), 2-chloropyridine (109-09-1, 99%), and 3-chloropyridine (626-60-8, 99%) were obtained from Sigma-Aldrich (St. Louis, MO). 3-

chlorothiophene (17249-80-8, 96%) was acquired from Acros-Organics. Agar powder (9002-18-0) was purchased from Alfa Aesar (Haverhill, MA). Tryptic soy broth was obtained from BD (Franklin Lakes, NJ). *Burkholderia cepacia* (ATCC25416 strain) was acquired from American Type Culture. The OverExpress™ E. coli C41(DE3) strain was obtained from Lucigen (Middleton, WI). Collection (ATCC). Groundwater was collected from Village Creek (Arlington, TX). Discovery® DSC-18 SPE cartridges (tube bed wt. 5 g) as well as capillary GC columns were obtained from Supelco (Millipore Sigma, Bellefonte, PA). The HPLC grade solvents: acetone, acetonitrile, dichloromethane, methanol, and ethanol were obtained from Sigma-Aldrich (St. Louis, MO). Deionized water was produced by Synergy 185 water purification system (Millipore, Billerica, MA).

7.6.2 Methods

7.6.2.1 Growth conditions for microorganisms

A 500 mL flask with a stirring magnetic bar was charged with 2 g of agar, 3 g of trypticase soy broth (TSB), and 100 mL of deionized (DI) water. The mixture was allowed to heat at 120 °C on hot plate until completely dissolved. The growth media was autoclaved at 121 °C at 15 psi for 30 min.

Molten trypticase soy agar (TSA) was transferred into 60 mm sterile petri dishes over flame and allowed to solidify at room temperature. Frozen solutions of *Escherichia coli (E. coli)* strain was streaked aseptically to sterilized media. Media was placed in incubator at 37 °C for 24 hours to culture bacteria.

To make the liquid media, 0.6 g of TBS was added to 20 mL of DI water. The media was autoclaved at 121 °C at 15 psi for 30 min. The *E. Coli* strains were inoculated to sterilized media

and flask was incubated at 200 rpm at 37 °C for 24 hours. A similar procedure was utilized for growing *Burkholderia cepacia (B. Cepacia)* bacteria.

7.6.2.2 Sample preparation and extraction

To monitor the biodegradation of organic compounds in bacterial samples, 10 µL of ^{14}N-pyridine and ^{15}N-pyridine were introduced into the 20 mL of microbial media. Moreover, a 500-ppm solution of pyridine isotopologues in groundwater was prepared. Three set of samples were prepared and incubated at 200 rpm at 37 °C. Samples were analyzed after 7 days and 14 days. To obtain cell free supernatants, cultures were centrifuged at 3500 rpm for 30 min. Pyridine isotopologues were extracted from the supernatant mixture using reversed-phase solid phase extraction (SPE). Dichloromethane was used to elute pyridine isotopologues from the C18 SPE cartridges. Extracted sample was concentrated to 100 µL of dichloromethane by removing excess solvent through rotary evaporation at 5 psi and 35 °C. The quantitative recovery yield was determined by extracting a 500-ppm standard solution of ^{14}N-pyridine and ^{15}N-pyridine from DI water and found to be 72% ± 4%. To monitor the changes in concentration of pyridine isotopologues, a calibration curve was constructed using 100, 200, 400, and 500 ppm standard solutions of both isotopologues in DI water. A regression coefficient (r^2) equal to 0.997 with a line equation of y = 0.0015x - 0.0146, and a regression coefficient (r^2) equal to 0.992 with a line equation of y = 0.0012x - 0.0238 were obtained to determine the concentration of ^{14}N-pyridine and ^{15}N-pyridine, respectively.

Similarly, 500 ppm solutions of $^{13}CH_3CN$, $CH_3{}^{13}CN$, and $CH_3C^{15}N$ isotopomers were prepared by adding 10 µL of each isotopologue to 20 mL of groundwater, as well as microbial media. Two set of samples were prepared and incubated at 200 rpm at 37 °C. The concentration of acetonitrile isotopomers were analyzed over a period of 14 days. Bacterial cultures were removed by

centrifuging samples at 3500 for 30 min. 1 mL of sample was transferred into a 10 mL headspace vial and heated at 80 °C for 20 minutes. The vapor phase enriched with acetonitrile isotopologues was extracted and injected to the GC-MRR. Specific calibration curves were constructed using 50, 100, 200, 400, and 500 ppm standard solutions of acetonitrile isotopologues in water. Line equations of y = 0.00623x - 0.07350, y = 0.00457x - 0.10967, and y = 0.00238x + 0.00017 with regression coefficient (r^2) of 0.99 were acquired from the calibration curves to measure the changes in concentrations of $^{13}CH_3CN$, $CH_3{}^{13}CN$, and $CH_3C^{15}N$, respectively.

7.6.2.3 GC-MRR conditions

A Hewlett Packard- HP 6890 series gas chromatograph equipped with split/splitless injection port was coupled with a BrightSpec W-band molecular rotational resonance (MRR) spectrometer. Hydrogen was used as carrier gas with constant flow rate for all analysis. Mixtures were injected neat with split ratio of 100:1. Injection temperature was set at 200 °C. A Supelcowax® 10 capillary GC column (L × I.D. 60 m × 0.25 mm, d_f 0.25 μm) was utilized for analysis of 5 organic solvents and their isotopologues. The GC oven was operated at gradient mode starting from 30 °C and 2 min hold time, then increased to 60 °C with rate of 5 °C/min, followed by a ramp of 10 °C/min to 100 °C. Hydrogen flow rate of 1.8 mL/min was used for analysis of organic solvents. The MRR initial chamber pressure was 4.86 mTorr and the chamber temperature was set at 60 °C.

A SLB®-IL60 capillary column (L × I.D. 30 m × 0.25 mm, d_f 0.25 μm) was employed for separation of chloro-heterocycles, bromoethane and thiophene. The gradient temperature program was started at 80 °C with a ramp of 5 °C/min till 120 °C, then increased to 220 °C at 15 °C/min. Hydrogen flow rate of 1.2 mL/min was used for this analysis. The MRR initial chamber pressure was 3.26 mTorr and the chamber temperature was set at 80 °C. GC-MRR analyses of the

acetonitrile and pyridine isotopic analytes extracted from biological matricies (Table 7.1) were analyzed using a Watercol™ 1910 GC column operated isothermally at 100 °C. Concentrations were determined by integrating the areas of the chromatographic peaks relative to the appropriate standard curve (see above Supporting Information, Section 7.6.2.2). Note that in this study, specific contributions of several spectral lines were added and monitored to get the chromatographic signal (i.e., peak) as described in Section 7.6.2.4 below. While not used in the current study of isotope ratios, changes in dipole moments and rotational constants are typically small and the ratio between MRR peak intensities also can be used directly as an accurate determination of isotopic ratios.

7.6.2.4 MRR data and analysis

MRR spectra were recorded using the segmented chirped-pulse FT-mmW technique, described in detail in Ref. 30 (numbering from the main paper). The excitation segment bandwidth was 720 MHz, and a total of 48 segments were used to attain a full bandwidth of 34,560 MHz (across the range 74,880-109,440 MHz). The excitation pulses were 250 ns in length. For each spectrum, a total of 10,000 FID signals were recorded at each segment, with duration 1.8 μs each. Signal averaging was performed by a digitizer with on-board FPGA signal accumulation capabilities. During each experiment, a broadband MRR spectrum was collected and archived to disk every 1.8 seconds. The resulting data were Fourier transformed using a Kaiser-Bessel apodization window (β=8) to suppress signal sidelobes, following the method described in Ref. 30. A single background measurement was also performed automatically at the beginning of each experiment to allow for removal of any spurious signals. A normalization procedure is performed by the user upon installation and periodically thereafter to characterize the MRR instrument response and ensure

accurate intensity quantification across spectra and between instruments. It should be noted that there have been some demonstrations of broadband chirped-pulse rotational spectroscopy for time resolved kinetic studies [1,2].

The total molecule chromatogram (TMC) was obtained by performing a peakpick on each Fourier transformed spectrum and summing the intensities of all the observed peaks. The extracted molecule chromatogram (EMC) for each compound (or isotopologue, or isotopomer) of interest was determined by identifying a list of transition frequencies for each with an intensity greater than approximately 30% of that of the strongest line of that compound. In this study, specific contributions of several spectral lines were added and monitored to get the chromatographic signals (i.e., peaks). In addition to increasing the signal-to-noise ratio of the chromatogram, it also reduces the error because MRR signal variations are frequency dependent. However, if too many weak lines are included, the overall signal-to-noise ratio begins to decrease, and we have found that 30% is typically a good tradeoff. Any overlaps or near-overlaps between the transition frequencies of different compounds were removed to avoid cross-contamination between their EMCs. For isotopologues and isotopomers of a single compound, the same transition quantum numbers were chosen in order to ensure unbiased determination of isotopic ratios. The raw data was then smoothed with an odd-point segmented Hamming filter in Matlab 2019.

7.6.2 *Reproducibility of GC-MRR response*

A 200 ppm solution containing $^{13}CH_3CN$, $CH_3{}^{13}CN$, and $CH_3C^{15}N$ in DI water was prepared and analyzed as per section 7.6.2.2, to examine the reproducibility of the GC-MRR response. The relative standard deviation (RSD%) for 5 successive injections was found to be approximately +/- 2.6 %, confirming satisfactory reproducibility of GCMRR detection (see Table S-1).

Table 7.S1 Peak areas, standard deviations, and relative standard deviations for standards of 3 acetonitrile isotopologues.

Compound	Peak area 1 (mV. Sec)	Peak area 2 (mV. Sec)	Peak area 3 (mV. Sec)	Peak area 4 (mV. Sec)	Peak area 5 (mV. Sec)	STD	RSTD%
$^{13}CH_3CN$	0.56	0.55	0.52	0.53	0.54	0.016	2.9
$CH_3{}^{13}CN$	0.79	0.75	0.75	0.75	0.74	0.019	2.6
$CH_3C^{15}N$	0.36	0.35	0.35	0.34	0.35	0.008	2.4

7.6.4 References for Supporting Information

[1] J.M. Oldham, C. Abeysekera, B. Joalland, L.N. Zack, K. Prozument, I.R. Sims, G.B. Park, R.W. Field, and A.G. Suits, *J. Chem. Phys.* 2014, 141, 154202.

[2] D.P. Zaleski, L.B. Harding, S.J. Klippenstein, B. Ruscic and K. Prozument, *J. Phys. Chem. Lett*. 2017, 8, 6180-6188.

Chapter 8. Conclusions

Geopolymer, -an advanced material from the field of construction engineering, has been reinvented into a product suitable for separation sciences using the principles of polymer chemistry, material science, and column technology. Chapter 2 discusses the first-ever synthesis of micron-sized geopolymer microspheres by reverse emulsion templating (or inverse suspension polymerization) and their complete characterization by SEM, EDS, XRD, laser diffraction, and surface and porosimetry. The intrinsic base stability, high hydrophilicity, and a unique selectivity of the geopolymer stationary phase make it a tough competitor to silica stationary phases. Among 37 tested commercial stationary phases, it was recognized as the most hydrophilic stationary phase. Chapter 3 discusses the manipulation of the original microstructure of geopolymer monoliths to induce the interconnected macroporosity in their otherwise impermeable structure. This was achieved by taking advantage of the sticky period, which occurs during suspension polymerization. Chapter 4 investigates the consequences of trace transition metals, present in original geopolymer stationary phases, on chromatographic peak shapes, and proposes highly pure transition metal-free geopolymers as an alternative. Chapter 5 discusses the chemical modifications of geopolymers by incorporating barium ions in their structures to extend their applications in separations of compounds bearing acidic functional groups. Chapter 6 introduces iron oxide coated geopolymer microspheres as an adsorbent for four different arsenic species viz arsenate, arsenite, monomethyl arsenate, and dimethyl arsenate.

Chapter 7 presents the coupling of gas chromatography with molecular rotational resonance spectroscopy (GC-MRR). The exceptional features of GC-MRR, such as ultra-high resolution (that exceeds that of NMR, FTIR, and most importantly, high-resolution mass spectrometry) and incredible chemical specificity, have been highlighted.

Appendix A List of Co-authors

Chapter 2. Wimalasinghe RM, Weatherly CA, Wahab MF, Thakur N, Armstrong DW. *Analytical Chemistry*. 2018, 90, 8139-46.

Chapter 3. Thakur N, Weatherly CA, Wimalasinghe RM, Armstrong DW. Journal of American Ceramic Society. 2019, 1024405-4409.

Chapter 4. Thakur N, Wahab MF, Khanal DD, Armstrong DW. Analytica Chimica Acta. 2019, 1081, 209-217.

Chapter 5. Khanal DD, Thakur N, Wahab MF, Armstrong DW. Talanta. 2020, 207, 120339.

Chapter 6. Thakur N, Armstrong DW.

Chapter 7. Armstrong DW, Talebi M, Thakur N, Wahab MF, Mikhoin AV, Muckel MT, Neill JL. Angewandte Chemie. 2020, 59, 192 –196.

Biographical Information

Nimisha Thakur was born in the small mountainous town, Solan, located in Himalayas, India. She obtained her Bachelor of Science (Honors School) and Master of Science (Honors School) degree in Chemistry from Panjab University, India. During her bachelor's studies, she interned at Bhabha Atomic Research Centre, Mumbai, India. She joined Dr. Daniel W. Armstrong's research group in 2017 for her Ph.D. studies in Analytical Chemistry. She has worked on synthesizing new pH stable stationary phases for high-performance liquid chromatography, tuning surface properties and porosity in ceramics, developing new adsorption media, and interfacing a new detector based on microwave spectroscopy with gas chromatography. She interned at BASF, Michigan in 2020, where she developed methods for analysis of bisphosphonates in corrosion stabilizer fluids. She has published seven articles in peer-reviewed journals and presented her work in various prestigious conferences. During the International Symposium for Capillary Chromatography (ISCC) 2019, she was awarded The Leslie S. Ettre Award by Perkin Elmer. She was also awarded President Spaniolo Graduate Award Fund and Dr. Charles K. Baker Character Fellowship by Department of Chemistry & Biochemistry, University of Texas at Arlington in April 2020.